UNIVERSIDADE FEDERAL DE SANTA MARIA
CENTRO DE CIÊNCIAS NATURAIS E EXATAS
PROGRAMA DE PÓS-GRADUAÇÃO EM CIÊNCIAS BIOLÓGICAS:
BIOQUÍMICA TOXICOLÓGICA

Pablo Andrei Nogara

ESTUDOS *in silico* APLICADOS A COMPOSTOS ORGÂNICOS DE MERCÚRIO E SELÊNIO EM SISTEMAS BIOLÓGICOS

TESE DE DOUTORADO

Santa Maria, RS
2020

Pablo Andrei Nogara

ESTUDOS *in silico* APLICADOS A COMPOSTOS ORGÂNICOS DE MERCÚRIO E SELÊNIO EM SISTEMAS BIOLÓGICOS

Tese apresentada ao Programa de Pós-Graduação em Ciências Biológicas: Bioquímica Toxicológica, da Universidade Federal de Santa Maria (UFSM, RS), como requisito parcial para obtenção do título de **Doutor em Ciências Biológicas: Bioquímica Toxicológica**.

Orientador: Prof. Dr. João Batista Teixeira da Rocha

Santa Maria, RS
2020

Nogara, Pablo Andrei
ESTUDOS in silico APLICADOS A COMPOSTOS ORGÂNICOS DE MERCÚRIO E SELÊNIO EM SISTEMAS BIOLÓGICOS / Pablo Andrei Nogara.- 2020.
160 p.; 30 cm

Orientador: João Batista Teixeira da Rocha
Tese (doutorado) - Universidade Federal de Santa Maria, Centro de Ciências Naturais e Exatas, Programa de Pós-Graduação em Ciências Biológicas: Bioquímica Toxicológica, RS, 2020

1. docagem 2. selenoproteínas 3. metilmercúrio 4. DFT 5. modelagem por homologia I. , João Batista Teixeira da Rocha II. Título.

Sistema de geração automática de ficha catalográfica da UFSM. Dados fornecidos pelo autor(a). Sob supervisão da Direção da Divisão de Processos Técnicos da Biblioteca Central. Bibliotecária responsável Paula Schoenfeldt Patta CRB 10/1728.

Pablo Andrei Nogara

ESTUDOS *IN SILICO* APLICADOS A COMPOSTOS ORGÂNICOS DE MERCÚRIO E SELÊNIO EM SISTEMAS BIOLÓGICOS

Tese apresentada ao Curso de Pós-Graduação em Ciências Biológicas: Bioquímica Toxicológica, da Universidade Federal de Santa Maria (UFSM, RS), como requisito parcial para obtenção do título de **Doutor em Ciências Biológicas: Bioquímica Toxicológica**.

Aprovado em 10 de agosto de 2020

João Batista Teixeira da Rocha, Dr. (UFSM)
(Presidente/Orientador)

Adriano Defini Andricopulo, Dr. (USP)

Cristiane Lenz Dalla Corte, Dr.ª (UFSM)

Karina dos Santos Machado, Dr.ª (FURG)

Oscar Endrigo Dorneles Rodrigues, Dr. (UFSM)

Santa Maria, RS
2020

“A imaginação é mais importante que o conhecimento”

Albert Einstein

"What man is a man that does not make the world better?"

Kingdom of Heaven, 2005

"Na natureza nada se cria, nada se perde, tudo se transforma"

Antoine Lavoisier

"Educação não transforma o mundo. Educação muda as pessoas.
Pessoas transformam o mundo"

Paulo Freire

"Nada é absoluto. Tudo muda, tudo se move, tudo gira, tudo voa e desaparece"

Frida Kahlo

“O nitrogênio em nosso DNA, o cálcio em nossos dentes, o ferro em nosso sangue, o carbono em nossas tortas de maçãs, ..., foram feitos no interior de estrelas em colapso.
Nós somos feitos de poeira das estrelas”

Carl Sagan

Dedico este trabalho aos meus pais Inês Fátima e Vilmar, e aos meus irmãos Cristian e Karise,
que sempre me apoiaram e ajudaram nos meus sonhos.
Esta conquista também é de vocês.

AGRADECIMENTOS

Agradeço a Deus e aos meus familiares que sempre me auxiliaram nesta jornada.

À Universidade Federal de Santa Maria e ao PPGBTox pela oportunidade e apoio durante a realização deste trabalho.

Ao prof. Dr. João Batista Teixeira da Rocha pela orientação, conselhos e apoio indispensáveis para a realização deste estudo.

À prof. Drª Laura Orian, bem como as demais professores e alunos integrantes do grupo de pesquisa *Theoretical Chemistry Group* (TCG) da *Università degli Studi di Padova* (UNIPD, Itália), pela oportunidade, ensinamentos, e apoio fundamentais para a conclusão deste estudo.

Aos colegas do Laboratório de Bioquímica Toxicológica pela amizade, pelas divagações, pela parceria nos mates, pela companhia e apoio "universitário" sempre necessários nos seminários e na compreensão e escrita de artigos.

Aos professores Dr. André Luis Silva da Silva e Rogério de Aquino Saraiva, que me mostraram e a auxiliaram nesse caminho científico.

Aos colegas e amigos do "Prédio 18 e 19" que sempre estiveram presentes.

Aos muitos antigos colegas de graduação e de pesquisa que desde 2010 me acompanharam e auxiliaram neste caminho.

Aos amigos e colegas da UNIPD que me receberam e ajudaram durante o Doutorado Sanduíche na Itália.

Aos demais professores, funcionários e alunos do PPBGTox e do Departamento de Bioquímica e Biologia Molecular pela disponibilidade e ajuda quando necessário.

Aos órgãos de fomento CNPq, CAPES, FAPERGS, e em especial ao CAPES-PrInt, pelo auxílio financeiro e a concessão da bolsa de estudos, bem como aos seus funcionários.

Agradeço a todos que de uma forma ou outra contribuíram para a realização desta tese.

RESUMO

ESTUDOS *in silico* APLICADOS A COMPOSTOS ORGÂNICOS DE MERCÚRIO E SELÊNIO EM SISTEMAS BIOLÓGICOS

AUTOR: Pablo Andrei Nogara
ORIENTADOR: Dr. João Batista Teixeira da Rocha

O metilmercúrio (MeHg) é uma potente neurotoxina, associado à inibição das selenoenzimas Glutationa Peroxidase (GPx) e Tioredoxina Redutase (TrxR), no entanto, o mecanismo de inibição do MeHg a nível molecular ainda precisa ser elucidado. Compostos orgânicos de Se, como o Ebselen (Ebs) e o disseleneto de difenila (DPDSe), têm demonstrado resultados promissores contra o toxicidade do MeHg. Por outro lado, os organosselênios também podem ser considerados tóxicos, uma vez que oxidam os grupos tióis proteicos da enzima ácido δ-aminolevulínico desidratase de mamífero (δ-AlaD). O uso de ferramentas *in silico*, tais como *docking* molecular, modelagem por homologia, e cálculos DFT são importantes, pois permitem uma análise a nível molecular. Além disso, novos moléculas sintéticas podem ser planejadas e virtualmente testadas. Assim, o presente trabalho tem o objetivo de compreender, à nível molecular, as interações químicas envolvidas entre organosselênios e MeHg com seus alvos biológicos, bem como propor novos compostos. Os resultados de *docking* molecular com a GPx e TrxR demonstraram que o MeHg é capaz de interagir nos seus sítio ativos, onde um ataque nucleofilico do resíduo de selenocisteina (Sec), poderia levar a formação do aduto Sec-SeHgMe, inibindo as enzimas. Os cálculos de DFT sugerem que Sec-SeHgMe poderia sofrer uma β-eliminação, formando assim a desidroalanina (Dha). Já as interações entre organosselênios e δ-AlaD mostraram que os selenóxidos, além de mais reativos que seus respectivos selenetos, possuem uma coordenação Zn··O o que poderia facilitar o ataque do tiolato da Cys124 ao átomo de Se. Por fim, novos compostos tio(seleno)semicarbazidas e derivados do Ebs são propostos para fins terapêuticos. Esses dados auxiliam no entendimento da toxicologia do MeHg e organosselênios, e podem guiar o desenvolvimento de futuros agentes quelantes de Hg com alta seletividade e com menor efeitos adversos.

Palavras chaves: docagem, selenoproteínas, metilmercúrio, DFT, modelagem por homologia.

ABSTRACT

in silico STUDIES APPLIED TO ORGANIC COMPOUNDS OF MERCURY AND SELENIUM IN BIOLOGICAL SYSTEMS

AUTHOR: Pablo Andrei Nogara
ADVISOR: João Batista Teixeira da Rocha, PhD

Methylmercury (MeHg) is a potent neurotoxin, which is associated with the inhibition of Glutathione Peroxidase (GPx) and Thioredoxin Reductase (TrxR) selenozymes, however, the mechanism of MeHg inhibition, at the molecular level, need to be elucidated. Organic selenium compounds, such as Ebselen (Ebs) and diphenyl diselenide (DPDSe), have shown promising results against MeHg toxicity. On the other hand, organoselenium compounds can also be considered toxic, since they are able to oxidize the thiol groups from the mammalian δ-aminolevulinic acid dehydratase (δ-AlaD). The use of *in silico* tools, such as molecular docking, homology modeling, and DFT calculations are important because they allow analysis at the molecular level. In addition, new synthetic molecules can be designed and virtually tested. Thus, the present work aims to understand, at the molecular level, the chemical interactions involved between organoselenium and MeHg molecules with their biological targets, as well as, to propose new and more effective compounds. The results of molecular docking with GPx and TrxR demonstrated that MeHg is capable of interacting in its active sites, where a nucleophilic attack from selenocysteine residue (Sec), could lead to the formation of the Sec-SeHgMe adduct, inhibiting the enzymes. DFT calculations suggest that Sec-SeHgMe could undergo β-elimination, leading to the dehydroalanine (Dha). The interactions between organoselenium compounds and δ-AlaD showed that selenoxides are more reactive than their respective selenides, and they have Zn···O coordination, which could facilitate the attack of the Cys124 thiolate on the Se atom. New compounds, such as pyridinyl(quinolyl)-thio(seleno)semicarbazides and Ebs derivatives are proposed for therapeutic purposes. These data help us to understand the toxicology of MeHg and organoselenium molecules and can guide the development of new Hg chelating agents with high selectivity and with less adverse effects.

Key words: Molecular docking, selenoproteins, methylmercury, DFT, homology modeling.

LISTA DE ILUSTRAÇÕES

LISTA DE TABELAS

LISTA DE QUADROS

LISTA DE ABREVIATURAS E SIGLAS

ACh	Acetilcolina
AChE	Acetilcolinesterase
ADF	*Amsterdam Density Functional*
Ala	Ácido δ-aminolevulínico
BAL	Dimercaprol / *British anti-Lewisite*
COVID-19	Doença do coronavírus 2019 / *Corona virus disease 2019*
Cys	Cisteína
DA	Doença de Alzheimer
DFT	Teoria do Funcional da Densidade / *Density Functional Theory*
Dha	Desidroalanina / *Dehydroalanine*
DMSA	Ácido dimercaptosuccínico / *dimercaptosuccinic acid*
DNA	Ácido Desoxirribonucleico / *deoxyribonucleic acid*
DCDSe	Disseleneto de dicolesterila / *dicholesteroyl diselenide*
DPDSe	Disseleneto de difenila / *diphenyl diselenide*
DSV	*Discovery Studio Visualizer*
Ebs	Ebselen
GPx	Glutationa peroxidase / *glutathione peroxidase*
GSH	Glutationa reduzida / *reduced glutathione*
GSSG	Glutationa oxidada
Hg	Mercúrio
Hist	Histamina
MeHg	Metilmercúrio / *methylmercury*
MerB	organomercurio-liase / *organomercurial lyase*
MM	Mecânica molecular
MQ	Mecânica quântica
Mpro	Protease principal / *main protease*
NAC	N-acetilcisteina
PAS	subsítio aniônico periférico / *peripheral anionic subsite*
PBG	Porfobilinogênio
PDB	Banco de dados de proteínas / *Protein Data Bank*
PSA	ácido fenilselenínico / *phenyl seleninic acid*
Py	Piridina
Qui	Quinolina
RMSD	Raiz do erro quadrático médio / *Root Mean Square deviation*
S	Enxofre
SAR	Relações estrutura-atividade / *structure-activity relationship*
SARS-COV-2	Coronavírus da síndrome respiratória aguda grave 2
Se	Selênio
Sec	Selenocisteína
SOD	Superóxido dismutase
Trx	Tiorredoxina / *thioredoxin*
TrxR	Tiorredoxina redutase / *thiredoxin reductase*
TrxSS	Tiorredoxina oxidada
δ-AlaD	ácido δ-aminolevulínico desidratase / *δ-aminolevulinic acid dehydratase*
–SH	Tiol
–SeH	Selenol

SUMÁRIO

1. INTRODUÇÃO

O entendimento dos mecanismos que geram a toxicidade de compostos naturais e sintéticos é essencial para o tratamento de intoxicações e doenças, bem como para o desenvolvimento de novos compostos com potencial uso terapêutico. O estudo das interações químicas entre macromoléculas e xenobióticos por meio de metodologias *in silico* podem auxiliar nesse processo, permitindo a compreensão do modo de ligação e a estimação da afinidade de ligantes por receptores (FRIEDMAN; BOYE; FLATMARK, 2013; RAIES; BAJIC, 2016; GUPTA; SHARMA; KUMAR, 2018). Nesse sentido, as interações entre organosselênios e metilmercúrio (MeHg) com seus alvos biológicos macromoleculares foram estudadas aplicando-se abordagens *in silico*, isto é, simulações computacionais (Figura 1.1), tais como *docking* molecular, modelagem por homologia, e cálculos da Teoria do Funcional da Densidade (DFT).

No Capítulo 1 foram estudados as interações dos compostos orgânicos de selênio com as enzimas ácido δ-aminolevulínico desidratase (δ-AlaD) e tiorredoxina redutase (TrxR), e no Capítulo 2 a ligação do MeHg na glutationa peroxidase (GPx) e TrxR foi investigada. Já no Capítulo 3, novos organosselênios foram planejados visando a inibição das enzimas acetilcolinesterase humana (AChE) e a principal protease viral (Mpro), além da remoção do Hg do organismo. Os resultados aqui apresentados podem auxiliar na compreensão da toxicologia e farmacologia dessas moléculas, bem como no *design* de novos compostos.

Figura 1.1. Visão geral dos temas abordados neste estudo.

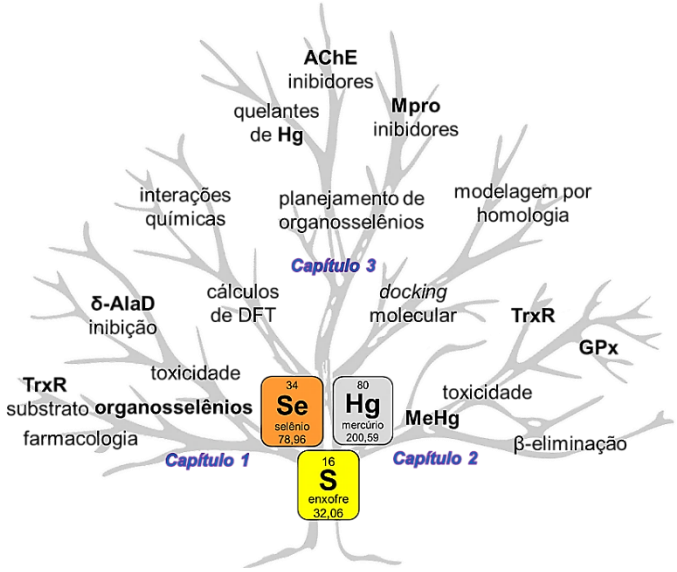

Fonte: autor.

1.1. METILMERCÚRIO

O elemento químico mercúrio (Hg), pertencente à família do zinco (Zn) (grupo 12 da tabela periódica) (Figura 1.2), é o único metal líquido em condições ambientes de temperatura e pressão (ponto de fusão = -38ºC), e apesar de ser encontrado naturalmente na forma do mineral cinabar (HgS), é considerado um poluente global pois ações antropogênicas (urbanização e industrialização) liberam mercúrio continuamente no meio ambiente (ARAÚJO; FARIA, 2003; NOGARA et al., 2019a).

Figura 1.2. Tabela periódica dos elementos químicos representada por elementos essenciais à vida.

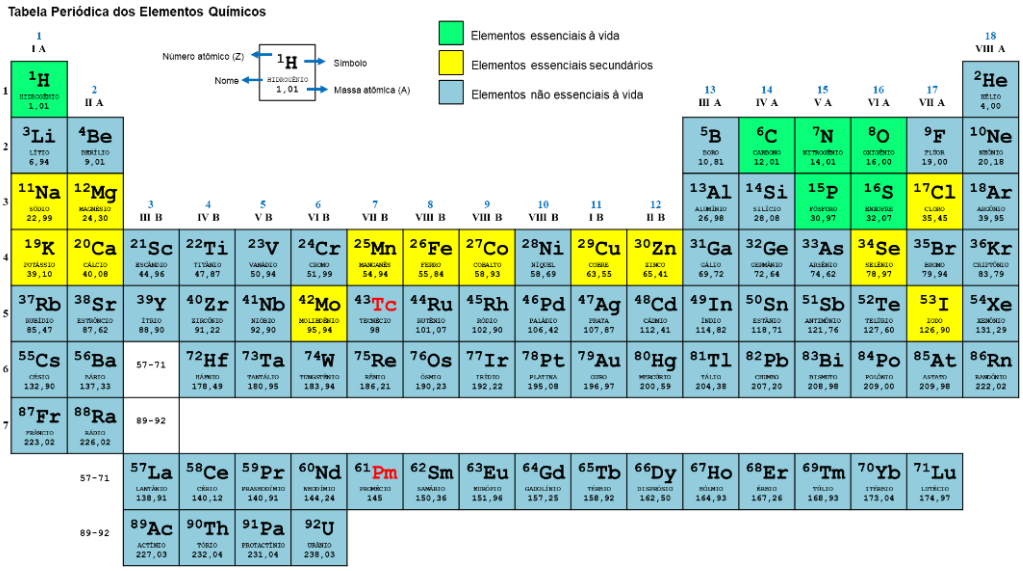

Fonte: autor. Adaptado de (ROCHA; PICCOLI; OLIVEIRA, 2017).

Indústrias utilizam Hg e/ou compostos de Hg na fabricação de medicamentos, fungicidas, amalgamas dentárias, ligas metálicas, entre outros. O cloreto de mercúrio ($HgCl_2$) é utilizado como antisséptico e como catalisador na indústria química (TCHOUNWOU et al., 2003; RICE et al., 2014; NOGARA et al., 2019b), e Hg^0 foi/é utilizado na mineração artesanal de ouro (Au), como observado no Brasil (MALM, 1998; KRISTENSEN; THOMSEN; MIKKELSEN, 2014). No nosso cotidiano, Hg pode ser encontrado em baterias/pilhas, termômetros, lâmpadas, amalgamas dentárias, conservantes de vacinas (tiomersal), bem como na queima de combustíveis fósseis e florestas (APÊNDICE 9.1) (NOGARA et al., 2019b).

À exceção de alguns micro-organismos fotossintetizantes que usam Hg como aceptor de elétrons (GREGOIRE; POULAIN, 2016), nenhuma forma de Hg tem alguma função biológica ou

fisiológica em organismos vivos, assim, a exposição a qualquer nível de Hg é tóxica (RENZONI; ZINO; FRANCHI, 1998; TCHOUNWOU et al., 2003; CLARKSON; MAGOS, 2006). Nesse sentido, o estudo das fontes de contaminação e das emissões naturais e antropogênicas de Hg são essenciais para a vida humana e do ecossistema (MASON; FITZGERALD; MOREL, 1994; PACYNA et al., 2006; PIRRONE et al., 2010; CHEN et al., 2017).

O Hg pode existir no ambiente em diferentes formas: mercúrio elementar (Hg^0), sais de mercúrio (Hg^{2+}), e mercúrio orgânico, tais como o metilmercúrio (MeHg). Devido à essa diversidade, a toxicidade do Hg depende de qual forma está presente. Hg^0 é rapidamente absorvido pelos pulmões e pelas membranas mucosas, enquanto que Hg^{2+} é fracamente absorvido. Já o MeHg é facilmente absorvido pelo intestino e deposita-se em muitos tecidos (BERNHOFT, 2012; OLIVEIRA et al., 2017).

A atenção sobre a toxicidade do Hg aumentou após o acidente na baia de Minamata, no Japão em 1956, onde o uso de Hg^{2+} como catalisador na síntese de acetaldeído, e seu descarte industrial indevido na baia resultou em uma alta contaminação. MeHg foi encontrado em peixes desta área, que acabaram sendo consumidos pela população local, sendo o principal causador da Doença de Minamata (uma síndrome neurológica). A exposição de humanos (em desenvolvimento ou adultos) ao MeHg resultou em casos catastróficos de neurotoxicidade (EKINO et al., 2007; GRANDJEAN et al., 2010; OLIVEIRA et al., 2017). Dessa forma, o MeHg é uma potente neurotoxina para humanos e animais, que pode ser biogmagnificado nas cadeias alimentares aquáticas, sendo formado por bactérias e fungos. Após o consumo de carnes contaminadas, o MeHg é absorvido pelo trato gastrointestinal e distribuído aos órgãos pela corrente sanguínea, sendo capaz de ultrapassar as barreiras placentária e hematoencefálica (HINTELMANN, 2010; UNEP, 2013; NOGARA et al., 2019a). Como tema dessa tese, os efeitos do MeHg serão priorizados em relação as outras formas de Hg.

O hidrargirismo ou mercurialismo resultante da intoxicação pela exposição ao Hg, apresenta sintomas que dependem do tipo de Hg, dose, tempo e forma de exposição. Dentre elas podemos citar a fraqueza muscular, dormência nas extremidade (mãos e pés), falta de coordenação e memória, diminuição da inteligência, dificuldade para enxergar, além de problemas renais. Em casos mais graves, a intoxicação pode provocar sequelas irreversíveis e morte (ARAÚJO; FARIA, 2003; BERNHOFT, 2012; OLIVEIRA et al., 2018).

Em nível molecular, a toxicidade de formas eletrofílicas de Hg (tais como Hg^{2+} e $MeHg^{+}$) podem ser explicados em termos químicos, através da Teoria Ácido-Base de Pearson. Hg^{2+} e $MeHg^{+}$ são eletrófilos moles e, consequentemente, em sistemas biológicos eles irão interagir com nucleófilos moles, especificamente os grupos tiol (–SH) e selenol (–SeH) presentes nos aminoácidos cisteína e selenocisteina, respectivamente (FARINA; ASCHNER; ROCHA, 2011; LOPACHIN; GAVIN, 2016; FARINA; ASCHNER, 2017).

Os agentes quelantes de Hg tem sido utilizados como tratamento, tais como o ácido dimercaptosuccínico (*dimercaptosuccinic acid*, DMSA), ácido 2,3-dimercapto-1-propanossulfônico (*2,3-dimercapto-1-propanesulfonic acid*, DMPS) e o dimercaprol (*British anti-Lewisite*, BAL), *N*-acetilcisteina (NAC), entre outros. Ambos possuem o grupo –SH, no qual espera-se formar complexos com Hg, que são excretados mais facilmente (BERNHOFT, 2012; KOSNETT, 2013; NOGARA et al., 2019a).

De maneira simplificada podemos dizer que a distribuição do MeHg no ambiente e no organismo é definida pela reação de Rabenstein. A reação de Rabenstein, em homenagem ao professor Dr. Dallas Rabenstein que foi pioneiro no estudo desse tipo de reação (RABENSTEIN, 1978; RABENSTEIN; EVANS, 1978; RABENSTEIN; ISAB; REID, 1982; RABENSTEIN; REID, 1984; ARNOLD; TAN; RABENSTEIN, 1986), é caracterizada pela troca de ligantes tióis e/ou selenóis ao átomo de Hg (Equação 1),

$$R–S(e)H + R'S–HgMe \leftrightarrow R–S(e)–HgMe + R'SH \quad (1)$$

onde R–S(e)H podem ser moléculas de alta massa molecular contendo –SH e/ou –SeH (tio/selenoproteínas), e R'S representa moléculas de baixa massa molecular contendo –SH (tais como cisteína, ácido lipoíco e glutationa (GSH)). Assim, considerando inicialmente o MeHg ligado a uma tiomolécula (R'S–HgMe), o átomo de Hg sofrerá um ataque nucleofílico do átomo de Se de outra molécula livre (R–SeH), onde o Se é considerado o nucleófilo ("rico em elétrons") e o Hg o eletrófilo ("pobre em elétrons"), formando a ligação Se–Hg (R–Se–HgMe) e substituindo a antiga ligação S–Hg. Apesar do MeHg formar adutos estáveis com a Cys, a ligação S–Hg é lábil, favorecida as reações de troca na presença de outras moléculas contendo grupos –SH ou –SeH. A labilidade da ligação química do Hg se refere a facilidade com que esta quebra e forma novas ligações com S e Se. (RABENSTEIN; EVANS, 1978; MELNICK; YURKERWICH; PARKIN, 2010; NOGARA et al., 2019a; OLIVEIRA et al., 2019; MADABENI et al., 2020).

1.2. SELENOENZIMAS COMO ALVOS DO MeHg

Os elementos químicos enxofre (S) e selênio (Se), da família dos calcogênios (grupo 16 da tabela periódica), são essenciais aos organismos vivos uma vez que estão presentes naturalmente em proteínas na forma dos aminoácidos cisteína (Cys, C), metionina (Met, M), e selenocisteína (Sec, U) (BROWN; ARTHUR, 2001; ROCHA; PICCOLI; OLIVEIRA, 2017; OLIVEIRA et al., 2019). O genoma humano codifica cerca de 214 mil Cys distribuídas em diversas proteínas, que podem conter um ou mais resíduos de Cys (GO; CHANDLER; JONES, 2015), por outro lado, apenas 25 selenoproteínas são codificadas (KRYUKOV et al., 2003).

Dentre as selenoproteínas destacam-se as enzimas glutationa peroxidase (GPx, EC 1.11.1.9) e tiorredoxina redutase (TrxR, EC 1.8.1.9), que atuam no sistema de defesa antioxidante (MUSTACICH; POWIS, 2000; STEINBRENNER; SIES, 2009; BRIGELIUS-FLOHÉ; MAIORINO, 2013). A atividade catalítica dessas enzimas ocorre através do grupo selenol (–SeH) da Sec presente nos sítios ativos (Figura 1.3). O selenol é análogo ao grupo tiol (–SH) encontrado na cisteína (Cys), no entanto, muito mais reativo frente aos eletrófilos, sendo um importante centro redox nas selenoproteínas (JOHANSSON; GAFVELIN; ARNÉR, 2005; ROCHA; PICCOLI; OLIVEIRA, 2017).

Figura 1.3. Estruturas e ciclos catalíticos da TrxR (A-B) e GPx (C-D). Os sítios ativos estão evidenciados.

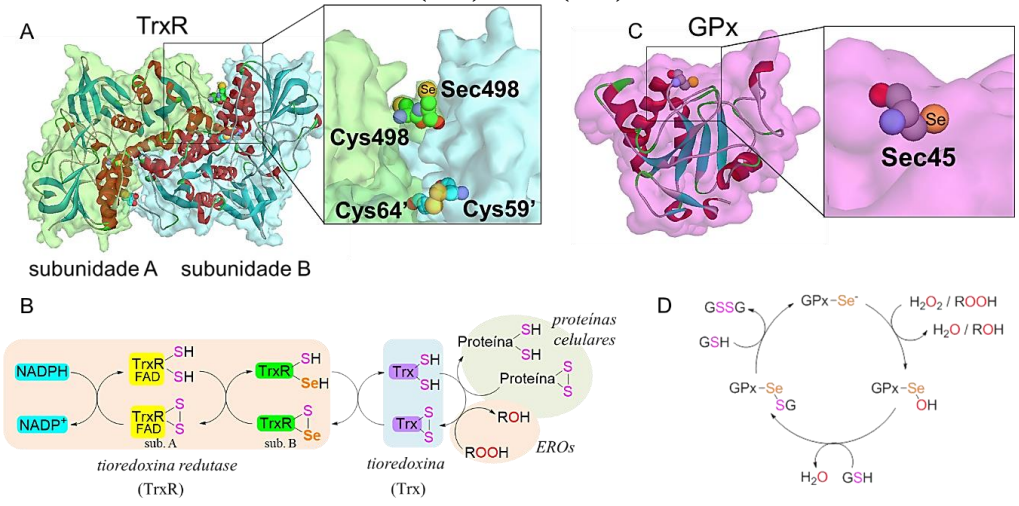

Fonte: Autor. As estruturas da TrxR (2J3N) e GPx (1GP1) foram obtidas do Banco de dados de proteínas (PDB).

A GPx e TrxR fazem parte do maior sistema redox intracelular: os sistemas glutationa (GSH/GSSG) e tiorredoxina (Trx/TrxSS) (STEINBRENNER; SIES, 2009). A GPx é responsável

pela degradação de peróxidos (de hidrogênio e lipídicos), utilizando como agente redutor a glutationa (GSH), que é oxidada a GSSG, de acordo com a Figura 1.3 (BRIGELIUS-FLOHÉ; MAIORINO, 2013). A TrxR, bem como a GPx, são responsáveis pela manutenção do ambiente redutor no interior das células, reduzindo espécies reativas de oxigênio (EROs) e outras tioproteínas, além de auxiliar na proliferação e apoptose celular. A TrxR é uma enzima homodimérica, contendo FAD (dinucleótido de flavina e adenina) e NADPH (fosfato de dinucleótido de nicotinamida e adenina) como coenzimas, que catalisa a redução da ponte dissulfeto da tiorredoxina oxidada (TrxSS) para gerar a tiorredoxina reduzida (Trx) (Figura 1.3) (ARNÉR; HOLMGREN, 2000; MUSTACICH; POWIS, 2000).

Estudos *in vitro* e *in vivo* têm demonstrado o efeito toxicológico do mercúrio inorgânico (Hg^{2+}) e orgânico (principalmente o MeHg), que podem estar relacionados à inibição da GPx e TrxR, devido a afinidade do Se pelo Hg. As inibições dessas enzimas podem estar diretamente relacionadas ao estresse oxidativo e à morte celular causados pela exposição ao Hg (CARVALHO et al., 2008; FRANCO et al., 2009; WAGNER et al., 2010; FARINA; ASCHNER; ROCHA, 2011; MEINERZ et al., 2017; BRANCO; CARVALHO, 2019; FARINA; ASCHNER, 2019). Sendo assim, a GPx e TrxR são alvos macromoleculares do MeHg, e consequentemente, compostos capazes de remover o MeHg dos seus sítios ativos poderiam ter efeitos benéficos. A presença de nanopartículas de seleneto de mercúrio (HgSe, conhecido como o mineral tiemanita) no cérebro e rins de mamíferos, indicando que o Hg poderia remover o Se de proteínas (KORBAS et al., 2010; GAJDOSECHOVA et al., 2016). No entanto, ainda não está claro na literatura se a ligação do MeHg à Sec poderia levar a formação da desidroalanina (do inglês, *dehydroalanine*, Dha), removendo assim o átomo de Se (MA et al., 2003).

1.3. COMPOSTOS ORGÂNICOS DE SELÊNIO

O uso do Se na síntese orgânica deu origem aos compostos de organosselênio, sendo o dietilseleneto o primeiro composto sintético produzido em 1836 por C. J. Löwig (LÖWIG, 1836; NOGARA; OLIVEIRA; ROCHA, 2020). Desde então muitos organosselênios tem sido sintetizados, dentre os quais o Ebselen (2-fenil-1,2-benzoselenazol-3-ona, Ebs) e o disseleneto de difenila (DPDSe) (Figura 1.4), que apresentam propriedades terapêuticas, tais como anti-inflamatória, cardioprotetora, neuroprotetora e antioxidante. Esta última devido sua capacidade de reduzir o peróxido de hidrogênio (H_2O_2) à água (H_2O), sendo considerados miméticos da GPx (isto

é, catalisam o mesmo tipo de reação química) (MUGESH; SINGH, 2000; NOGUEIRA; ZENI; ROCHA, 2004; SANTI; SANTORO; BATTISTELLI, 2010; ORIAN; TOPPO, 2014; BARBOSA et al., 2017). Além disso, híbridos de organosselênios e medicamentos conhecidos têm sido estudados com o intuito de desenvolver novos fármacos com propriedades concomitantes dos compostos originais, como observado em híbridos de Ebselen e donepezila, que são inibidores da acetilcolinesterase (AChE), um importante alvo terapêutico na Doença de Alzheimer (LUO et al., 2013).

Figura 1.4. Fórmula estrutural de compostos organocalcogênicos e seus derivados.

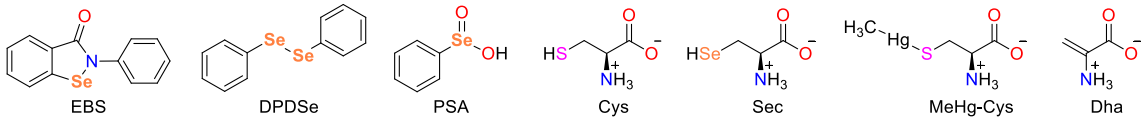

Fonte: Autor.

Devido a sua capacidade de reagir covalentemente com resíduos de Cys, o Ebs tem sido estudado como antiviral, inibindo cisteíno-proteases (ex. Mpro) responsáveis pela replicação viral, como recentemente estudados para o caso da COVID-19 (JIN et al., 2020; ULLRICH; NITSCHE, 2020). Além disso, tem se relatado que os organosselênios também são capazes de oxidar grupos tióis proteicos (NOGUEIRA; ROCHA, 2011; BARBOSA et al., 2017), como se observa na enzima ácido δ-aminolevulínico desidratase de mamífero (δ-AlaD), que apresenta três resíduos de Cys desprotonados (Apêndice 9.2) coordenados a um íon de Zn (II) (NOGUEIRA et al., 2003; JAFFE, 2004; ROCHA et al., 2012). Desta forma, apresentam efeitos toxicológicos, pois a δ-AlaD é uma importante enzima envolvida na síntese das porfirinas (JAFFE, 2000).

A δ-AlaD (ou porfobilinogênio sintase, EC 4.2.1.24) catalisa a condensação assimétrica de duas moléculas de ácido aminolevulínico, formando o porfobilinogênio (PBG) (Figura 1.5), que é o precursor da síntese das porfirinas. As porfirinas são essenciais ao organismo humano, pois o grupo prostético heme está envolvido no transporte de oxigênio (hemoglobina e mioglobina), metabolismo de xenobióticos (citocromo P450) e na proteção contra peróxidos (peroxidases e catalases) (JAFFE, 2000; HEINEMANN; JAHN; JAHN, 2008). No entanto, nem todas as formas da δ-AlaD são inibidas por organosselênios. Estudos tem mostrado que o DPDSe não é capaz de inibir a δ-AlaD de plantas (FARINA et al., 2002).

Figura 1.5. Reação catalisada pela δ-AlaD.

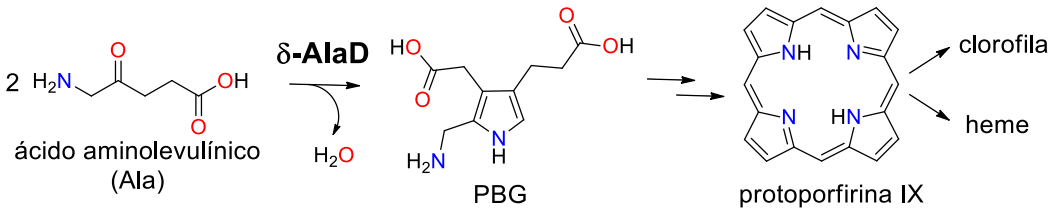

Fonte: Autor.

1.4. MODELAGEM MOLECULAR *in silico*

As técnicas de modelagem molecular, através do uso de computadores, podem permitir a compreensão dos mecanismos moleculares envolvidos em determinada atividade biológica. As simulações computacionais fornecem uma representação tridimensional dos processos moleculares envolvidos, como a interação proteína-ligante, e dessa maneira, podemos visualizar os sítios de ligação, identificar as interações químicas e os resíduos de amino ácidos envolvidos. Além disso, propriedades moleculares, tais como geometria, reatividade, e energias de reações, podem ser estudadas. Portanto, o uso da modelagem molecular é essencial na toxicologia e farmacologia de moléculas, bem como no desenvolvimento de novos fármacos (RODRIGUES, 2001; FRIEDMAN; BOYE; FLATMARK, 2013; FERREIRA et al., 2015; GENHEDEN et al., 2017; JAGGER et al., 2020; MARKOVIC; BEN-SHABAT; DAHAN, 2020).

Basicamente os estudos de modelagem molecular *in silico* envolvem dois tipos de métodos teóricos, os baseados na mecânica molecular clássica (MM) e os baseados na mecânica quântica (MQ) (FRIESNER, 2005; SANT'ANNA, 2009; PATRICK, 2013; LEWARS, 2016). Na MM os átomos são considerados como esferas carregadas e as ligações químicas se comportam como osciladores harmônicos, sem considerar os elétrons. Esse método pode ser aplicado em sistemas com grande número de átomos (centenas/milhares), como em proteínas. Por outro lado, na MQ são consideradas as interações entre núcleo e elétrons dos átomos da molécula, utilizando aproximações da equação de onda de Schrödinger ($H\Psi=E\Psi$), podendo ser aplicados em pequenos sistemas de algumas dezenas de átomos, devido ao seu alto custo computacional. Os métodos de Born-Oppenheimer (que considera os núcleos estáticos e os elétrons dinâmicos) e da teoria do funcional da densidade - *density functional theory*, DFT - (que calcula a probabilidade da densidade eletrônica) são alguns exemplos de métodos quânticos. Além disso, há os métodos semiempíricos, no qual a equação de onda é calculada com muitas aproximações e alguns parâmetros são obtidos

a partir de dados empíricos. Desta forma são mais rápidos que os métodos DFT, podendo ser aplicados em sistemas com centenas de átomos, no entanto, são menos precisos (SANT'ANNA, 2009; JOHANSSON; KAILA; SUNDHOLM, 2013; CUI; ELSTNER, 2014). Um dos principais objetivos da MQ é a compreensão do comportamento da matéria a nível atômico-molecular, além da previsão de propriedades físico-químicas. A equação de Schrödinger descreve o comportamento quântico dos átomos, considerando as coordenadas de todos os núcleos e elétrons do sistema. No entanto a resolução exata desta equação para sistemas grandes é muito complicada, principalmente devido as repulsões eletrônicas, sendo necessário várias aproximações para seu uso prático. O modelo DFT é um método alternativo, baseado no conceito de densidade eletrônica (ρ), derivado da probabilidade de encontrar uma partícula num determinado ponto e momento. Assim, a energia do sistema é expressa como uma função da densidade eletrônica (uma única variável de três coordenadas cartesianas), o que é muito mais simples do que os métodos fundamentados em funções de onda (3N variáveis, onde N é o número de elétrons do sistema) (DUARTE, 2001; RODRIGUES, 2001; SANT'ANNA, 2009; FRIEDMAN; BOYE; FLATMARK, 2013).

As estruturas tridimensionais de ligantes e receptores são de extrema importância na modelagem molecular, uma vez que estas estão associadas as suas funções moleculares e biológicas. As estruturas podem ser obtidas experimentalmente por cristalografia de raios X e ressonância magnética nuclear, ou podem ser criados modelos virtuais destas. A modelagem de proteínas por homologia é uma importante ferramenta para a obtenção de modelos 3D proteicos, no qual a estrutura da proteína de interesse é construída utilizando uma proteína molde (de estrutura conhecida), sendo suas sequencias primárias semelhantes (ARNOLD et al., 2006; FRIEDMAN; BOYE; FLATMARK, 2013; SCHMIDT; BERGNER; SCHWEDE, 2014).

Dentre as metodologias *in silico* existentes, o *docking* molecular (também denominado ancoragem, docagem, ou atracamento molecular) destaca-se por simular as interações entre macromoléculas (proteínas, enzimas, DNA) e ligantes (substrato, inibidor, agonista). Este método molecular consiste na predição do modo de ligação do ligante no sítio de ligação de um alvo determinado, além da estimação da afinidade pelo receptor, através da previsão da energia livre de ligação - ΔG (MORRIS et al., 1998; KITCHEN et al., 2004; CHEN, 2015). Dentre os programas de *docking* molecular, a família de softwares AutoDock (AutoDock4 e AutoDock Vina) são amplamente utilizados em estudos de ancoramento proteína-ligante. Ambos são de código livre para uso acadêmico e possuem como opções de docagem proteína-ligante: rígido-rígido, rígido-

flexível, e a proteína com as cadeias laterais flexíveis. O Vina se destaca devido sua velocidade de cálculo e precisão na estimação do modo de ligação de moléculas. A sua função de pontuação (*score*) considera interações estéricas, repulsivas, hidrofóbicas, ligações de hidrogênio, e penalidades de ligações rotacionáveis, no qual para cada termo é associado um valor (peso) pré-determinado. O algoritmo de busca (*Iterated Local Search*) realiza mudanças conformacionais no ligante criando diversas novas poses de ligação, buscando a de menor energia segundo o *score*. (CHANG et al., 2010; TROTT; OLSON, 2010; FORLI et al., 2016). Além disso, programas de dinâmica molecular podem ser utilizados para obtenção da conformação mais estável da estrutura proteica (refinamento estrutural). Neste processo ocorrem estiramentos das ligações e alterações conformacionais (angulares), simulando um "aquecimento", para que as barreiras de energia entre as conformações sejam vencidas (CARVALHO et al., 2003; HOLLINGSWORTH; DROR, 2018).

Os softwares de cálculos quânticos como o *Gaussian* (FRISCH et al., 2009) e o ADF (*Amsterdam Density Functional*) (TE VELDE et al., 2001) são programas amplamente utilizados. Eles calculam propriedades químicas e físicas, tais como: geometria molecular, potencial eletrostático, frequências de vibração, propriedades termodinâmicas e cinéticas, entre outras. Devido ao alto custo computacional dos métodos quânticos, métodos híbridos como o MQ/MM (método de simulação molecular que combina a precisão da MQ e a velocidade da MM) permitem o estudo de processos químicos mais complexos, como em soluções e em proteínas (FRIESNER, 2005; SANT'ANNA, 2009; KAMP; MULHOLLAND, 2013).

No entanto, estudos direcionados ao entendimento das interações entre organosselênios e proteínas alvo e entre selenoproteínas e espécies de mercúrio através de modelagem molecular ainda são raros na literatura. Além disso, esses poucos estudos utilizaram modelos que simplificam muito a estrutura proteica, isto é, poucos resíduos de aminoácidos (geralmente apenas um) são considerados nos cálculos e simulações (BAYSE; ALLISON, 2007; HOWELL, 2009; HEVERLY-COULSON; BOYD, 2010; ORIAN; TOPPO, 2014). Tendo em vista a importância de fatores estéricos, e que uma proteína pode possuir vários sítios de ligações (podendo levar a interações químicas com resíduos fora do sítio ativo), metodologias *in silico*, que considerem toda a estrutura proteica alvo, tornam-se necessárias para acelerar os avanços na farmacologia e toxicologia de compostos orgânicos de selênio e mercúrio.

2. JUSTIFICATIVA

Como estudos *in vitro* e *in vivo* encontrados na literatura demonstram que proteínas contendo grupos tióis são oxidadas por organosselênios, assim como selenoproteínas são inibidas por mercúrio (BARBOSA et al., 2017; NOGARA et al., 2019a), mais estudos são necessários para a compreensão de seus mecanismos de ação em nível molecular.

Desse modo, a intensificação de estudos *in silico* que determinem o modo de interação a nível molecular entre organosselênios e MeHg com seus alvos celulares podem melhorar a compreensão da reatividade, toxicologia e farmacologia destas moléculas. Além disso, estudos de simulações computacionais de compostos orgânicos de selênio podem auxiliar no desenvolvimento de novas moléculas que possam interagir com alvos moleculares específicos, diminuindo seus efeitos indesejados.

3. OBJETIVOS

3.1. OBJETIVO GERAL

Descrever as características estruturais e de reatividade envolvidas na interação entre organosselênios e MeHg com seus alvos macromoleculares, através de modelagem molecular *in silico*, além de planejar novos compostos organosselênios.

3.2. OBJETIVOS ESPECÍFICOS

3.2.1. Compreender o mecanismo de inibição da enzima δ-AlaD por organosselênios e seus respectivos selenóxidos, através de *docking* molecular;

3.2.2. Investigar o modo de ligação de organosselênios com a TrxR;

3.2.3. Simular as interações químicas entre espécies de MeHg e as enzimas TrxR e GPx;

3.2.4. Compreender a formação de Dha através de cálculos de DFT;

3.2.5. Propor novos compostos de Se, com possíveis atividades terapêuticas frente a intoxicação por MeHg, e na inibição das enzimas AChE humana e Mpro viral.

4. DESENVOLVIMENTO

Para uma melhor compreensão dos temas aqui estudados, o desenvolvimento desta tese está estruturado em três capítulos (Figura 1.1), de acordo com os objetivos propostos.

No Capítulo 1 refere-se à ligação dos compostos orgânicos de selênio com alvos biológicos, isto é, as enzimas δ-AlaD e TrxR. O Capítulo 2 apresenta as interações do MeHg com as selenoenzimas GPx, TrxR, e no Capítulo 3 são apresentados o planejamento de novos organosselênios.

Para os capítulos 1 e 2, os itens Materiais e Métodos, Resultados e Discussões, e Bibliografia encontram-se nos próprios artigos e manuscritos, que estão organizados de acordo com as normas das respectivas revistas científicas.

4.1. CAPÍTULO 1: INTERAÇÕES BIOLÓGICAS DE ORGANOSSELÊNIOS

Considerando que a δ-AlaD é um alvo biológicos dos compostos organosselênios, estudos *in silico* foram realizados para melhor entender as interações químicas envolvidas e um provável mecanismo de inibição. Os resultados podem ser encontrados nos artigos:

(a) **Nogara, P.A**. and Rocha, J.T.R., In silico studies of mammalian δ-AlaD interactions with Selenides and Selenoxides, *Molecular Informatics*, **2018**, 37 (4), 1700091, DOI: 10.1002/minf.201700091.

(b) **Nogara, P.A.**, Orian, L. and Rocha, J.T.R., The Se…S/N interactions as a possible mechanism of δ-aminolevulinic acid dehydratase enzyme inhibition by organoselenium compounds: A computational study, *Computational Toxicology*, **2020**, 15, 100127, DOI: 10.1016/j.comtox.2020.100127.

Além disso, sabendo-se que organosselênios podem ser substratos da TrxR, estudos de *docking* molecular foram realizados, e publicados no artigo:

(c) Sudati, J.H., **Nogara, P.A**., Saraiva, R.A., Wagner, C., Alberto, E.E., Braga, A.L., Fachinetto, R., Piquini, P.C., Rocha, J.B.T., Diselenoamino acid derivatives as GPx mimics and as substrates of TrxR: in vitro and in silico studies, *Organic and Biomolecular Chemistry*, **2018**, 16, 3777–3787, DOI: 10.1039/c8ob00451j.

Vale ressaltar aqui que os dados das simulações de *docking* foram obtidos pelo autor **Nogara, P.A**., e os experimentos *in vitro* foram realizados pela autora Sudati, J.H., por isso, ambos compartilharam a primeira autoria do artigo.

4.1.1. Artigo 1: Estudos *in silico* das interações da δ-AlaD de mamíferos com selenetos e selenóxidos

Nogara, P.A. and Rocha, J.T.R., In silico studies of mammalian δ-AlaD interactions with Selenides and Selenoxides, *Molecular Informatics*, **2018**, 37 (4), 1700091, DOI: 10.1002/minf.201700091.

Graphical Abstract

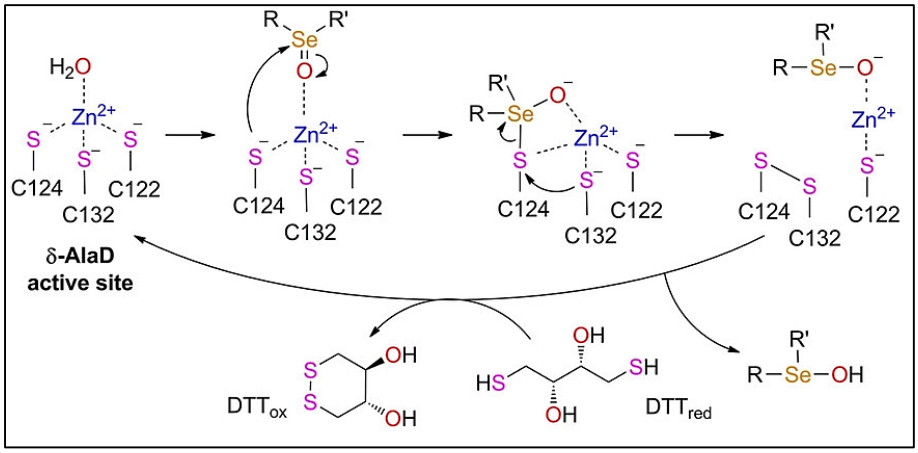

Full Paper

www.molinf.com

molecular informatics

DOI: 10.1002/minf.201700091

In Silico Studies of Mammalian δ-ALAD Interactions with Selenides and Selenoxides

Pablo Andrei Nogara*[a] and João Batista Teixeira Rocha*[a]

Abstract: Previous studies have shown that the mammalian δ-aminolevulinic acid dehydratase (δ-ALAD) is inhibited by selenides and selenoxides, which can involve thiol oxidation. However, the precise molecular interaction of selenides and selenoxides with the active center of the enzyme is unknown. Here, we try to explain the interaction of selenides and the respective selenoxides with human δ-ALAD by *in silico* molecular docking. The *in silico* data indicated that Se atoms of selenoxides have higher electrophilic character than their respective selenides. Further, the presence of oxygen increased the interaction of selenoxides with the δ-ALAD active site by O…Zn coordination. The interaction of S atom from Cys124 with the Se atom indicated the importance of the nucleophilic attack of the enzyme thiolate to the organoselenium molecules. These observations help us to understand the interaction of target proteins with organoselenium compounds.

Keywords: Organoselenium · molecular docking · δ-ALAD · *in silico* · semi empirical

1 Introduction

The enzyme δ-aminolevulinic acid dehydratase (δ-ALAD) or porphobilinogen synthase (E.C. 4.2.1.24) catalyzes the asymmetric condensation of two molecules of 5-aminolevulinic acid (ALA) to form the monopyrrole porphobilinogen (PBG). The PBG is the precursor of tetrapyrroles, such as coproporphyrin (which is an intermediate in heme synthesis) and porphyrins (which is an intermediate in chlorophyll synthesis). Consequently, δ-ALAD participates in biosynthetic pathways that are essential to aerobic life in the earth.[1–3] Thus, molecules that interfere with the tetrapyrrole biosynthesis can disrupt the cell metabolism.

The mammalian δ-ALAD can be inhibited by various metals, such as Cu^{2+}, Ag^{+}, Cd^{2+}, Hg^{2+}, Al^{3+}, Ga^{3+}, In^{3+}, Tl^{3+}, Sn^{2+}, Pb^{2+} and Bi^{3+}; and by inorganic and organic forms of selenium and tellurium compounds.[4] Accordingly, some studies have been published demonstrating that organic selenides **(1–3)** are weaker inhibitors of δ-ALAD than their respective selenoxides **(1–3(R, S))** (Figure 1 and Table 1). And it has been postulated that the selenoxides inhibit the δ-ALAD by oxidazing sulfhydryl groups from cysteinyl residues, since inhibitory effect of selenoxides was antagonized by dithiotreitol (DTT).[5,6]

Recently, *in silico* methods have been gaining importance as predicting tool of protein-ligand interactions at the atomic-level. It is frequently used in the discovery and optimization of novel molecules with affinity to particular targets. In this way, the molecular docking can be an important tool to predict the binding pose of a small molecule in specific proteins.[7–13]

Here we aim to explain at the molecular level the mechanism by which the selenoxides inhibit mammalian δ-ALAD and try to explain why they are more potent inhibitors of the enzyme than their selenide analogs.

2 Material and Methods

2.1 Molecular Docking

The 3D structure of human δ-ALAD was obtained from the Protein Data Bank (http://www.rcsb.org/pdb/) with the code: 5HMS.[14] The Chimera 1.8 software[15] was used to remove the chain B, water and other molecules, and to add hydrogen atoms to the protein. The ligands were built in the software Avogadro 1.1.1,[16] following the semi empirical PM6[17] geometry optimization with the program MOPAC2012.[18] The ligands and protein in the *pdbqt* format were generated by AutoDockTools,[19] where the ligands were considered flexible (with PM6 charges), and the enzyme rigid (with Gasteiger charges). The Zn^{2+} partial charge (0.302) was determined using a system that contains only the three cysteinyl residues (Cys122, Cys124 and Cys132), the Zn^{2+} ion and a molecule of water (which was included to complete the tetrahedral geometry of zinc). In order to mantain the amide bonds an acetyl group was added to the amine-terminal group and a methylamine was bound to the the carboxyl-terminal region. During the PM6 optimization, the Cα was considered frozen. AutoDock Vina

[a] *P. Andrei Nogara, J. Batista Teixeira Rocha*
Departamento de Bioquímica e Biologia Molecular, Centro de Ciências Naturais e Exatas, Universidade Federal de Santa Maria, Santa Maria, RS, Brazil
E-mail: pbnogara@gmail.com
jbtrocha@yahoo.com.br

1.1.1[20] program was used for the blind docking using a gridbox of 52×50×52 Å and the coordinates x=16.932, y=39.661, z=70.64, with an exhaustiveness of 100. Since only the compound 2 bound in the active site, we performed a more refined analisys, allowing the volumos residues located closed to the active site flexible. Specifically a gridbox of 20 Å^3 with the coordinates x=9.185, y=34.319, z=73.794 was used for the local docking in the active site region, allowing the side chains of Ser168, Lys199, Tyr205, Arg209, Arg221, Tyr224 and Gln225 residues to be flexible. The docking results were analyzed using the Accelrys Discovery Studio 3.5 software.[21]

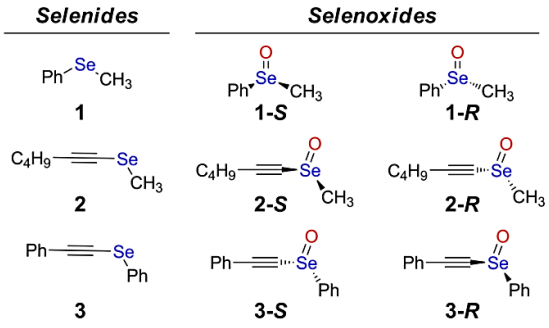

Figure 1. Chemical formula of selenides (**1-3**) and selenoxides (**1-3(R, S)**).

Table 1. Thermodynamic parameters obtained for the interaction of selenides and selenoxides with human ALAD.

Compound	△G (kcal/mol)		IC_{50} (μM)[c]
	1° conformer[a]	mean[b]	
1	−5.3	−5.03	>400
1-R	−5.8	−5.52	104
1-S	−4.5	−4.40	
2	−5.6	−5.45	>400
2-R	−5.9	−5.86	72
2-S	−6.0	−5.72	
3	−5.7	−5.65	250
3-R	−5.7	−5.65	45
3-S	−6.1	−6.05	

[a] △G from the conformer with the lowest negative energy in the cluster most populated; [b] △G mean from the cluster most populated; [c] Data from references[5,6] for the racemic mixture of isomers R and S.

2.2 Semi Empirical Optimization

To verify if the protein environment alters the partial charge of selenium atom of the compounds, when they were inside of δ-ALAD structure, a single point PM6 optimization was carry out. The ligands and the flexible residues were bound with the rigid protein file manually. The chemical bonds of the side chains of flexibles residues were built in the Accelrys Discovery Studio, and the hydrogen atoms were added in the Chimera 1.8 software. The file was saved in the *pdb* format. The total charge of the systems were found in the Avogadro program (with the key word: CHARGES) with the extension MOPAC. And after that, a single point optimization were made with the method PM6. In this step it was necessary to certify the protonation state of cysteinyl residues (as well as the other residues). Furthermore, the nature of the chemical bonds of selenium and the flexible residues with the rigid part of protein had to be check when run in different programas (i.e. Avogrado, Chimera, AutoDock Tools and Vina).

3 Results and Discussion

Initially, a blind docking comprising all the 3D structure of human δ-ALAD (PDB: 5HMS) was performed to determine the most favorable binding sites of the selenides and selenoxides compounds. The data analysis indicated that only the molecules **2** and **2-R** bound to the active site and interacted with the Zn, with the distance of Se to Zn of approximately 3 Å (data not show). The compounds **1**, **1-R**, **1-S**, **2-S**, **3**, **3-R** and **3-S** did not interact directly with the active site, but they bound to the loop located at the entrance of the active site (residues 205–225). These residues can cause a steric hindrance, do not allowing the entrance of the compounds to active site. In order to further characterize the interaction with this region, another docking were carried out leaving the side chains of the more voluminous residues (i.e., Tyr205, Arg209, Arg221, Tyr224 and Gln225) flexible. To increase the mobility of the ligands during the docking in the active site, the side chains of Ser168 and Lys199 were also considered flexible. The binding mode selected was based in the conformational cluster analysis, which usually generates 20 conformers. From these, the ten conformers with the most nergative energy were grouped in clusters, when the calculated RMSD ≤ 2 Å.[22,23] The best-cluster was considered the most populated and the conformer selected was the one with the lowest energy (△G) inside this cluster.

The flexible molecular docking indicated that the compound **1** interacted in the active site of δ-ALAD with Lys199 and Arg209 by cation-π stacking, and with the Ser168 by a H-bond (Figure 2A). In addition, Se atom of compound **1** interacted with Zn with a distance of 3.57 Å (Table 2). The selenoxide **1-R** (Figure 2B) bound to the enzyme in similar way to the selenide **1**, making cation-π interactions with Lys199, Arg209 and Arg221, and H-bond with Ser168 (due the presence of oxygen in **1-R**). The distance of Se to the Zn was practically the same obseved with **1** (3.51 Å). In contrast, the selenoxide **1-S** bound at the entrance of the active site, far from the zinc atom. The

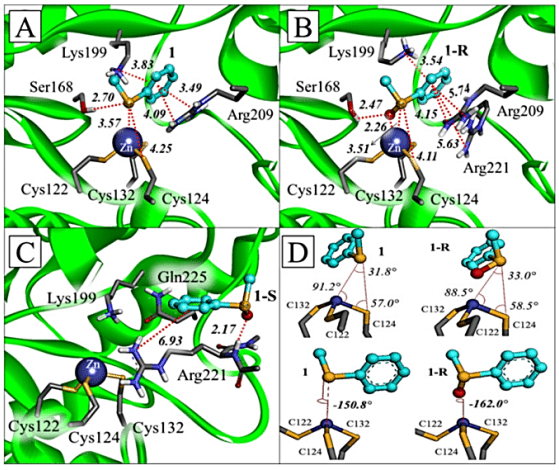

Figure 2. Interactions between selenide **1** (A) and selenoxides **1-R** (B) and **1-S** (C) with side chain residues of the δ-ALAD. The atomic angles between Se atoms of ligands with Zn and cysteinyl residues of the protein is depicted in (D). The δ-ALAD protein is represented in green color and only the side chains of the main residues are demonstrated. The selenide and selenoxides **1** were depicted with carbon atoms with light blue color. The cation-π and H-bonds interactions are represented by red dot lines, with the distances in Å (in bold).

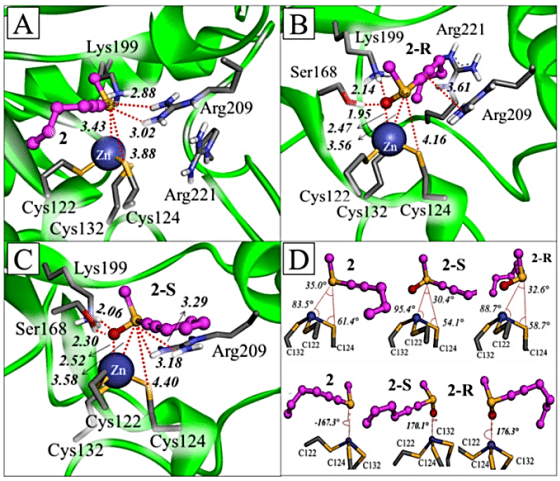

Figure 3. Interactions between selenide **2** (A) and selenoxides **2-R** (B) and **2-S** (C) with side chain residues of the δ-ALAD. The atomic angles between Se atoms of the ligands with Zn and cysteinyl residues of the protein is depicted in (D). The δ-ALAD protein is depicted in green color and only the side chains of the main residues are demonstrated. The selenide and selenoxides **2** were depicted with carbon atoms in pink color. The cation-π and H-bonds interactions are represented by red dot lines, with the distances in Å (in bold).

selenoxide **1-S** interacted with the Arg221 by cation-π and H-bonds (Figure 2C) and this isomer probably does not contribute to the inhibition of δ-ALAD. The angles between Zn and S (Cys124) with the Se atoms of the **1** and **1-R** were similar (Figure 2D). The dihedral angles (C–Se–Zn–S for **1** or O–Se–Zn–S for **1-R**) also had similar geometry (Figure 2D).

The docking results for the selenide **2** showed that this compound bound in the active site interacting with Arg209 and with the zinc ion (3.43 Å) (Figure 3A). The selenoxide **2-R** presented a distinct conformation when compared with **2**, particularly the alificatic carbon chain (represented in pink in Figure 3B). The **2-R** molecule showed H-bonds with Ser168 and Lys199 and a cation-π interactions between the guanidinium moiety of Arg209 and the electron rich triple bond of **2-R**. The distance between the Se atom and the zinc was slightly longer (3.56 Å) than that found for compound **2** (3.43 Å). For the selenoxide isomer **2-S**, the alifatic carbon chain also presented a different conformation when compared with **2** and **2-R** (Figure 3C). The great flexibility of the alifatic chain probably contributed to these different interactions with the enzyme. The oxygen atom from **2-S** made H-bonds with Lys199 and Ser168 and the distance of the Se atom to Zn (3.58 Å) was similar to that found for **2-R**. The angles between Se in the selenide/selenoxides **2** with Zn and S (Cys124) were similar. The angles between Se–Zn–S varied from 83.5 to

Table 2. Structural data obtained in the docking of selenides and selenoxides with δ- ALAD.

Comp.	Distance (Å) Se···S[a]	Se···Zn	O···Zn	Angle O–Zn–S[a]	V (Å^3)[b]
1	4.25	3.57	–	–	165.35
1-R	4.11	3.51	2.26	110.04	174.47
1-S	–	–	–	–	175.19
2	3.88	3.43	–	–	182.34
2-R	4.16	3.56	2.47	113.09	193.11
2-S	4.40	3.58	2.52	119.52	194.20
3	4.15	3.08	–	–	263.06
3-R	4.01	2.94	–	–	273.93
3-S	4.75	3.73	2.31	117.22	273.26

[a] S from Cys124; [b] Data from PM6 optimization in MOPAC, with only the compounds.

95.4°; while the angles between Se–S–Zn varied from 54.1 to 61.4°; and the angles between Zn–Se–S varied from 30.4 to 35.0° (Figure 3D). The dihedral angles between S–Zn–Se–O(C)) were found to be close to 170°.

In the case of selenide **3**, the simulation indicated that one of benzene rings made cation-π interactions with Arg221 and the other ring made σ-π stacking interaction with Phe79. The distance of Se to Zn (3.08 Å) was shorter to those found for compounds **1** and **2** (Figure 4A and Table 2). The selenoxide **3-R** demonstrated similar interactions with Arg221 and Phe79, however, the presence of oxygen atom in **3-R** allow H-bonds with Ser168 and Lys199 (Figure 4B). The distance of Se to Zn (2.94 Å) slightly shorter than that found for **3**. Similarly to those interactions observed with **3** and **3-R**, the selenoxide **3-S** presented σ-π stacking with Phe79 and cation-π interactions with Arg221 and H-bonds with Ser168 (Figure 4C). In constrast, the distance of Se to Zn (3.73 Å) was longer than those found with **3** and **3-R**. The analysis of the atomic angles (Figure 4D) indicated similarities, with the angles between Se–Zn–S varying from 100.3° to 102.3°, the angles between Se–S–Zn varying from 46.3 to 50.2°, and the angles between Zn–Se–S varying from 27.5 to 36.4°. The dihedral angles between S–Zn–Se–O were found to be close to 155°.

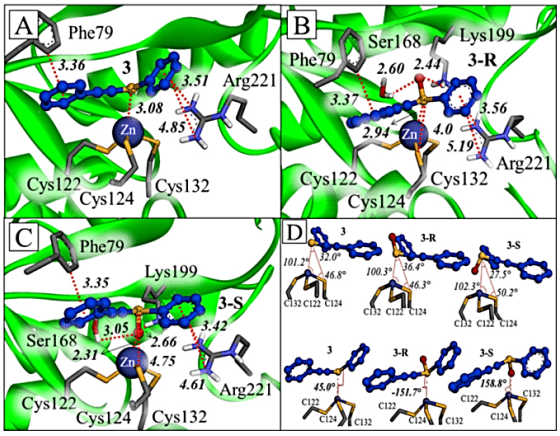

Figure 4. Interactions between selenide **3** (A) and selenoxides **3-R** (B) and **3-S** (C) with side chain residues of the δ-ALAD. The atomic angles between Se atoms of the ligands with Zn and cysteinyl residues of the protein is depicted in (D). The δ-ALAD protein is depicted in green color and only the side chains of the main residues are demonstrated. The selenide and selenoxides **3** were depicted with carbon atoms in blue. The cation-π and H-bonds interactions are represented by red dot lines, with the distances in Å (in bold).

The coordination of the oxygen from the selenoxide group with zinc (O…Zn) contributed to decrease the $\triangle G_{binding}$ of ligands **1-R, 2-R, 2-S and 3-S**, indicating a more favorable interaction than their respective selenides (Table 1). The exeptions were **1-S** that did not bind in the active site, and the **3-R** that did not display the O···Zn interaction. These observations were obtained both for the conformer of lower energy and for the overall $\triangle G_{mean}$ of the cluster (Table 1). The Lewis acid-base coordination between oxygen and zinc atoms are in accordance with the hard and soft acids and bases (HSAB) interactions, demonstrated by Pearson (1968).[24] Where the base is an atom, molecule, or ion which has at least one pair of free electrons, and the acid is an atom, molecule, or ion which has a vacant orbital where a pair of electrons can be accommodated.[24] In general, the selenoxides presented a more favorable binding energy with mammalian δ-ALAD than the selenides. *In vitro* studies indicated that the selenoxides can oxidized cysteinyl residues in the δ-ALAD, which has been shown to be prevented by DTT (dithiothreitol).[5,6] Thus, the coordination O···Zn can facilitate the nucleophilic attack of S atom from Cys124 into the Se atom, due its orientation and short distances (3.88–4.75 Å; Table 2, Figures 2, 3 and 4). The distance of O···Zn interactions found in the docking analysis (2.26–2.52) are in agreement with experimental data obtained by X-ray crystal structures of proteins (2.26–2.57 (PDB 1 L6S)). In addition, the angles between O–Zn–S from the selenoxides and the enzyme (110–119°) obtained here are in accordance with literature data (105° ± 7).[25–27]

The electrostatic potential map is an important tool to find reactive sites in a molecule/system; generally, the negative regions/species tend to attack the positively charged sites (a nucleophilic attack). The regions positively charged are the preferred sites for attack by specific nucleophiles. In addition, the electrostatic potential map helps us to understand the attraction and/or repulsion interactions between molecules. Consequently, charge density can explain the more preferable site for a nucleophilic attack.[28–31]

According to the electrostatic potential map of selenides **1–3** (Figure 5 and Table 3), the Se atom is slightly polarized. In contrast, the Se atom is highly polarized in the selenoxides **1-R, 1-S, 2-R, 2-S** and **3-R, 3-S.** The partial positive charge of Se atom is depicted in blue and the partial negative charge of O is shown in red in Figure 5. Overall, the selenium atom in selenoxides **1-R** and **1-S** has a positive charge which was about 20 times higher than that of Se atom in selenide **1** (Table 3). In the selenoxides **2-R, 2-S, 3-R** and **3-S**, the Se atom had positive charges that were 5 times higher than their selenides **2** and **3**. Hence, the presence of the oxygen atom has an electron-withdrawing effect, decreasing the electron density in the Se atom. The high positivity of Se atoms in **2**, **2-R**, **2-S**, **3**, **3R** and **3-S**, when compared to **1,1-R** and **1-S** (see charges in Table 3) can be explained by the presence of the triple bond in selenides and selenoxides **2** and **3**.

After the molecular docking, hydrogen atoms were added manually in each enzyme-inhibitor complexes. Then a PM6 single point optimization was performed with the

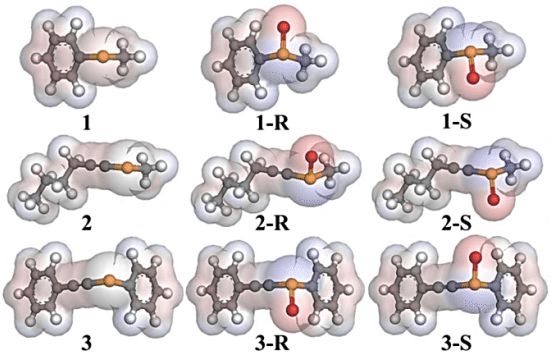

Figure 5. Electrostatic potential map of selenides **1–3** and selenoxides **1-R, S-3-R, S**. The partial charges were obtained from PM6 optimization and the maps built in the Accelrys Discovery Studio 3.5. The negative regions are indicated by the red color, while the positive regions in the selenides and selenoxides are represented by the blue regions.

enzyme-organoselenium compound complex, to verify if the Se charge could be altered inside of protein. The partial charges of Se atoms had little changes and the electrophile character of Se atoms was maintained.

The Se···S interaction is crucial to the cysteine oxidation (–S–S–), because it can facilitate the nucleophilic attack of thiol moiety (in this case Cys124) in the Se atom in the selenides and selenoxides **1–3**. The intermediate formed, with the selenylsulfide bond (–Se–S–), converts the S atom in the Cys124 into an electrophile center. Consequently, the S atom of Cys124 can now suffer a nucleophilic attack from the vicinal cysteinyl residues in the active center of δ-ALAD. The nucleophilic attack at the Cys124 forms a disulfide bridge (–S–S–) in δ-ALAD. Similar interactions between Se and S have been described in glutathione peroxidase and thioredoxin reductase and other theoretical works with sulfhydryl- and/or selenohydryl-containing proteins.[32–37] In this study, the Se···S distances ranged from 3.88 to 4.75 Å (Table 2) indicating a possible nucleophilic attack from the S atom of Cys124 in the Se atom in the selenides and selenoxides. In addition, the analysis of electrostatic potential map of the active site of δ-ALAD (Figure 6 and Table 3) confirmed the nucleophilic character of cysteinyl residues (negative charged regions around the S atom is depicted in red, Figure 6). The partial charges of S atoms observed in the enzyme-selenide/selenoxide complexes is shown in Table 3. The Cys124 and Cys132 residues presented higher negative charges than Cys122. However, as the Cys124 is closer and present a better spatial alignment with the Se atom of selenides/selenoxides than Cys132, we propose that the Cys124 is the first cystenyl residue which reacts with the organoselenium compounds. Since Cys122 is closer to the Cys124, one could propose that the disulfide bond would be formed between Cys124 and Cys122. However, since the S atom of Cys132 is more negative and has a better orientation than Cys122, we propose here that the –S–S– bond will be formed between Cys124 and Cys132 (Figure 6).

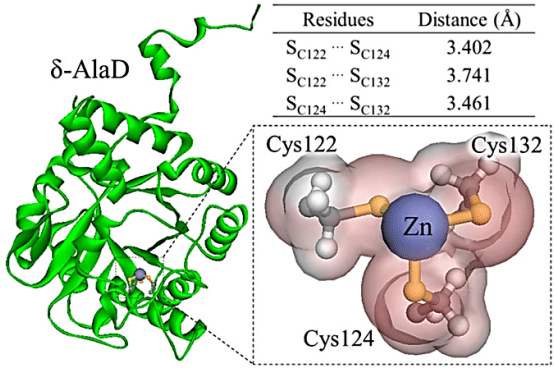

Figure 6. Electrostatic potential map of active site of mamalian δ-ALAD. The partial charges were obtained from PM6 single point optimization with entire enzyme, and the map build in the Accelrys Discovery Studio 3.5. The negative and positive regions are depicted in red and blue, respectively. The distances between thiolate groups of the cysteinyl residues inside the catalytic active site of δ-ALAD enzyme (5HMS) are indicated above in the small table.

Table 3. Partial charges obtained from PM6 single point optimization of selenides, selenoxides and enzyme-inhibitor complex.

Atom	Se[a]	Se	Zn	S_{C122}	S_{C124}	S_{C132}	O
1	0.048	0.180	0.467	−0,513	−0,636	−0,616	–
1-R	0.879	0.964	0.406	−0,529	−0,656	−0,631	−0,555
1-S	0.880	0.882	0.520	−0,521	−0,609	−0,634	−0,776
2	0.181	0.062	0.477	−0,529	−0,638	−0,610	–
2-R	0.980	1.058	0.455	−0,529	−0,666	−0,602	−0,665
2-S	0.979	0.909	0.497	−0,550	−0,658	−0,636	−0,711
3	0.181	0.240	0.522	−0,550	−0,631	−0,684	–
3-R	0.971	0.978	0.476	−0,511	−0,594	−0,670	−0,804
3-S	0.972	0.966	0.482	−0,556	−0,621	−0,686	−0,688

[a] These charges refer to the optimization with the selenides and selenoxides alone (before the docking).

The findings obtained here are in agreement with previous studies from our group that indicated the importance of Cys124 in the initial step of reaction between organoselenium compounds with δ-ALAD.[38,39]

The theoretical molecular volume analysis of the compounds indicated that the presence of oxygen atom in the selenoxides increased the molecular volume by 9–11 Å^3. Although the selenides and selenoxides **1-R**, **1-S**, **2-R** and **2-S** presented lower volume than **3-R** and **3-S**, the selenoxides **3-R** and **3-S** presented higher inhibitory potency than the selenoxides **1** and **2**. Probably the presence of the two benzene rings are essential to better accomodate the selenoxides in active site of δ-ALAD (Table 2).

Here we highlight the importance of flexible protein molecular docking that can provide better data when compared with the rigid docking. The presence of cation-π stacking with Arg209 and Arg221 was essential to stabilize the inhibitors in the δ-ALAD active site. In addition, the selenoxides have more reactive selenium atoms than selenides due to the presence of oxygen atom, which increased the electrophilicity of the Se atom and made H-bonds with Ser168. Thus, the presence of the selenoxide group increased the reactivity and the stability of the inhibitors with the enzyme. It is worth mentioning that the alkyne selenides (**2-3**) presented selenium atoms more eletrophilic than **1** (Table 3).

4 Conclusions

The *in silico* results presented here are in accordance with experimental data and help us to understand the reactivity of organoselenium compounds with sulfhydryl proteins. The oxidation of selenides to selenoxides increase the electrophilic character of selenium atom. Besides, the presence of oxygen atom can improve the interaction of selenoxides inside the catalytic site of δ-ALAD, by Lewis acid-base interactions (O···Zn coordination) (Figure 7). These observations encourage us to use *in silico* models for the understanding of experimental *in vitro* and *in vivo* data. However, more studies are necessary to prove the formation of the disulfide bridge (–S–S–) between Cys124 and Cys132 residues.

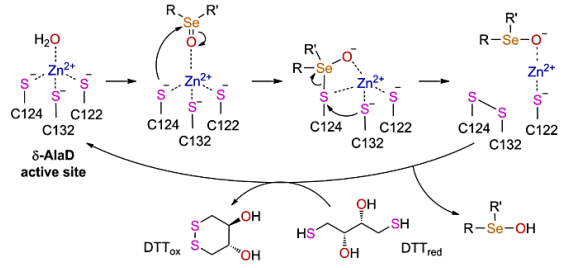

Figure 7. Proposed mechanism of mammalian δ-ALAD inhibition by selenoxides.

Conflict of Interest

None declared.

Acknowledgements

The authors would like to thank the financial support by FAPERGS/CNPq 12/2014-PRONEX: no. 16/2551-0000, CAPES, CNPq – Brazil, INCT-EN: For Cerebral Diseases, Excitotoxicty and Neuroprotection.

References

[1] R. S. Ajioka, J. D. Phillips, J. P. Kushner, *Biochim. Biophys. Acta.* **2006**, *1763*, 723–736.
[2] S. Sassa, *Semin. Liver Dis.* **1998**, *18*, 95–101.
[3] N. Mochizuki, R. Tanaka, B. Grimm, T. Masuda, M. Moulin, A. G. Smith, A. Tanaka, M. J. Terry, *Trends Plant Sci.* **2010**, *15*, 488–98.
[4] J. B. T Rocha, R. A Saraiva, S. C. Garcia, F. S. Gravina, C. W. Nogueira, *Toxicol. Res.* **2012**, *1*, 85–102.
[5] M. Farina, V. Folmer, R. C. Bolzan, L. H. Andrade, G. Zeni, A. L. Braga, J. B. T. Rocha, *Toxicol. Lett.* **2001**, *119*, 27–37.
[6] R. C. Bolzan, V. Folmer, M. Farina, G. Zeni, C. W. Nogueira, J. B. T. Rocha, T. Emanuelli, *Pharmacol. Toxicol.* **2002**, *90*, 214–219.
[7] A. Roncaglioni, E. Benfenati, *Chem. Soc. Rev.* **2008**, *37*, 441–50.
[8] F. Ballante, G. R. Marshall, *J. Chem. Inf. Model.* **2016**, *56*, 54 – 72.
[9] M. Löwer, E. Proschak. *Mol. Inf.* **2011**, *30*, 398–404.
[10] A. Koutsoukas, B. Simms, J. Kirchmair, P. J. Bond, A. V. Whitmore, S. Zimmer, M. P. Young, J. L. Jenkins, M. Glick, R. C. Glen, A. Bender, *J. Proteomics.* **2011**, *74*, 2554–2574.
[11] S. Ekins, J. Mestres, B. Testa, *Br. J. Pharmacol.* **2007**, *152*, 9–20.
[12] G. Sliwoski, S. Kothiwale, J. Meiler, E. W. Jr. Lowe, *Pharmacol. Rev.* **2013**, *31*, 334–395.
[13] B. O. Villoutreix, M. A. Kuenemann, J. L. Poyet, H. Bruzzoni-Giovanelli, C. Labbé, D. Lagorce, O. Sperandio, M. A. Miteva. *Mol. Inf.* **2014**, *33*, 414–437.
[14] N. Mills-Davies, D. Butler, E. Norton, D. Thompson, M. Sarwar, J. Guo, R. Gill, N. Azim, A. Coker, S. P. Wood, P. T. Erskine, L. Coates, J. B. Cooper, N. Rashid, M. Akhtar, P. M. Shoolingin-Jordan, *Acta Crystallogr. Sect. D* **2017**, *73*, 9–21.
[15] E. F. Pettersen, T. D. Goddard, C. C. Huang, G. S. Couch, D. M. Greenblatt, E. C. Meng, T. E. Ferrin, *J. Comput. Chem.* **2004**, *25*, 1605–1162.
[16] M. D. Hanwell, D. E. Curtis, D. C. Lonie, T. Vandermeersch, E. Zurek, G. R. Hutchison, *J. Cheminf.* **2012**, *4*, 1–17.
[17] J. J. P. Stewart, *J. Mol. Model.* **2007**, *13*, 1173–1213.
[18] J. J. P. Stewart, MOPAC 2012, **2012**. Stewart Computational Chemistry. Colorado Springs, CO, USA. http://OpenMOPAC.net
[19] G. M. Morris, R. Huey, W. Lindstrom, M. F. Sanner, R. K. Belew, D. S. Goodsell, A. J. Olson, *J. Comput. Chem.* **2009**, *30*, 2785–2791.
[20] O. Trott, A. J. Olson, *J. Comput. Chem.* **2010**, *31*, 455–461.
[21] Dassault Systèmes BIOVIA, Discovery Studio Modeling Environment, Release 2017, San Diego: Dassault Systèmes, **2016**.

[22] F. Ballante, G. R. Marshall, *J. Chem. Inf. Model.* **2016**, *56*, 54 – 72.
[23] A. M. Ruvinsky, A. V. Kozintsev, *J. Comput. Chem.* **2005**, *26*, 1089–1095.
[24] R. G. Pearson, J . *Chem. Educ.* **1968**, *45*, 581–587.
[25] E. K. Jaffe, J. Kervinen, J. Martins, F. Stauffer, R. Neier, A. Wlodawer, A. Zdanov, *J. Biol. Chem.* **2002**, *277*, 19792–19799.
[26] H. Zheng, M. Chruszcz, P. Lasota, L. Lebioda, W. Minor, *J. Inorg. Biochem.* **2008**, *102*, 1765–1776.
[27] I. L. Alberts, K. Nadassy, S. J. Wodak, *Protein Sci.* **1998**, *7*, 1700–1716.
[28] N. O. Eddy, B. I. Ita. *Int. J. Quantum Chem.* **2011**, *111*, 3456–3474.
[29] C. Cojocaru, A. Airinei, N. Fifere, *Springer Plus*, **2013**, *2*, 1–19.
[30] T. C. Ngo, D. Q. Dao, N. M. Thong, P. C. Nam, *RSC Adv.* **2016**, *6*, 30824–30834.
[31] A. Vektariene, G. Vektaris, J. Svoboda, *Arkivoc* **2009**, *vii*, 311–329.
[32] D. Bhowmick, G. Mugesh, *Org. Biomol. Chem.* **2015**, *13*, 10262–10272.
[33] T. Sandalova, L. Zhong, Y. Lindqvist, A. Holmgren, G. Schneider, *Proc. Natl. Acad. Sci. USA* **2001**, *98*, 9533–9538.
[34] S. Antony, C. A. Bayse, *Inorg. Chem.* **2013**, *52*, 13803–13805.
[35] C. A. Bayse, P. Pavlou, *Org. Biomol. Chem.* **2011**, *9*, 8006–8015.
[36] P. B. Lutz, C. A. Bayse, *J. Inorg. Biochem.* **2016**, *157*, 94–103.
[37] L. P. Wolters, L. Orian, *Curr. Org. Chem.* **2016**, *2*, 189–197.
[38] R. A. Saraiva, D. C. Bueno, P. A. Nogara, J. B. T. Rocha, *J. Toxicol. Environ. Health A.* **2012**, *75*, 1012–1022.
[39] N. V. Barbosa, C. W. Nogueira, P. A. Nogara, A. F. de Bern, M. Aschner, J. B. T. Rocha, *Metallomics*, in press, DOI, 10.1039/c7mt00083a.

Received: July 14, 2017
Accepted: October 18, 2017
Published online on November 6, 2017

4.1.2. Artigo 2: Interações Se···S/N como um possível mecanismo de inibição da enzima ácido δ-aminolevulínico desidratase por compostos organosselênios: um estudo computacional

Nogara, P.A., Orian, L. and Rocha, J.T.R., The Se…S/N interactions as a possible mechanism of δ-aminolevulinic acid dehydratase enzyme inhibition by organoselenium compounds: A computational study, *Computational Toxicology*, **2020**, 15, 100127, DOI: 10.1016/j.comtox.2020.100127.

O *Supporting information* deste artigo encontra-se disponível no APÊNDICE 9.3.

Graphical Abstract

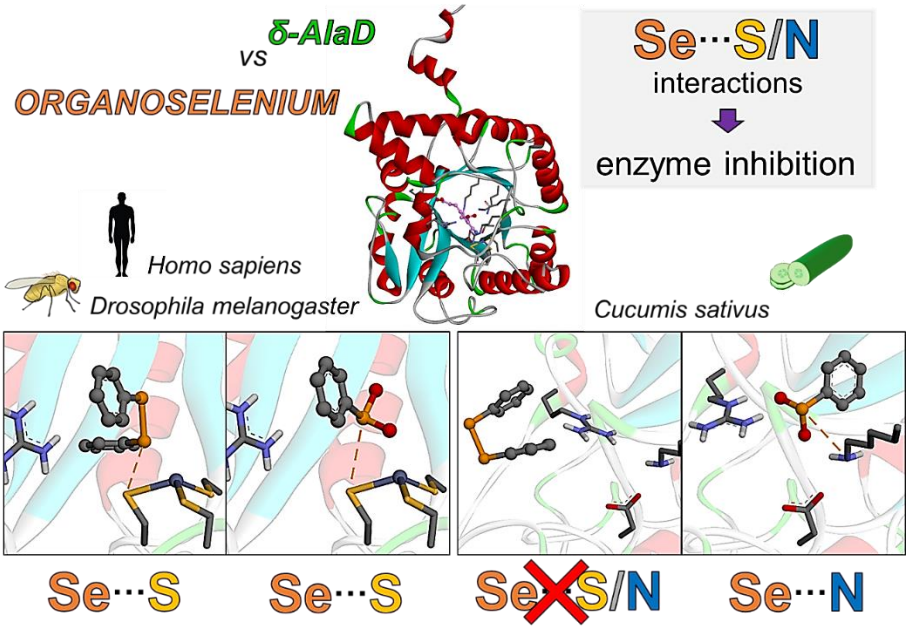

Computational Toxicology 15 (2020) 100127

Contents lists available at ScienceDirect

Computational Toxicology

journal homepage: www.elsevier.com/locate/comtox

The Se···S/N interactions as a possible mechanism of δ-aminolevulinic acid dehydratase enzyme inhibition by organoselenium compounds: A computational study

Pablo Andrei Nogara[a], Laura Orian[b], João Batista Teixeira Rocha[a,*]

[a] Departamento de Bioquímica e Biologia Molecular, Universidade Federal de Santa Maria (UFSM), Santa Maria 97105-900, RS, Brazil
[b] Dipartimento di Scienze Chimiche, Università degli Studi di Padova, Via Marzolo 1, 35131 Padova, Italy

ARTICLE INFO

Keywords:
Porphobilinogen synthase
Protein homology modeling
Docking
DFT calculations
In silico analysis

ABSTRACT

Organoselenium compounds present many pharmacological properties and are promising drugs. However, toxicological effects associated with inhibition of thiol-containing enzymes, such as the δ-aminolevulinic acid dehydratase (δ-AlaD), have been described. The molecular mechanism(s) by which they inhibit thiol-containing enzymes at the atomic level, is still not well known. The use of computational methods to understand the physical–chemical properties and biological activity of chemicals is essential to the rational design of new drugs. In this work, we propose an *in silico* study to understand the δ-AlaD inhibition mechanism by diphenyl diselenide (DPDS) and its putative metabolite, phenylseleninic acid (PSA), using δ-AlaD enzymes from *Homo sapiens* (*Hs*δ-AlaD), *Drosophila melanogaster* (*Dm*δ-AlaD) and *Cucumis sativus* (*Cs*δ-AlaD). Protein modeling homology, molecular docking, and DFT calculations are combined in this study. According to the molecular docking, DPDS and PSA might bind in the *Hs*δ-AlaD and *Dm*δ-AlaD active sites interacting with the cysteine residues by Se···S interactions. On the other hand, the DPDS does not access the active site of the *Cs*δ-AlaD (a non-thiol protein), while the PSA interacts with the amino acids residues from the active site, such as the Lys291. These interactions might lead to the formation of a covalent bond, and consequently, to the enzyme inhibition. In fact, DFT calculations (mPW1PW91/def2TZVP) demonstrated that the selenylamide bond formation is energetically favored. The *in silico* data showed here are in accordance with previous experimental studies, and help us to understand the reactivity and biological activity of organoselenium compounds.

1. Introduction

The utilization of selenium (Se) in organic synthesis has been producing a vast number of organoselenium compounds since the second half of the 19th century. For instance, Ebselen (EBS) was synthesized in 1924, and nowadays is the most investigated of the organoselenium compounds (Fig. 1A) [1]. Diphenyl diselenide (DPDS) is the simplest diaryl diselenide and has been tested as a pharmacological agent [2]. The organoselenium derivatives present many pharmacological properties, such as anti-inflammatory, cardioprotective, neuroprotective, and antioxidant, this last one due to their ability to reduce hydrogen peroxide (H_2O_2) to water (H_2O). Therefore, these compounds are considered mimetics of the glutathione peroxidase (GPx) enzyme and are promising drugs [3–6].

In addition, EBS and DPDS can oxidize thiol groups of proteins [3,4,7] as observed in the mammalian enzyme δ-aminolevulinic acid dehydratase (*m*δ-AlaD) or porphobilinogen synthase (PBGS) (EC 4.2.1.24). Since the δ-AlaD is an important enzyme involved in the porphyrins' synthesis, its inhibition can have toxicological consequences [8–11]. The δ-AlaD catalyzes the asymmetric condensation of two molecules of 5-aminolevulinic acid (δ-aminolevulinic acid – 5-Ala), forming the porphobilinogen (PBG), which is the precursor of porphyrins' synthesis (Fig. 1B). In the enzyme active site, each substrate binds at two different subsites (A and P), leading to the regioselective product PBG. The acetic acid and propanoic acid side-chains of PBG originate from the subsites A and P, respectively [12–14]. Porphyrins are essential to living beings, particularly to the aerobic life, due to the heme prosthetic group, which is involved in the transport of oxygen (hemoglobin and myoglobin), xenobiotic metabolism (cytochrome P450), protection against peroxides (peroxidases and catalases), and chlorophyll synthesis [13,15–17]. There are two major classes of δ-AlaD: the Zn-dependent enzymes (that are present in mammals, fungi

* Corresponding author.
E-mail address: jbtrocha@yahoo.com.br (J.B.T. Rocha).

https://doi.org/10.1016/j.comtox.2020.100127
Received 3 March 2020; Received in revised form 29 May 2020; Accepted 3 June 2020
Available online 09 June 2020

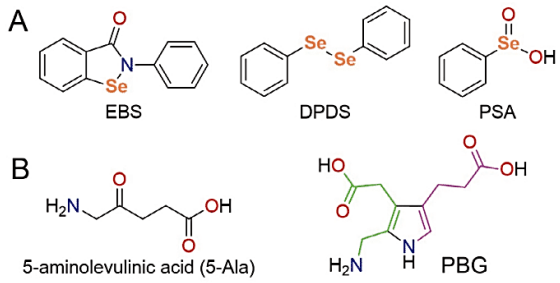

Fig. 1. (A) The structural formula of some organoselenium compounds, (B) the 5-aminolevulinic acid (5-Ala) substrate and porphobilinogen (PBG) product of the δ-AlaD.

and some bacteria, such as *Escherichia coli*) [15,18,19], and the Mg-dependent enzymes, that are found mainly in plants, protozoa and other bacteria [13,20–22].

Studies have demonstrated that the DPDS can inhibit the δ-AlaD enzyme from human (*Hs*δ-AlaD) and rodents [10,11,23–28]. The δ-AlaD from *Drosophila melanogaster* (*Dm*δ-AlaD) can also be inhibited by DPDS [29]. In contrast, DPDS do not inhibit δ-AlaD from cucumber, *Cucumis sativus* (*Cs*δ-AlaD); nevertheless, its putative metabolite, the phenylseleninic acid (PSA), can inhibit the *Cs*δ-AlaD [30]. In fact, the toxicity of organoselenium compounds could be associated with their metabolic oxidation by flavin-containing monooxygenases [4,31,32]. However, the inhibition mechanism(s) involved in these cases has not been established yet.

To complement and better understand the *in vivo* and *in vitro* data, *in silico* methods have been used to analyze, simulate, and predict the pharmacology and toxicity of chemicals [33–37]. There are many types of computational methods, where the molecular docking stands out by simulating the interactions between macromolecules (proteins and DNA) and ligands (substrate, inhibitor, and agonist). This method consists in predicting the binding mode of the ligand at the binding site of a given target, in addition to the estimation of affinity for the receptor, by predicting binding free energy (ΔG) [38–41]. Quantum mechanical methods, such as the density functional theory (DFT) approach, are frequently used in the study of structures, reactions, and molecular properties [42–44], but are strictly limited to systems of few hundreds of atoms. In addition, the protein homology modeling has been successfully employed to predict the 3D protein structure, which is essential in many cases when the tertiary or quaternary structure must be studied [45–49].

Different *in silico* methods have been adopted to predict the reactivity, toxicity, and pharmacology of organoselenium compounds and selenoproteins [44,50–58]. Here, to better understand the toxicological effects of organoselenium molecules, and how they interact with target proteins, we propose an *in silico* approach combining protein homology modeling, molecular docking simulations, and DFT calculations (Scheme 1). Based on the difference of DPDS and PSA inhibition behavior on δ-AlaD enzymes, this study aims to compare the intermolecular interactions between the *Hs*δ-AlaD, *Dm*δ-AlaD and *Cs*δ-AlaD enzymes and the DPDS and PSA organoselenium compounds, to gain insight into their mechanisms of inhibition.

2. Materials and methods

2.1. Protein homology modeling

First, the homology analysis of the primary structure of δ-AlaD enzymes from cucumber (*Cucumis sativus*), fruit fly (*Drosophila melanogaster*), human (*Homo sapiens*), mouse (*Mus musculus*), zebrafish (*Danio rerio*), cockroach (*Blattella germanica*), protozoa (*Toxoplasma gondii*), yeast (*Saccharomyces cerevisiae*), archaeon (*Pyrobaculum calidifontis*) and bacteria (*Chlorobaculum parvum*, *Escherichia coli*, *Pseudomonas aeruginosa*, *Staphylococcus aureus* and *Wolbachia*) were performed. The FASTA amino acid sequences for δ-AlaD enzymes were obtained from the the National Center for Biotechnology Information – NCBI (https://www.ncbi.nlm.nih.gov/pubmed/), UniProt (http://www.uniprot.org/) and Protein Data Bank – PDB (http://www.rcsb.org/pdb), according to the respective codes: *Blattella germanica*: UniProt (A0A2P8XHW3_BLAGE); *Chlorobaculum parvum*: PDB (2C1H); *Cucumis sativus*: UniProt (A0A0A0LQK9_CUCSA); *Danio rerio*: NCBI (NP_001017645.1); *Drosophila melanogaster*: UniProt (Q9VTV9_DROME); *Escherichia coli*: PDB (1L6S); *Homo sapiens*: PDB (1E51); *Mus musculus*: NCBI (NP_001263375.1); *Pseudomonas aeruginosa*: PDB (1GZG); *Pyrobaculum calidifontis*: PDB (5LZL); *Saccharomyces cerevisiae*: PDB (1H7N); *Staphylococcus aureus*: UniProt (HEM2_STAAR); *Toxoplasma gondii*: PDB (3OBK); *Wolbachia*: NCBI (WP_041571452.1). Regarding of FASTA from PDB, it was used the FASTA associated with the corresponding PDB file on the database (we do not extract the FASTA from the PDB file). The Clustal Omega server (http://www.ebi.ac.uk/Tools/msa/clustalo) was used to make the multiple sequence alignment, and the similarity between the δ-AlaD sequences was calculated from the Geneious program (https://www.geneious.com) (Fig. 2, S1, S2 and Table S1).

Since there is no available three-dimensional structure of *Dm*δ-AlaD and *Cs*δ-AlaD, the Swiss-Model (https://swissmodel.expasy.org) [59], Phyre2 [60], and Geno3D servers [61] were used to obtain their structures, using the amino acid sequence of the *Cucumis sativus* and *Drosophila melanogaster* δ-AlaD, taken from UniProt with the codes A0A0A0LQK9_CUCSA and Q9VTV9_DROME, respectively. The 3D structures of the *Chlorobaculum parvum* (PDB: 2C1H [62]), *Pseudomonas aeruginosa* (PDB: 1GZG [63]), and *Toxoplasma gondii* (PDB: 3OBK [21]) where used as template to build the *Cs*δ-AlaD models, while the *Escherichia coli* (PDB: 1L6S [64]), *Pyrobaculum calidifontis* (PDB: 5LZL [18]), and *Saccharomyces cerevisiae* (PDB: 1H7N [19]) structures where used as template to build the *Dm*δ-AlaD models. The validation of the protein models were carried out by the programs: Verify 3D [65,66], ProSA [67], PROCHECK [68,69], and ERRAT [70]. The Ramachandran plot was made by the PDBsum server (www.ebi.ac.uk/pdbsum/) [71]. More details can be found in the Supporting information.

2.2. Molecular docking

To carry out the docking simulations, the *Hs*δ-AlaD was obtained from PDB with the code 1E51 [72], and the *Dm*δ-AlaD-1L6S and *Cs*δ-AlaD-3OBK models were obtained from protein homology modeling by the Swiss-model program (as described above). The CHIMERA 1.8 program [73] was used to add the hydrogen atoms to the proteins. The Lys199/195/291 and Lys252/248/344 residues were considered neutral (deprotonated) [14], which was confirmed by H++ analysis (http://biophysics.cs.vt.edu). The ligands (PBG and the organoselenium compounds) were built in the Avogadro 1.1.1 software [74], followed by a geometric optimization using the MOPAC program (http://openmopac.net/MOPAC2012.html) with the semi-empirical method PM6 (with the water dielectric constant) [75]. The PSA was considered deprotonated (pka = 4.79) [76] during the docking simulations. The protein and ligands were converted to the *pdbqt* format with the AutoDockTools [77], with the Gasteiger and MOPAC charges, respectively. The partial charge (0.302) of the Zn^{2+} ion from *Hs*δ-AlaD and *Dm*δ-AlaD were obtained from a previous study [51].

The AutoDockVina 1.1.1 software [78] was used for the docking simulations, with exhaustiveness of 100. The best docking protocol was obtained using the ligands and the side chain of Arg209 and Lys252 residues from *Hs*δ-AlaD (Arg205 and Lys248 from *Dm*δ-AlaD-1L6S, and Arg301 and Lys344 from *Cs*δ-AlaD-3OBK) flexible. The grid boxes (with spacing of 1 Å) were centered in the active site of the enzymes *Hs*δ-AlaD (coordinates: x = 31.63; y = 73.65; z = 57.08), *Dm*δ-AlaD-1L6S

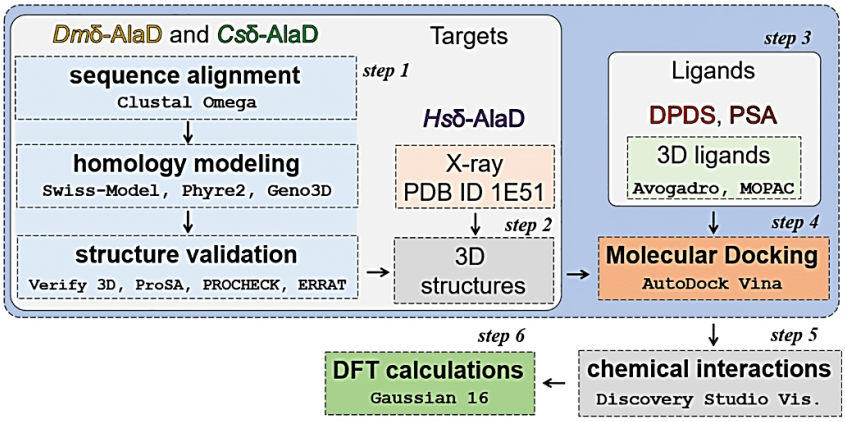

Scheme 1. Overview of all the steps involved in this study.

(coordinates: x = 19.72; y = 83.35; z = 52.14), and *Cs*δ-AlaD-3OBK (coordinates: x = -64.60; y = -77.40; z = 28.05), with a size of 25 × 25 × 25 Å, in both cases. The Discovery Studio Visualizer 17.2.0. (DSV) program (https://www.3dsbiovia.com/) was used to analyze the results, where the conformers of lowest binding free energy (ΔG) were selected as the best model. The molecular docking protocols were validated by the RMSD (root-mean-square deviation) values from the PBG molecules, which give the relationship between the experimental and the theoretical data in a receptor-ligand complex. RMSD values lower than 2.0 Å indicate good quality of data reproduction (Fig. S4) [41,79,80] (details can be found in the Supporting Information).

2.3. Density functional theory calculations

All quantum chemistry calculations have been performed using density functional theory (DFT) approach as implemented in Gaussian 09 rev. E.01 program [81]. mPW1PW91 (Perdew-Wang hybrid functional) [82] was used, in combination with the def2TZVP (Triple zeta quality with polarization functions) basis set for all the atoms [83,84].Full geometry optimizations were carried out in gas phase; solvation (water) effects were taken into account in subsequent single point calculations at the same level of theory using PCM approximation [85].

3. Results and discussion

3.1. Protein sequence comparison and homology modeling

Considering that DPDS inhibits the *Hs*δ-AlaD [11] and *Dm*δ-AlaD [29] and does not inhibit *Cs*δ-AlaD [30], we initially compared the primary structure of the δ-AlaD enzymes (including other different species) through multiple sequence alignment (Fig. 2, Fig. S1/S2 and Table S1). The analysis of the sequence alignment data demonstrated that are two groups of proteins, i.e. Group A, which includes the species that present Cys residues in the active site (*Saccharomyces cerevisiae, Drosophila melanogaster, Danio rerio, Homo sapiens, Mus musculus, Escherichia coli, Pyrobaculum calidifontis and Staphylococcus aureus*), and Group B, which includes the species that have Asp residues (*Toxoplasma gondii, Cucumis sativus, Wolbachia, Pseudomonas aeruginosa* and *Chlorobaculum parvum*) (Fig. S2). Interestingly, the *Blattella germanica* δ-AlaD is small when compared to the other species (146 *vs* ~ 330 residues) and has not the Cys region of the active site; however, the catalytic Lys residues are conserved (Fig. S1). According to the phylogenetic tree (Fig. S2) it belongs to Group A.

In general, the three cysteine residues from the active site of Group A δ-AlaD were replaced by two aspartate residues and one alanine residue in Group B (Fig. 2 and Fig. S1/S2) indicating a significant change in the nature of the active site. In addition, the Arg221 (in the human protein) were replaced by a Lys residue in the δ-AlaD from Group B (Lys313 in *Cs*δ-AlaD). As the Lys and Arg are basic and positively charged residues, practically, the same physical–chemical properties

```
S.cerevisiae    FGVPLIPGTKDPVGTAADDPAGPVIQGIKFIREYFPE-LYIICDVCLCEYTSHGHCGVLY 147
D.melanogaster  FGVVD-PDMKDEQASNADSAKNPVVLALPKLREWFPD-LLIACDVCICPYSSHGHCGLLG 134
B.germanica     ------------------------------------------------------------ 0
D.rerio         FGVPA-KVAKDERGSGADADDTPAVLAVKKLRSTFPE-LVLACDVCLCPYTSHGHCGILR 138
H.sapiens       FGVPS-RVPKDERGSAADSEESPAIEAIHLLRKTFPN-LLVACDVCLCPYTSHGHCGLLS 136
M.musculus      FGVPS-RVPKDEQGSAADSEDSPTIEAVRLLRKTFPS-LLVACDVCLCPYTSHGHCGLLS 136
P.calidifontis  FGVLP-DELKNPEGTGGYDPEGVVPRAIRLIKEIFGDRVLVFADVCLCEYTDHGHCGVVK 139
E.coli          FGISH---HTDETGSDAWREDGLVARMSRICKQTVPE-MIVMSDTCFCEYTSHGHCGVLC 133
S.aureus        FGVPN---SKDDIGTGAYIHDGVIQQATRIAKKMYDD-LLIVADTCLCEYTDHGHCGVID 132
T.gondii        FPKVD-DELKSVMAEESYNPDGLLPRAIMALKEAFPD-VLLLADVALDPYSSMGHDGVVD 150
Wolbachia       FPVVD-SKLKSENAEEAYNSDNLICKAIRAIKLKVPG-IGIIADVALDPYTTHGHDGILK 137
C.sativus       FPKVP-DALKTPTGDEAYNDNGLVPRTIRLLKDKYPD-LVIYTDVALDPYSSDGHDGIVR 229
C.parvum        FGIP---EQKTEDGSEAYNDNGILQQAIRAIKKAVPE-LCIMTDVALDPFTPFGHDGLVK 139
P.aeruginosa    FPVTP-VEKKSLDAAEAYNPEGIAQRATRALRERFPE-LGIITDVALDPFTTHGQNGILD 143
```

Fig. 2. Multiple alignments of the δ-AlaD amino acids sequence of different organisms. Only a fragment from the active site of the proteins are shown. The residues from the active site are highlighted: Cys (yellow); residues that remain conserved (cyan), residues that are not conserved when compared to the human enzyme (green and pink). The complete alignment is shown in Fig. S1. (For interpretation of the references to color in this figure legend, the reader is referred to the web version of this article.)

are conserved. These observations are in accordance with previous studies of Kervinen et al. (2001) [86] where five δ-AlaD enzymes (from *Pisum sativum*, *Pseudomonas aeruginosa*, *Bradyrhizobium japonicum*, *Escherichia coli,* and *H. sapiens*) sequences were analysed, and the metal-binding region determined.

Here, based on these observations, we can suppose that DPDS does not inhibit the *Cs*δ-AlaD because this enzyme does not present Cys residues in its active site. However, it does not explain why PSA inhibits the *Cs*δ-AlaD. For a better understanding of the interactions between inhibitors and enzymes, the molecular docking simulations were performed. Taking into account that there are no *Cs*δ-AlaD and *Dm*δ-AlaD structures available, the 3D model of these enzymes were built using protein homology modelling.

Homology modeling is the most accurate method to build protein structure models [87–89]. Among the different programs developed for this purpose, in this study we have chosen the Swiss-Model [59], Phyre2 [60], and Geno3D [61] to create the *Dm*δ-AlaD and *Cs*δ-AlaD structures. Taking in account the primary structure similarity between the δ-AlaD enzymes (Fig. 2, Figs. S1–S2 and Table S1), three templates were selected for *Dm*δ-AlaD (PDB ID: 1H7N, 1L6S and 5LZL) and three for *Cs*δ-AlaD (PDB ID: 1GZG, 2C1H, and 3OBK). Each template was used in the protein homology modeling with the three programs above cited, to find the best protein model. The 3D structure models of *Dm*δ-AlaD and *Cs*δ-AlaD built were validated using the programs: Verify 3D [65,66], ProSA [67], PROCHECK [68,69], and ERRAT [70] (Tables S1–S2).

According to the data in Tables S2 and S3, the best *Dm*δ-AlaD and *Cs*δ-AlaD models were obtained from the PDB ID 1L6S and PDB ID 3OBK templates, respectively, using the Swiss-Model program, which turned out to be the most performant program for this task. *Dm*δ-AlaD-1L6S and *Cs*δ-AlaD-3OBK models showed a satisfactory protein structure, because the validation parameters are in the range of native protein structure (see the Supporting information), and they were used for the molecular docking simulations.

Despite the differences in the primary structure between the *Homo sapiens* δ-AlaD, *Dm*δ-AlaD and *Cs*δ-AlaD, the comparison of the tertiary structure of the three enzymes exhibited a very similar organization of the residues, with the simulated PBG binding pose presenting practically the same conformation and interactions (Fig. 3). Here, we highlighted the major difference in the active site of both enzymes. As shown in Fig. 3AB, in *Hs*δ-AlaD and *Dm*δ-AlaD the thiolates of the Cys residues are coordinated to a zinc ion (Zn^{2+}), where this metal nucleus acts as a Lewis acid and Zn···N coordination with the amino moiety (Lewis base) from PBG is formed. This Zn···N interaction is essential to the catalysis of the δ-AlaD, because it specifically guides one molecule of 5-Ala substrate in subsite A, before the cyclization to pyrrole ring [86,90]. In fact, the Cys mutations cause a dramatic reduction in the enzyme activity [12]. On the other hand, according to the docking simulation between the PBG and *Cs*δ-AlaD, the orientation of one molecule of 5-Ala substrate is likely driven by the H-bonds between the amino moiety from 5-Ala and the carboxylate groups of Asp217 and Asp225 residues (Fig. 3C). The PBG binding pose obtained by the docking in *Cs*δ-AlaD is very similar to the crystallographic data collected from *T. gondii* δ-AlaD [21]. Interestingly, Asp217 and Asp225 are the residues that correspond to Cys124 and Cys132 residues in the human enzyme, respectively (Figs. 2 and 3).

In addition, in the case of *Cs*δ-AlaD, the Mg^{2+} ion is not present in the active site (Fig. 3C), and does not participate directly in the catalysis. However, the Mg^{2+} is essential to enzyme function, as observed in *E. coli*, *Bradyrhizobium japonicum*, *Pseudomonas aeruginosa,* and *P. sativum,* due to the H-bonding network around this metal ion maintaining the quaternary structure of δ-AlaD [13–15,86]. This difference in the active site of δ-AlaD from different species must be taken into account in the design of selective inhibitors with useful applications, such as in the case of δ-AlaD from *Wolbachia* [91–93] and *Staphylococcus aureus* [94]. Moreover, due to the similarity of the active site from δ-AlaD of the group B, the use of plant δ-AlaD (such as cucumber) can provide a simple, practical and cheap *in vitro* assay to find new selective inhibitors.

3.2. Organoselenium molecular docking study

Molecular docking simulations were carried out to understand the δ-AlaD inhibition by DPDS and PSA. According to the docking between the *Hs*δ-AlaD and DPDS, this latter interacts with the enzyme active site mainly by hydrophobic interactions (π-π stacking with Phe79, Tyr205 and Phe208 residues and alkyl-π with Pro125). The selenium atoms of DPDS interact with the carboxylic group of Asp120 and with the Zn^{2+} ion, besides the thiolate group from Cys124 (Fig. 4A). The putative DPDS metabolite, PSA, also interacts in the *Hs*δ-AlaD active site, by π-π stacking with Tyr205 and Phe208, H-bond with Ser168, and interactions with Tyr196 (anion-π interaction between the seleninate and the phenyl moieties), Asp120 (repulsive electrostatic interaction between the seleninate and carboxyl groups), and zinc ion (coordination). In addition, Se···S interaction with Cys124 is observed (Fig. 4B).

The simulation of DPDS with the *Dm*δ-AlaD demonstrated that this organoselenium compound could access the active site making hydrophobic interactions with Arg205, Pro212 (alkyl and phenyl groups), Phe204 and Tyr201 (phenyl and phenyl moieties), besides interacting with Arg217 via H-bond (selenyl and guanidinyl groups [95,96]) (Fig. 4C). In addition, the DPDS showed a Se···S interaction with Cys122. The PSA molecule also binds in the *Dm*δ-AlaD active site, through hydrophobic π-π stacking with Phe204 and Tyr201 (phenyl and phenyl moieties), through H-bonds with Ser165, Lys195, and Gln221 (seleninate and OH, NH and C=O groups, respectively), and Zn···O coordination. Similarly to DPDS, the PSA also showed Se···S interaction with Cys122 (Fig. 4D).

On the other hand, the docking simulations between the *Cs*δ-AlaD and DPDS demonstrated that it does not enter in the *Cs*δ-AlaD active site. In fact, DPDS binds in the superficial region of the enzyme, close to the entrance of the active site, interacting with the Lys313 (phenyl and carbon chain) and presenting an intramolecular π-π stacking (phenyl-phenyl) (Fig. 4E). In contrast, PSA can access the active site of *Cs*δ-AlaD (Fig. 4F), making H-bonds with Arg301 and Lys291 residues, stabilized by electrostatic interaction with Asp217, and π-π stacking with Phe330 (phenyl and phenyl moieties).

Finally, we simulated the interactions of other putative oxidized organoselenium forms [97] (Fig. S5) to verify if these molecules are able to interact with the δ-AlaD enzymes, and its binding partner. For *Hs*δ-AlaD, all organoselenium molecules show Se···S interaction (3.1–5 Å) with the Cys124 residue (Fig. S6), except *R,R*-DPDS(O). Conversely, for *Dm*δ-AlaD, only *S,R*-DPDS(O), *R*-DPDS(O) and PhSeOH show Se···S interaction (4–4.4 Å) (Fig. S7). In relation of the *Cs*δ-AlaD, we verified that all the selenoxide forms of DPDS do not bind in the active site (Fig. S8), as observed with DPDS. However, like PSA, PhSeOH enters in the active site and interacts with Lys291. These data suggest that for *Cs*δ-AlaD small organoselenium electrophilic moieties can indeed inhibit the enzyme. In addition, the stereochemistry of the compounds play an essential role in the binding mode in the enzyme.

The predicted binding free energy (ΔG_{bind}) for the *Hs*δ-AlaD indicates that the interaction of DPDS with the enzyme is energetically more favored than the interaction PSA-enzyme (Table 1). In contrast, ΔG_{bind} for *Dm*δ-AlaD suggests a more favorable PSA-enzyme than DPDS enzyme binding. Similarly, in *Cs*δ-AlaD, PSA showed (negatively) larger binding energy than DPDS. Finally, the presence of oxygen atoms in the oxidized forms of DPDS enabled the formation of H-bonds facilitating thermodynamically the binding.

In the *Hs*δ-AlaD and *Dm*δ-AlaD enzymes, both PSA and DPDS presented similar binding pose, interacting with amino acid residues from the active site. Notably, Cys124 and Cys122 (*Hs*δ-AlaD and *Dm*δ-AlaD, respectively), stabilization occurs via Se···S interaction (Fig. 4A–D). However, for *Cs*δ-AlaD, only PSA binds in the active site, and no Se···S

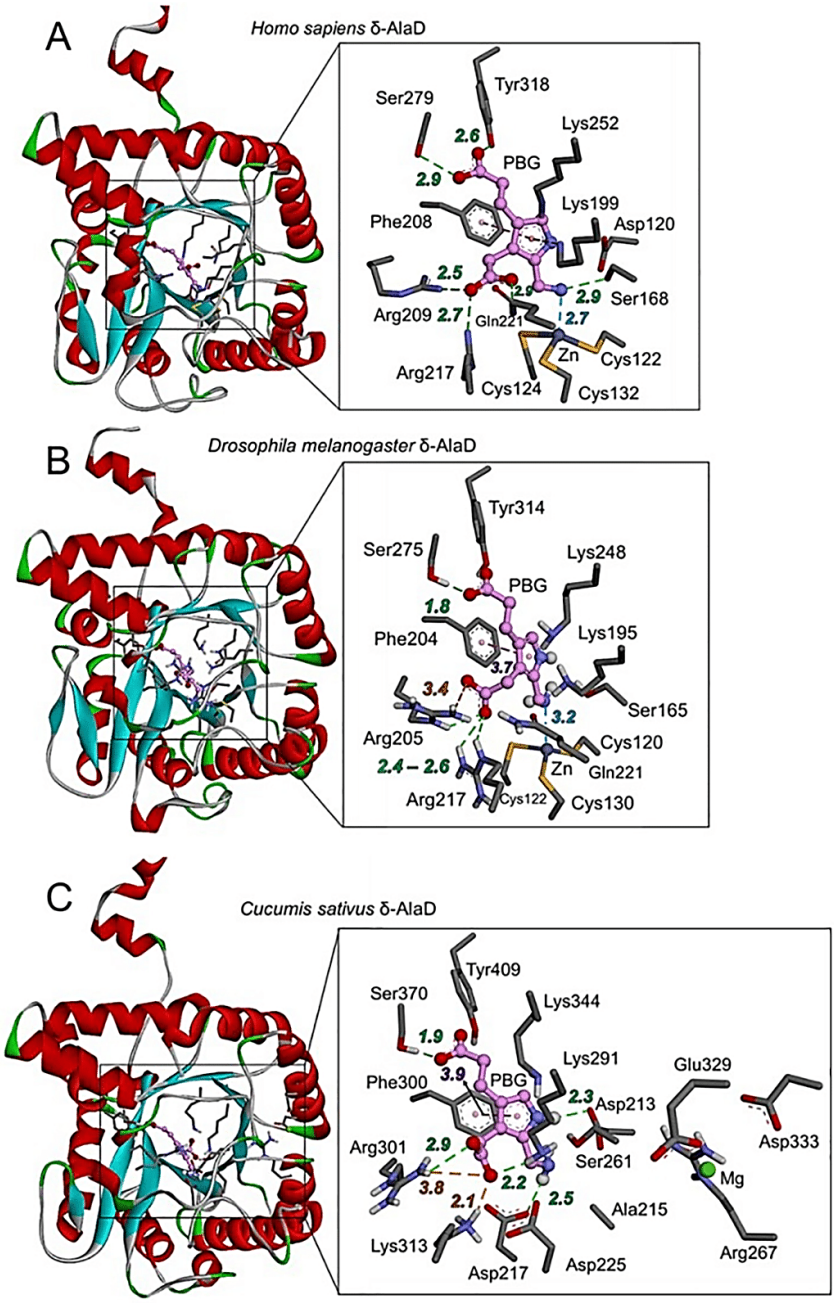

Fig. 3. Comparison between the 3D structures of δ-AlaD from *Homo sapiens* (A), *Drosophila melanogaster* (B) and *Cucumis sativus* (C). The active site is highlighted, and the carbon atoms of PBG are represented in pink color. (A) Human δ-AlaD structure from the crystal PDB ID 1E51 [72], and (B) *Dm*δ-AlaD and (C) *Cs*δ-AlaD from protein homology modeling, with the PBG binding pose from the molecular docking. The hydrogen atoms were omitted for clarity. H-bonds, electrostatic (charge-charge) and hydrophobic (π–π) interactions, besides the zinc coordination, are represented by green, orange, purple, and blue dotted lines, respectively; all distances are in Å. (For interpretation of the references to color in this figure legend, the reader is referred to the web version of this article.)

interaction is present because the *Cs*δ-AlaD does not have Cys residues in the active site (Fig. 4E–F). These outcomes strongly suggest that organoselenium compounds binding in the active sites could prevent the entrance of the substrate 5-Ala, thus inhibiting the enzymes.

The previous *in vitro* assays have indicated that the mechanism of *Hs*δ-AlaD (or mammalian δ-AlaD) and *Dm*δ-AlaD inhibition by organoselenium compounds involves Cys oxidation because dithiothreitol (DTT_{red}) could reactivate the enzyme from these sources [10,11,24,29,30,98]. The Se···S interaction could lead to the formation of the selenenyl sulfide bond (Se–S) [99,100], an adduct between the protein and the selenium compound, by means of a nucleophilic attack of the thiolate moiety of Cys124(122) to the Se atom of either DPDS or PSA. In fact, previous experimental as well as theoretical studies have indicated that Se-S bound can be easily formed between reduced thiol-containing molecules and diselenide- (Se-Se) and seleninic acid (R-SeO_2H)-containing molecules [99,101,110,102–109].

In the next step, a vicinal thiol group – from Cys122(120) and/or Cys132(130) – could perform a nucleophilic attack to the electrophilic S

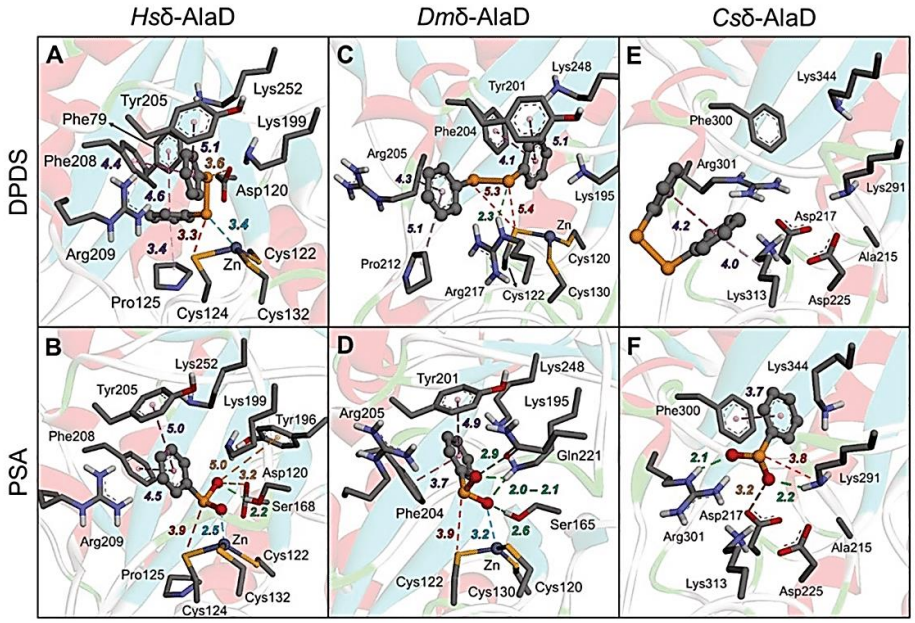

Fig. 4. Molecular docking of organoselenium compounds with *Hs*δ-AlaD (A, B), *Dm*δ-AlaD (C, D) and *Cs*δ-AlaD (E, F). (A, C, and E) DPDS binding pose in *Hs*δ-AlaD, *Dm*δ-AlaD, and *Cs*δ-AlaD enzymes, respectively. (B, D, and F) PSA binding pose in *Hs*δ-AlaD, *Dm*δ-AlaD, and *Cs*δ-AlaD, respectively. H-bonds (green), hydrophobic (π-π, alkyl-π) (purple), cation-π, anion-π, electrostatic interactions (orange), and zinc coordination (blue), are represented by dotted lines; all the distances are in Å. The ligands and the amino acids lateral chains are represented by ball and stick, and stick models, respectively. (For interpretation of the references to color in this figure legend, the reader is referred to the web version of this article.)

Table 1
Predicted ΔG_{bind} (kcal/mol) from molecular docking.

Enzyme	*Hs*δ-AlaD	*Dm*δ-AlaD	*Cs*δ-AlaD
DPDS	−6.2	−5.9	−5.2
PSA	−5.1	−6.1	−5.9
R,R-DPDS(O)	−7.0	−8.0	−5.1
S,R-DPDS(O)	−7.0	−7.9	−6.7
S,S-DPDS(O)	−6.1	−6.1	−4.8
R-DPDS(O)	−7.0	−6.5	−5.2
S-DPDS(O)	−6.3	−6.0	−5.1
PhSeOH	−4.6	−5.8	−4.8

atom of the Se–S bond, leading to the disulfide bridge (S–S) formation, i.e., thiol oxidation, and the release of zinc ion [7,99,108,111–113]. In fact, the distances between the S atoms are 3.7–4.6 Å for both *Hs*δ-AlaD and *Dm*δ-AlaD. Previous studies suggested that the cysteine oxidation (S–S) in the *Hs*δ-AlaD active site involves Cys124 and Cys132 residues. The Cys124 residue is the first thiolate that reacts with diselenides or selenides/selenoxides, forming the Se–S intermediate; then, Cys132 reacts with this intermediate leading the disulfide bridge, denaturing the active site [51,114].

*Cs*δ-AlaD has no Cys residues in the active site and consequently, the Cys oxidation mechanism is not possible. PSA, likely due to its polarity, has a better affinity for the active site of *Cs*δ-AlaD (where polar and basic residues are present). PSA has a highly electrophilic Se atom [30,115,116]. Its Hirshfeld partial charge is higher than the one computed for Se in DPDS and in the other selenium compounds of this study, indicating a deficiency of electrons (Table S4). In addition, due to the short distance between the Se atom and the amino group from Lys291 (Se···N = 3.8 Å, Fig. 4F), a nucleophilic attack from the Lys291 on PSA could occur, forming a seleninamide moiety (Ph-**Se(O)NH**-Lys), i.e., an adduct between the enzyme and the organoselenium moiety, which might inhibit the *Cs*δ-AlaD. The seleninamide formation from seleninic acid has already been reported in the literature [115,117]. The formation of seleninamide could prevent the reaction between the Lys291 residue and the 5-Ala substrate (the Schiff base formation, which is an essential step in the δ-AlaD catalytic cycle [14,15]). The *in vitro* study of Farina et al. (2002) [30] showed that in the presence of DTT_{red} the *Cs*δ-AlaD is not inhibited. A possible explanation is that the sulfur atom from DTT could react with the seleninamide adduct, forming a thioseleninate moiety (Ph-**Se(O)S**-DTT) releasing the free Lys291 and consequently reactivating the enzyme (Ph-**Se(O)NH**-Lys + DTT-**SH** → Ph-**Se(O)S**-DTT + Lys-$\mathbf{NH_2}$). In fact, the thioseleninate intermediate can be formed via a reaction between seleninamide and thiol molecules [5,100,118,119].

The reaction between the PSA and the active site in *Cs*δ-AlaD was investigated by means of DFT calculations. For this purpose, we set up a model reaction, using $EtNH_2$ as a model of the Lys residue and PSA in the protonated form (PhSeOOH), as it should be due to its proximity to Arg301 (Fig. 4F) and because water is a better leaving group than hydroxyl anion. Our results (Fig. 5) indicate that the seleninamide formation is energetically favored, both in the gas and water phase. The reactant complex ($PhSeOOH{\cdot}EtNH_2$) is characterized by an H-bond between the hydroxyl and amino groups and by a short distance Se···N (3.8 Å), promoting the release of a water molecule and the formation of the Se–N bond in the product complex ($PhSeONHEt{\cdot}H_2O$) (Fig. 5A).

The proximity between electrophilic forms of organoselenium molecules and nucleophilic moieties from critical amino acids residues (in this case Se···S/N interactions from Cys124, Cys122, and Lys291, from *Hs*δ-AlaD, *Dm*δ-AlaD, and *Cs*δ-AlaD, respectively) could lead to covalent bonds formation, and consequently, these adducts can impair the functions of enzymes, inhibiting them. This mechanism could justify the toxicity of some organoselenium compounds.

The understanding of the mechanism of organoselenium compounds toxicity will be crucial in the designing of new molecules less toxic and more selective in relation to pharmacological targets. In this sense, the

A

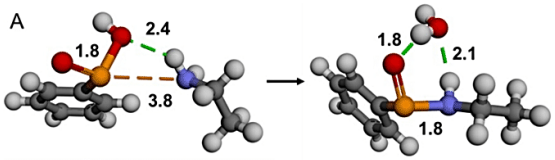

B

Molecule	Phase	
	Gas	Water
$PhSeOOH + EtNH_2$	0.0	0.0
$PhSeOOH \cdot EtNH_2$	-5.2	-1.1
$PhSeONHEt \cdot H_2O$	-11.1	-7.2
$PhSeONHEt + H_2O$	-0.9	-1.6

Fig. 5. The reaction of PSA with Lys residue model ($EtNH_2$) modeled at (PCM)-mPWPW91/def2PVTZ level of theory. (A) Intermolecular interactions of reagent and product complexes; the distances are in Å. (B) Energetics (kcal/mol) of the reaction in the gas and water phase. $PhSeOOH + EtNH_2$ and $PhSeONHEt + H_2O$ correspond to the reagents and products, while $PhSeOOH \cdot EtNH_2$ and $PhSeONHEt \cdot H_2O$ are the reactant and product complexes, respectively. All energy values are relative to the free reactants.

potential role of metabolites of a given drug can also be informative, as suggested by our present study. Organoselenium molecules have promising biological activity, and Ebselen is under clinical trials as potential lithium mimetic for bipolar disorder [120]. Of particular importance, Ebselen has been recently used against SARS-CoV-2 *in vitro* and presented antiviral activity possibly by inhibiting the main protease (Mpro) enzyme from the virus of COVID-19 [121]. Selenothymidines (selenium-containing AZT derivatives) are potential pharmacological agents against cancer [122]. DPDS presents many therapeutics properties (anxiolytic, antidepressant-like, anticancer, neuroprotective, and others) and its mechanism of action involves the modulation of the cellular redox status [123]. DPDS could modulate any protein having reactive thiol groups due to the lack of specific molecular targets. In this way, new DPDS derivatives with higher selectivity for specific protein targets still need to be developed.

4. Conclusion

The present work, entirely performed *in silico* and combining multiscale approaches, provides an efficient explanation to experimental *in vitro* data, giving evidence that DPDS inhibits *Hs*δ-AlaD and *Dm*δ-AlaD enzymes, but does not inhibit *Cs*δ-AlaD [11,29,30]. The molecular docking simulations between the selected organoselenium molecules and δ-AlaD could provide a possible explanation for this observation. The homology modeling showed that *Cs*δ-AlaD does not present Cys residues in the active site, and consequently, DPDS has not a substrate to oxidize. On the other hand, the putative metabolite PSA could access the active site, interacting with the Lys291 residue (Se···N), preventing the entrance of the 5-Ala substrate, and consequently inhibiting the *Cs*δ-AlaD. By DFT calculations, we have demonstrated that the reaction between PSA and Lys is indeed energetically favored. In *Hs*δ-AlaD and *Dm*δ-AlaD enzymes, both DPDS and PSA can access the active site, interacting with Cys124 (122), by Se···S interaction, which could lead to Cys oxidation, and, consequently, protein denaturation and enzyme inhibition. This type of study is essential to understand the reactivity and selectivity of organoselenium compounds in biological systems and can lead to better rational drug design. On the basis of these promising computational results, further studies are prompted. In addition, due to its protein similarity and organoselenium binding pose, *Dm*δ-AlaD rather than *Hs*δ-AlaD could be used as a model to test the toxicity of new organoselenium molecules.

CRediT authorship contribution statement

Pablo Andrei Nogara: Conceptualization, Methodology, Investigation, Validation, Writing - original draft. **Laura Orian:** Methodology, Resources, Writing - review & editing, Supervision, Funding acquisition. **João Batista Teixeira Rocha:** Methodology, Resources, Writing - review & editing, Supervision, Funding acquisition.

Declaration of Competing Interest

The authors declare that they have no known competing financial interests or personal relationships that could have appeared to influence the work reported in this paper.

Acknowledgments

The authors would like to thank the financial support by Coordination for Improvement of Higher Education Personnel CAPES/PROEX (n° 23038.005848/2018-31; n°0737/2018; n°88882.182123/2018-01), the CAPES/PrInt – Projeto Institucional de Internacionalização (n° 88887.374997/2019-00), the National Council for Scientific and Technological Development (CNPq), and the Rio Grande do Sul Foundation for Research Support (FAPERGS - Brazil). DFT calculations were carried out on Galileo (CINECA: Casalecchio di Reno, Italy) thanks to the ISCRA Grant HP10CUVVQU: "MEthylMErcury and Selenoproteins (MEMES).

Appendix A. Supplementary data

Supplementary data to this article can be found online at https://doi.org/10.1016/j.comtox.2020.100127.

References

[1] J.B.T. Rocha, B.C. Piccoli, C.S. Oliveira, Biological and chemical interest in selenium: a brief historical account, Arkivoc part ii (2017): 457–491. https://doi.org/10.3998/ark.5550190.p009.784.
[2] A.S. Weisberger, L.G. Suhrland, Studies on analogues of L-cysteine and L-cystine III. The effect of selenium cystine on Leukemia, Blood 11 (1956) 19–30.
[3] C.W. Nogueira, G. Zeni, J.B.T. Rocha, Organoselenium and organotellurium compounds: toxicology and pharmacology, Chem. Rev. 104 (2004) 6255–6285, https://doi.org/10.1021/cr0406559.
[4] C.W. Nogueira, J.B.T. Rocha, Toxicology and pharmacology of selenium: emphasis on synthetic organoselenium compounds, Arch. Toxicol. 85 (2011) 1313–1359, https://doi.org/10.1007/s00204-011-0720-3.
[5] G. Mugesh, H.B. Singh, Synthetic organoselenium compounds as antioxidants: glutathione peroxidase activity, Chem. Soc. Rev. 29 (2000) 347–357, https://doi.org/10.1039/a908114c.
[6] C. Santi, S. Santoro, B. Battistelli, Organoselenium compounds as catalysts in nature and laboratory, Curr. Org. Chem. 14 (2010) 2442–2462, https://doi.org/10.2174/138527210793358231.
[7] N.V. Barbosa, C.W. Nogueira, P.A. Nogara, A.F. De Bem, M. Aschner, J.B.T. Rocha, Organoselenium compounds as mimics of selenoproteins and thiol modifier agents, Metallomics 9 (2017) 1703–1734, https://doi.org/10.1039/c7mt00083a.
[8] D.M. Bissell, J.C. Lai, R.K. Meister, P.D. Blanc, Role of delta-aminolevulinic acid in the symptoms of acute porphyria, Am. J. Med. 128 (2015) 313–317, https://doi.org/10.1016/j.amjmed.2014.10.026.
[9] S. Sassa, ALAD porphyria, Semin. Liver Dis. 18 (1998) 95–101, https://doi.org/10.1055/s-2007-1007145.
[10] J.B.T. Rocha, R.A. Saraiva, S.C. Garcia, F.S. Gravina, C.W. Nogueira, Aminolevulinate dehydratase (δ-ALA-D) as marker protein of intoxication with metals and other pro-oxidant situations, Toxicol. Res. (Camb) 1 (2012) 85–102, https://doi.org/10.1039/c2tx20014g.
[11] C.W. Nogueira, V.C. Borges, G. Zeni, J.B.T. Rocha, Organochalcogens effects on d-aminolevulinate dehydratase activity from human erythrocytic cells in vitro, Toxicology 191 (2003) 169–178, https://doi.org/10.1016/S0300-483X(03)00250-6.
[12] E.K. Jaffe, The porphobilinogen synthase catalyzed reaction mechanism, Bioorg. Chem. 32 (2004) 316–325, https://doi.org/10.1016/j.bioorg.2004.05.010.
[13] E.K. Jaffe, The remarkable character of porphobilinogen synthase, Acc. Chem. Res. 49 (2016) 2509–2517, https://doi.org/10.1021/acs.accounts.6b00414.

[14] E.K. Jaffe, Porphobilinogen synthase, the first source of Heme's asymmetry, J. Bioenerg. Biomembr. 27 (1995) 169–179, https://doi.org/10.1007/BF02110032.

[15] E.K. Jaffe, S. Ali, L.W. Mitchell, K.M. Taylor, M. Volin, G.D. Markham, Characterization of the role of the stimulatory magnesium of escherichia coli porphobilinogen synthase, Biochemistry 34 (1995) 244–251, https://doi.org/10.1021/bi00001a029.

[16] I.U. Heinemann, M. Jahn, D. Jahn, The biochemistry of heme biosynthesis, Arch. Biochem. Biophys. 474 (2008) 238–251, https://doi.org/10.1016/j.abb.2008.02.015.

[17] G. Layer, J. Reichelt, D. Jahn, D.W. Heinz, Structure and function of enzymes in heme biosynthesis, Protein Sci. 19 (2010) 1137–1161, https://doi.org/10.1002/pro.405.

[18] N. Mills-Davies, D. Butler, E. Norton, D. Thompson, M. Sarwar, J. Guo, R. Gill, N. Azim, A. Coker, S.P. Wood, P.T. Erskine, L. Coates, J.B. Cooper, N. Rashid, M. Akhtar, P.M. Shoolingin-Jordan, Structural studies of substrate and product complexes of 5-aminolaevulinic acid dehydratase from humans, Escherichia coli and the hyperthermophile Pyrobaculum calidifontis, Acta Crystallogr. Sect. D Struct. Biol. 73 (2017) 9–21, https://doi.org/10.1107/S2059798316019525.

[19] P.T. Erskine, R. Newbold, A.A. Brindley, S.P. Wood, P.M. Shoolingin-Jordan, M.J. Warren, J.B. Cooper, The X-ray structure of yeast 5-aminolaevulinic acid dehydratase complexed with substrate and three inhibitors, J. Mol. Biol. 312 (2001) 133–141, https://doi.org/10.1006/jmbi.2001.4947.

[20] K.M. Cheung, P. Spencer, M.P. Timko, P.M. Shoolingin-Jordan, Characterization of a recombinant pea 5-aminolevulinic acid dehydratase and comparative inhibition studies with the Escherichia coli dehydratase, Biochemistry 36 (1997) 1148–1156, https://doi.org/10.1021/bi961215h.

[21] E.K. Jaffe, D. Shanmugam, A. Gardberg, S. Dieterich, B. Sankaran, L.J. Stewart, P.J. Myler, D.S. Roos, Crystal structure of Toxoplasma gondii porphobilinogen synthase: insights on octameric structure and porphobilinogen formation, J. Biol. Chem. 286 (2011) 15298–15307, https://doi.org/10.1074/jbc.M111.226225.

[22] A.B. Reitz, U.D. Ramirez, L. Stith, Y. Du, G.R. Smith, E.K. Jaffe, Pseudomonas aeruginosa porphobilinogen synthase assembly state regulators: hit discovery and initial SAR studies, Arkivoc 2010 (2010) 175–188, https://doi.org/10.3998/ark.5550190.0011.815.

[23] N.B.V. Barbosa, J.B.T. Rocha, G. Zeni, T. Emanuelli, M.C. Beque, A.L. Braga, Effect of organic forms of selenium on δ-aminolevulinate dehydratase from liver, kidney, and brain of adult rats, Toxicol. Appl. Pharmacol. 149 (1998) 243–253, https://doi.org/10.1006/taap.1998.8373.

[24] E.N. Maciel, R.C. Bolzan, A.L. Braga, J.B.T. Rocha, Diphenyl diselenide and diphenyl ditelluride differentially affect δ-aminolevulinate dehydratase from liver, kidney, and brain of mice, J. Biochem. Mol. Toxicol. 14 (2000) 310–319, https://doi.org/10.1002/1099-0461(2000)14:6<310::aid-jbt3>3.3.co;2-4.

[25] R. Fachinetto, L.A. Pivetta, M. Farina, R.P. Pereira, C.W. Nogueira, J.B.T. Rocha, Effects of ethanol and diphenyl diselenide exposure on the activity of δ-aminolevulinate dehydratase from mouse liver and brain, Food Chem. Toxicol. 44 (2006) 588–594, https://doi.org/10.1016/j.fct.2005.10.014.

[26] I.J. Kade, M.W. Paixão, O.E.D. Rodrigues, E.O. Ibukun, A.L. Braga, G. Zeni, C.W. Nogueira, J.B.T. Rocha, Studies on the antioxidant effect and interaction of diphenyl diselenide and dicholesteroyl diselenide with hepatic δ-aminolevulinic acid dehydratase and isoforms of lactate dehydrogenase, Toxicol. Vitr. 23 (2009) 14–20, https://doi.org/10.1016/j.tiv.2008.08.008.

[27] I.J. Kade, V.C. Borges, L. Savegnago, E.O. Ibukun, G. Zeni, C.W. Nogueira, J.B.T. Rocha, Effect of oral administration of diphenyl diselenide on antioxidant status, and activity of delta aminolevulinic acid dehydratase and isoforms of lactate dehydrogenase, in streptozotocin-induced diabetic rats, Cell Biol. Toxicol. 25 (2009) 415–424, https://doi.org/10.1007/s10565-008-9095-5.

[28] D.S. Ávila, A.L. Braga, I.J. Kade, N.B.V. Barbosa, J.B.T. Rocha, O.E.D. Rodrigues, C.W. Nogueira, M.W. Paixão, Comparative studies on dicholesteroyl diselenide and diphenyl diselenide as antioxidant agents and their effect on the activities of Na+/K+ ATPase and δ-aminolevulinic acid dehydratase in the rat brain, Neurochem. Res. 33 (2008) 167–178, https://doi.org/10.1007/s11064-007-9432-8.

[29] R.M. Golombieski, D.A.S. Graichen, L.A. Pivetta, C.W. Nogueira, E.L.S. Loreto, J.B.T. Rocha, Diphenyl diselenide [(PhSe)2] inhibits Drosophila melanogaster δ-aminolevulinate dehydratase (δ-ALA-D) gene transcription and enzyme activity, Comp. Biochem. Physiol. - C Toxicol. Pharmacol. 147 (2008) 198–204, https://doi.org/10.1016/j.cbpc.2007.09.007.

[30] M. Farina, N.B.V. Barbosa, C.W. Nogueira, V. Folmer, G. Zeni, L.H. Andrade, A.L. Braga, J.B.T. Rocha, Reaction of diphenyl diselenide with hydrogen peroxide and inhibition of delta-aminolevulinate dehydratase from rat liver and cucumber leaves, Brazilian J. Med. Biol. Res. 35 (2002) 623–631, https://doi.org/10.1590/S0100-879X2002000600001.

[31] R.J. Krause, S.C. Glocke, A.R. Sicuri, S.L. Ripp, A.A. Elfarra, Oxidative metabolism of seleno-L-methionine to L-methionine selenoxide by flavin-containing monooxygenases, Chem. Res. Toxicol. 19 (2006) 1643–1649, https://doi.org/10.1021/tx0601915.

[32] G.P. Chen, D.M. Ziegler, Liver microsome and flavin-containing monooxygenase catalyzed oxidation of organic selenium compounds, Arch. Biochem. Biophys. 312 (1994) 566–572, https://doi.org/10.1006/abbi.1994.1346.

[33] J.C. Madden, G. Pawar, M.T.D. Cronin, S. Webb, Y. Tan, A. Paini, In silico resources to assist in the development and evaluation of physiologically-based kinetic models, Comput. Toxicol. 11 (2019) 33–49, https://doi.org/10.1016/j.comtox.2019.03.001.

[34] R. Friedman, K. Boye, K. Flatmark, Molecular modelling and simulations in cancer research, Biochim. Biophys. Acta - Rev. Cancer. 2013 (1836) 1–14, https://doi.org/10.1016/j.bbcan.2013.02.001.

[35] R.A. Hodos, B.A. Kidd, K. Shameer, B.P. Readhead, J.T. Dudley, In silico methods for drug repurposing and pharmacology, Wiley Interdiscip. Rev. Syst. Biol. Med. 8 (2016) 186–210, https://doi.org/10.1002/wsbm.1337.

[36] A.B. Raies, V.B. Bajic, In silico toxicology: computational methods for the prediction of chemical toxicity, Wiley Interdiscip. Rev. Comput. Mol. Sci. 6 (2016) 147–172, https://doi.org/10.1002/wcms.1240.

[37] C.L. Mellor, F.P. Steinmetz, M.T.D. Cronin, Using molecular initiating events to develop a structural alert based screening work flow for nuclear receptor ligands associated with hepatic steatosis, Chem. Res. Toxicol. 29 (2016) 203–212, https://doi.org/10.1021/acs.chemrestox.5b00480.

[38] D.B. Kitchen, H. Decornez, J.R. Furr, J. Bajorath, Docking and scoring in virtual screening for drug discovery: methods and applications, Nat. Rev. Drug Discov. 3 (2004) 935–949, https://doi.org/10.1038/nrd1549.

[39] Y. Chen, Beware of docking!, Trends Pharmacol. Sci. 36 (2015) 78–95, https://doi.org/10.1016/j.tips.2014.12.001.

[40] R. Grzywa, E. Dyguda-Kazimierowicz, M. Sieńczyk, M. Feliks, W.A. Sokalski, J. Oleksyszyn, The molecular basis of urokinase inhibition: from the nonempirical analysis of intermolecular interactions to the prediction of binding affinity, J. Mol. Model. 13 (2007) 677–683, https://doi.org/10.1007/s00894-007-0193-8.

[41] T.L. Gonzalez, J.M. Rae, J.A. Colacino, R.J. Richardson, Homology models of mouse and rat estrogen receptor-α ligand-binding domain created by in silico mutagenesis of a human template: molecular docking with 17β-estradiol, diethylstilbestrol, and paraben analogs, Comput. Toxicol. 10 (2019) 1–16, https://doi.org/10.1016/j.comtox.2018.11.003.

[42] R.O. Jones, Density functional theory: its origins, rise to prominence, and future, Rev. Mod. Phys. 87 (2015) 897–923, https://doi.org/10.1103/RevModPhys.87.897.

[43] A.J. Cohen, P. Mori-Sánchez, W. Yang, Challenges for density functional theory, Chem. Rev. 112 (2012) 289–320, https://doi.org/10.1021/cr200107z.

[44] R.A. Saraiva, P.A. Nogara, R.F. Costa, E.M. Bezerra, H.N.H. Veras, I.R.A. Menezes, U.L. Fulco, E.L. Albuquerque, V.N. Freire, J.B.T. Rocha, Interaction energy profile for diphenyl diselenide in complex with δ-aminolevulinic acid dehydratase enzyme using quantum calculations and a molecular fragmentation method, Comput. Toxicol. 7 (2018) 9–19, https://doi.org/10.1016/j.comtox.2018.05.002.

[45] J. Carlsson, R.G. Coleman, V. Setola, J.J. Irwin, H. Fan, A. Schlessinger, A. Sali, B.L. Roth, B.K. Shoichet, Ligand discovery from a dopamine D3 receptor homology model and crystal structure, Nat. Chem. Biol. 7 (2011) 769–778, https://doi.org/10.1038/nchembio.662.

[46] K.S. Nascimento, D.A. Araripe, V.R. Pinto-Junior, V.J.S. Osterne, F.W.V. Martins, A.H.B. Neco, G.A. Farias, B.S. Cavada, Homology modeling, molecular docking, and dynamics of two α-methyl-d-mannoside-specific lectins from Arachis genus, J. Mol. Model. 24 (2018) 251, https://doi.org/10.1007/s00894-018-3800-y.

[47] J.L.R. Scaini, A.D. Camargo, V.R. Seus, A. von Groll, A.V. Werhli, P.E.A. da Silva, K. dos S. Machado, Molecular modelling and competitive inhibition of a Mycobacterium tuberculosis multidrug-resistance efflux pump, J. Mol. Graph. Model. 87 (2019) 98–108, https://doi.org/10.1016/j.jmgm.2018.11.016.

[48] J.H. Kim, S.K. Kim, J.H. Lee, Y.J. Kim, W.A. Goddard, Y.C. Kim, Homology modeling and molecular docking studies of Drosophila and Aedes sex peptide receptors, J. Mol. Graph. Model. 66 (2016) 115–122, https://doi.org/10.1016/j.jmgm.2016.03.014.

[49] Å Mortensen, S. Mæhre, K. Kristiansen, E.S. Heimstad, G.W. Gabrielsen, B.M. Jenssen, I. Sylte, Homology modeling to screen for potential binding of contaminants to thyroid hormone receptor and transthyretin in glaucous gull (Larus hyperboreus) and herring gull (Larus argentatus), Comput. Toxicol. 13 (2020): 100120. https://doi.org/10.1016/j.comtox.2020.100120.

[50] J. He, D. Li, K. Xiong, Y. Ge, H. Jin, G. Zhang, M. Hong, Y. Tian, J. Yin, H. Zeng, Inhibition of thioredoxin reductase by a novel series of bis-1,2-benzisoselenazol-3(2H)-ones: organoselenium compounds for cancer therapy, Bioorganic Med. Chem. 20 (2012) 3816–3827, https://doi.org/10.1016/j.bmc.2012.04.033.

[51] P.A. Nogara, J.B.T. Rocha, In silico studies of mammalian δ-ALAD interactions with selenides and selenoxides, Mol. Inform. 36 (2017) 1–8, https://doi.org/10.1002/minf.201700091.

[52] L. Orian, S. Toppo, Organochalcogen peroxidase mimetics as potential drugs: a long story of a promise still unfulfilled, Free Radic. Biol. Med. 66 (2014) 65–74, https://doi.org/10.1016/j.freeradbiomed.2013.03.006.

[53] L.P. Wolters, L. Orian, Peroxidase activity of organic selenides: mechanistic insights from quantum chemistry, Curr. Org. Chem. 20 (2016) 189–197, https://doi.org/10.2174/1385272819666150724233655.

[54] E. Fragoso, R. Azpiroz, P. Sharma, G. Espinosa-Pérez, F. Lara-Ochoa, A. Toscano, R. Gutierrez, O. Portillo, New organoselenium compounds with intramolecular Se···O/ Se···H interactions: NMR and theoretical studies, J. Mol. Struct. 1155 (2018) 711–719, https://doi.org/10.1016/j.molstruc.2017.11.054.

[55] C.A. Bayse, B.D. Allison, Activation energies of selenoxide elimination from Se-substituted selenocysteine, J. Mol. Model. 13 (2007) 47–53, https://doi.org/10.1007/s00894-006-0128-9.

[56] L. Orian, P. Mauri, A. Roveri, S. Toppo, L. Benazzi, V. Bosello-Travain, A. De Palma, M. Maiorino, G. Miotto, M. Zaccarin, A. Polimeno, L. Flohé, F. Ursini, Selenocysteine oxidation in glutathione peroxidase catalysis: an MS-supported quantum mechanics study, Free Radic. Biol. Med. 87 (2015) 1–14, https://doi.org/10.1016/j.freeradbiomed.2015.06.011.

[57] M. Bortoli, M. Torsello, F.M. Bickelhaupt, L. Orian, Role of the chalcogen (S, Se, Te) in the oxidation mechanism of the glutathione peroxidase active site, ChemPhysChem 18 (2017) 2990–2998, https://doi.org/10.1002/cphc.201700743.

[58] M.D. Tiezza, G. Ribaudo, L. Orian, Organodiselenides: organic catalysis and drug design learning from glutathione peroxidase, Curr. Org. Chem. 23 (2019)

1381–1402, https://doi.org/10.2174/1385272822666180803123137.
[59] K. Arnold, L. Bordoli, J. Kopp, T. Schwede, The SWISS-MODEL workspace: a web-based environment for protein structure homology modelling, Bioinformatics 22 (2006) 195–201, https://doi.org/10.1093/bioinformatics/bti770.
[60] L.A. Kelly, S. Mezulis, C. Yates, M. Wass, M. Sternberg, The Phyre2 web portal for protein modelling, prediction, and analysis, Nat. Protoc. 10 (2015) 845–858, https://doi.org/10.1038/nprot.2015-053.
[61] C. Combet, M. Jambon, G. Deléage, C. Geourjon, Geno3D: automatic comparative molecular modelling of protein, Bioinformatics 18 (2002) 213–214, https://doi.org/10.1093/bioinformatics/18.1.213.
[62] L. Coates, G. Beaven, P.T. Erskine, S.I. Beale, S.P. Wood, P.M. Shoolingin-Jordan, J.B. Cooper, Structure of Chlorobium vibrioforme 5-aminolaevulinic acid dehydratase complexed with a diacid inhibitor, Acta Crystallogr. Sect. D Biol. Crystallogr. 61 (2005) 1594–1598, https://doi.org/10.1107/S0907444905030350.
[63] F. Frère, W.D. Schubert, F. Stauffer, N. Frankenberg, R. Neier, D. Jahn, D.W. Heinz, Structure of porphobilinogen synthase from pseudomonas aeruginosa in complex with 5-fluorolevulinic acid suggests a double schiff base mechanism, J. Mol. Biol. 320 (2002) 237–247, https://doi.org/10.1016/S0022-2836(02)00472-2.
[64] E.K. Jaffe, J. Kervinen, J. Martins, F.R. Stauffer, R. Neier, A. Wlodawer, A. Zdanov, Species-specific inhibition of porphobilinogen synthase by 4-oxosebacic acid, J. Biol. Chem. 277 (2002) 19792–19799, https://doi.org/10.1074/jbc.M201486200.
[65] D. Eisenberg, R. Luthy, J.U. Bowie, VERIFY 3D: assessment of protein models with three-dimensional profiles, Methods Enzymol. 277 (1997) 396–404.
[66] J.U. Bowie, R. Luthy, D. Eisenberg, A method to identify protein sequences that fold into a known three-dimensional structure, Science (80-.). 253 (1991): 164–170. https://doi.org/10.1126/science.1853201.
[67] M. Wiederstein, M.J. Sippl, ProSA-web: interactive web service for the recognition of errors in three-dimensional structures of proteins, Nucleic Acids Res. 35 (2007) 407–410, https://doi.org/10.1093/nar/gkm290.
[68] R.A. Laskowski, M.W. MacArthur, D.S. Moss, J.M. Thornton, PROCHECK: a program to check the stereochemical quality of protein structures, J. Appl. Crystallogr. 26 (1993) 283–291, https://doi.org/10.1107/S0021889892009944.
[69] G.N. Ramachandran, V. Sasisekharan, Conformation of polypeptides and proteins, Adv. Protein Chem. 23 (1968) 283–438, https://doi.org/10.1016/S0065-3233(08)60402-7.
[70] C. Colovos, T.O. Yeates, Verification of protein structures: patterns of nonbonded atomic interactions, Protein Sci. 2 (1993) 1511–1519, https://doi.org/10.1002/pro.5560020916.
[71] R.A. Laskowski, PDBsum: summaries and analyses of PDB structures, Nucleic Acids Res. 29 (2001) 221–222, https://doi.org/10.1093/nar/29.1.221.
[72] N. Mills-Davies, D. Thompson, J. Cooper, S. Wood, P.M. Shoolingin-Jordan, Crystal structure of native human erythrocyte 5-aminolaevulinic acid dehydratase, RCSB PDB (2000), https://doi.org/10.2210/pdb1E51/pdb.
[73] E.F. Pettersen, T.D. Goddard, C.C. Huang, G.S. Couch, D.M. Greenblatt, E.C. Meng, T.E. Ferrin, UCSF Chimera - a visualization system for exploratory research and analysis, J. Comput. Chem. 25 (2004) 1605–1612, https://doi.org/10.1002/jcc.20084.
[74] M.D. Hanwell, D.E. Curtis, D.C. Lonie, T. Vandermeersch, E. Zurek, G.R. Hutchison, Avogadro: an advanced semantic chemical editor, visualization, and analysis platform, J. Cheminform. 4 (2012) 1–17, https://doi.org/10.1186/1758-2946-4-17.
[75] J.J.P. Stewart, Optimization of parameters for semiempirical methods V: Modification of NDDO approximations and application to 70 elements, J. Mol. Model. 13 (2007) 1173–1213, https://doi.org/10.1007/s00894-007-0233-4.
[76] J.D. McCullough, E.S. Gould, The dissociation constants of some mono-substituted benzeneseleninic acids, J. Am. Chem. Soc. 71 (1949) 674–676, https://doi.org/10.1021/ja01170a083.
[77] G.M. Morris, R. Huey, W. Lindstrom, M.F. Sanner, R.K. Belew, D.S. Goodsell, A.J. Olson, AutoDock4 and AutoDockTools4: automated docking with selective receptor flexibility, J. Comput. Chem. 30 (2009) 2785–2791, https://doi.org/10.1002/jcc.21256.
[78] O. Trott, A.J. Olson, AutoDock Vina: improving the speed and accuracy of docking with a new scoring function, efficient optimization, and multithreading, J. Comput. Chem. 31 (2010) 455–461, https://doi.org/10.1002/jcc.21334.
[79] J.L. Stigliani, V. Bernardes-Génisson, J. Bernadou, G. Pratviel, Cross-docking study on InhA inhibitors: a combination of Autodock Vina and PM6-DH2 simulations to retrieve bio-active conformations, Org. Biomol. Chem. 10 (2012) 6341–6349, https://doi.org/10.1039/c2ob25602a.
[80] C.P. Vianna, W.F. De Azevedo, Identification of new potential Mycobacterium tuberculosis shikimate kinase inhibitors through molecular docking simulations, J. Mol. Model. 18 (2012) 755–764, https://doi.org/10.1007/s00894-011-1113-5.
[81] M.J. Frisch, G.W. Trucks, H.B. Schlegel, G.E. Scuseria, M.A. Robb, J.R. Cheeseman, G. Scalmani, V. Barone, G.A. Petersson, H. Nakatsuji, X. Li, M. Caricato, A. Marenich, J. Bloino, B.G. Janesko, R. Gomperts, B. Mennucci, H.P. Hratchian, J.V. Ortiz, A.F. Izmaylov, J.L. Sonnenberg, D. Williams-Young, F. Ding, F. Lipparini, F. Egidi, J. Goings, B. Peng, A. Petrone, T. Henderson, D. Ranasinghe, V.G. Zakrzewski, J. Gao, N. Rega, G. Zheng, W. Liang, M. Hada, M. Ehara, K. Toyota, R. Fukuda, J. Hasegawa, M. Ishida, T. Nakajima, Y. Honda, O. Kitao, H. Nakai, T. Vreven, K. Throssell, J.A. Montgomery Jr., J.E. Peralta, F. Ogliaro, M. Bearpark, J.J. Heyd, E. Brothers, K.N. Kudin, V.N. Staroverov, T. Keith, R. Kobayashi, J. Normand, K. Raghavachari, A. Rendell, J.C. Burant, S.S. Iyengar, J. Tomasi, M. Cossi, J.M. Millam, V. Klene, C. Adamo, R. Cammi, V. Ochterski, R.L. Martin, K. Morokuma, O. Farkas, J.B. Foresman, D.J. Fox, Gaussian 09 (2009).
[82] C. Adamo, V. Barone, Exchange functionals with improved long-range behavior and adiabatic connection methods without adjustable parameters: the mPW and mPW1PW models, J. Chem. Phys. 108 (1998) 664–675, https://doi.org/10.1063/1.475428.
[83] T.H. Dunning, Gaussian basis functions for use in molecular calculations. IV. The representation of polarization functions for the first row atoms and hydrogen, J. Chem. Inf. Model. 55 (1971): 3958–3966. https://doi.org/10.1063/1.1676685.
[84] S. Antony, C.A. Bayse, Modeling the mechanism of the glutathione peroxidase mimic ebselen, Inorg. Chem. 50 (2011) 12075–12084, https://doi.org/10.1021/ic201603v.
[85] J. Tomasi, B. Mennucci, R. Cammi, Quantum mechanical continuum solvation models, Chem. Rev. 105 (2005) 2999–3094, https://doi.org/10.1021/cr9904009.
[86] J. Kervinen, E.K. Jaffe, F. Stauffer, R. Neier, A. Wlodawer, A. Zdanov, Mechanistic basis for suicide inactivation of porphobilinogen synthase by 4,7-Dioxosebacic acid, an inhibitor that shows dramatic species selectivity, Biochemistry 40 (2001) 8227–8236, https://doi.org/10.1021/bi010656k.
[87] V.K. Vyas, R.D. Ukawala, M. Ghate, C. Chintha, homology modeling a fast tool for drug discovery: current perspectives, Indian J. Pharm. Sci. 74 (2012) 1–17.
[88] T. Schmidt, A. Bergner, T. Schwede, Modelling three-dimensional protein structures for applications in drug design, Drug Discov. Today. 19 (2014) 890–897, https://doi.org/10.1016/j.drudis.2013.10.027.
[89] Z. Xiang, Advances in homology protein structure modeling, Curr. Protein Pept. Sci. 7 (2006) 217–227, https://doi.org/10.2174/138920306777452312.
[90] E. Erdtman, E.A.C. Bushnell, J.W. Gauld, L.A. Eriksson, Computational insights into the mechanism of porphobilinogen synthase, J. Phys. Chem. B. 114 (2010) 16860–16870, https://doi.org/10.1021/jp103590d.
[91] C.S. Lentz, D. Stumpfe, J. Bajorath, M. Famulok, A. Hoerauf, K.M. Pfarr, New chemotypes for wALADin1-like inhibitors of delta-aminolevulinic acid dehydratase from Wolbachia endobacteria, Bioorganic Med. Chem. Lett. 23 (2013) 5558–5562, https://doi.org/10.1016/j.bmcl.2013.08.052.
[92] C.S. Lentz, V. Halls, J.S. Hannam, B. Niebel, U. Strübing, G. Mayer, A. Hoerauf, M. Famulok, K.M. Pfarr, A selective inhibitor of heme biosynthesis in endosymbiotic bacteria elicits antifilarial activity in vitro, Chem. Biol. 20 (2013) 177–187, https://doi.org/10.1016/j.chembiol.2012.11.009.
[93] B. Wu, J. Novelli, J. Foster, R. Vaisvila, L. Conway, J. Ingram, M. Ganatra, A.U. Rao, I. Hamza, B. Slatko, The heme biosynthetic pathway of the obligate wolbachia endosymbiont of brugia malayi as a potential anti-filarial drug target, PLoS Negl. Trop. Dis. 3 (2009) e475, https://doi.org/10.1371/journal.pntd.0000475.
[94] P.S. Kumar, Y.N. Kumar, U.V. Prasad, S. Yeswanth, V. Swarupa, G. Sowjenya, K. Venkatesh, L. Srikanth, V.K. Rao, P.V. Sarma, In silico designing and molecular docking of a potent analog against Staphylococcus aureus porphobilinogen synthase, J. Pharm. Bioallied Sci. 6 (2014) 158–166, https://doi.org/10.4103/0975-7406.135246.
[95] K.K. Mishra, S.K. Singh, P. Ghosh, D. Ghosh, A. Das, The nature of selenium hydrogen bonding: gas phase spectroscopy and quantum chemistry calculations, Phys. Chem. Chem. Phys. 19 (2017) 24179–24187, https://doi.org/10.1039/c7cp05265k.
[96] V.R. Mundlapati, D.K. Sahoo, S. Ghosh, U.K. Purame, S. Pandey, R. Acharya, N. Pal, P. Tiwari, H.S. Biswal, Spectroscopic evidences for strong hydrogen bonds with selenomethionine in proteins, J. Phys. Chem. Lett. 8 (2017) 794–800, https://doi.org/10.1021/acs.jpclett.6b02931.
[97] G. Ribaudo, M. Bellanda, I. Menegazzo, L.P. Wolters, M. Bortoli, G. Ferrer-Sueta, G. Zagotto, L. Orian, Mechanistic insight into the oxidation of organic phenylselenides by H2O2, Chem. - A Eur. J. 23 (2017) 2405–2422, https://doi.org/10.1002/chem.201604915.
[98] C.V. Klimaczewski, P.A. Nogara, N.V. Barbosa, J.B.T. da Rocha, Interaction of metals from group 10 (Ni, Pd, and Pt) and 11 (Cu, Ag, and Au) with human blood δ-ALA-D: in vitro and in silico studies, Environ. Sci. Pollut. Res. 25 (2018) 30557–30566, https://doi.org/10.1007/s11356-018-3048-1.
[99] P.B. Lutz, C.A. Bayse, Chalcogen bonding interactions between reducible sulfur and selenium compounds and models of zinc finger proteins, J. Inorg. Biochem. 157 (2016) 94–103, https://doi.org/10.1016/j.jinorgbio.2016.01.013.
[100] K.N. Sands, T.G. Back, Key steps and intermediates in the catalytic mechanism for the reduction of peroxides by the antioxidant ebselen, Tetrahedron 74 (2018) 4959–4967, https://doi.org/10.1016/j.tet.2018.05.027.
[101] M. Abdo, Z. Sun, S. Knapp, Biohybrid-Se-S-coupling reactions of an amino acid derived seleninate, Molecules 18 (2013) 1963–1972, https://doi.org/10.3390/molecules18021963.
[102] L. Engman, D. Stern, Thiol/diselenide exchange for the generation of benzeneselenolate ion. catalytic reductive ring-opening of α,β-epoxy ketoness, J. Org. Chem. 59 (1994): 5179–5183. https://doi.org/10.1021/jo00097a019.
[103] R.M. Rosa, R. Roesler, A.L. Braga, J. Saffi, J.A.P. Henriques, Pharmacology and toxicology of diphenyl diselenide in several biological models, Brazilian J. Med. Biol. Res. 40 (2007) 1287–1304, https://doi.org/10.1590/S0100-879X2006005000171.
[104] Y. Xue, X. Xia, B. Yu, L. Tao, Q. Wang, S.W. Huang, F. Yu, Selenylsulfide bond-launched reduction-responsive superparamagnetic nanogel combined of acid-responsiveness for achievement of efficient therapy with low side effect, ACS Appl. Mater. Interfaces 9 (2017) 30253–30257, https://doi.org/10.1021/acsami.7b06818.
[105] M. Kunstelj, K. Fidler, Š. Škrajnar, M. Kenig, V. Smilović, M. Kusterle, S. Caserman, I. Zore, V.G. Porekar, S. Jevševar, Cysteine-specific PEGylation of rhG-CSF via selenylsulfide bond, Bioconjug. Chem. 24 (2013) 889–896, https://doi.org/10.1021/bc3005232.
[106] D. Steinmann, T. Nauser, W.H. Koppenol, Selenium and sulfur in exchange reactions: a comparative study, J. Org. Chem. 75 (2010) 6696–6699, https://doi.org/

10.1021/jo1011569.
[107] M. Bortoli, L.P. Wolters, L. Orian, F.M. Bickelhaupt, Addition-elimination or nucleophilic substitution? Understanding the energy profiles for the reaction of chalcogenolates with dichalcogenides, J. Chem. Theory Comput. 12 (2016) 2752–2761, https://doi.org/10.1021/acs.jctc.6b00253.
[108] J.L. Kice, T.W.S. Lee, Oxidation-reduction reactions of organoselenium compounds. 1. Mechanism of the reaction between seleninic acids and thiols, J. Am. Chem. Soc. 100 (1978): 5094–5102. https://doi.org/10.1021/ja00484a031.
[109] P. Prabhu, B.G. Singh, M. Noguchi, P.P. Phadnis, V.K. Jain, M. Iwaoka, K.I. Priyadarsini, Stable selones in glutathione-peroxidase-like catalytic cycle of selenonicotinamide derivative, Org. Biomol. Chem. 12 (2014) 2404–2412, https://doi.org/10.1039/c3ob42336k.
[110] B.K. Sarma, G. Mugesh, Antioxidant activity of the anti-inflammatory compound ebselen: a reversible cyclization pathway via selenenic and seleninic acid intermediates, Chem. Eur. J. 14 (2008) 10603–10614, https://doi.org/10.1002/chem.200801258.
[111] G.R. Haenen, B.M. De Rooij, N.P. Vermeulen, A. Bast, Mechanism of the reaction of ebselen with endogenous thiols: dihydrolipoate is a better cofactor than glutathione in the peroxidase activity of ebselen, Mol. Pharmacol. 37 (1990) 412–422.
[112] W. Hassan, J.B. Teixeira Rocha, Interaction profile of diphenyl diselenide with pharmacologically significant thiols, Molecules 17 (2012) 12287–12296, https://doi.org/10.3390/molecules171012287.
[113] J. Chiou, S. Wan, K.F. Chan, P.K. So, D. He, E.W.C. Chan, T.H. Chan, K.Y. Wong, J. Tao, S. Chen, Ebselen as a potent covalent inhibitor of New Delhi metallo-β-lactamase (NDM-1), Chem. Commun. 51 (2015) 9543–9546, https://doi.org/10.1039/c5cc02594j.
[114] R.A. Saraiva, D.C. Bueno, P.A. Nogara, J.B.T. Rocha, Molecular docking studies of disubstituted diaryl diselenides as mammalian δ -aminolevulinic acid dehydratase enzyme inhibitors, J. Toxicol. Environ. Heal. Part A 75 (2012) 1012–1022, https://doi.org/10.1080/15287394.2012.697810.
[115] H.J. Reich, R.J. Hondal, Why nature chose selenium, ACS Chem. Biol. 11 (2016) 821–841, https://doi.org/10.1021/acschembio.6b00031.
[116] C. Santi, C. Tidei, Electrophilic selenium/tellurium reagents: reactivity and their contribution to green chemistry, in: PATAI'S Chem. Funct. Groups, 2013, pp. 1–87. https://doi.org/10.1002/9780470682531.pat0720.
[117] V.P. Singh, H.B. Singh, R.J. Butcher, Synthesis and glutathione peroxidase-like activities of isoselenazolines, Eur. J. Org. Chem. 3 (2011) 5485–5497, https://doi.org/10.1002/ejoc.201100899.
[118] T.G. Back, B.P. Dyck, A novel camphor-derived selenamide that acts as a glutathione peroxidase mimetic, J. Am. Chem. Soc. 119 (1997) 2079–2083, https://doi.org/10.1021/ja963602k.
[119] H.J. Reich, C.P. Jasperse, Organoselenium chemistry. Redox chemistry of selenocysteine model systems, J. Am. Chem. Soc. 109 (1987): 5549–5551. https://doi.org/10.1021/ja00252a055.
[120] N. Singh, A.C. Halliday, J.M. Thomas, O. Kuznetsova, R. Baldwin, E.C.Y. Woon, P.K. Aley, I. Antoniadou, T. Sharp, S.R. Vasudevan, G.C. Churchill, A safe lithium mimetic for bipolar disorder, Nat. Commun. 4 (2013) 1332–1337, https://doi.org/10.1038/ncomms2320.
[121] Z. Jin, X. Du, Y. Xu, Y. Deng, M. Liu, Y. Zhao, B. Zhang, X. Li, L. Zhang, C. Peng, Y. Duan, J. Yu, L. Wang, K. Yang, F. Liu, R. Jiang, X. Yang, T. You, X. Liu, X. Yang, F. Bai, H. Liu, X. Liu, L.W. Guddat, W. Xu, G. Xiao, C. Qin, Z. Shi, H. Jiang, Z. Rao, H. Yang, Structure of Mpro from COVID-19 virus and discovery of its inhibitors, Nature (2020), https://doi.org/10.1038/s41586-020-2223-y.
[122] M.S. Wagner, E. Schultze, T.L. Oliveira, P.M.M. de Leon, H.S. Thurow, V.F. Campos, I. Oliveira, D. de Souza, O.E.D. Rodrigues, T. Collares, F.K. Seixas, Revitalizing the AZT through of the selenium: an approach in human triple negative breast cancer cell line, Front. Oncol. 8 (2018) 525, https://doi.org/10.3389/fonc.2018.00525.
[123] P.A. Nogara, C.S. Oliveira, J.B.T. Rocha, Chemistry and pharmacology of synthetic organoselenium compounds, in: B.C. Ranu, B. Banerjee (Eds.), Organoselenium Chem., De Gruyter, Berlin, 2020, pp. 305–346. https://doi.org/10.1515/9783110625110-008.

4.1.3. Artigo 3: Disselenetos derivados de aminoácidos como miméticos da GPx e substratos da TrxR: estudos *in vitro* e *in silico*

Sudati, J.H., **Nogara, P.A.**, Saraiva, R.A., Wagner, C., Alberto, E.E., Braga, A.L., Fachinetto, R., Piquini, P.C., Rocha, J.B.T., Diselenoamino acid derivatives as GPx mimics and as substrates of TrxR: in vitro and in silico studies, *Organic & Biomolecular Chemistry*, **2018**, 16, 3777–3787, DOI: 10.1039/c8ob00451j.

Graphical Abstract

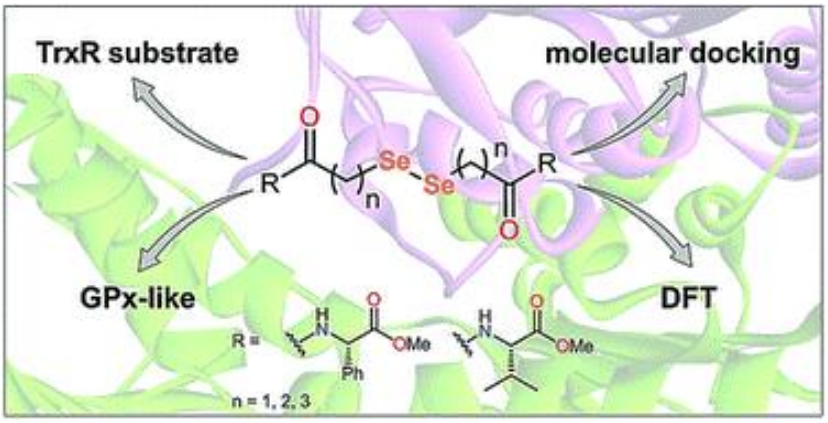

Organic & Biomolecular Chemistry

PAPER

View Article Online
View Journal | View Issue

Cite this: *Org. Biomol. Chem.*, 2018, **16**, 3777

Diselenoamino acid derivatives as GPx mimics and as substrates of TrxR: *in vitro* and *in silico* studies

Jéssie Haigert Sudati, †[a,b] Pablo Andrei Nogara, †[b] Rogério Aquino Saraiva, [c] Caroline Wagner, [d] Eduardo Eliezer Alberto, [e] Antonio Luiz Braga, [f] Roselei Fachinetto, [b] Paulo Cesar Piquini [g] and João Batista Teixeira Rocha *[b]

Received 21st February 2018,
Accepted 23rd April 2018

DOI: 10.1039/c8ob00451j

rsc.li/obc

Excessive production of reactive species in living cells usually has pathological effects. Consequently, the synthesis of compounds which can mimic the activity of antioxidant enzymes has inspired great interest. In this study, a variety of diselenoamino acid derivatives from phenylalanine and valine were tested to determine whether they could be functional mimics of glutathione peroxidase (GPx) and substrates for liver thioredoxin reductase (TrxR). Diselenides **C** and **D** showed the best GPx mimicking properties when compared with **A** and **B**. We suppose that the catalytic activity of diselenide GPx mimics depends on the steric effects, which can be influenced by the number of carbon atoms between the selenium atom and the amino acid residue and/or by the amino acid lateral residue. Compounds **C** and **D** stimulated NADPH oxidation in the presence of partially purified hepatic mammalian TrxR, indicating that they are substrates for TrxR. Our study indicates a possible dissociation between the two pathways for peroxide degradation (*i.e.*, *via* a substrate for TrxR or *via* mimicry of GPx) for compounds tested in this study, except for PhSeSePh, and the antioxidant activity of diselenoamino acids can also be attributed to their capacity to mimic GPx and to be a substrate for mammalian TrxR.

Introduction

Glutathione peroxidase (GPx) isoforms are selenium-containing enzymes with antioxidant properties. GPx1 is composed of four identical subunits, and each subunit contains one selenocysteinyl residue which undergoes a redox cycle as shown in Scheme 1.[1–3]

GPx isoforms protect aerobic organisms from oxidative stress using glutathione (GSH) as a source of reducing equivalents for decomposing peroxides such as H_2O_2, *t*-butyl hydroperoxide, and lipid hydroperoxides, according to Scheme 1 and the reaction:[4]

$$H_2O_2 + 2GSH \rightarrow GSSG + 2H_2O \quad (1)$$

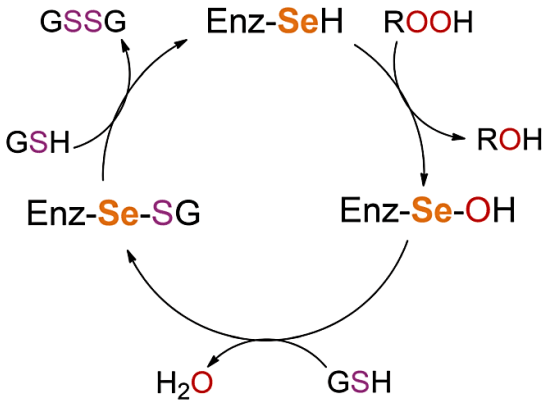

Scheme 1 GPx catalytic cycle.

The potential therapeutic use of GPx has some shortcomings such as instability, limited cellular accessibility and poor availability, which are a consequence of the high molecular weight of GPx. Consequently, considerable efforts have been made to find low molecular weight compounds that could mimic the properties of GPx and facilitate the understanding of its reaction mechanisms.[5–23]

[a]*Universidade Federal do Pampa (Unipampa), Dom Pedrito, RS, Brazil*
[b]*Departamento de Bioquímica e Biologia Molecular, CCNE, Universidade Federal de Santa Maria (UFSM), Santa Maria, RS, Brazil. E-mail: jbtrocha@yahoo.com.br*
[c]*Universidade Federal Rural de Pernambuco, Serra Talhada, PE, Brazil*
[d]*Universidade Federal do Pampa (Unipampa), Caçapava do Sul, RS, Brazil*
[e]*Departamento de Química, Universidade Federal de Minas Gerais (UFMG), Belo Horizonte, MG, Brazil*
[f]*Departamento de Química, Universidade Federal de Santa Catarina (UFSC), Florianópolis, SC, Brazil*
[g]*Departamento de Física, CCNE, Universidade Federal de Santa Maria (UFSM), Santa Maria, RS, Brazil*
†These authors contributed equally to this work.

Ebselen was the first compound suggested for hydroperoxide-inactivating therapy.[24] The reaction catalyzed by ebselen and some organoselenium compounds can be considered similar to that catalyzed by GPx. In effect, after interacting with a thiol (RSH), ebselen and diselenides can form selenol intermediates, which can decompose different types of peroxides (Scheme 1).[25] Furthermore, ebselen can react directly with peroxides, forming a selenoxide intermediate,[3,17–20] though this route is not thermodynamically favored compared to the one forming selenol and selenenic acid.[3,19] However, studies using high and non-physiological concentrations (high mmol L^{-1}) of peroxide have demonstrated that the selenol intermediates of ebselen and derivatives are not formed to an appreciable extent.[17,18,21,22] According to this, synthetic organoselenium and organotellurium compounds have been screened as potential mimetic candidates of native GPx.[7–9,26–29]

Zhao and his colleagues have shown that ebselen is a good substrate for mammalian thioredoxin reductase (TrxR), which produces the ebselen selenol intermediate. This selenol intermediate can decompose hydrogen peroxide using electrons derived from NADPH instead of –SH groups (Scheme 2).[30]

Similarly, diphenyl diselenide and analogs can be reduced to their selenol intermediates by TrxR.[31] The pharmacological antioxidant properties of ebselen and diselenides can be mediated either by their thiol peroxidase-like activity or *via* their reduction catalyzed by TrxR (Schemes 1 and 2). The catalytic mechanism of GPx mimetics can be altered depending on the structure of the organoselenium molecule and the reactivity of its respective intermediates toward thiols and peroxides.[3,6,20–23] Furthermore, diselenide compounds can also oxidize thiol-containing molecules (including low- and high-molecular-mass thiol groups) without decomposing peroxides, as presented in eqn (2), which can impart toxicological properties to diselenides mediated by excessive depletion of endogenous thiol groups.[3,32–35]

$$2\mathrm{RSH} + \mathrm{R'SeSeR'} \rightarrow \mathrm{RSSR} + 2\mathrm{R'SeH} \quad (2)$$

Consequently, the determination of the thiol oxidase activity of organoselenium compounds is also an important step in the screening of the new potential antioxidant diorganylchalcogenides, because compounds with high thiol oxidase activity can be potentially toxic.[34–36] In contrast, weak thiol-oxidizing molecules, such as diphenyl diselenide, can modulate the antioxidant defenses by interacting with thiol-containing proteins (*e.g.*, KEAP-1).[3,37,38] The interaction with KEAP-1 can activate the antioxidant responsive element (ARE), which increases the expression of antioxidant enzymes (*e.g.*, GPx).[38]

Considering the fact that ebselen and diphenyl diselenide have antioxidant properties, which can be attributed to their peroxidase-like activity and/or to their reduction catalyzed by TrxR, in this paper, four new diselenoamino acid derivatives (Fig. 1) were used as potential mimics of native Gpx and/or as potential substrates of mammalian TrxR. Furthermore, we have also determined the antioxidant properties and the thiol oxidase activity of these diselenoamino acid derivatives.

With particular biological and chemical significance, these diselenides are analogs of naturally occurring amino acids and possess in their structures an amino group that could potentially interact with the selenol intermediates formed after their direct reduction by a thiol or indirectly *via* reduction catalyzed by the mammalian TrxR. In effect, literature data have indicated that amino groups in the aryl organic moiety can considerably increase the thiol-peroxidase like activity of a variety of diselenides.[3,39]

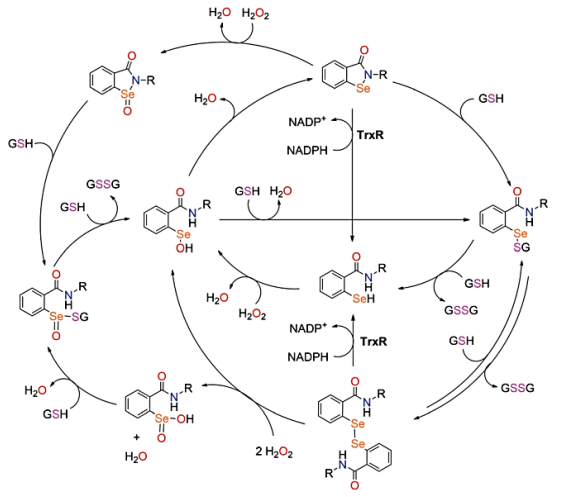

Scheme 2 Ebselen-derivatives as the TrxR substrate and its general GPx-like cycle.

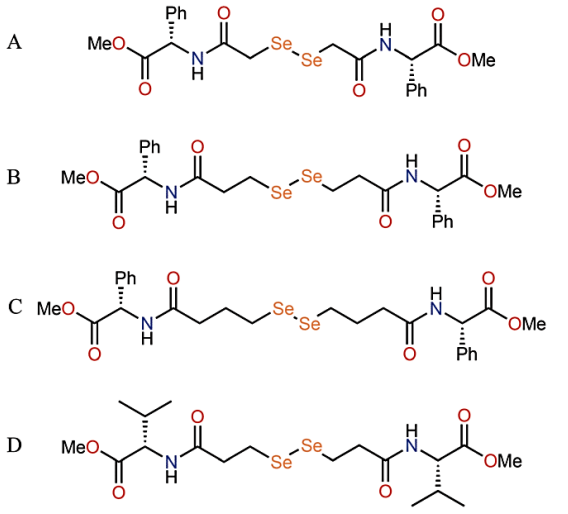

Fig. 1 Structure of diselenoamino acid derivatives. L-Phenylalanine (**A–C**) and L-valine (**D**) derivatives.

Results and discussion

GPx-like activity

Taking advantage of the modular characteristic of our catalysts, we evaluated the influence of the carbon chain length between the diselenide and amino acid moieties on the decomposition of H_2O_2 catalyzed by them (Fig. 2). Compound **A**, with the shortest carbon chain length between selenium atoms and the amino groups, was the less effective catalyst of the thiol-mediated reduction of hydrogen peroxide (T_{50} = 93.03 ± 5.77 min). In contrast, compounds **B**, **C** and **D** were better mimetics of GPx than diphenyl diselenide (T_{50} = 51.80 ± 2.83 min). Diselenide **D**, derived from L-valine (and with two carbon atoms between Se and the amino groups), showed the best GPx-like activity (T_{50} = 42.18 ± 2.75 min) followed by compounds **C** (three carbon atoms of distance from the Se to N atoms, T_{50} = 45.15 ± 3.17 min) and **B** (two carbon atoms of distance from the Se to the N atoms, T_{50} = 51.38 ± 2.45 min).

On the basis of the GPx mimetic properties of compounds **C** and **D**, we evaluated the reduction of H_2O_2 using different concentrations of this substrate and different concentrations of the catalysts. T_{50} values decreased as the concentration of H_2O_2 or the catalysts increased (Table 1).

Thiol oxidase activity

In addition to their reactions with peroxides, the GPx activity of organoselenium compounds also depends on the reactivity with thiols. Indeed, it has been shown that the GPx activity of selenium compounds depends not only on the reactivity of the selenol intermediates towards hydrogen peroxide, but also on the reactivity of the selenenyl sulfide intermediates with thiols.[40] Thus, the reactivity with thiol groups could influence the GPx-like activity of selenium compounds.[3] In addition, taking into account that the pharmacological and toxicological properties of organoselenium compounds are related to protein thiol oxidation,[3,11] we evaluated the thiol oxidase activity of these molecules using different thiol sources (GSH, captopril, and DTT) to better understand the reactivity of them towards organoselenium compounds. Thiol groups of DTT were oxidized more efficiently by the catalysts than monothiols. The high reactivity of DTT can be explained by the presence of a vicinal dithiol in its structure that facilitates the interaction of diselenides with thiols. Additionally, the formation of an intramolecular 6-membered ring in the oxidized DTT (DTTox) is thermodynamically stable.[41] In a similar way to that observed in the GPx-like assay, compounds **C** and **D** were more efficient oxidants of GSH (monothiol) and DTT (dithiol) than compounds **A** and **B** (Table 2). The oxidation of the captopril thiol group was faster for compound **D** than **A**, **B** and PhSeSePh (Table 2). In summary, the diselenoamino acid **D** presented the highest thiol oxidase activity.

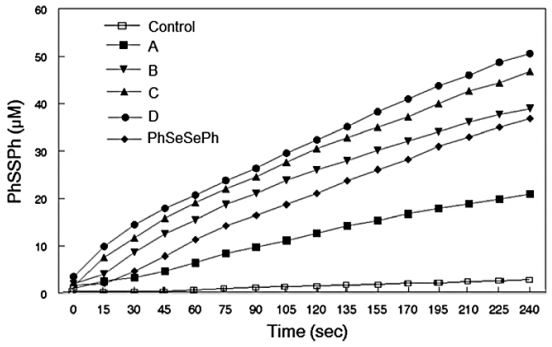

Fig. 2 GPx-like activity of catalysts **A**–**D** and PhSeSePh. [MeOH (1 mL); **A**–**D** and PhSeSePh (25 μM); PhSH (1.9 mM); H_2O_2 (5 mM)].

Table 1 T_{50} values (min) for oxidation of PhSH by the catalysts **C**, **D** and diphenyl diselenide **(PhSe)$_2$** at varying concentrations of H_2O_2

		H_2O_2[c,d] (mM)			
	[ ] μM	5	10	15	30
Control	—	131.66	95.3	92.07	84.69
C[a,b]	5	85.56	56.98	38.51	26.25
	10	79.51	49.23	31.21	22.33
	25	45.11	45.75	33.85	21.15
D[a,b]	5	93.88	74.04	43.22	31.22
	10	79.85	62.83	42.10	22.06
	25	37.64	34.98	20.96	17.78
(PhSe)$_2$[a,b]	5	82.18	54.95	48.25	31.90
	10	69.42	42.92	41.51	26.88
	25	52.56	28.66	24.65	15.66

[a] Under these conditions, in the absence of catalyst, H_2O_2 did not show any significant oxidation of PhSH. [b] MeOH (1 mL), catalyst (5, 10, 15, 30 μM), PhSH (1.9 mM), H_2O_2 (5, 10, 15 and 30 mM). [c] T_{50} is the time required, in minutes, to reduce the thiol concentration to 50% after the addition of H_2O_2. [d] The experimental error (S.E.M.) was less than 10%, data not shown.

Table 2 Oxidation of GSH, Captropil, and DTT catalyzed by diselenoamino acid derivatives (100 μM). Values are expressed as % of –SH consumed after 120 min of reaction in relation to the time zero of reaction (mean ± SD from 4 independent experiments performed in duplicate). Numbers not sharing the same superscript letters are statistically different from each other using the LSD multiple range tests, $p < 0.05$

	% SH consumed		
	GSH	Captropil	DTT
Control	6.37 ± 0.35	6.85 ± 1.35	8.54 ± 2.5
A	16.73 ± 2.1[a]	25.09 ± 7.93[a]	18.3 ± 1.62[a]
B	20.14 ± 3.93[a]	24.00 ± 3.81[a]	21.88 ± 6.93[a]
C	28.18 ± 4.7[b]	26.36 ± 1.50[a,b]	44.20 ± 8.74[b]
D	31.79 ± 1.6[b]	32.75 ± 4.4[b]	63.71 ± 4.56[c]
(PhSe)$_2$	25.52 ± 1.15[b]	21.63 ± 1.84[a]	57.80 ± 7.68[c]

Global hardness, reactivity indexes, and electrostatic potentials

The hard and soft acids and bases (HSAB) principle states that hard (or soft) Lewis acids prefer to interact with hard (or soft) Lewis bases. The global hardness, η, and global softness, S, of a reactant can be determined by total energy calculations, using the formula:

$$\eta = 1/S = (I - A)/2 \quad (3)$$

where I and A represent the ionization potential and the electron affinity of the isolated reactant, respectively. The local version of these quantities, *i.e.*, the local hardness, $\eta(r)$, and local softness, $s(r)$, allows one to infer the electrophilic and nucleophilic regions of the isolated reactants. Actually, the electrophilic and nucleophilic regions of a given chemical species can be formally associated (within density functional theory or DFT) with specific local softness maps, $s^+(r)$ and $s^-(r)$ respectively, which are defined in terms of charge density differences as:

$$s^+(r) = (\rho_{N+1}(r) - \rho_N(r)) \times S \quad (4)$$

$$s^-(r) = (\rho_N(r) - \rho_{N-1}(r)) \times S \quad (5)$$

where $\rho_N(r)$ represents the electronic charge density of a system with N electrons at a point r.[42–45]

We have used density functional theory to optimize the molecular structures of compounds **A–D**, PhSeSePh and PhSH in the neutral charge state. Once these structures were optimized, we then performed static, *i.e.*, fixed geometry calculations for the positively and negatively charged states. From these calculations, we can determine the vertical ionization potentials and electron affinities, global hardness, and local softness maps for all compounds **A–D**, PhSeSePh, and PhSH.

In the reactions, we were interested in knowing if compounds **A–D** and PhSeSePh can act like Lewis acids or Lewis bases, *i.e.* they can gain or lose electrons to the thiol molecule, PhSH. Taking this into account, one could visualize the nucleophilic and the electrophilic regions of these compounds by looking at their $s^-(r)$ and $s^+(r)$ maps, respectively. Fig. 3 shows the calculated $s^-(r)$ and $s^+(r)$ maps for each of these molecules. They all have the same kind of information, namely both the nucleophilic and the electrophilic regions are around the Se atoms, with the charge differences in $s^-(r)$ resembling the charge distributions of Se p-like orbitals pointing perpendicularly to the Se–Se bond, while the $s^+(r)$ maps resemble Se p-like orbitals oriented along the Se–Se bond. This confirms that the Se atoms are the most reactive sites for nucleophilic as well as electrophilic attacks, as should be expected. In the $s^-(r)$ and $s^+(r)$ maps for the PhSH molecule, the softness maps reveal different reactive characteristics when the system is subjected to nucleophilic or electrophilic attacks. For electrophilic attacks, the most reactive region of PhSH is seen to be on the S atom, while for nucleophilic attacks the carbon atoms at the *ortho* and *meta* positions of the phenyl group are seen as the most reactive regions. Which of these maps should be looked at will depend on the characterization of each reactant as acids and/or bases. In this study, PhSH will act as a nucleophile.

Table 3 shows the calculated values of vertical ionization potentials and electron affinities as well as the global hardness for the studied reactants. It can be seen that all systems have not so different values for the global hardness, with PhSeSePh being the softest of them. Comparing these values with those

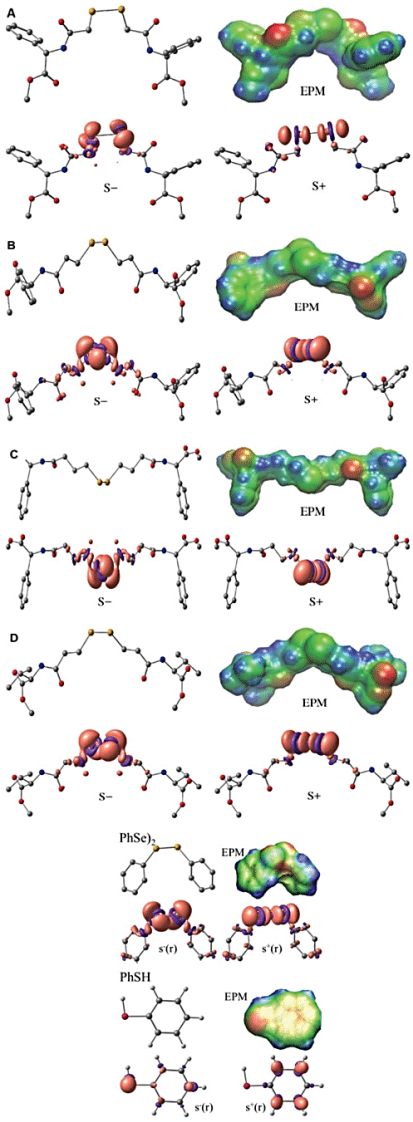

Fig. 3 Illustrative data obtained by density functional calculations for compounds **A–D**, PhSeSePh and PhSH. The optimized structures are shown at the top-left corner, and the electrostatic potential maps (EPM) at the top-right corner. The $s^-(r)$ and $s^+(r)$ local softness maps are shown at the bottom-left and bottom-right corners, respectively.

Table 3 Calculated vertical ionization potentials, I, vertical electron affinities, A, and global hardness, η, for compounds **A–D**, PhSeSePh, and PhSH (optimized in the Gaussian program)

	A	**B**	**C**	**D**	PhSeSePh	PhSH
I (eV)	6.62	6.40	6.37	6.41	6.40	6.26
A (eV)	2.08	1.89	1.85	1.89	2.46	0.90
η (eV)	2.27	2.25	2.26	2.26	1.97	2.67

for common acids and bases,[46] it can be seen that all species are soft acids or bases. The similarity among the calculated η values does not allow us to establish any clear tendency for a favourable reaction between PhSH with one of compounds **A–D** and PhSeSePh.

In order to further investigate the reactivity of compounds **A–D** and PhSeSePh with PhSH, we have determined their electrostatic potential maps, which can be seen in Fig. 3. The electrostatic potential maps for compounds **A–D** and PhSeSePh can be classified into two groups. For compounds **B**, **C** and **D**, the region around the Se atoms shows a neutral (green) or slightly positive (blue) charge distribution. On the other hand, compound **A** and PhSeSePh show a negative (red) charge distribution around the Se atoms. In the electrostatic potential map of PhSH, there is a clear negatively charged region around the S atom, indicating the nucleophile region. Once the reaction is supposed to occur between the S atom of PhSH and the Se atoms at compounds **A–D** and PhSeSePh, the electrostatic potential data on Fig. 3 show that the reactions of PhSH with compounds **B**, **C** and **D** should be the most favorable ones, since in these cases the more negatively charged region around the S atom in PhSH will approach the more positively charged region around Se atoms on compounds **B**, **C** and **D**. Reactions of PhSH with compound **A** and also PhSeSePh will be electrostatically less favorable, due to the electrostatic repulsion between the two negatively charged regions. However, PhSeSePh presented a good GPx-like activity, in this case, we think that in the reaction medium the Se–Se bond of PhSeSePh can be polarizable (with the support of the benzene rings that can stabilize the negative partial charge on the Se atom, by resonance), making the other Se atom more electrophile. This is in agreement with the reaction rate data in Fig. 2. As expected, for the electrostatic reactions, PhSH will act as the base, while compounds **A–D** will be the Lewis acids.

One important point to be stressed is that charge distribution around the Se atoms is largely influenced by the position of the carbonyl group (C═O) relative to the Se centres. In addition, the closest the carbonyl group is from the Se atoms the less reactive is the molecule (compound **A**), as can be seen from the molecular structures in Fig. 3 and the data in Fig. 2, probably due to the steric effect between the carbonyl moiety and the Se atom. For the thiol group of PhSH to react with the diselenides, it is necessary that the pair of electrons from the S atom (HOMO orbital) interact with the non-bonding orbital (LUMO) from compounds **A–D**. The proximity of carbonyl or the lateral chain groups to the Se can cause a steric effect and hinder the reaction. In Table 4 and Fig. 4, we verify that compound **A** presents the carbonyl closer to the Se atom than the other molecules (**B–D**). In this way, increasing the number of carbons between the carbonyl and Se atom decreases the steric effect and increases the reactivity of the molecules. In addition, **D** is a valine derivative, whereas **A–C** are phenylalanine derivatives, so the isopropyl moiety of the lateral chain in **D** presents a lower steric effect than the benzene ring in **A–C**, and possibly this fact can be involved in the reactivity of these molecules.

Table 4 Mean distances between the Se atom and carbonyl/lateral chain moieties, and the lowest predicted binding free energy from the conformations of compounds **A–D** and PhSeSePh optimized in the Gaussian program. x = 2 (**A**, **B**, **C**); x = 1 (**D**)

Distance (Å)	**A**	**B**	**C**	**D**	PhSeSePh
NHC═O···Se	4.16	4.77	5.53	4.80	–
Cα···Se	4.51	6.71	7.78	6.64	–
CH_x···Se	5.40	7.76	8.06	7.45	–
MeOC═O···Se	4.39	7.49	9.06	7.68	–
$\Delta G_{binding}$ (kcal mol^{-1})	−7.9	−7.7	−8.5	−6.7	−6.2

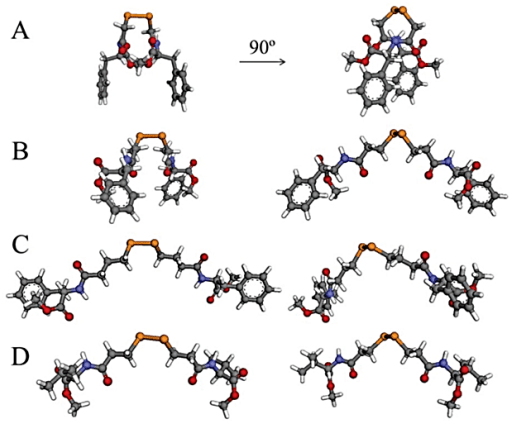

Fig. 4 Overview of the steric effect on the Se atom in diselenides **A–D**. Structures optimized in the Gaussian program.

Diselenoamino acid derivatives as substrates for mammalian TrxR

The reactivity of diselenoamino acid derivatives with the rat hepatic thioredoxin reductase (TrxR) is depicted in Fig. 5. Compounds (**C** and **D**) stimulated NADPH oxidation in the presence of partially purified hepatic TrxR, indicating that they are substrates of mammalian TrxR at 5 and 15 μM (Fig. 5A and B). Diphenyl diselenide was a much better substrate of TrxR than its analogs, causing about 13% (at 5 μM) and 19% (at 15 μM) oxidation of NADPH after 5 min of reaction (Fig. 5). The order of reactivity of hepatic TrxR with 5 μM of diselenoamino acid derivatives was **D** ≥ **C** ≥ **B** ≥ **A**. At 15 μM, the trend of reactivity was the same, but compounds **A** and **B** oxidized less NADPH than observed at 5 μM, indicating that at 15 μM they were probably inhibiting the TrxR activity. In contrast, the oxidation of NADPH increased from 7.5% to 11% (compound **D**) and from 6 to 9% (compound **C**). The inhibition of TrxR by similar concentrations of organoselenium compounds (including diselenides) has been reported in the literature.[30,31] The oxidation of NADPH was almost completely blocked by 1 μM $AuCl_3$ (about 97%) in all tested compounds.

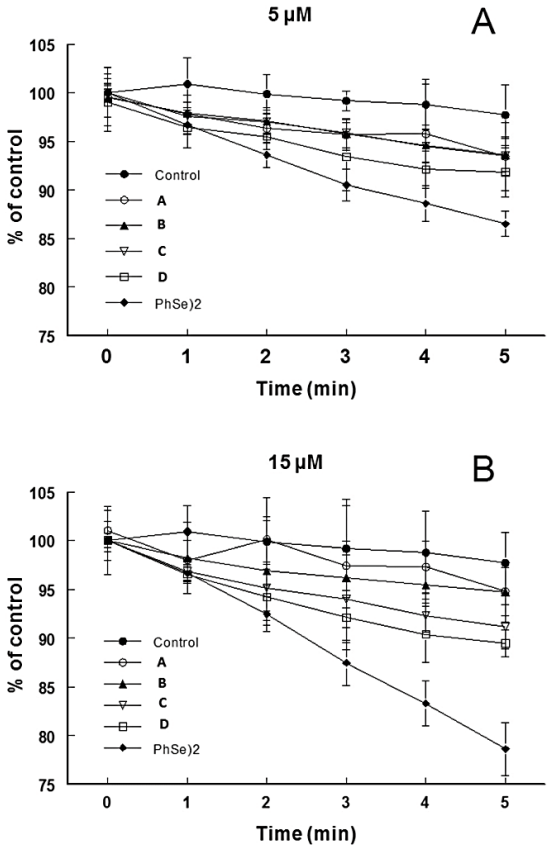

Fig. 5 Reduction of different diseleno amino acids (**A–C**) and PhSeSePh by NADPH catalyzed by hepatic TrxR. Diselenides were tested at the concentrations of 5 μM (painel A) and 15 μM (painel B).

Docking simulation between diselenoamino acid compounds and TrxR-1

According to the *in vitro* results, diphenyl diselenide and other organoselenium compounds can act as a substrate of TrxR. The postulated mechanism has indicated that the C-terminal from TrxR-1 in the reduced form (free selenol of Sec498 and the thiol of Cys497) can interact with organoselenium compounds.[30,47,48] Based on this mechanism, docking simulations between the catalytically active site (C-terminal region) of rat TrxR-1 and organodiselenide compounds (**A–D** and PhSeSePh) were performed to propose a molecular mechanism of binding.

The docking conformation from the lowest free energy of binding (ΔG_{bind}) obtained from the AutoDock Vina program revealed that the phenyl rings of PhSeSePh are attracted by hydrophobic residues (*i.e.*, W407 and L409) located in the active site pocket. The Se–Se region is positioned at a distance of 5.6–6.7 Å from the free selenol of U498 (Fig. 6). In addition, the phenyl rings present an intramolecular π–π stacking. The

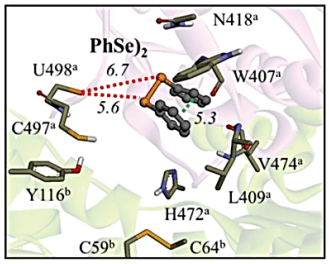

Fig. 6 Virtual model of the lowest free energy conformation of diphenyl diselenide – **(PhSe)$_2$** – docked into the redox-active site of TrxR-1. Red dotted lines show the distance (in Å) between Se from diphenyl diselenide and Se from Sec498 (U498). The green dotted line represents the π–π stacking. *a* and *b* indicate the chains of TrxR-1.

lowest free energy conformations of compounds **A–D** are shown in Fig. 7. The analysis indicated that all molecules can interact with the selenolate from TrxR (U498), with the distance Se···Se varying from about 4.0 to 6.0 Å. The amide and carboxyl moieties in compounds **A–D** can form H-bonds with the polar groups of the amino acid residues N418, W407, V474, L409, H472, Y116, and C497. The carboxyl groups of **A** and **B** interacted by H-bonds with N418 and W407 and with V474 and L409 and their phenyl rings presented an intramolecular π–π stacking (Fig. 7). On the other hand, in compounds **C** and **D**, one carboxyl moiety interacted with V474 and L409, and the other carboxyl group made an H-bond with H472 (Fig. 7C and D). In addition, the carbonyl moiety of the amide bond interacts by an H-bond with Y116 and/or C497.

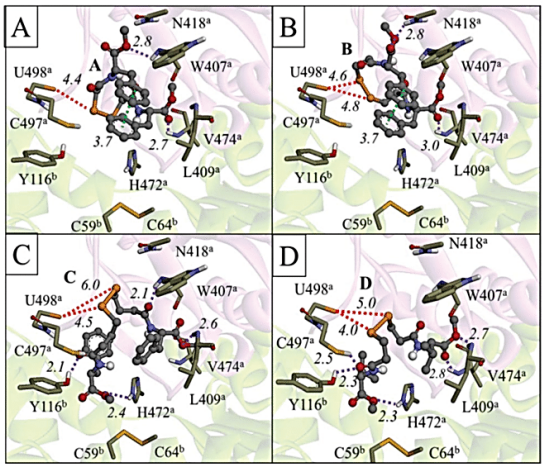

Fig. 7 Virtual models of the lowest free energy conformations of diselenoamino acid derivatives **A–D** docked into the redox-active site of TrxR-1, proposed by the AutoDock Vina program. Purple dotted lines show H-bonds (in Å). Red dotted lines show the distance (in Å) between the Se atom from **A–D** and Se from Sec498 (U498). The green dotted line represents the π–π stacking. *a* and *b* indicate the chains of TrxR-1.

The analysis of free energy binding obtained in the AutoDock Vina (Table 4) indicated that there is no correlation between the ΔG_{bind} and the NADPH oxidation. This can be explained because the molecular docking simulated the first step of the reaction, *i.e.*, the interaction between the enzyme (TrxR) and ligand (diselenides molecules), and not all the steps involved in the catalysis. Thus, although PhSeSePh and **D** present a higher ΔG_{bind} than **A–C**, they were better substrates of TrxR than their analogues. Based on these features, we suppose that the diselenoamino acids **C** and **D** are a better substrate of TrxR-1 than **A–B**, due to the lower steric effects, and have a higher degree of freedom in the active site of TrxR-1 than **A–B** (that have intermolecular π–π stacking, which decreases their flexibility). The diphenyl diselenide is a better TrxR substrate probably due to its lower steric effect and higher degree of freedom than **D**.

Thiobarbituric acid reactive substance measurement

The thiobarbituric acid reactive substance (TBARS) assay is widely used to measure lipid peroxidation and antioxidant activity.[49] Fe(II) induced a significant increase in TBARS formation ($p < 0.05$) in rat brain homogenates that were blocked with PhSeSePh at 40 and 80 μM (the positive control, Fig. 8). The diselenoamino acid derivatives **C** and **D** exhibited only a weak antioxidant activity against iron-induced lipid peroxidation (Fig. 8), while compounds **A** and **B** were ineffective. Possibly, the protective effect against lipid peroxidation presented by diselenides **A–D** could be mediated by a different mechanism other than *via* their thiol peroxidase activity.

Comparisons of the relative activities

The comparisons of the relative activities of the diselenoamino acids **A–D** and diphenyl diselenide as thiol peroxidase-like mimetics, thiol oxidase agents, and TrxR substrates are shown in Table 5. According to the GPx-like, thiol oxidase, TrxR substrate activity and TBARS results, compounds **C** and **D** presented the best antioxidant activities that were slightly lower than the positive control PhSeSePh.

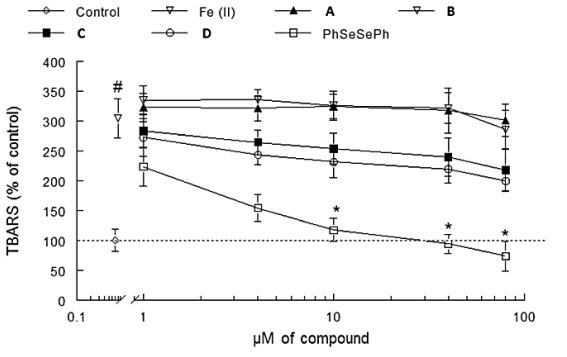

Fig. 8 Effect of different concentrations of compounds **A–D** and PhSeSePh (used as a positive control) on TBARS formation induced by Fe(II). Values are expressed as mean ± S.E.M from 3 to 4 independent experiments performed in triplicate. *represents the difference in relation to Fe(II)-induced TBARS when compared to those induced by Fe(II) and treated with compounds.

Table 5 Comparisons of the relative activities (GPx-like, thiol oxidase, Trx substrate activity and TBARS) of diselenoamino acid compounds **A–D**. Relative activities were calculated in relation to the control (arbitrary value of 1.00), *i.e.*, activity determined in the absence of diselenoamino acid compounds. For TBARS, calculations were related to **$(PhSe)_2$** and it means the inhibition percentage

	[ ] μM	Control	A	B	C	D	$(PhSe)_2$
Gpx-like	5	1.0	—	—	2.91	3.49	2.5
	10	1.0	—	—	2.08	2.72	3.32
	15	1.0	—	—	2.71	4.39	3.73
	25	1.0	—	—	4.0	4.76	5.4
Thiol oxidase	100[a]	1.0	2.62	3.16	4.42	5.0	4.0
	100[b]	1.0	3.66	3.5	3.84	4.78	3.15
	100[c]	1.0	2.14	2.56	5.17	7.46	6.76
TrxR	5	1.0	2.39	2.46	2.61	3.26	5.65
	15	1.0	2.11	2.17	3.91	4.79	8.26
TBARS	100	—	0.14	0.32	0.43	0.48	1.0

[a] GSH. [b] Captropil. [c] DTT.

Experimental

Chemicals

Tris-HCl, thiobarbituric acid (TBA), and malonaldehyde bis-(dimethyl acetal; MDA) were obtained from Sigma (St Louis, MO, USA). Ferrous sulfate, chlorhydric acid, and acetic acid were obtained from Merck (Rio de Janeiro, RJ, Brazil). All other chemicals were of analytical grade and obtained from standard commercial suppliers. The selenoamino acids **A–D** were synthesized according to Alberto (2009).[5]

Animals

Male Wistar rats (±3 months old), weighing between 270–320 g, from our own breeding colony (Animal Householding, UFSM, Brazil) were kept in cages with free access to foods and water in a room with controlled temperature (22 °C ± 3) and in a 12 h light/dark cycle with lights on at 7:00 am. The animals were maintained and used in accordance with the guidelines of the Brazilian Association for Laboratory Animal Science (COBEA).

Preparation of brain homogenates

Rats were euthanized by decapitation and the encephalic tissue (whole brain) was rapidly dissected, placed on ice and weighed. Tissues were immediately homogenized in cold 10 mM Tris-HCl, pH 7.5 (1/10, w/v). The homogenate was centrifuged for 10 min at 4000*g* to yield a pellet that was discarded and a low-speed supernatant (S1) was used in the experiments.

Determination of GPx like activity

A catalytic GPx-like model reaction (H_2O_2 + 2PhSH → $2H_2O$ + PhSSPh) was performed according to Iwaoka and Tomoda's

method (1994).[50] The reaction was initiated by the addition of H_2O_2 (to the final concentrations of 5, 10, 15 and 30 mM) to a methanol solution containing thiophenol (PhSH at 1.9 mM), diphenyl diselenide (PhSeSePh, which was used as positive control) or the diselenoamino acids **A–D** at different concentrations (5, 10, 15 and 25 μM). The reactions were carried out at 30 °C and monitored by UV spectroscopy at 305 nm. T_{50} values (the time required to consume 50% of PhSH) were calculated for each compound. During the assay, appreciable (if any) formation of the dehydroalanine-derivatives from the diselenoamino acid derivative beta-hydride elimination was not observed. Indeed, one aspect that has to be considered here is the low stability of the selenenic intermediate formed after the reaction of selenol intermediates with peroxides,[51,52] and although the formation of selenenic acid intermediates of the compounds used here can be unstable and susceptible to beta-hydride elimination of the Se moiety, the presence of an excess of reducing thiol compounds in the assay medium possibly hampered the degradation and the beta-elimination of the selenium moiety. The reaction of the thiol/thiolate reducing agents with selenenic acid is normally very fast and transforms the unstable intermediate (–SeOH) into a more stable (R–S–Se–R′) intermediate. Anyway, in order to clarify this issue, the investigation of beta-elimination of Se from diselenides should be done with sensitive analytical procedures.

Determination of thiol oxidase activity

Thiol oxidase activity was determined according to Ellman's method.[53] The thiol content was determined in the absence of a biological sample. The system allows determining whether or not the new diselenide compounds oxidize low-molecular-mass thiol compounds (reduced glutathione or GSH (1 mM), captopril (1 mM) or dithiothreitol or DTT (0.5 mM)). Diselenoamino acid compounds (**A–D**) and PhSeSePh (100 μM) were dissolved in MeOH and incubated (37 °C) in a reaction medium containing 50 mM Tris/HCl buffer (pH 7.4) and the thiol compounds. Basal thiol levels are around 100 nmol mL^{-1} because an aliquot of 100 μL was removed from the initial concentration of thiol. Then, it was added to the final reaction system, containing the Ellman's reagent DTNB and 100 mM Tris/HCl buffer (pH 7.4). Samples were read at 412 nm. Standard curves were constructed using GSH, captopril or DTT.

Thioredoxin reductase assay

TrxR from rat liver was partially purified as described in Wagner *et al.*, 2010.[54] TrxR activity was determined according to Zhao *et al.*[30,47] in a buffer containing 50 mM Tris-HCl, 1 mM EDTA, pH 7.5, 100 μL of TrxR (10 μg protein per mL of reaction medium) and 100 μM of NADPH. Reactions were started with the addition of diselenoamino acid derivatives.

Docking simulation between organoselenide compounds and the rat TrxR

Docking simulation of the organoselenium compounds with TrxR-1 was carried out using AutoDock Vina 1.1.1.[55,56] The crystal structure of rat (*Rattus novergicus*) TrxR-1 was obtained from the RCSB Protein DataBank (http://www.rcsb.org/pdb/) and used as the macromolecule (PDB entry code: 1H6V).[57] The chains A and B from the 1H6V structure were used in the docking, whereas the water molecules and other chains were removed. The hydrogen atoms were added by the Chimera 1.8 software.[58] The rat TrxR-1 has a selenocysteinyl residue (Sec498 or U498) in the catalytic site;[48,57] consequently, the sulfur atom of Cys498 (from chain A) was replaced by selenium (to create the Sec498). The Sec498 was considered deprotonated (Se^-), because the pka of Sec is near 5.[59] The ligands (diselenoamino acids **A–D** and PhSeSePh) were built and optimized in the software Avogadro 1.1.1,[60] with the universal force field (UFF) (5000 steps),[61] followed by a semi-empirical PM6[62] geometry optimization using the program MOPAC2012.[63] The ligands and protein were generated in the *pdbqt* format using AutoDockTools, where the ligands were considered flexible (with PM6 charges), and the enzyme rigid (with Gasteiger charges).[64] The selenium atom partial charge (−0.814) of the Sec498 was obtained by semi-empirical PM6 single point calculation with the dielectric constant of water in the MOPAC program, using the residues at 5 Å of distance from the Se atom. The grid was centered in the selenium atom in the C-terminal region (x = 2.894; y = 10.929; z = 156.561). The grid box size was set at 30 × 30 × 30 Å (x, y and z dimensions) and the spacing between grid points was set at 1.0 Å. The conformers with the lower binding free energy were analyzed in the Accelrys Discovery Studio 3.5.[65]

Computational details

First-principles calculations based on density functional theory (DFT) were performed using the Gaussian 09 package.[66] The hybrid B3LYP functional was employed to treat the exchange and correlation functional,[67,68] with the molecular orbitals being described by the 6-311G Gaussian basis set[69] augmented with diffuse and polarization functions. Geometry optimizations were performed and the obtained geometries were verified to consider only real vibrational frequencies. All calculations (geometry optimizations and vibrational frequencies) were performed using methanol as the solvent (dielectric constant = 32.613), through the Polarizable Continuum Model.[70]

Thiobarbituric acid reactive substances (TBARS)

TBARS production was determined as described by Ohkawa, H. *et al.*[71] and Puntel *et al.*[72] Aliquots of the homogenate (200 μL) from tissues were incubated at 37 °C in a water bath in the presence of different concentrations of diselenide compounds (0–80 μM) and with the freshly prepared Fe(II) (10 μM). The color reaction was developed by adding 200 μL 8.1% SDS (sodium dodecyl sulfate) to the reaction mixture containing S1 from rat brain. This was subsequently followed by the addition of 500 μL of an acetic acid/HCl (pH 3.4) mixture and 500 μL of 0.6% thiobarbituric acid (TBA). This mixture was incubated at 100 °C for 1 h. TBARS were measured at 532 nm and the absor-

bance was compared with the standard curve using malondialdehyde (MDA).

Statistical analyses

Values were expressed as mean ± S.E.M. Statistical analysis was performed by one-way ANOVA, followed by Duncan's multiple range tests when appropriated. The results were considered statistically significant for $P < 0.05$.

Conclusions

In summary, we have evaluated a new class of chiral diselenoamino acid derivatives as GPx mimics, catalyzing the reduction of H_2O_2 to water at the expense of thiophenol using a very low amount of catalyst. The diselenides tested in this work showed promising mimetic properties. Taking the results together, we suppose that under *in vivo* physiological conditions (*i.e.*, low concentrations of peroxides nmol L^{-1} to μmol L^{-1} and high concentrations of reducing thiols mmol L^{-1}) the diselenides can be transformed to the selenol intermediates by the TrxR enzyme isoforms and, consequently, present the peroxide scavenger activity through the GPx-like cycle as shown in Scheme 2. The direct interaction of thiols with diselenides is also possible, but the relative contributions of each pathway to their antioxidant effects have not yet been clarified. Our study showed that there are two key factors for improving the catalytic efficiency of GPx mimics tested in our study. First, diselenides are influenced by the steric effect of the aminoacid residue (best catalyst: compound **D**), and second, the number of carbon atoms between the amino acid moiety and the Se atom in the diselenide structure (best catalyst: compound **C**). We conclude that these conditions are significant considering the design mimics with high catalytic efficiency. This investigation of compounds able to imitate selenium-containing enzymes may yield useful agents as artificial catalysts for medical applications, and the antioxidant activity of diselenoamino acid derivatives can be attributed to their capacity to mimic GPx and to be a substrate for mammalian TrxR.

Conflicts of interest

The authors declare no conflicts of interest.

Acknowledgements

The authors would like to acknowledge the financial support by FAPERGS/CNPq 12/2014-PRONEX: no. 16/2551-0000, CAPES, CNPq – Brazil, INCT-EN: For Cerebral Diseases, Excitotoxicty and Neuroprotection. The calculations were performed using the computational facilities of CPAD/UFSM.

References

1 L. Flohe, *Curr. Top. Cell. Regul.*, 1985, **27**, 473.
2 F. Ursini, M. Maiorino, R. Brigelius-Flohe, K. D. Aumann, A. Roveri, D. Schomburg and L. Flohe, *Methods Enzymol.*, 1995, **252**, 38.
3 N. V. Barbosa, C. W. Nogueira, P. A. Nogara, A. F. de Bem, M. Aschner and J. B. T. Rocha, *Metallomics*, 2017, **9**, 1703.
4 M. Iwaoka and S. Tomoda, *J. Am. Chem. Soc.*, 1994, **116**, 2557.
5 E. E. Alberto, L. C. Soares, J. H. Sudati, A. C. A. Borges, J. B. T. Rocha and A. L. Braga, *Eur. J. Org. Chem.*, 2009, 4211.
6 D. Bhowmick and G. Mugesh, *Org. Biomol. Chem.*, 2015, **13**, 10262.
7 A. L. Braga, E. E. Alberto, L. C. Soares, J. B. T. Rocha, J. H. Sudati and D. H. Roos, *Org. Biomol. Chem.*, 2009, **7**, 43.
8 R. F. S. Canto, F. A. R. Barbosa, V. Nascimento, A. S. de Oliveira, I. M. C. Brighente and A. L. Braga, *Org. Biomol. Chem.*, 2014, **12**, 3470.
9 P. Prabhu, B. G. Singh, M. Noguchi, P. P. Phadnis, V. K. Jain, M. Iwaoka and I. Priyadarsini, *Org. Biomol. Chem.*, 2014, **12**, 2404.
10 S. J. Balkrishna, S. Kumar, G. K. Azad, B. S. Bhakuni, P. Panini, N. Ahalawat, R. S. Tomar, M. R. Dettyc and S. Kumar, *Org. Biomol. Chem.*, 2014, **12**, 1215.
11 J. B. T. Rocha and C. W. Nogueira, *J. Braz. Chem. Soc.*, 2010, **21**, 2055.
12 K. Selvakumar, P. Shah, H. B. Singh and R. J. Butcher, *Chem. – Eur. J.*, 2011, **17**, 12741.
13 S.-C. Yu, D.-M. Ri and H. Kühn, *J. Organomet. Chem.*, 2018, **862**, 86.
14 R. Kheirabadi, M. Izadyar and M. R. Housaindokht, *J. Phys. Chem. A*, 2018, **122**, 36.
15 B. K. Sarma and G. Mugesh, *J. Am. Chem. Soc.*, 2005, **127**, 11477.
16 R. Morgenstern, I. A. Cotgreave and L. Engman, *Chem.-Biol. Interact.*, 1992, **84**, 77.
17 H. Fischer and N. Dereu, *Bull. Soc. Chim. Belg.*, 1987, **96**, 757.
18 B. K. Sarma and G. Mugesh, *Chem. – Eur. J.*, 2008, **14**, 10603.
19 S. Antony and C. A. Bayse, *Inorg. Chem.*, 2011, **50**, 12075.
20 L. P. Wolters and L. Orian, *Curr. Org. Chem.*, 2016, **20**, 189.
21 K. Satheeshkumar and G. Mugesh, *Chem. – Eur. J.*, 2011, **17**, 4849.
22 V. Nascimento, E. E. Alberto, D. W. Tondo, D. Dambrowski, M. R. Detty, F. Nome and A. L. Braga, *J. Am. Chem. Soc.*, 2012, **134**, 138.
23 G. Ribaudo, M. Bellanda, I. Menegazzo, L. P. Wolters, M. Bortoli, G. Ferrer-Sueta, G. Zagotto and L. Orian, *Chem. – Eur. J.*, 2017, **23**, 2405.
24 A. Wendel, M. Fausel, H. Safayhi, G. Tiegs and R. A. Otter, *Biochem. Pharmacol.*, 1984, **33**, 3241.

25 C. W. Nogueira, G. Zeni and J. B. Rocha, *Chem. Rev.*, 2004, **104**, 6255.
26 D. F. Meinerz, J. H. Sudati, D. B. Santos, A. Frediani, E. E. Alberto, J. Allebrandt, J. L. Franco, N. B. Barbosa, M. Aschner and J. B. T. Rocha, *Arch. Toxicol.*, 2011, **85**, 43.
27 S. Shaaban, A. Negm, M. A. Sobh and L. A. Wessjohann, *Eur. J. Med. Chem.*, 2015, **5**, 190.
28 V. P. Singh, J. F. Poon, R. J. Butcher, X. Lu, G. Mestres, M. K. Ott and L. Engman, *J. Org. Chem.*, 2015, **80**, 7385.
29 B. K. Sarma and G. Mugesh, *Org. Biomol. Chem.*, 2008, **6**, 965.
30 R. Zhao and A. Holmgren, *J. Biol. Chem.*, 2002, **42**, 39456.
31 A. de Freitas, A. de Souza Prestes, C. Wagner, J. H. Sudati, D. Alves, L. O. Porciúncula, I. J. Kade and J. B. T. Rocha, *Molecules*, 2010, **15**, 7699.
32 N. B. Barbosa, J. B. Rocha, G. Zeni, T. Emanuelli, M. C. Beque and A. L. Braga, *Toxicol. Appl. Pharmacol.*, 1998, **149**, 243.
33 E. N. Maciel, R. C. Bolzan, A. L. Braga and J. B. T. Rocha, *J. Biochem. Mol. Toxicol.*, 2000, **14**, 310.
34 M. Farina, N. V. Barbosa, C. W. Nogueira, V. Folmer, G. Zeni, L. H. Andrade, A. L. Braga and J. B. T. Rocha, *Braz. J. Med. Biol. Res.*, 2002, **35**, 623.
35 T. H. Lugokenski, L. G. Muller, P. S. Taube, J. B. T. Rocha and M. E. Pereira, *Drug Chem. Toxicol.*, 2011, **34**, 66.
36 L. S. Galant, M. M. Braga, D. de Souza, A. F. de Bem, L. Sancineto, C. Santi and J. B. T. da Rocha, *Free Radical Res.*, 2017, **51**, 657.
37 F. L. Lovato, J. B. Teixeira da Rocha and C. L. Dalla Corte, *Chem. Res. Toxicol.*, 2017, **30**, 1134.
38 A. F. de Bem, B. Fiuza, P. Calcerrada, P. M. Brito, G. Peluffo, T. C. Dinis, M. Trujillo, J. B. Rocha, R. Radi and L. M. Almeida, *Nitric Oxide*, 2013, **31**, 20.
39 S. R. Wilson, P. A. Zucker, R. R. C. Huang and A. Spector, *J. Am. Chem. Soc.*, 1989, **111**, 5936.
40 B. Mishra, K. I. Priyadarsini, H. Mohan and G. Mugesh, *Bioorg. Med. Chem. Lett.*, 2006, **16**, 5334.
41 J. Fuchs, L. Packer and G. Zimmer, *Lipoic acid in health and disease*, Macel Dekker Inc., New York, 1997.
42 F. A. Bulat, E. Chamorro, P. Fuentealba and A. Toro-Labbe, *J. Phys. Chem. A*, 2004, **108**, 342.
43 P. K. Chattaraj, S. Duleya and L. R. Domingo, *Org. Biomol. Chem.*, 2012, **10**, 2855.
44 L. R. Domingo and P. Perez, *Org. Biomol. Chem.*, 2011, **9**, 7168.
45 R. M. LoPachin, T. Gavin, A. DeCaprio and D. S. Barber, *Chem. Res. Toxicol.*, 2012, **25**, 239.
46 R. G. Parr and R. G. Pearson, *J. Am. Chem. Soc.*, 1983, **105**, 7512.
47 R. Zhao, H. Masayasu and A. Holmgren, *Proc. Natl. Acad. Sci. U. S. A.*, 2002, **99**, 8579.
48 A. Holmgren, *Antioxid. Redox Signaling*, 2000, **2**, 811.
49 M. A. Ghani, C. Barril, D. R. Bedgood Jr. and P. D. Prenzler, *Food Chem.*, 2017, **230**, 195.
50 M. Iwaoka and S. Tomoda, *J. Am. Chem. Soc.*, 1994, **116**, 2557.
51 L. Orian, P. Mauri, A. Roveri, S. Toppo, L. Benazzi, V. Bosello-Travain, A. De Palma, M. Maiorino, G. Miotto, M. Zaccarin, A. Polimeno, L. Flohé and F. Ursini, *Free Radicals Biol. Med.*, 2015, **87**, 1.
52 S. Ma and R. M. Caprioli, *J. Am. Soc. Mass Spectrom.*, 2003, **14**, 593.
53 G. L. Ellman, *Arch. Biochem. Biophys.*, 1959, **82**, 70.
54 C. Wagner, J. H. Sudati, C. W. Nogueira and J. B. T. Rocha, *Biometals*, 2010, **23**, 1171.
55 O. Trott and A. J. Olson, *J. Comput. Chem.*, 2010, **31**, 455.
56 R. A. Saraiva, D. C. Bueno, P. A. Nogara and J. B. Rocha, *J. Toxicol. Environ. Health, Part A*, 2012, **75**, 1012.
57 T. Sandalova, L. Zhong, Y. Lindqvist, A. Holmgren and G. Schneider, *Proc. Natl. Acad. Sci. U. S. A.*, 2001, **98**, 9533.
58 E. F. Pettersen, T. D. Goddard, C. C. Huang, G. S. Couch, D. M. Greenblatt, E. C. Meng and T. E. Ferrin, *J. Comput. Chem.*, 2004, **25**, 1605.
59 B. J. Byun and Y. K. Kang, *Biopolymers*, 2011, **95**, 345.
60 M. D. Hanwell, D. E. Curtis, D. C. Lonie, T. Vandermeersch and E. Zurek, *J. Cheminf.*, 2012, **4**, 1.
61 A. K. Rappe, C. J. Casewit, K. S. Colwell, W. A. Goddard III and V. M. Skiff, *J. Am. Chem. Soc.*, 1992, **114**, 10024.
62 J. J. P. Stewart, *J. Mol. Model.*, 2007, **13**, 1173.
63 J. J. P. Stewart, *MOPAC2012*, Stewart Computational Chemistry, Colorado Springs, CO, USA, 2012, http://OpenMOPAC.net.
64 G. M. Morris, R. Huey, W. Lindstrom, M. F. Sanner, R. K. Belew, D. S. Goodsell and A. J. Olson, *J. Comput. Chem.*, 2009, **30**, 2785.
65 Dassault Systèmes BIOVIA, *Discovery Studio Modeling Environment, Release 2017*, Dassault Systèmes, San Diego, 2016.
66 M. J. Frisch, G. W. Trucks, H. B. Schlegel, G. E. Scuseria, M. A. Robb, J. R. Cheeseman, G. Scalmani, V. Barone, B. Mennucci, G. A. Petersson, H. Nakatsuji, M. Caricato, X. Li, H. P. Hratchian, A. F. Izmaylov, J. Bloino, G. Zheng, J. L. Sonnenberg, M. Hada, M. Ehara, K. Toyota, R. Fukuda, J. Hasegawa, M. Ishida, T. Nakajima, Y. Honda, O. Kitao, H. Nakai, T. Vreven, J. A. Montgomery Jr., J. E. Peralta, F. Ogliaro, M. Bearpark, J. J. Heyd, E. Brothers, K. N. Kudin, V. N. Staroverov, R. Kobayashi, J. Normand, K. Raghavachari, A. Rendell, J. C. Burant, S. S. Iyengar, J. Tomasi, M. Cossi, N. Rega, J. M. Millam, M. Klene, J. E. Knox, J. B. Cross, V. Bakken, C. Adamo, J. Jaramillo, R. Gomperts, R. E. Stratmann, O. Yazyev, A. J. Austin, R. Cammi, C. Pomelli, J. W. Ochterski, R. L. Martin, K. Morokuma, V. G. Zakrzewski, G. A. Voth, P. Salvador, J. J. Dannenberg, S. Dapprich, A. D. Daniels, Ö. Farkas, J. B. Foresman, J. V. Ortiz, J. Cioslowski and D. J. Fox, *Gaussian 09 Rev. A.2*, Gaussian, Inc., Wallingford, CT, 2009.
67 A. D. Becke, *J. Chem. Phys.*, 1993, **98**, 1372.
68 C. Lee, W. Yang and R. G. Parr, *Phys. Rev. B: Condens. Matter Mater. Phys.*, 1988, **37**, 785.

69 R. Krishnan, J. S. Binkley, R. Seeger and J. A. Pople, *J. Chem. Phys.*, 1980, **72**, 650.
70 J. Tomasi, B. Mennucci and R. Cammi, *Chem. Rev.*, 2005, **105**, 2999.
71 H. Ohkawa, N. Ohishi and K. Yagi, *Anal. Biochem.*, 1979, **95**, 351.
72 R. L. Puntel, C. W. Nogueira and J. B. T. Rocha, *Neurochem. Res.*, 2005, **30**, 417.

4.2. CAPÍTULO 2: INTERAÇÕES BIOLÓGICAS DO MeHg

Para uma melhor compreensão da toxicologia do MeHg, foram realizadas simulações do modo de ligação de quatro diferentes espécies químicas de MeHg (MeHgOH, MeHgCl, MeHgCys, e MeHgGSH) com as enzimas GPx e TrxR. Os dados obtidos estão descritos na forma de um manuscrito intitulado: ***Interaction between methylmercury and the selenoenzymes GPx and TrxR***, a ser submetido para *Journal of Molecular Modeling*.

Além disso, visto que o MeHg poderia se ligar ao átomo de Se da Sec presente no sítio ativo da GPx, cálculos de DFT foram realizados para verificar a viabilidade do aduto Sec–HgMe sofrer uma reação de β-eliminação, levando assim a formação da desidroalanina (Dha). Os resultados foram representados através de um manuscrito ***β-elimination reaction from methyl(mercury)chalcogen oxides: a theoretical study***, que será submetido para a revista *ChemPhysChem*.

4.2.1. Manuscrito 1: Interações entre metilmercúrio e as selenoenzimas GPx e TrxR

Interaction between methylmercury and the selenoenzymes GPx and TrxR

P. A. Nogara[a,b], M. Bortoli[b], L. Orian[b], and J. B. T. Rocha[a*]

[a] Departamento de Bioquímica e Biologia Molecular, Universidade Federal de Santa Maria (UFSM), Santa Maria, 97105-900, RS, Brazil; *Corresponding author: jbtrocha@yahoo.com.br

[b] Dipartimento di Scienze Chimiche, Università degli Studi di Padova, Via Marzolo 1 35131 Padova, Italy.

Abstract

MeHg is a potent neurotoxin that can inhibit the function of essential selenoenzymes involved in the antioxidant system, such as glutathione peroxidase (GPx) and thioredoxin reductase. Here, we proposed a molecular mechanism of inhibition based on the docking simulations between MeHg species and GPx and TrxR enzymes. In this sense, four MeHg molecules were studied (MeHgOH, MeHgCl, MeHgCys, and MeHgGSH). The possibility of an adequate orientation between the selenol group from selenocysteine and the Hg moiety, indicates that the formation of Se-Hg could occur, inhibiting the proteins.

1- Introduction

Methylmercury (MeHg) is a neurotoxin that is found in food, such as fish and rice. MeHg's toxicity is mediated by its interaction with thiol (R-SH) and/or selenol (R-SeH) groups in proteins, due to the presence of the cysteine and selenocysteine residues [1]. However, the identification of MeHg's targets is elusive. Previous studies have been indicating that the selenoenzymes glutathione peroxidase (GPx) [2] and thioredoxin reductase (TrxR) [3, 4] are inhibited by MeHg (IC_{50} = 2 μM and 19.7 nM, respectively), due to the high affinity between the Hg and Se atoms. The GPx and TrxR are important antioxidant enzymes involved in the metabolism of reactive oxygen species (ROS). High levels of ROS results in oxidative stress and could cause cell death [5]. In this way, the GPx and TrxR inhibition by MeHg could be involved in the neurotoxicity of this chemical.

Mercuric selenide (HgSe) nanoparticles have been found in mammals' brains and liver, indicating that the Hg species could remove Se atoms from proteins [6, 7]. In fact, previous studies

demonstrated that the GPx inhibition could be due to the Se atom lost, leading to the formation of dehydroalanine (Dha) [8, 9]. However, we do not know if the binding of MeHg in selenoenzymes has this same effect. Here, we performed docking simulations between the TrxR-1 and GPx-1, with the methylmercury hydroxide (MeHgOH), methylmercury chloride (MeHgCl), and methylmercury-cysteine (MeHgCys) to understand the enzyme-inhibitor complex formation.

2- Materials and Methods

AutoDock Vina program was used in the docking simulations. The 3D structures of the GPx-1 and TrxR-1, both as dimers, were obtained from the Protein Data Bank (PDB) with the codes 1GP1 and 2J3N, respectively. The grid box of 15 $Å^3$ was centered on the selenium atom from the enzymes. Before, the structures of the enzymes were submitted to molecular dynamics simulations (MD) to obtain a more realistic protein conformation. First, the initial enzyme structures were solvated with TIP3P water (21495 water molecules for GPx1 and 33566 for TrxR) in a truncated octahedral box. Afterward, the systems were minimized, heated to the target temperature (298.15 K) with a constant volume constraint for 400 ps, and equilibrated for 4 ns at constant temperature and pressure (1 bar). The MD simulations were carried out for 500 ns in the same conditions of the equilibration, using the Langevin thermostat and a Monte Carlo barostat. The non-standard AMBER force field parameters for Sec were taken from the literature [10]. The structure of the ligands (MeHgOH, MeHgCl, MeHgCys, and MeHgGSH) were obtained by DFT calculations using the program ADF (Amsterdam Density Functional) using the functional and correction BLYP/D3BJ, the TZ2P base and the relativistic correction ZORA (zeroth-order regular approximation), in the water phase model [11]. The initial structure of Cys was obtained from Wilke et al. 2009 [12]. The partial charges of Mulliken were used in the ligands in the docking simulations [13]. As the Vina does not have parameters for Hg, for the docking simulations, we used Zn due to its similarities [14, 15]. However, the charge and geometric were maintained from DFT optimization. The ligand conformer with the lowest binding energy and with the best Se…Hg orientation was selected as the model of interaction.

3- Results and Discussion

Taking into account that it is difficult to know what is the MeHg specie inside of the organism, here we used four MeHg molecule models (considering the cell environment and the

presence of water, Cl anions, and the thiols of low molecular mass (LMM-SH), such as Cys and GSH). According to the docking simulations (Figures 1 and 2), the MeHgOH, MeHgCl, MeHgCys, and MeHgGSH could access the active site of GPx-1 and Trx-1 in a favourable thermodynamical process (Table 1). Despite the MeHgCys and MeHgGSH presented the lowest ΔG values (more stable complex), it does not mean that they are better inhibitor than MeHgOH and MeHgCl. It could be due to the correlation between the number of heavy atoms (≠ H) in the molecules and the predicted binding energies [16].

Table 1. Binding free energy, ΔG (kcal/mol), predicted by AutoDock Vina.

Enzyme	MeHgOH	MeHgCl	MeHgCys	MeHgGSH
GPx-1	-1.8	-1.5	-3.3	-4.1
TrxR-1	-1.9	-1.3	-3.2	-4.6

In the GPx-1, MeHgOH and MeHgCl presented similar binding pose, with Se···Hg interaction distances ranging from 4.6 to 5.4 Å. In addition, the hydroxyl moiety of MeHgOH shown H-bonds with the Asn82 and Gly46 residues, while the chlorine atom of MeHgCl interacted with Arg177 by electrostatic interaction (Figure 1). The MeHg moiety of MeHgCys showed the same Se···Hg distance that MeHgCl (5.4 Å). In addition, MeHgCys interacted with the Asn159 backbone via H-bonds, and with Phe145 by anion-π interactions. MeHgGSH showed the highest Se···Hg distance (6.1 Å) when compared with the other molecules, and presented H-bond with Thr147, anion-π and salt-bridge interactions with His79, Arg50, and Arg177 residues, respectively.

In the same way, for the TrxR-1 the MeHgOH and MeHgCl presented similar binding poses, interacting with the Sec498 by Se···Hg (3.6 Å) and with the Cys497 by H-bonds (2.5 – 3.0 Å) (Figure 2). MeHgCys interacts by H-bonds with His108 and Ser111 residues, besides of Se…Hg interaction of 4.1 Å. MeHgGSH exhibited H-bonds with Ser111, Gln494, and Asn419 residues, and the Hg atom is 5.1 Å far from Se. In addition, the carboxylic group of MeHgGSH made an intramolecular interaction with the Hg atom.

Due to the relatively short distances between the enzymes and the MeHg compounds, possibly, a nucleophilic attack could occur from the Se to the Hg atom, forming the Se–Hg bond and consequently inhibiting the enzymes. In general, TrxR-1 showed the shortest Se···Hg distance (3.6 – 5.1 Å) than GPx1 (4.6 – 6.1 Å), and it could be involved in the highest inhibition of TrxR by MeHg, than GPx.

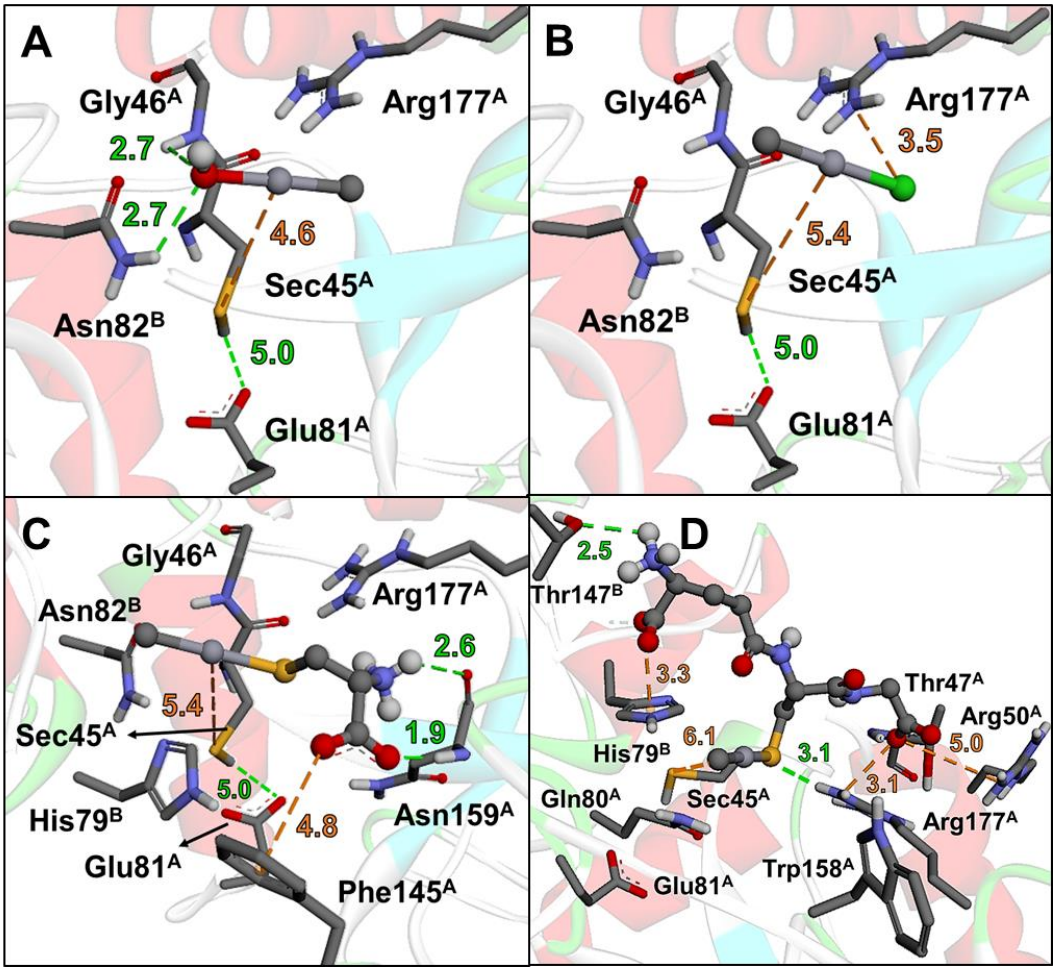

Figure 1. Docking simulations between the GPx-1 and the MeHgOH (A), MeHgCl, MeHgCys (C), and MeHgGSH molecules (D). In the residue names, A and B means the protein subunit.

In the GPx, the proximity between the carboxylic group of Glu81 and the selenol moiety from Sec45 suggests that the Glu81 could remove the proton from the –SeH (Figure 1). However, previous in silico studies, considering the GPx during the catalytic cycle, suggest that it is the substrate hydrogen peroxide (H_2O_2) which will deprotonate the Sec residue in the first step of the reaction [9, 10]. This process is facilitated when the Trp residue from the catalytic tetrad acts as a base removing a water proton, and this water will accept a proton from H_2O_2 (Sec_Se-**H** + HOO**H** + HO**H** + N(H)_Trp → Sec_Se^- + **H**OOH + **H**OH + **H**N^+(H)_Trp). In this sense, the presence of a water molecule and the Trp residue (a base) could be necessary to activate the nucleophilic attack of SeH on the MeHg. Here, the Trp158 does not interact directly with the MeHg species, indicating that the base could be represented by other residues, like the Glu81. In addition, the Arg177 and one/two water molecules can be necessary to make the proton exchange (Figure 3). The Glu81 and

water will deprotonate the Sec45, and the selenolate formed will react with the Hg from MeHg species. With the exception of the MeHgCl (where the Cl- anion is stabilized by a salt bridge with Arg177) and MeHgGSH (which the Arg177 donates a proton to the thiolate moiety), a water molecule could be necessary to deliver a proton to the hydroxyl and cysteinyl groups.

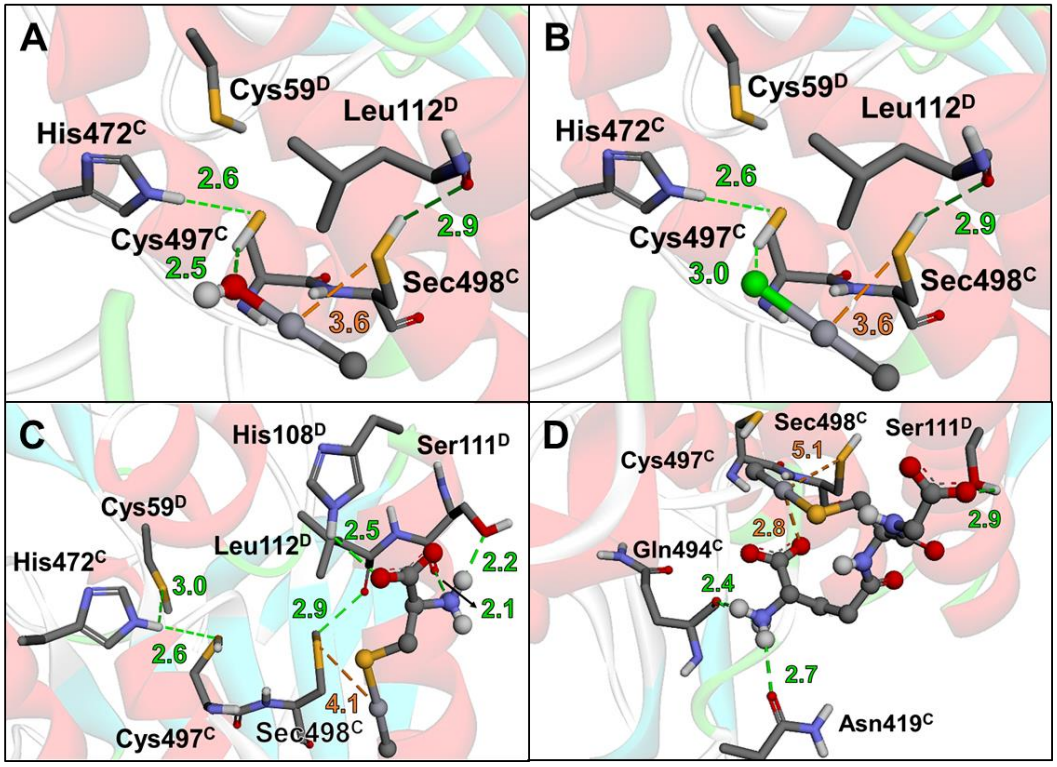

Figure 2. Docking simulations between the TrxR-1 and the MeHgOH (A), MeHgCl, MeHgCys (C), and MeHgGSH molecules (D). In the residue names, C and D means the protein subunit.

DFT studies suggest that the triad Sec498-His472-Glu477 is essential for the proton transfer and the activation of selenolate in the TrxR [17]. However, here we do not observe this H-bond network between Sec498, His472, and Glu477, probably due to the different protein conformation obtained from molecular dynamics. The proton from the –SeH also could be directly transferred to the inhibitor, as proposed for adamantane–azole gold(I) complexes [18]. The covalent bond formation between the reduced selenol and an inhibitor, such as gold, nitrosoureas, chlorodinitrobenzene, and curcumin derivatives, is well accepted as the mechanism of TrxR inhibition [19].

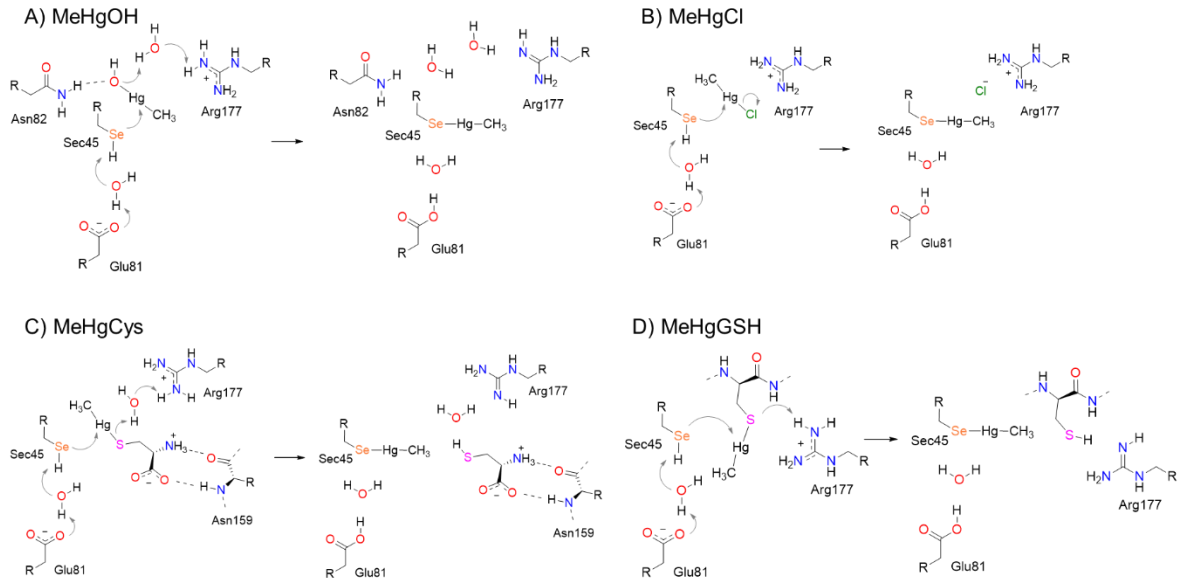

Figure 3. Possible mechanism of GPx inhibition by MeHgOH (A), MeHgCl (B), MeHgCys (C), and MeHgGSH (D).

Here, we proposed a new mechanism to TrxR inhibition by MeHg based on the docking simulations (Figure 4). Considering that Cys497 is able to remove the proton from the selenol group of Sec498 (due to the proximity between the residues), for the MeHgOH and MeHgCl the proton exchange occurs between -OH/-Cl groups, Cys497, and Sec498, leading to the formation of water/chloridric acid and the Se–Hg bond. On the other hand, for MeHgCys and MeHgGSH, the proton exchange could occur directly between Sec498, water, and MeHgCys/GSH.

Although the chemical mechanisms of inhibition are represented by a concerted mechanism (Figures 3 and 4), a stepwise reaction could occur. More studies are necessary to validate the proposed way. Maybe other molecular dynamic simulations in the presence of water molecules are necessary to verify the conformation change in the active site and the interactions of residues that can act as proton donors/acceptors.

It is important to mention here that the possibility of LMM-SH-MeHg molecules to interacts in the active site of selenoenzymes indicates that the MeHg can be delivered due to the substrate-enzyme interaction, once the MeHg is bonded in the substrate (GSH or Trx).

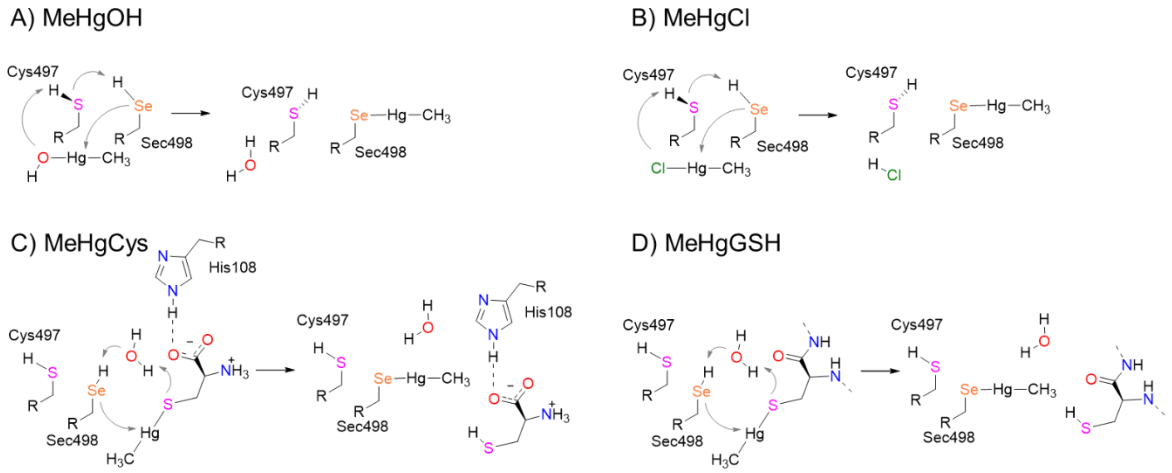

Figure 4. Proposed TrxR mechanism of inhibition by MeHgOH (A), MeHgCl (B), MeHgCys (C), and MeHgGSH (D).

4- Conclusion

The present study demonstrated that different MeHg species could interact in the active site of TrxR and GPx enzymes. The adequate orientation between the selenol group from Sec residue and the MeHg moiety suggests that a nucleophilic attack from Se to Hg could occur. The presence of water molecules in the reaction is important and needs to be more studied. The possible formation of the Se-Hg bond could be involved in the selenoenzymes inhibition by MeHg molecules.

5- References

1. Nogara PA, Oliveira CS, Schmitz GL, et al (2019) Methylmercury's chemistry: From the environment to the mammalian brain. Biochim Biophys Acta - Gen Subj 1863:129284. https://doi.org/10.1016/j.bbagen.2019.01.006

2. Farina M, Campos F, Vendrell I, et al (2009) Probucol increases glutathione peroxidase-1 activity and displays long-lasting protection against methylmercury toxicity in cerebellar granule cells. Toxicol Sci 112:416–426. https://doi.org/10.1093/toxsci/kfp219

3. Carvalho CML, Chew EH, Hashemy SI, et al (2008) Inhibition of the human thioredoxin system: A molecular mechanism of mercury toxicity. J Biol Chem 283:11913–11923. https://doi.org/10.1074/jbc.M710133200

4. Wagner C, Sudati JH, Nogueira CW, Rocha JBT (2010) In vivo and in vitro inhibition of mice thioredoxin reductase by methylmercury. BioMetals 23:1171–1177. https://doi.org/10.1007/s10534-010-9367-4

5. Steinbrenner H, Sies H (2009) Protection against reactive oxygen species by selenoproteins. Biochim Biophys Acta - Gen Subj 1790:1478–1485. https://doi.org/10.1016/j.bbagen.2009.02.014

6. Gajdosechova Z, Lawan MM, Urgast DS, et al (2016) In vivo formation of natural HgSe nanoparticles in the liver and brain of pilot whales. Sci Rep 6:1–11. https://doi.org/10.1038/srep34361

7. Korbas M, Odonoghue JL, Watson GE, et al (2010) The chemical nature of mercury in human brain following poisoning or environmental exposure. ACS Chem Neurosci 1:810–818. https://doi.org/10.1021/cn1000765

8. Cho CS, Lee S, Lee GT, et al (2010) Irreversible inactivation of glutathione peroxidase 1 and reversible inactivation of peroxiredoxin ii by H2O2 in red blood cells. Antioxidants Redox Signal 12:1235–1246. https://doi.org/10.1089/ars.2009.2701

9. Orian L, Mauri P, Roveri A, et al (2015) Selenocysteine oxidation in glutathione peroxidase catalysis: An MS-supported quantum mechanics study. Free Radic Biol Med 87:1–14. https://doi.org/10.1016/j.freeradbiomed.2015.06.011

10. Bortoli M, Torsello M, Bickelhaupt FM, Orian L (2017) Role of the Chalcogen (S, Se, Te) in the Oxidation Mechanism of the Glutathione Peroxidase Active Site. ChemPhysChem 18:2990–2998. https://doi.org/10.1002/cphc.201700743

11. Madabeni A, Nogara PA, Orian L, et al (2020) Chalcogen-mercury bond formation and disruption in model Rabenstein's reactions: A computational analysis. J Comput Chem June:1–10. https://doi.org/10.1002/jcc.26371

12. Wilke JJ, Lind MC, Schaefer III HF, et al (2009) Conformers of Gaseous Cysteine. J Chem Theory Comput 5:1511–1523. https://doi.org/10.1021/ct900005c

13. Hoffmeyer RE, Singh SP, Doonan CJ, et al (2006) Molecular mimicry in mercury toxicology. Chem Res Toxicol 19:753–759. https://doi.org/10.1021/tx0503449

14. Forli S, Huey R, Pique ME, et al (2016) Computational protein–ligand docking and virtual drug screening with the AutoDock suite. Nat Protoc 11:905–919. https://doi.org/10.1038/nprot.2016.051

15. Klimaczewski CV, Nogara PA, Barbosa NV, da Rocha JBT (2018) Interaction of metals from group 10 (Ni, Pd, and Pt) and 11 (Cu, Ag, and Au) with human blood δ-ALA-D: in vitro and in silico studies. Environ Sci Pollut Res 25:30557–30566. https://doi.org/10.1007/s11356-018-3048-1

16. Chang MW, Ayeni C, Breuer S, Torbett BE (2010) Virtual screening for HIV protease inhibitors: A comparison of AutoDock 4 and Vina. PLoS One 5:1–9. https://doi.org/10.1371/journal.pone.0011955

17. Brandt W, Wessjohann LA (2005) The functional role of selenocysteine (Sec) in the catalysis mechanism of large thioredoxin reductases: Proposition of a swapping catalytic triad including a Sec-His-Glu state. ChemBioChem 6:386–394. https://doi.org/10.1002/cbic.200400276

18. Garcia A, Machado RC, Grazul RM, et al (2016) Novel antitumor adamantane-azole gold(I) complexes as potential inhibitors of thioredoxin reductase. J Biol Inorg Chem 21:275–292. https://doi.org/10.1007/s00775-016-1338-y

19. Saccoccia F, Angelucci F, Boumis G, et al (2014) Thioredoxin Reductase and its Inhibitors. Curr Protein Pept Sci 15:621–646. https://doi.org/10.2174/1389203715666140530091910

4.2.2. Manuscrito 2: Reação de β-eliminação a partir de óxidos de metil(mercúrio)calcogênios: um estudo teórico

β-elimination reaction from methyl(mercury)chalcogen oxides: a theoretical study

P. A. Nogara[a,b], A. Madabeni[b], M. Bortoli[b], J. B. T. Rocha[a*], and L. Orian[b*]

[a] Departamento de Bioquímica e Biologia Molecular, Universidade Federal de Santa Maria (UFSM), Santa Maria 97105-900, RS, Brazil
[b] Dipartimento di Scienze Chimiche, Università degli Studi di Padova, Via Marzolo 1, 35131 Padova, Italy
[*] Corresponding authors. E-mail address: laura.orian@unipd.it (L. Orian), jbtrocha@yahoo.com.br (J.B.T. Rocha).

Abstract

The synthesis of dehydroalanine (Dha) plays an important role in the antibiotic peptides synthesis, enzyme inhibition, and in the activation of synthetic organochalcogen molecules as prodrugs. Dha formation via β-elimination was investigated by DFT calculations using the methyl (Me) and methylmercury (MeHg) groups attached to the chalcogen atoms (S, Se, and Te). Our data suggested that is not necessary for the second oxidation of chalcogen atom to conduct the β-elimination. The β-elimination reaction exhibited a trend to be more favorable from 'S' to 'Te', and the reactions of 'HgMe' compounds are more favorable than the 'Me' molecules. This data helps us to better understand the glutathione peroxidase (GPx) and thioredoxin reductase (TrxR) inhibition and the metabolism of organic chalcogen compounds.

1. Introduction

Dehydroalanine (Dha) is an α,β-unsaturated amino acid, which occurs naturally in antibiotic peptides (lantibiotics) and in post-translational modifications (PTMs) of proteins. It is found in the position corresponding to the serine (Ser), cysteine (Cys), and selenocysteine (Sec) residues. The PTMs can occur via phosphorylation, glycosylation, methylation, acetylation, and lipidation of amino acid residues[1–4].

Cys and Sec residues are converted to Dha, via syn-β-elimination, as the result of their alkylation and/or oxidation to its corresponded sulfoxides and selenoxides[2,3]. The β-elimination occurs by intramolecular abstraction of the α-hydrogen by the sulfoxide/selenoxide moiety, leading to a sulfenic/selenenic acid and dehydroalanine (2-aminoacrylic acid). This mechanism is also used

to generate unsaturated compounds in synthetic organic chemistry and the incorporation of Dha in peptides (as a chemical precursor for the insertion of unnatural amino acids)[1,5–7]. In addition, pyruvate was identified as a product of Se-alkyl-L-selenocysteine (Sec-SeR, R= alkyl) after its chemical oxidation by hydrogen peroxide, and also upon incubation with rat liver microsomes[8]. In this case, Dha is hydrolyzed into pyruvate and ammonia.

However, the formation of Dha has been reported to inhibit the function of cysteine- and selenocysteine-containing proteins and enzymes, such as albumin[9], peroxiredoxin (Prx)[10], glyceraldehyde-3-phosphate dehydrogenase (GAPDH)[11], thioredoxin reductase (TrxR)[12], and glutathione peroxidase (GPx)[2,4,13,14]. For example, small electrophilic compounds, such as 1-chloro-2,4-dinitrobenzene (CDNB), reacts with S/Se atoms from Cys/Sec residues. After the oxidation, the S/Se moiety undergoes β-elimination to produce Dha[5,12]. In fact, the alkylation of Sec residues could lead to the Dha formation, indicating the loss of selenium from rat selenoprotein P and GPx in vitro[3]. On the other hand, the Dha formation plays an important role in the pharmacological action of S,Se,Te-conjugates as prodrugs due to chemopreventive and antitumor activities of S, Se, and Te moieties[15,16]. Similar to selenocystine, and selenomethionine (Mse), the amino acid methylselenocysteine (MeSec) can occur naturally in plants[17]. The oxidative decomposition of MeSeCys could generate methylseleninic acid (MeSeOOH), the simplest organoselenium with pharmacological properties, such as anticancer activity[18].

Methylmercury (MeHg) is a neurotoxicant found in fish and cereals. Industrial and anthropogenic activities have been increasing the mercury pollution[19,20] and, consequently have contributed to the biomagnification of MeHg in the aquatic food chain[21,22]. MeHg toxicity is associated with the overproduction of reactive oxygen production (ROS) and the disrupting of proteins function, due to its interaction with Cys and Sec residues[23,24]. TrxR and GPx, which are targets of MeHg, are important selenoenzymes involved in the cell antioxidant defense, reducing peroxides[4,23,25]. The binding of MeHg to Sec residues could facilitate the release of Se from proteins, likely via β-elimination reaction, which could lead to the formation of inorganic mercury selenide (HgSe). In fact, HgSe formation could be associated with selenium depletion (which disrupts the synthesis of selenoenzymes), and the selenium deficiency could increase MeHg neurotoxicity[17,23].

In this sense, the study about the potential formation of Dha from alkyl- and methylmercury-amino acids are essential for better understand their pharmacological and

toxicological mechanism of action. For this purpose, the influence of the chalcogen atom type (S, Se, and Te), its oxidation states, and the presence of Hg atom was investigated. The goal of the present study is to investigate the β-elimination reactions of methyl(mercury)chalcogen molecules, by DFT calculations. In fact, computational methods have been applied to understand the amino acids[26–29] and synthetic chalcogen-molecules reactions[30,31], indicating to be a powerful tool to be used. Here, we have used the methyl group as a model of alkyl moiety. For this purpose, as a model of amino acid structures, we used only atoms from the side chain, where the carboxylic acid and amino groups attached to the alpha-carbon were replaced by hydrogen (Figure 1). Hydrogen peroxide (H_2O_2) was used as the oxidant because it is one of the natural substrates of Sec- or Cys-containing GPx enzymes[32].

2. Materials and Methods

All Density Functional Theory (DFT) calculations were done with the Amsterdam Density Functional (ADF) program[33,34], using the TZ2P basis set, zeroth-order regular approximation (ZORA)[35], and the BLYP functional[36,37], including Grimme dispersion (BLYP-D3(BJ))[38]. As a previous study demonstrated, BLYP-D3(BJ) is an adequate level of theory to study structural and energetic features from chalcogen-mercury molecules[39]. The side chain model molecules {(ethylthio)methylmercury [EtSHgMe], (ethylselanyl)methylmercury [EtSeHgMe], (ethyltellanyl)methylmercury [EtTeHgMe], ethylmethylsulfide [EtSMe], ethylmethylselenide [EtSeMe], and ethylmethyltelluride [EtTeMe]}, and its respective mono- and dioxides were geometrically optimized in the gas phase, including the frequency calculations. All minima stationary points have real frequencies, and transition states have one imaginary frequency corresponding to the connection between reactants to products. The value 627.509 was used to convert Hartree to kcal/mol unities. The energy variation (ΔE) was determined following the equations: $\Delta E = \sum E_{products} - \sum E_{reactants}$ and $\Delta E^{\ddagger} = \sum E_{TS} - \sum E_{reactants}$.

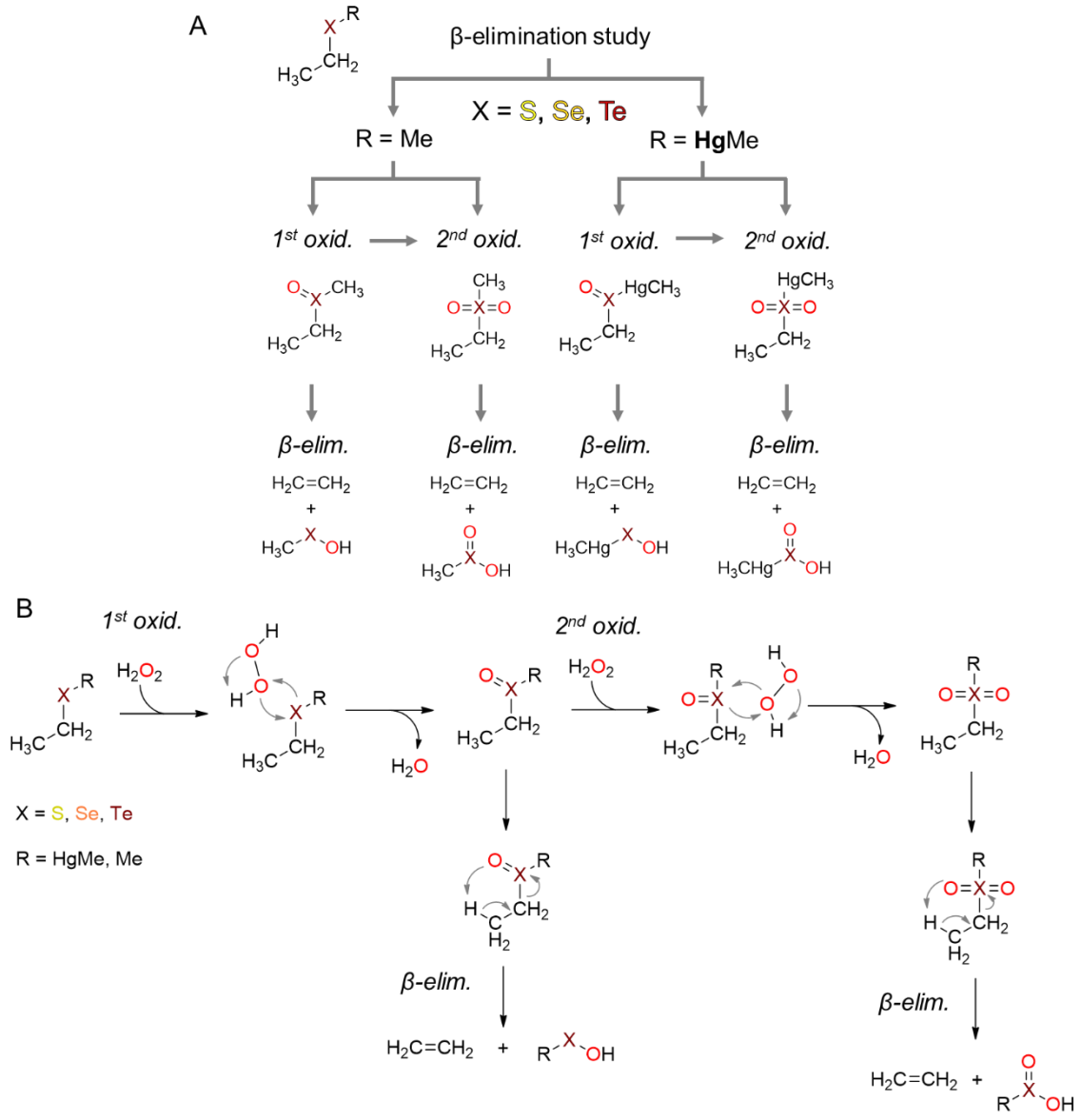

Figure 1. Design of the β-elimination study (A) and general reactions (B). The oxidation reaction occurs with H_2O_2 and releasing H_2O. β-elimination follows an intramolecular reaction.

3. Results and discussion

The global reaction energies of monoxides and dioxides formation from EtS(Hg)Me, EtSe(Hg)Me, and EtTe(Hg)Me are energetically favorable (Table 1 and Figure 2). The first oxidation of R= Me molecules (-37 to -48 kcal/mol) are more favorable than the R= HgMe species (-29 to -39 kcal/mol), however, the second oxidation global energy of 'HgMe' molecules are lower than the R= Me species, with exception of 'S' compounds. The first oxidation transition state (TS) energies of the R= HgMe and R= Me molecules demonstrated that activation energy decrease from

'S' to 'Te' ('HgMe': 8 to 0.5 kcal/mol; 'Me': 8 to -1 kcal/mol). However, the second oxidation transition state energies for R= Me molecules increase (9 to 12 kcal/mol) in relation to the first oxidation, especially for $EtSeO_2Me$ and $EtTeO_2Me$. For the R= HgMe species, the energy for 'S' decreases, for 'Se' keeps practically the same, and for 'Te' the energy increase, when compared with the first oxidation.

The β-elimination reaction showed a favorable energetic trend from 'S' to 'Te', in both cases with R= HgMe and R = Me (Table 1 and Figure 3). The EtS(Hg)Me species showed the highest transition state (22 to 42 kcal/mol) and global energies (12 to 24 kcal/mol), when compared with EtSe(Hg)Me (transition state: 13 to 21 kcal/mol; global: -13 to 4 kcal/mol), and EtTe(Hg)Me species (transition state: 10 to 16 kcal/mol; global: -23 to 0.5 kcal/mol).

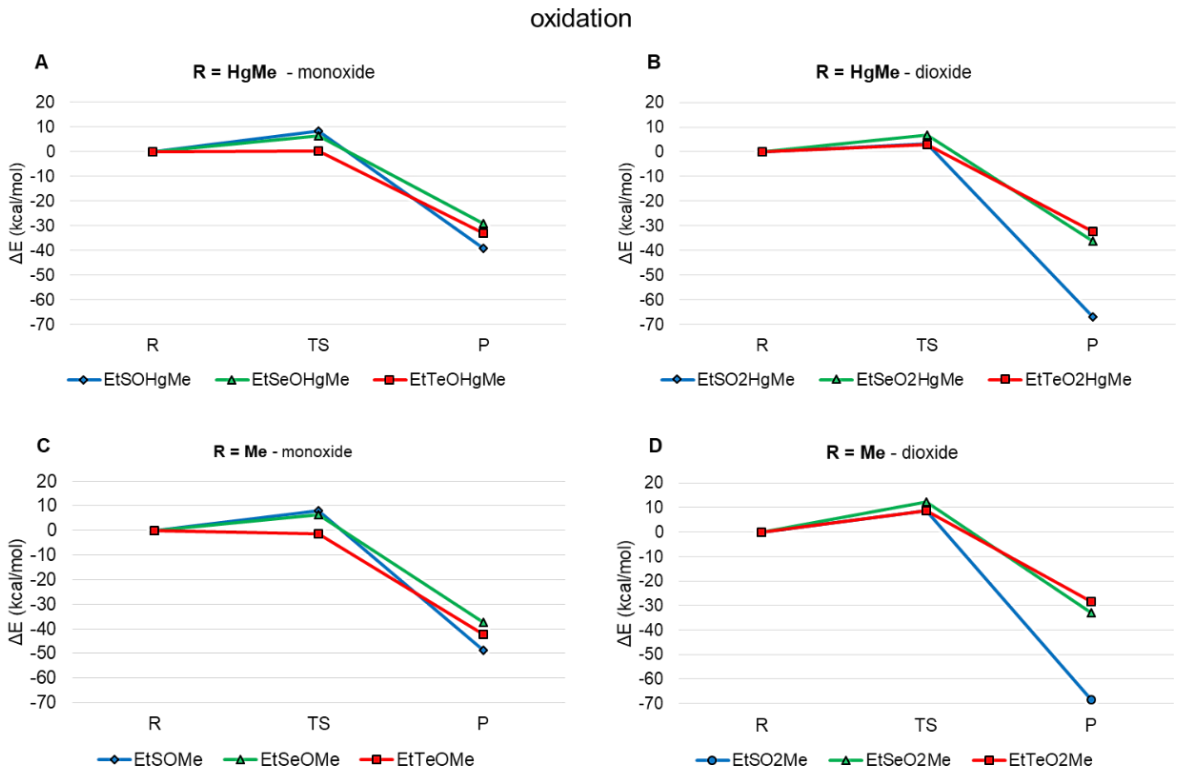

Figure 2. Oxidation reaction energies (kcal/mol) for EtS(Hg)Me (♦ blue), EtSe(Hg)Me (▲ green), and EtTe(Hg)Me (■ red). Reactions (X = S, Se, Te): (A) $EtXHgMe + H_2O_2 \rightarrow EtXOHgMe + H_2O$; (B) $EtXOHgMe + H_2O_2 \rightarrow EtXO_2HgMe + H_2O$; (C) $EtXMe + H_2O_2 \rightarrow EtXOMe + H_2O$; (D) $EtXOMe + H_2O_2 \rightarrow EtXO_2Me + H_2O$. R, TS, and P mean reactants, transition state, and products, respectively. ZORA-BLYP(BJ)/TZ2P.

In general, the monoxides of R= HgMe and Me presented the lowest β-elimination TS (10 to 25 kcal/mol) when compared to its corresponded dioxides (12 to 42 kcal/mol). However, the global reaction energies of dioxides are lower than the monoxides, with the exception of 'S' molecules. The monoxides with R= HgMe showed a lower transition state and global reaction energies than the R= Me species. The transition state energy from R= HgMe dioxides showed the lowest values when compared with the dioxides with R= Me, however, for the global reaction energy occurs the opposite.

Table 1. Oxidation and β-elimination reaction energies (ΔE in kcal/mol). Energies relative to the most stable free reactants. ZORA-BLYP(BJ)/TZ2P.

Reaction		**oxidation**			**β-elimination**	
Molecule	**R**	**TS**	**P**	**R**	**TS**	**P**
EtSOHgMe	0.00	8.41	-39.02	0.00	21.83	12.14
EtSeOHgMe	0.00	6.41	-29.10	0.00	13.14	-1.62
EtTeOHgMe	0.00	0.33	-32.88	0.00	10.96	-5.93
$EtSO_2HgMe$	0.00	3.34	-67.00	0.00	35.51	24.08
$EtSeO_2HgMe$	0.00	6.62	-36.12	0.00	16.43*	-7.66
$EtTeO_2HgMe$	0.00	3.04	-32.50	0.00	12.37*	-17.60
EtSOMe	0.00	8.00	-48.61	0.00	25.66	18.54
EtSeOMe	0.00	6.43	-37.49	0.00	16.21	4.12
EtTeOMe	0.00	-1.39	-42.16	0.00	14.37	0.61
$EtSO_2Me$	0.00	8.75	-68.34	0.00	41.93	22.47
$EtSeO_2Me$	0.00	12.35	-32.91	0.00	20.58	-12.86
$EtTeO_2Me$	0.00	8.69	-28.30	0.00	15.61	-23.39

* Energy obtained from the structures with the Hg···O distance fixed (constrain). R, TS, and P mean reactants, transition state, and products, respectively.

From the kinetic point of view, the β-elimination reactions of 'HgMe' compounds are more favorable than the R= Me molecules, and the reaction trends occur according to 'Te' > 'Se' >> 'S'. In addition, the data showed here indicates that is not necessary the second oxidation to conduct the β-elimination.

A previous study of Cys, Sec, and Tec oxidation, using a cluster model of GPx, presented the same trend as reported here, where the Tec showed the lowest TS energies when compared

with Sec and Cys (7, 17 and 25 kcal/mol, respectively; the level of theory: B3LYP-D3(BJ)/6-311G(d,p),cc-pVTZ(-PP))[32]. In addition, the hydroperoxide reduction by Sec is thermodynamically and kinetically more favored than Cys, in the oxidative stress regulator (OxyR), glyceraldehyde 3-phosphate dehydrogenase (GAPDH), and peroxiredoxin (Prx) models [40]. The chalcogen atom type presents a high effect in the β-elimination reaction, while the effect of MeHg and Me groups is less marked. In fact, Bayse and Allison (2007)[31] reported that the inductive effects of alkyl and aryl groups have a small effect in the activation energies (13 to 16 kcal/mol, level of theory: B3LYP/mPW1PW91) for selenocysteine β-elimination.

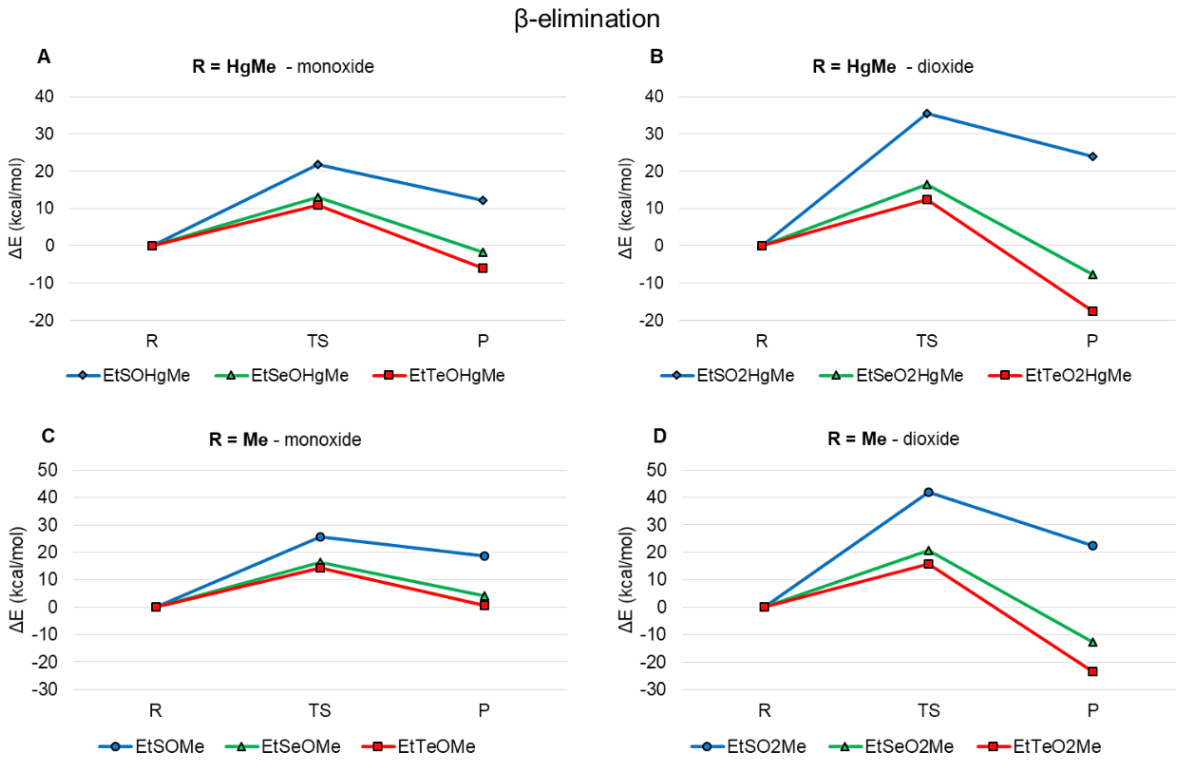

Figure 3. β-elimination reaction energies (kcal/mol) for EtS(Hg)Me (♦ blue), EtSe(Hg)Me (▲ green), and EtTe(Hg)Me (■ red). Reactions (X = S, Se, Te): (A) EtXOHgMe → CH_2=CH_2 + MeHgXOH; (B) $EtXO_2HgMe$ → CH_2=CH_2 + $MeHgXO_2H$; (C) EtXOMe → CH_2=CH_2 + MeXOH; (D) $EtXO_2Me$ → CH_2=CH_2 + $MeXO_2H$. R, TS, and P mean reactants, transition state, and products, respectively. ZORA-BLYP(BJ)/TZ2P.

4. Conclusions

According to the data presented here for the Dha formation, it is not necessary the second oxidation of the chalcogen atom to conduct the β-elimination, i.e., the TS energies indicate that

after the first chalcogen atom oxidation, the β-elimination could occur. This information helps us to better understand the chemical behavior of amino acids after its alkylation or reaction with MeHg, in special the Cys and Sec from GPx and TrxR. Besides, these data suggest that synthetic Te-compounds could be easier activated than the S,Se-molecules in organic chalcogen prodrugs.

Conflicts of interest

There are no conflicts to declare.

Acknowledgements

All the calculations were carried out on Galileo (CINECA: Casalecchio di Reno, Italy) thanks to the ISCRA (Italian SuperComputing Resource Allocation) Grant MEMES (MEthylMErcury and Selenoproteins). J. B. T. R. and P. A. N. would like to thank the financial support by Coordination for Improvement of Higher Education Personnel (nº 23038.004173/2019-93; nº 0493/2019; nº 88882.182123/2018-01) and the Institutional Internationalization Project (CAPES/PrInt) (nº. 88887.374997/2019-00).

Supporting information

O *Supporting information* deste artigo encontra-se disponível no APÊNDICE 9.4.

5-References

1. Chalker, J. M. et al. Methods for converting cysteine to dehydroalanine on peptides and proteins. Chem. Sci. 2, 1666–1676 (2011).
2. Rhee, S. G. & Cho, C. S. Blot-based detection of dehydroalanine-containing glutathione peroxidase with the use of biotin-conjugated cysteamine. in Methods in enzymology (eds. Cadenas, E. & Packer, L.) 474, 23–34 (Elsevier Inc., 2010).
3. Ma, S., Caprioli, R. M., Hill, K. E. & Burk, R. F. Loss of selenium from selenoproteins: Conversion of selenocysteine to dehydroalanine in vitro. J. Am. Soc. Mass Spectrom. 14, 593–600 (2003).
4. Orian, L. et al. Selenocysteine oxidation in glutathione peroxidase catalysis: An MS-supported quantum mechanics study. Free Radic. Biol. Med. 87, 1–14 (2015).
5. Reddy, K. M. & Mugesh, G. Modelling the Inhibition of Selenoproteins by Small Molecules Using Cysteine and Selenocysteine Derivatives. Chem. - A Eur. J. 25, 8875–8883 (2019).
6. Reich, H. J., Wollowitz, S., Trend, J. E., Chow, F. & Wendelborn, D. F. Syn Elimination of Alkyl Selenoxides. Side Reactions Involving Selenenic Acids. Structural and Solvent Effects on Rates. J. Org. Chem. 43, 1697–1705 (1978).

7. Okeley, N. M., Zhu, Y. & Van Der Donk, W. A. Facile chemoselective synthesis of dehydroalanine-containing peptides. Org. Lett. 2, 3603–3606 (2000).

8. Rooseboom, M., Commandeur, J. N. M., Floor, G. C., Rettie, A. E. & Vermeiden, N. P. E. Selenoxidation by flavin-containing monooxygenases as a novel pathway for β-elimination of selenocysteine Se-conjugates. Chem. Res. Toxicol. 14, 127–134 (2001).

9. Bar-Or, R., Rael, L. T. & Bar-Or, D. Dehydroalanine derived from cysteine is a common post-translational modification in human serum albumin. Rapid Commun. Mass Spectrom. 22, 711–716 (2008).

10. Jeong, J., Kim, Y., Kyung Seong, J. & Lee, K. J. Comprehensive identification of novel post-translational modifications in cellular peroxiredoxin 6. Proteomics 12, 1452–1462 (2012).

11. Jeong, J. et al. Novel oxidative modifications in redox-active cysteine residues. Mol. Cell. Proteomics 10, 1–13 (2011).

12. Nordberg, J., Zhong, L., Holmgren, A. & Arnér, E. S. J. Mammalian thioredoxin reductase is irreversibly inhibited by dinitrohalobenzenes by alkylation of both the redox active selenocysteine and its neighboring cysteine residue. J. Biol. Chem. 273, 10835–10842 (1998).

13. Wang, S. K., Weaver, J. D., Zhang, S. & Lei, X. G. Knockout of SOD1 promotes conversion of selenocysteine to dehydroalanine in murine hepatic GPX1 protein. Free Radic. Biol. Med. 51, 197–204 (2011).

14. Cho, C. S. et al. Irreversible inactivation of glutathione peroxidase 1 and reversible inactivation of peroxiredoxin ii by H2O2 in red blood cells. Antioxidants Redox Signal. 12, 1235–1246 (2010).

15. Andreadou, I., Menge, W. M. P. B., Commandeur, J. N. M., Worthington, E. A. & Vermeiden, N. P. E. Synthesis of novel Se-substituted selenocysteine derivatives as potential kidney selective prodrugs of biologically active selenol compounds: Evaluation of kinetics of β-elimination reactions in rat renal cytosol. J. Med. Chem. 39, 2040–2046 (1996).

16. Rooseboom, M., Vermeulen, N. P. E., Durgut, F. & Commandeur, J. N. M. Comparative study on the bioactivation mechanisms and cytotoxicity of Te-phenyl-L-tellurocysteine, Se-Phenyl-L-selenocysteine, and S-Phenyl-L-cysteine. Chem. Res. Toxicol. 15, 1610–1618 (2002).

17. Oliveira, C. S., Piccoli, B. C., Aschner, M. & Rocha, J. B. T. Chemical Speciation of Selenium and Mercury as Determinant of Their Neurotoxicity. in Neurotoxicity of Metals, Advances in Neurobiology (eds. Aschner, M. & Costa, L. G.) 18, 53–83 (Springer International Publishing, 2017).

18. Bartolini, D. et al. Selenocompounds in Cancer Therapy: An Overview. in Advances in Cancer Research (eds. Tew, K. D. & Galli, F.) 136, 259–302 (Elsevier Inc., 2017).

19. Zhao, S. et al. A review on mercury in coal combustion process: Content and occurrence forms in coal, transformation, sampling methods, emission and control technologies. Prog. Energy Combust. Sci. 73, 26–64 (2019).

20. Outridge, P. M., Mason, R. P., Wang, F., Guerrero, S. & Heimbürger-Boavida, L. E. Updated Global and Oceanic Mercury Budgets for the United Nations Global Mercury Assessment 2018. Environ. Sci. Technol. 52, 11466–11477 (2018).

21. Hong, Y.-S., Kim, Y.-M. & Lee, K.-E. Methylmercury Exposure and Health Effects. J. Prev. Med. Public Heal. 45, 353–363 (2012).

22. Karagas, M. R. et al. Evidence on the Human Health Effects of Low-Level Methylmercury Exposure. Environ. Health Perspect. 120, 799–806 (2012).

23. Nogara, P. A. et al. Methylmercury's chemistry: From the environment to the mammalian brain. Biochim. Biophys. Acta - Gen. Subj. 1863, 129284 (2019).

24. Franco, J. L. et al. Methylmercury neurotoxicity is associated with inhibition of the antioxidant enzyme glutathione peroxidase. Free Radic. Biol. Med. 47, 449–457 (2009).

25. Arnér, E. S. J. Focus on mammalian thioredoxin reductases - Important selenoproteins with versatile functions. Biochim. Biophys. Acta - Gen. Subj. 1790, 495–526 (2009).

26. Parks, J. M. & Smith, J. C. Modeling Mercury in Proteins. in Methods in Enzymology (ed. Voth, G. A.) 578, 103–122 (Elsevier Inc., 2016).

27. Asaduzzaman, A. M., Khan, M. A. K., Schreckenbach, G. & Wang, F. Computational studies of structural, electronic, spectroscopic and thermodynamic properties of methylmercury-amino acid complexes and their Se analogues. Inorg. Chem. 49, 870–878 (2010).

28. Asaduzzaman, A. et al. Environmental mercury chemistry - in silico. Acc. Chem. Res. 52, 379–388 (2019).

29. Musaev, D. G. Elucidating the role of the pyridoxal 5̀-phosphate (PLP)-dependent β-lyases in selenocysteine se-conjugates metabolism: A density functional study. J. Phys. Chem. B 108, 18756–18761 (2004).

30. Ribaudo, G. et al. Fluoxetine scaffold to design tandem molecular antioxidants and green catalysts. RSC Adv. 10, 18583 (2020).

31. Bayse, C. A. & Allison, B. D. Activation energies of selenoxide elimination from Se-substituted selenocysteine. J. Mol. Model. 13, 47–53 (2007).

32. Bortoli, M., Torsello, M., Bickelhaupt, F. M. & Orian, L. Role of the Chalcogen (S, Se, Te) in the Oxidation Mechanism of the Glutathione Peroxidase Active Site. ChemPhysChem 18, 2990–2998 (2017).

33. te Velde, G. et al. Chemistry with ADF. J. Comput. Chem. 22, 931–967 (2001).

34. Baerends, E. J. et al. ADF2018, SCM, Theoretical Chemistry, Vrije Universiteit, Amsterdam, The Netherlands, https://www.scm.com.

35. Van Lenthe, E., Baerends, E. J. & Snijders, J. G. Relativistic total energy using regular approximations. J. Chem. Phys. 101, 9783–9792 (1994).

36. Lee, C., Yang, W. & Parr, R. G. Development of the Colic-Salvetti correlation-energy formula into a functional of the electron density. Phys. Rev. B 37, 785–789 (1988).

37. Becke, A. D. Density-fnnctional exchange-energy approximation with correct asymptotic behavior. Phys. Rev. A 38, 3098–3100 (1988).

38. Grimme, S., Ehrlich, S. & Goerigk, L. Effect of the Damping Function in Dispersion Corrected Density Functional Theory. J. Comput. Chem. 32, 1456–1465 (2011).

39. Madabeni, A. et al. Chalcogen-mercury bond formation and disruption in model Rabenstein's reactions: A computational analysis. J. Comput. Chem. June, 1–10 (2020).

40. Dalla Tiezza, M. et al. A dual attack on the peroxide bond. The common principle of peroxidatic cysteine or selenocysteine residues. Redox Biol. 34, 101540 (2020).

4.3. CAPÍTULO 3: PLANEJAMENTO DE NOVOS ORGANOSSELÊNIOS

Neste capítulo serão abordados o planejamento de novos compostos orgânicos de selênio, visando uma maior seletividade em relação aos seus alvos macromoleculares. Nesse sentido três classes de compostos foram estudados:

(a) Piridinil(quinolil)-tio(seleno)semicarbazidas como agentes sequestrantes de MeHg;
(b) Derivados do Ebselen como possíveis inibidores da acetilcolinesterase (AChE);
(c) Selenazoil-peptideos como potenciais inibidores da Mpro do SARS-COV-2.

Além disso, avaliou-se computacionalmente a possível toxicidade dessas moléculas através do servidor pkCSM (PIRES; BLUNDELL; ASCHER, 2015).

4.3.1. Piridinil(quinolil)-tio(seleno)semicarbazidas como agentes sequestrantes de MeHg

De acordo com o Capítulo 2, o MeHg poderia se ligar covalentemente ao átomo de Se da GPx, o que causaria sua inibição. Nesse sentido, o planejamento de agentes sequestrantes de MeHg é essencial, isto é, projetar compostos capazes de remover o MeHg do sítio ativo da enzima.

Estudos sugerem que ação farmacológica do Ebs e DPDSe na toxicidade causada pelo MeHg podem estar relacionada com a formação dos complexos Ebs-SeHgMe e PhSeHgMe, que poderiam ser menos tóxicos e facilmente excretáveis (BARBOSA et al., 2017; MEINERZ et al., 2017). Assim, agentes quelantes de MeHg poderiam auxiliar no tratamento de sua intoxicação. Ebs e DPDSe são substratos da TrxR, sendo assim, podem ser reduzidos para suas formas de selenolato/selenol, os quais agiriam como sequestrantes de MeHg (Figura 4.3.1.1) (ZHAO; HOLMGREN, 2002; LU; BERNDT; HOLMGREN, 2009; SAUSEN DE FREITAS et al., 2010; FARINA; ROCHA; ASCHNER, 2011).

Figura 4.3.1.1. Redução do Ebs e DPDSe pela TrxR, e ligação com MeHg.

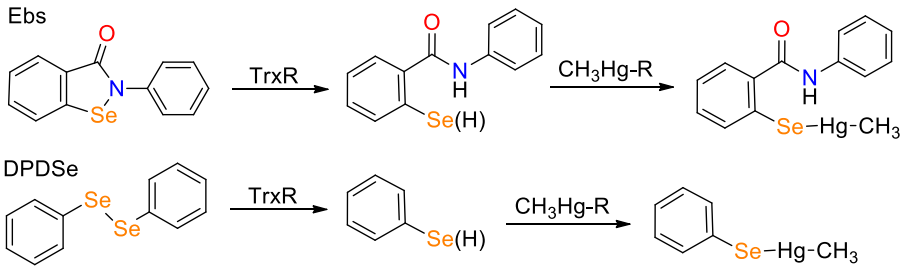

Fonte: Autor.

Além disso, a possibilidade do complexo formado promover a clivagem da ligação C–Hg dever ser destacada, uma vez que Hg^{2+} possui uma menor toxicidade que o MeHg (MELNICK; PARKIN, 2007; BANERJEE; ROY, 2017; NOGARA et al., 2019a). De fato, compostos imidazoilselonas demonstram essa capacidade através da formação de complexos com MeHg (BANERJEE; ROY, 2017), dessa forma sendo considerados miméticos da enzima organomercurio-liase (MerB). A MerB é um enzima bacteriana que catalisa a desmetilação do MeHg, e para isso, dois resíduos de Cys e um de Asp são essenciais. As Cys se coordenam ao MeHg e o Asp doa um próton para o grupo metila, promovendo assim a protólise do MeHg ($[Cys_2\text{-}HgCH_3]^-$ + Asp-COOH → Cys-Hg-Cys + $Asp\text{-}COO^-$ + CH_4) (PARKS et al., 2009). Outra classe

de quelantes são as piridinil e quinolil tio(seleno)semicarbazidas, ligantes tridentados, que tem sido relatados como bons complexantes de metais (Sn, Cu, Zn, Cd, Hg, and Ru), podendo formar dois anéis de 5 membros (TODOROVIĆ et al., 2006; CHANDRA; PARMAR; KUMAR, 2009; MOLTER et al., 2012; NIRMALA et al., 2014; ROGOLINO et al., 2017). No entanto, não se tem relatos de estudos com MeHg.

Considerando a importância do desenvolvimento de compostos capazes de formarem complexos com MeHg, bem como de removê-lo do sítio ativo de enzimas, e promover a clivagem da ligação C–Hg, piridinil(quinolil)-tio(seleno)semicarbazidas (Figura 4.3.1.2) foram estudadas por *docking* molecular com a GPx. Nessas moléculas os grupos ácido carboxílicos (COOH) e hidroxila (OH) podem ser essenciais para a clivagem da ligação C–Hg, pois poderiam atuar como doadores de prótons. Além disso, os putativos metabólitos Ebs–Se^-/SeH e $PhSe^-$/SeH foram estudados, originados do Ebs e DPDSe, respectivamente.

Figura 4.3.1.2. Estruturas de piridinil(quinolil)-tio(seleno)semicarbazidas. O mecanismo proposto para a formação do complexo com MeHg e sua protólise é mostrado.

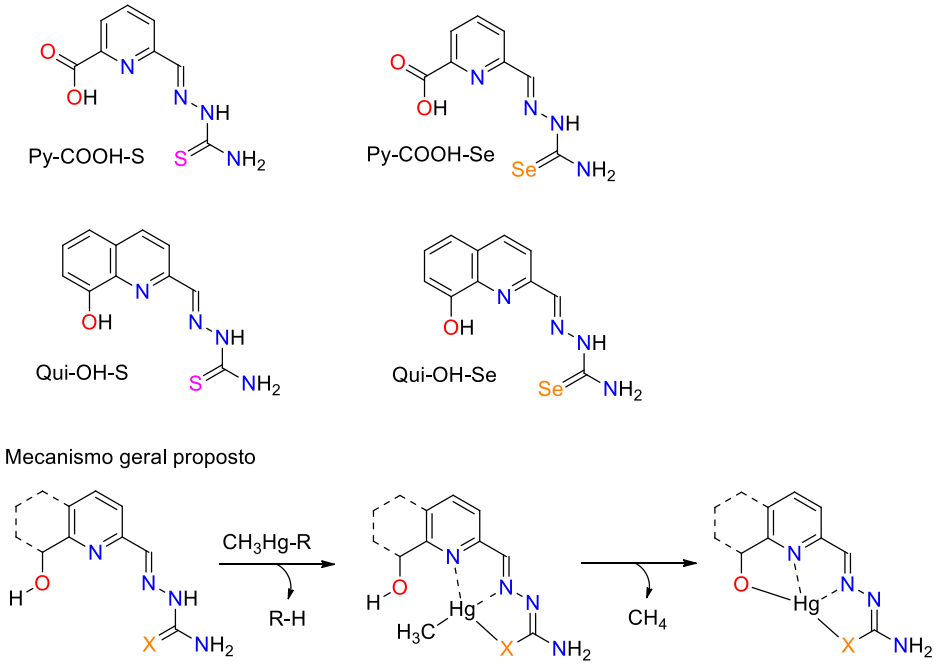

Fonte: autor. R = Sec, Cys, Cl, ou OH.

4.3.1.1. Materiais e métodos

Considerando que não há estrutura tridimensional disponível da GPx ligada ao MeHg, um modelo desta foi criado. Para isso os resíduos Sec45, Gln80, Trp158 e Asn159, foram removidos estrutura PDB ID 1GP1, e o grupo MeHg foi adicionado manualmente ao átomo de Se da Sec45, com o programa Avogadro. Este cluster foi otimizado geometricamente com o método semiempírico PM6 (MOPAC), onde somente o MeHg foi permitido se mover. Após o MeHg foi adicionado ao arquivo da proteína (1GP1), formando assim a molécula Sec–HgMe. Antes de converter o arquivo para *pdbqt*, através de um editor de texto o átomo de Hg foi trocado por Zn, conservando assim e cargas parciais obtidos do PM6. O programa Vina foi utilizado (TROTT; OLSON, 2010), com o *gridbox* de 15Å^3 centrado no sítio ativo (26,13 x 47,17 x 48,31). De maneira similar, os ligantes foram obtidos através da otimização com o PM6 (STEWART, 2007). Os dados foram analisados no programa *Discovery Studio Visualizer* (DSV) (DASSAULT SYSTÈMES BIOVIA, 2017). As simulações com a δ-AlaD foram realizadas de acordo com a literatura (NOGARA; ORIAN; ROCHA, 2020).

4.3.1.2. Resultados e discussões

As simulações de *docking* demonstraram que os metabólitos Ebs-SeH e PhSeH, tanto na forma protonada (–SeH) como desprotonada (–Se$^-$), interagem no sítio da GPx apresentando interações entres os átomos de Se e Hg (de 3,4 a 4,3 Å) (Quadro 4.3.1.1). Da mesma maneira, os compostos Qui-OH-Se, Qui-OH-S, Py-COOH-Se e Py-COOH-S mostraram um modo de ligação similar e uma boa orientação com o Hg da Sec45, com as distâncias S/Se$^{\cdots}$Hg variando de 3.2 a 5.1 Å. Os resíduos de Trp158 e Arg177 apresentam um papel importante na estabilização dos ligantes no sítio ativo, através de interações hidrofóbicas e ligações de H, respectivamente. Essas orientações também auxiliam na adequada conformação dos ligantes para interagir com o MeHg. Considerando que o pH fisiológico (pH =7,4), realizou-se também o *docking* com grupos carboxílicos desprotonados (Py-COO-Se e Py-COO-S). Somente para o Py-COO-S uma pequena mudança conformacional foi observada, diminuindo a distância S$^{\cdots}$Hg de 4,6 para 3,2 Å, quando comparado com Py-COOH-S.

Quadro 4.3.1.1. Simulações de docking com a GPxHgMe. Os valores de ΔG (kcal/mol) estão em parênteses. As linhas pontilhas nas cores verde, laranja e em rosa, representam ligações de hidrogênio, interações eletrostáticas e hidrofóbicas, respectivamente, com as distâncias em Å.

Ebs-SeH (-4,8)	Ebs-Se$^-$ (-5,0)
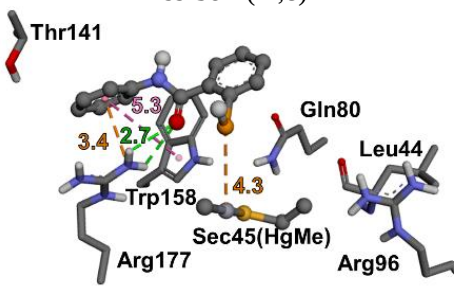	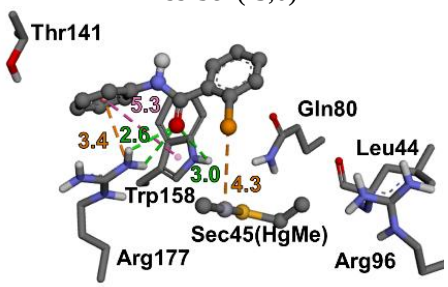
PhSeH (-2,7)	PhSe$^-$ (-2,9)
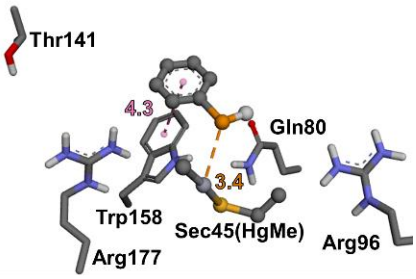	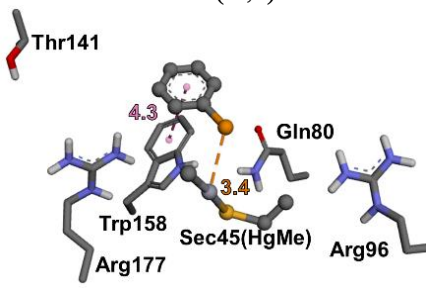
Qui-OH-Se (-5,1)	Qui-OH-S (-5,1)
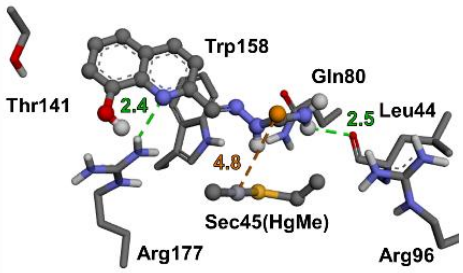	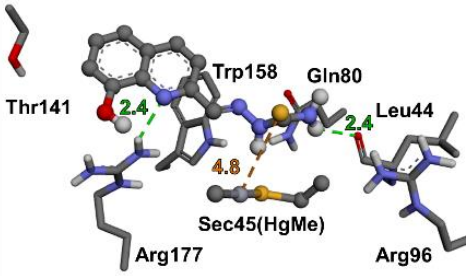
Py-COOH-Se (-4,5)	Py-COOH-S (-4,5)
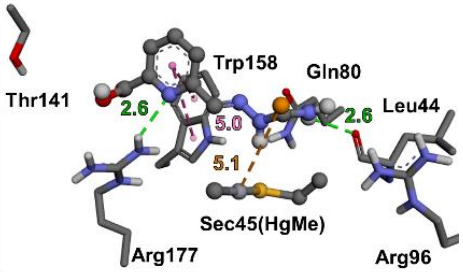	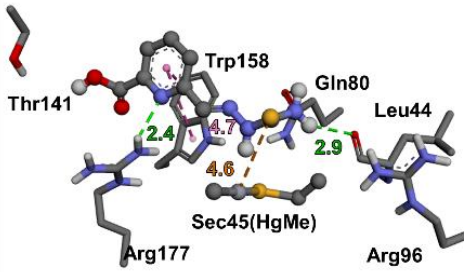
Py-COO-Se (-4,5)	Py-COO-S (-4,6)
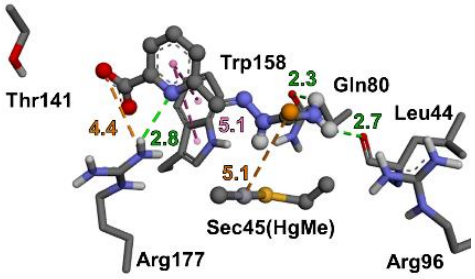	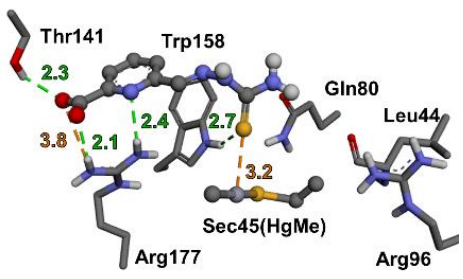

Desta forma podemos observar que os compostos de S e Se poderiam interagir com a GPx inibida por MeHg, e assim, remover essa toxina, reativando a função enzimática. No entanto, considerando que o MeHg está ligado ao átomo de Se da Sec45, compostos de S poderiam ter uma maior dificuldade para remover o metal, uma vez que estudos teóricos e práticos sugerem que a afinidade do Hg por calcogênios segue a ordem: S < Se < Te (MELNICK; YURKERWICH; PARKIN, 2010; MADABENI et al., 2020).

Além disso, considerando que a enzima δ-AlaD é um alvo para organosselênios, como método de predição de toxicidade o *docking* das piridinil(quinolil)-tio(seleno)semicarbazidas foram realizados (Quadro 4.3.1.2).

Quadro 4.3.1.2. Simulações de docking com a δ-AlaD. Os valores de ΔG (kcal/mol) estão em parênteses. As linhas pontilhas nas cores verde, laranja e em rosa, representam ligações de hidrogênio, interações eletrostáticas e hidrofóbicas, respectivamente, com as distâncias em Å.

Qui-OH-Se (-5,2) 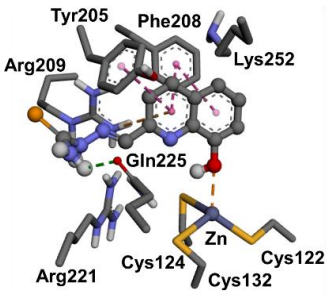	Qui-OH-S (-5,3) 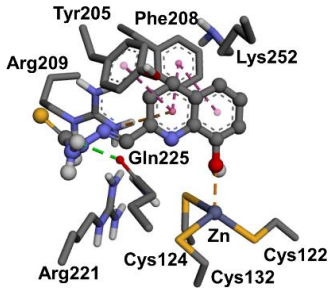
Py-COOH-Se (-4,6) 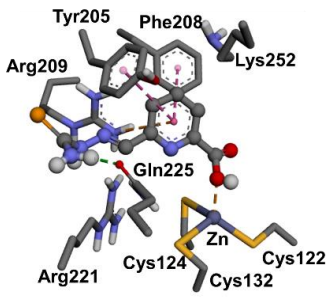	Py-COOH-S (-4,7) 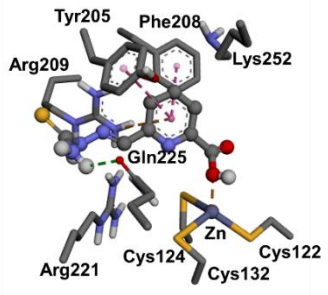
Py-COO-Se (-4,9) 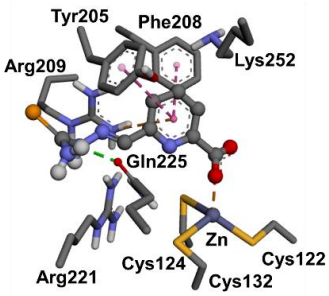	Py-COO-S (-4,8) 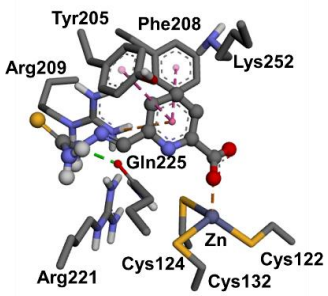

Ambas as moléculas apresentaram um modo similar de interação, no qual a porção tio(seleno)carbazida se posicionou na região mais afastada do sitio ativo, enquanto que os grupos –OH e –COOH mostraram uma coordenação com o átomo de Zn catalítico (~2,5 Å). Além disso, interações hidrofóbicas com os resíduos de Tyr205 e Phe208 foram observadas. Os grupos –OH e –COOH além de poderem desempenhar um papel como doadores de prótons na possível clivagem da ligação C–Hg do MeHg, o átomo de oxigênio se coordena com o Zn do sítio ativo da δ-AlaD, impedindo assim a interação S···Se que pode estar associada a toxicidade de organosselênios (SARAIVA et al., 2012; NOGARA; ROCHA, 2018; NOGARA; ORIAN; ROCHA, 2020).

4.3.2. Derivados do Ebselen como possíveis inibidores da acetilcolinesterase (AChE)

A doença de Alzheimer (DA) é um processo neurodegenerativo patológico crônico, caracterizado principalmente por déficit na aprendizagem e perda de memória (HAMPEL et al., 2018). É um distúrbio neurológico caracterizado pelo baixo nível do neurotransmissor acetilcolina (ACh) no hipocampo e córtex, e pela formação de placas amilóides extracelulares e emaranhados neurofibrilares intracelulares que conduzem à neurotoxicidade (FOLCH et al., 2016; HAMPEL et al., 2018). A ACh possui um papel fundamental nos processos de aprendizagem e memória, através da ativação de receptores nicotínicos e muscarínicos no sistema nervoso central, onde a enzima acetilcolinesterase (AChE) é responsável pelo controle da neurotransmissão colinérgica, uma vez que esta catalisa a hidrólise da ACh nas fendas sinápticas. Sendo assim, atualmente um dos tratamento para DA inclui inibidores da AChE (ou *acetylcholinesterase inhibitors,* AChEIs), pois, a inibição da AChE aumenta os níveis de ACh, melhorando a transmissão colinérgica (FOLCH et al., 2016; HAMPEL et al., 2018; SHARMA, 2019). Dentre estes inibidores podemos citar o o donepezil, galantamina e rivastigmina.

Apesar de muitos ensaios clínicos com novos AChEIs, nenhum dos potenciais candidatos tem sido bem sucedidos nos estudos da Fase III (MEHTA; ADEM; SABBAGH, 2012; GALIMBERTI; SCARPINI, 2016; AKINCIOGLU; GÜLÇIN, 2020). Além disso, considerando a variabilidade inter-paciente na resposta ao tratamento da DA e que os AChEIs possuem alguns efeitos colaterais (náusea, vômito e diarreia) (NOETZLI; EAP, 2013), o desenvolvimento de novos AChEIs que poderão ser utilizados no tratamento da DA é de crucial importância.

Nos vertebrados existem dois tipos de colinesterases, a AChE e a butirilcolinesterase (BChE), ambas catalisam a hidrólise da ACh, no entanto a AChE é a principal (DVIR et al., 2010; BAJDA et al., 2013). As duas enzimas apresentam uma identidade de 54% na sequência de aminoácidos, no entanto, a AChE é encontrada principalmente nas células neuronais, enquanto que a BChE é no plasma. Nesse sentido a AChE é o principal alvo no tratamento da DA (MEHTA; ADEM; SABBAGH, 2012; REALE et al., 2018). A hidrólise da ACh ocorre na parte inferior do sítio ativo da AChE, onde se localiza a tríade catalítica composta pelos resíduos Ser203, Glu334 e His447 (Figura 4.3.2.1). Além disso, resíduos aromáticos como triptofano, tirosina e fenilalanina, possuem um papel importante no processo (DVIR et al., 2010).

Figura 4.3.2.1. Estrutura e ciclo catalítico da AChE.

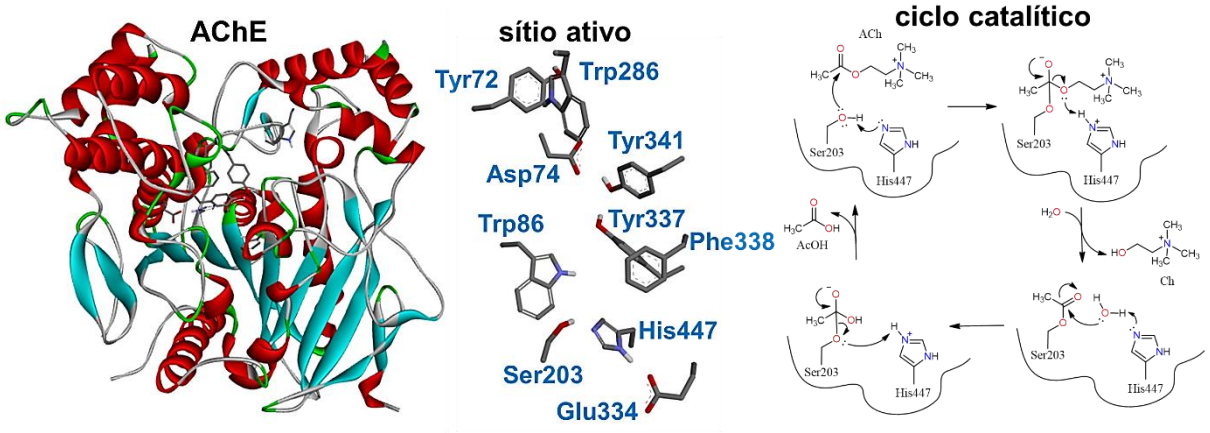

Fonte: autor. Estrutura obtida do PDB: 4EY6.

Inibidores híbridos tem sido estudados como alvo da AChE, dentre eles podemos citar os híbridos de donepezila e ebselen. Ambas as moléculas são estruturalmente parecidas, devido a presença de um anel benzênico fundido a um anel de 5 membros com uma carbonila (LUO et al., 2013; CHIERRITO et al., 2017) (Quadro 4.3.2.1). Além de ser um inibidor da AChE (IC_{50} = 41 μM) (LUO et al., 2013), o ebselen é considerado um composto não tóxico, podendo ser recomendado para o tratamento de transtornos bipolares e infecções virais respiratórias, tais como a COVID-19 (SINGH et al., 2013b; CAPPER et al., 2018; JIN et al., 2020; SIES; PARNHAM, 2020), assim sendo um importante bloco estrutural para derivatizações.

Aqui por meio de estudos de *docking* molecular, novos híbridos de donepezila-ebselen foram estudados com o intuito de encontrar novos possíveis candidatos a inibidores da AChE. Inicialmente foram estudadas as interações da ACh, donepezila e ebselen com AChE, e a partir disso novas modificações estruturais foram realizadas (afim de aumentar a afinidade pela enzima) até encontrar um candidato adequado.

4.3.2.1. Materiais e métodos

As simulações de *docking* com a AChE foram realizadas de acordo com a literatura (SILVA et al., 2020). A estrutura PDB 4EY6 foi utilizada e as moléculas de água conservadas (HOH: 704, 705, 707, 773, 803, 805 e 815) foram mantidas durante o *docking*. O programa Vina foi utilizado (TROTT; OLSON, 2010), com o *gridbox* de 30$Å^3$ centrado no sítio ativo da AChE (-13,25 x 46,76 x 33,52), e os ligantes foram obtidos através da otimização com o método PM6 (STEWART, 2007).

Os resultados foram analisados no programa *Discovery Studio Visualizer* (DSV) (DASSAULT SYSTÈMES BIOVIA, 2017). As simulações com a enzima δ-AlaD foram realizadas de acordo como foi apresentado no Capitulo 2 (NOGARA; ORIAN; ROCHA, 2020).

4.3.2.2. Resultados e discussões

O Quadro 4.3.2.1 mostra os dados obtidos. Inicialmente os modos de ligação do donepezila (neutro (B) e protononado (C)) obtidos do *docking* foram comparados com os dados cristalográficos (A), no qual se observou que ambos possuem uma conformação similar, demonstrando um bom desempenho do programa Vina. A porção 1,2-dimetoxibenzeno interage hidrofobicamente com o resíduo Trp286, a piperidina com Phe338 e Tyr337, e o grupo benzil se aproxima do Trp86. O substrato ACh (D) demonstrou ligações de H com a Gly122 e Ser203, e interações eletrostáticas com o Trp86 e Glu202, o que está de acordo com seu mecanismo de hidrólise (DVIR et al., 2010; ROSENBERRY et al., 2017). O ebselen (E) demonstrou interações hidrofóbicas entre o grupo benzoisoselenazol e o Trp84, e entre o grupo fenila e as tirosinas 124 e 341, além de ligações de H com uma molécula de água. A partir daqui, modificações estruturais foram realizadas, e primeiramente híbridos donepezila-ebselen foram testados (F–H). Neste caso o anel piperidina foi substituído pela piridina (Py), uma vez que análogos com o grupo piperidina já são descritos na literatura (LUO et al., 2013). Neste caso, as três moléculas apresentaram um modo de ligação similar ao donepezila, no qual o anel benzoisoselenazol interage com o Trp286, e os grupos Py e benzila se acomodam na parte intermediaria e inferior do sitio, entre os resíduos Tyr124, Tyr337, Trp86 e His447. Vale ressaltar que um grupamento etila unindo o anel benzoisoselenazol aos grupos Py/fenila (G–H), propiciam uma melhor interação hidrofóbica com o Trp86, que um grupo metila (F).

No entanto, os valores da energia livre de ligação (ΔG) até aqui apresentados foram superiores (-8,1 a -9,7 kcal/mol) ao próprio donepezila (-10,4 kcal/mol), sugerindo que essas moléculas teriam uma menor afinidade pela AChE, quando comparados com o clássico inibidor. Assim, híbridos entre Ebselen e histamina (Hist) foram testados (I–K). As simulações de encaixe sugerem que o grupo imidazol neutro interage na parte inferior do sítio (Trp86 e His447), enquanto que suas formas protonadas e metiladas se ligam na parte superior e intermediaria, entre os resíduos Trp286, Try337 e Tyr124. No entanto, os valores de ΔG foram superiores (-7,6 a -7,8 kcal/mol) ao próprio Ebselen (-8,1 kcal/mol).

Considerando que a interação com os resíduos da parte inferior do sítio são importantes, híbridos entre Ebselen, histamina e tacrina (Tha) foram simulados, uma vez que a literatura demonstra que híbridos ebselen-tacrina são bons inibidores da AChE (IC_{50} = 2,5 a 657 nM), e que a porção tetrahidroacridina da Tha propicia uma interação com o Trp86 (MAO et al., 2013). Para isso foram criados dois isômeros, um no qual o grupo Tha é unido a His através de um grupo etila ligado ao Nτ (Ebs-Hist-Thaτ), e outra molécula através do Nπ (Ebs-Hist-Thaπ). Surpreendentemente, a molécula Ebs-Hist-Thaτ (L) mostrou um ΔG (-11,6 kcal/mol) superior ao donepezila, indicando ser um bom inibidor. No entanto, inesperadamente o grupo Tha interagiu na parte superior do sitio, interagindo hidrofobicamente com os resíduos Leu289 e Trp286, enquanto que o grupo benzoisoselenazol se ligou na parte inferior, próximo ao Trp86, assim como o próprio Ebselen (E). O isômero Ebs-Hist-Thaπ (M) apresentou um modo de ligação similar, no entanto seu ΔG (-10,6 kcal/mol) foi superior ao Ebs-Hist-Thaτ, indicando um processo menos favorável. O próximo passo foi considerar a influência dos grupos metoxilas ligados no anel benzoisoselanazol (uma vez que o donepezila possui esses grupos). No entanto, apesar da molécula Ebs-Hist-Thaτ-OMe (N) apresentar um modo de ligação similar ao donepezila, no qual o grupo 1,2-dimetoxibenzeno interage com o Trp286, o seu valor de ΔG (-10,0 kcal/mol) indica um processo menos favorável que o seu análogo Ebs-Hist-Thaτ (L).

Considerando que o Itopride (O) é um inibidor da AChE (IC_{50} = 2 μM) (IWANAGA et al., 1994), e que sua estrutura é similar ao donepezila e Ebselen, híbridos entre Itopride e ebselen (Q, R) foram simulados com AChE. Primeiramente o próprio itopride neutro (O) e protonado (P) foram testados, onde observou-se que ambos possuem uma interação similar ao donepezila, com a porção 1,2-dimetoxibenzeno interagindo com o Trp286, enquanto que a outra extremidade da molécula se aproxima do Trp86. No entanto seus valores de ΔG (-8,5 e -8,2 kcal/mol) são superiores ao donepezila, o que está de acordo com os valores de IC_{50}, sendo que o donepezila é um inibidor mais potente (IC_{50} = 0,038 μM) (LUO et al., 2013). No entanto, os Ebs-itopride (Q, R) não demonstraram nenhuma melhora nos valores energéticos (ΔG = -7,6 e -8,3 kcal/mol), apesar dos modos de ligações serem parecidos com o donepezila.

Quadro 4.3.2.1. Moléculas, interações, e energia livre de ligação (ΔG, kcal/mol). As linhas pontilhas nas cores verde, laranja e em rosa, representam ligações de hidrogênio (1,5 a 3 Å), interações eletrostáticas (2,5 a 6 Å) e hidrofóbicas (3 a 6 Å), respectivamente, com as distâncias em Å.

<table>
<tr>
<td>A (AChE)
Donepezila
 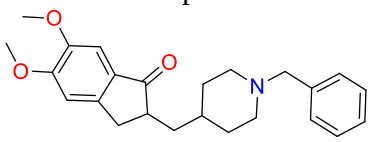
PDB ID 4EY7
 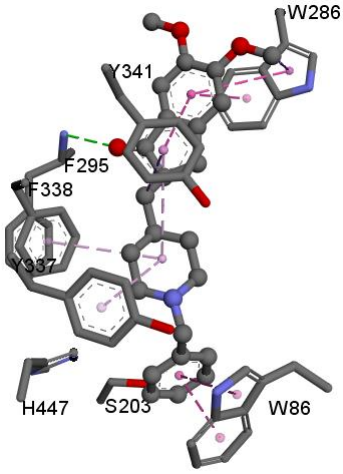
</td>
<td>B (AChE)
Donepezila-H
 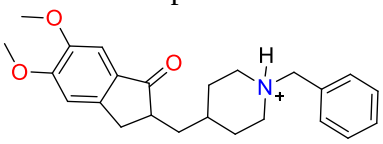
(-10.4)
 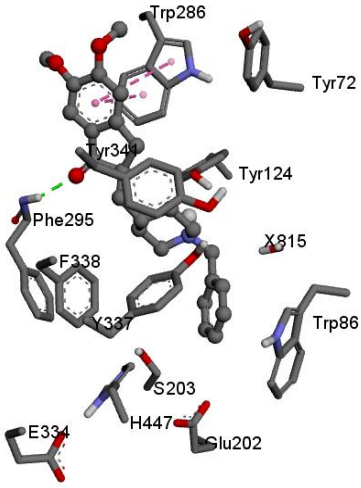
</td>
</tr>
<tr>
<td>C (AChE)
Donepezila
 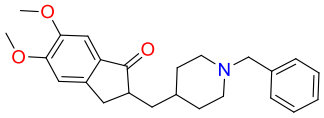
(-10.2)
 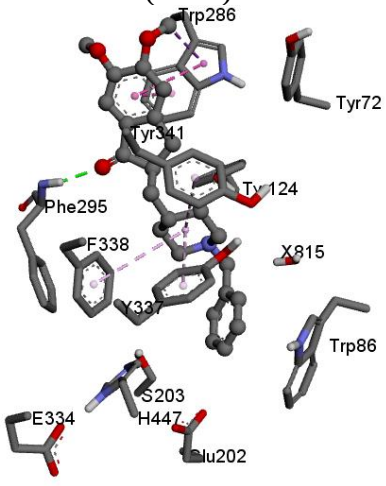
</td>
<td>D (AChE)
ACh
 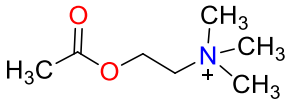
(-5.0)
 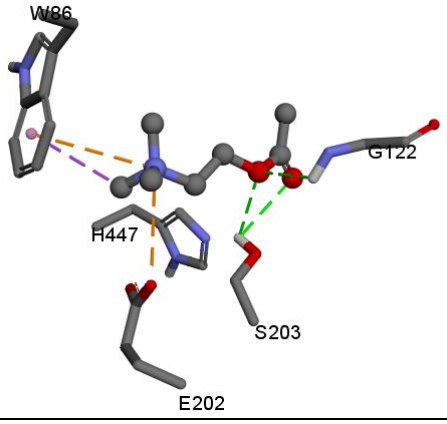
</td>
</tr>
</table>

E (AChE)
Ebs

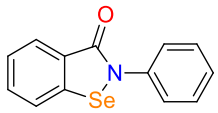

(-8.1)

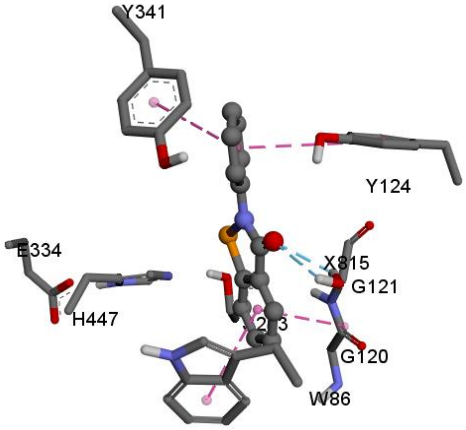

F (AChE)
Ebs-1Py-Ph

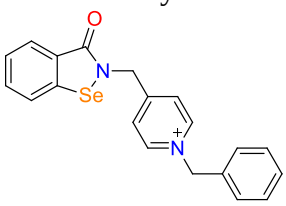

(-9.6)

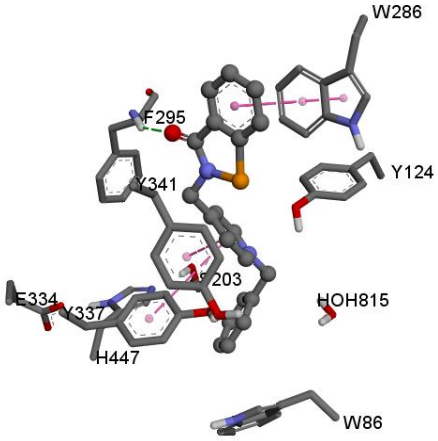

G (AChE)
Ebs-2Py-Ph

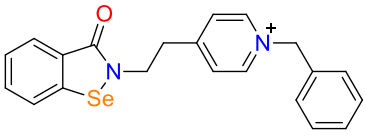

(-9.6)

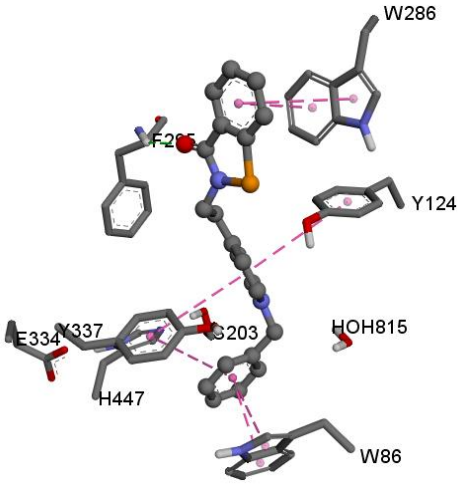

H (AChE)
Ebs-2Ph-Py

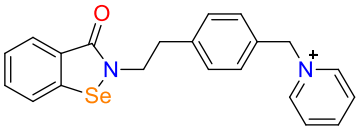

(-9.7)

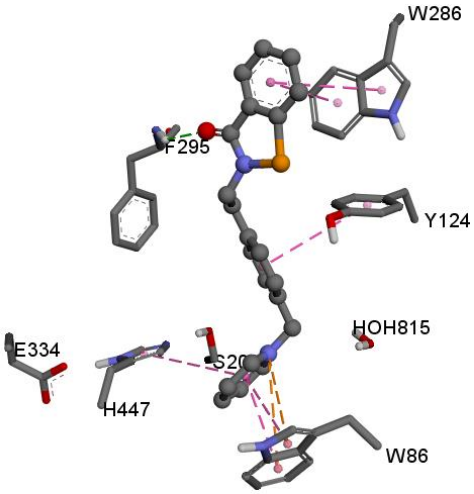

I (AChE) Ebs-Hist 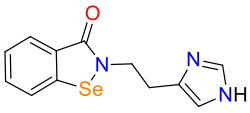 (-7.7) 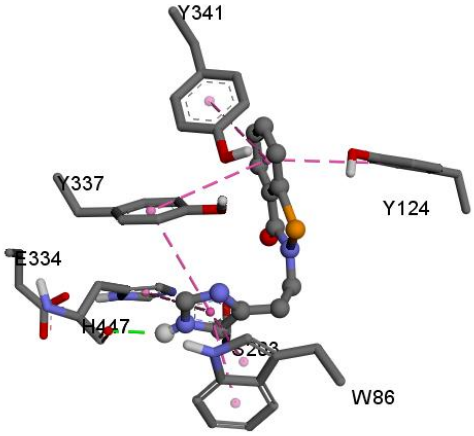	J (AChE) Ebs-HistH 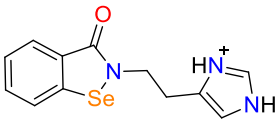 (-7.6) 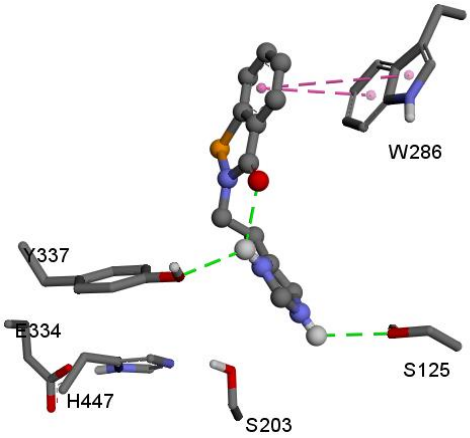
K (AChE) Ebs-HistMe$_2$ 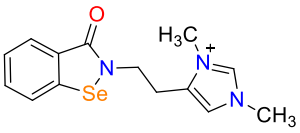 (-7.8) 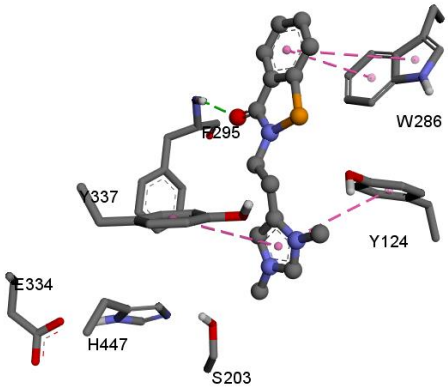	L (AChE) Ebs-Hist-Thaτ 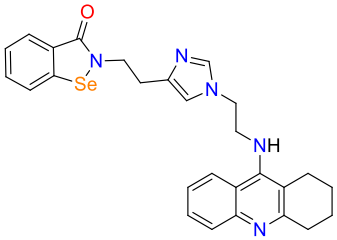 (-11.6) 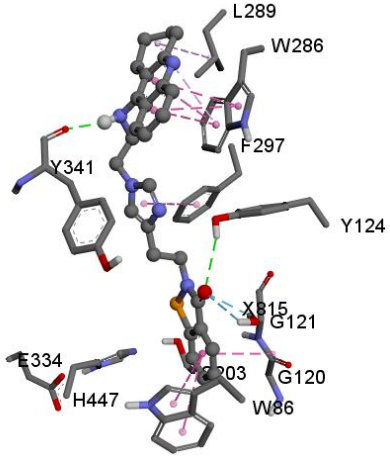

M (AChE)
Ebs-Hist-Thaπ

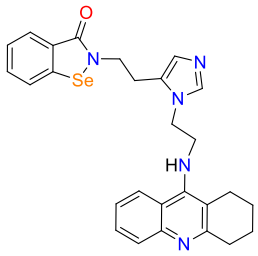

(-10.6)

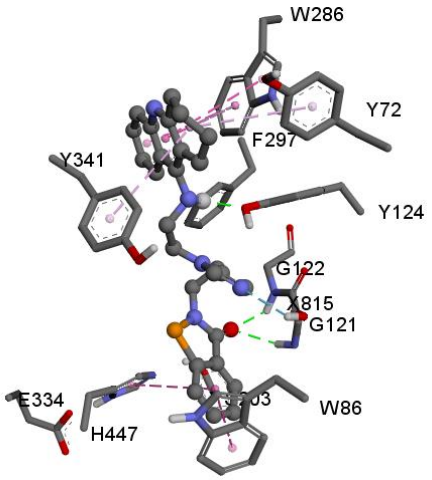

N (AChE)
Ebs-Hist-Thaτ-OMe

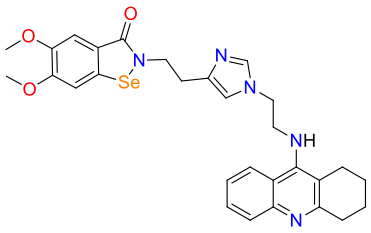

(-10.0)

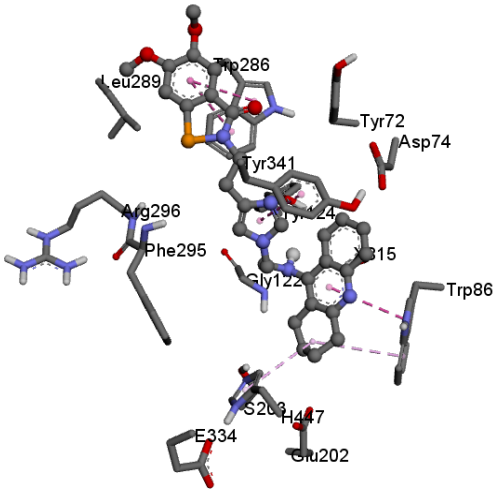

O (AChE)
Itopride

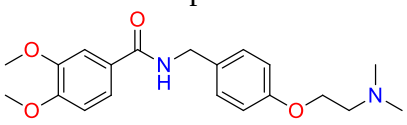

(-8.5)

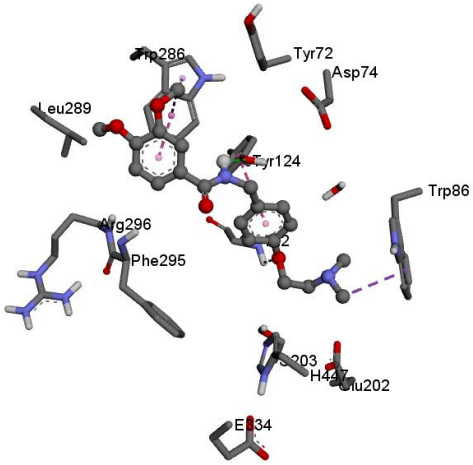

P (AChE)
Itopride-H

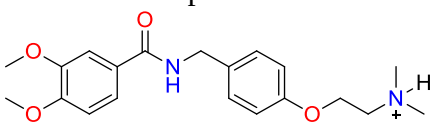

(-8.2)

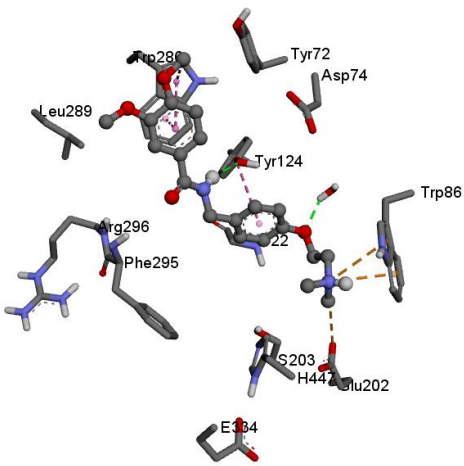

Q (AChE)
Se-Itopride

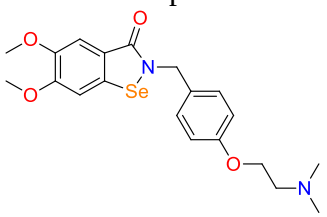

(-7.6)

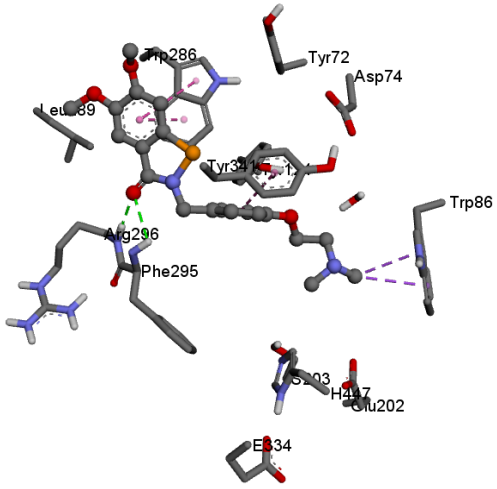

R (AChE)
Se-Itopride-H

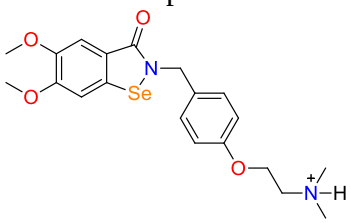

(-8.3)

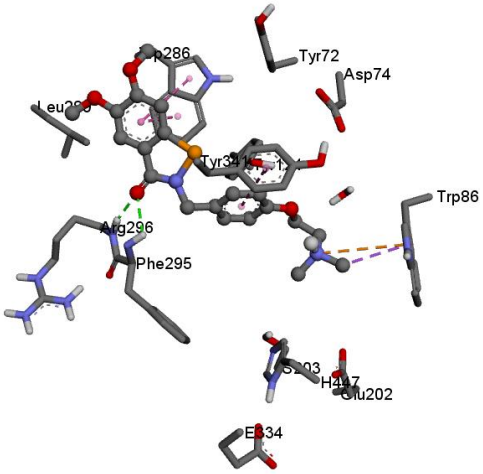

S (δ-AlaD)
Ebs

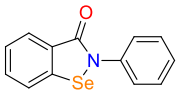

(-7.2)

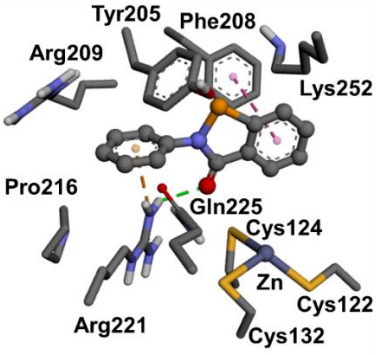

T (δ-AlaD)
Ebs-His-Tha

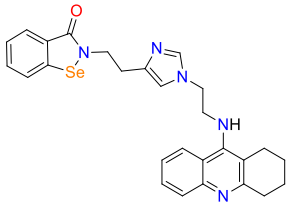

(-7.2)

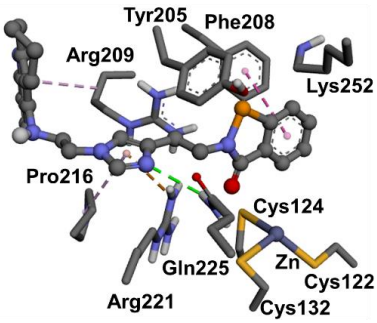

Dessa maneira, através deste estudo a molécula Ebs-Hist-Thaτ (L) apresentou os melhores resultados, podendo ser um potencial inibidor da AChE. A interação do grupo Tha no subsítio

aniônico periférico (*Peripheral Anionic Subsite*, PAS), constituído pelos resíduos Trp286, Tyr72, Tyr341 e Asp74, pode desempenhar um papel importante, uma vez que o PAS é alvo de várias toxinas e também de fármacos promissores (DVIR et al., 2010; BAJDA et al., 2013). Sendo assim, desenvolvimento de novos agentes anticolinesterásicos que interagem no PAS é um campo promissor na busca pelo tratamento do DA (SINGH et al., 2013a).

Considerando o possível uso de Ebs-Hist-Thaτ como inibidor da AChE, é importante determinar uma possível toxicidade desta molécula. Para isso o *docking* com a δ-AlaD foi realizado (Quadro 4.3.2.1, S–T). Assim como observado para o próprio Ebselen (S), a molécula Ebs-Hist-Thaτ (T) não apresentou a interação S···Se (entre os resíduos e Cys e o anel isoselenazol), o que poderia ser uma indicação da não inibição δ-AlaD (SARAIVA et al., 2012; NOGARA; ROCHA, 2018; NOGARA; ORIAN; ROCHA, 2020). Apesar de estudos indicarem que o ebselen inibe a δ-AlaD (IC_{50} = 100 μM), a sua potência é menor quando comparado com o DPDSe (IC_{50} = 9–40 μM), o qual apresenta a interação S···Se (ROCHA et al., 2012; NOGARA; ORIAN; ROCHA, 2020).

4.3.3. Selenazoil-peptideos como potenciais inibidores da Mpro do SARS-COV-2

O desenvolvimento de drogas antivirais é de suma importância para à erradicação de patógenos virais, principalmente as quais não há vacinas para o tratamento das doenças, como nos casos de infecção por vírus da imunodeficiência humana (HIV), vírus da hepatite C (HCV), vírus do papiloma humano (HPV), herpesvírus, vírus da febre hemorrágica, e para a maioria das infecções pelo vírus do trato respiratório (adenovírus, rinovírus, vírus da parainfluenza, e mais recentemente, o coronavírus da síndrome respiratória aguda grave 2 (SARS-CoV-2 ou 2019-nCoV), causador da COVID-19) (DE CLERCQ, 2002; MORSE et al., 2020; YAN et al., 2020). Embora vários antivirais têm sido desenvolvidos, muitos nem sempre são eficazes ou bem tolerados, apresentando efeitos colaterais e resistência viral (DE CLERCQ, 2002). Sendo assim, há a necessidade continua por agentes antivirais mais eficazes, principalmente nos casos de novos surtos, endemias, epidemias e pandemias (exemplo a COVID-19).

O planejamento (*design*) e desenvolvimento de um novo fármaco (antiviral, por exemplo) é um processo lento e complexo, que pode levar 12 a 15 anos e custar mais de 1 bilhão de dólares (HUGHES et al., 2011). Para acelerar esse processo, a utilização de métodos *in silico* permite uma rápida e eficiente avaliação da possível aplicação de moléculas. As relações estrutura-atividade (ou *structure-activity relationship*, SAR) são essenciais para muitos processos de descoberta de medicamentos, pois permitem construir uma variedade de modelos e assim identificar grupos farmacofóricos, priorizar, e sugerir modificações estruturais úteis na molécula (GUHA, 2013).

A determinação do alvo biológico é uma etapa fundamental na busca de fármacos. Nesse sentido as proteases virais, tais como do vírus da dengue e Zika (NITSCHE, 2019), e mais recentemente a do SARS-Cov-2 (JIN et al., 2020), tem demonstrado serem alvos promissores. As proteases virais são muito importantes no ciclo de vida viral, pois realizam modificações pós-traducionais nas proteínas virais tornando-as 'funcionais' (DE CLERCQ, 2002; LI; DE CLERCQ, 2020; MORSE et al., 2020).

O genoma do coronavirus apresenta 16 proteínas não-estruturais (NSP) que inicialmente estão na forma de duas grandes poliproteínas (PP1a e PP1ab), sendo processadas por duas enzimas (cisteino-proteases), a protease *papain-like* (PLpro) e a protease principal (Mpro, ou 3-*chymotrypsin-like* – 3CLpro). PLpro é responsável pela clivagem do N-terminal da PP, liberando NSP1, NSP2 e NSP3, enquanto que a Mpro, também denominada NSP5, libera as proteínas NSP4-

NSP16, clivando em 11 sítios da PP1ab (CHEN; LIU; GUO, 2020; WU et al., 2020). A sequência Leu-Gln↓Ser-Gly (↓ indica o sítio de clivagem da ligação peptídica) é encontrada em muitos desses sítios (DU et al., 2004; ULLRICH; NITSCHE, 2020; ZHANG et al., 2020).

Desse modo, essas proteases são importantes alvos no tratamento da Covid-19, uma vez que sua inibição interrompe a replicação viral (MORSE et al., 2020; SIES; PARNHAM, 2020). De fato, inibidores de proteases, tais como disulfiram, lopinavir e ritonavir, tem demonstrado resultados promissores no combate a SARS, MERS e SARS-Cov-2 (LI; DE CLERCQ, 2020; LIM et al., 2020; MORSE et al., 2020; YAN et al., 2020). Jin e colaboradores (JIN et al., 2020; SIES; PARNHAM, 2020) demonstraram que o ebselen é um potente inibidor da Mpro do SARS-Cov-2 (IC_{50} = 0.67 μM), podendo se ligar covalentemente ao resíduo de cisteína catalítico (Cys145) (Figura 4.3.3.1), através da formação da ligação S–Se. Desta forma, a Mpro pode ser considerada um alvo para organosselênios. De fato, o grupo 1,2-selenazoil pode reagir com o grupo tiol de Cys, como observado para a superóxido dismutase (SOD), TrxR e transpeptidase da *Mycobacterium tuberculosis* (WANG et al., 2012; CAPPER et al., 2018; MUNNIK et al., 2019), sendo assim um bom candidato a bloco precursor para inibidores de cisteíno-proteases.

Figura 4.3.3.1. Estrutura da Mpro do SARS-Cov-2 e *design* de selenazoil-peptideos.

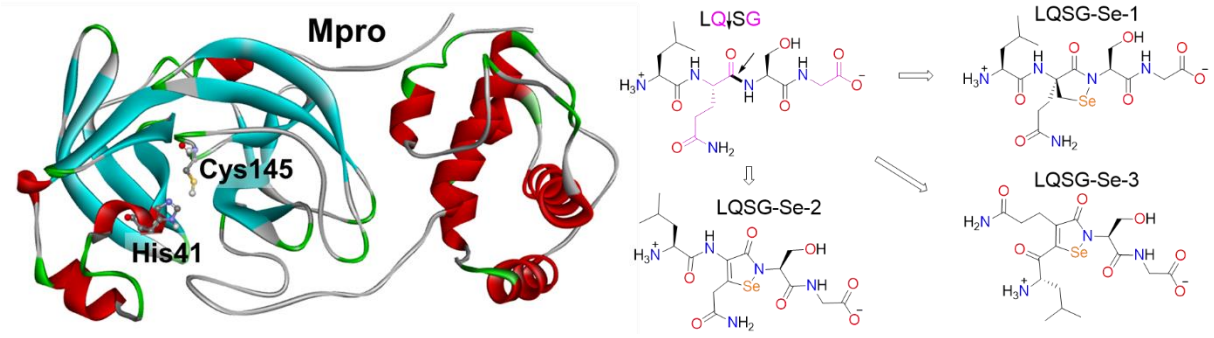

Fonte: autor. ↓ indica o sítio de clivagem da ligação peptídica.

O planejamento e/ou a otimização da atividade biológica de compostos orgânicos por meio de modificações estruturais guiadas por estudos de SAR e *docking* molecular tem sido utilizada com bons resultados, demonstrando ser uma boa metodologia a ser aplicada (GOGOI et al., 2016; NIKOLIC et al., 2016; JANG et al., 2018; KATSAMAKAS; HADJIPAVLOU-LITINA, 2018; SAXENA; DUBEY, 2019), reduzindo assim o tempo e custos associados na síntese de vários compostos, que muitas vezes são testados baseados na tentativa e erro.

Nesse sentido, adicionou-se o grupo 1,2-selenazol na sequência de clivagem da Mpro (Leu-Gln-Ser-Gly, ou LQSG), com o intuito de planejar novos inibidores dessa enzima (Figura 4.3.3.1).

4.3.3.1. Materiais e métodos

O programa AutoDock Vina foi utilizado para as simulações de encaixe (TROTT; OLSON, 2010). A estrutura da Mpro foi obitida do PDB com o código 6LU7, onde íons, moléculas orgânicas e de água foram removidos, e os átomos de H adicionados com o programa Chimera (PETTERSEN et al., 2004). O *gridbox* com as dimensões de 25 x 35 x 25 Å foi centrado no sítio ativo da enzima (-14,04 x 17,44 x 66,22), e os ligantes foram obtidos através da otimização geométrica com o método PM6 (STEWART, 2007). Os resultados foram analisados no programa *Discovery Studio Visualizer* (DSV) (DASSAULT SYSTÈMES BIOVIA, 2017). As simulações com a enzima δ-AlaD foram realizadas conforme foi apresentado no Capítulo 2 (NOGARA; ORIAN; ROCHA, 2020).

4.3.3.2. Resultados e discussões

Primeiramente realizou-se o *redocking* do inibidor N3 (Figura 4.3.3.2), co-cristalografado com a enzima Mpro (PDB 6LU7), onde a melhor configuração de *docking* apresentou um RMSD (do inglês *Root Mean Square deviation*, que significa a medida da distância média entre os átomos de duas moléculas sobrepostas) de 2,1 Å, o que é levemente superior ao aconselhado (2,0 Å) (STIGLIANI et al., 2012). Este valor pode estar associado ao fato que o inibidor N3 está covalentemente ligado a Cys145 da Mpro, e no entanto, o AutoDock Vina não é capaz de simular este tipo de interação/reação.

Para melhor compreender como a Mpro cliva a ligação peptídica, realizou-se o *docking* com o peptídeo LQSG (substrato), onde foi possível verificar que a carbonila da ligação peptídica da Gln-Ser realiza ligações de H com os grupos amino dos resíduos Gly143 e Ser144, além de estar 3,9 Å de distância da grupo tiol da Cys145 (B). Este modo de ligação está de acordo com o mecanismo catalítico da Mpro, no qual o próton do grupo tiol é removido pela His41, e o tiolato gerado irá reagir com a carbonila da Gln (ZHANG et al., 2020). Além disso, o resíduo de Leu do peptídeo interage hidrofobicamente com os resíduos His41 e Met49 da enzima, e a cadeia lateral da Gln faz uma ligação de H com a His163.

Figura 4.3.3.2. Simulações de docking com a Mpro. Os valores de ΔG (kcal/mol) estão em parênteses.

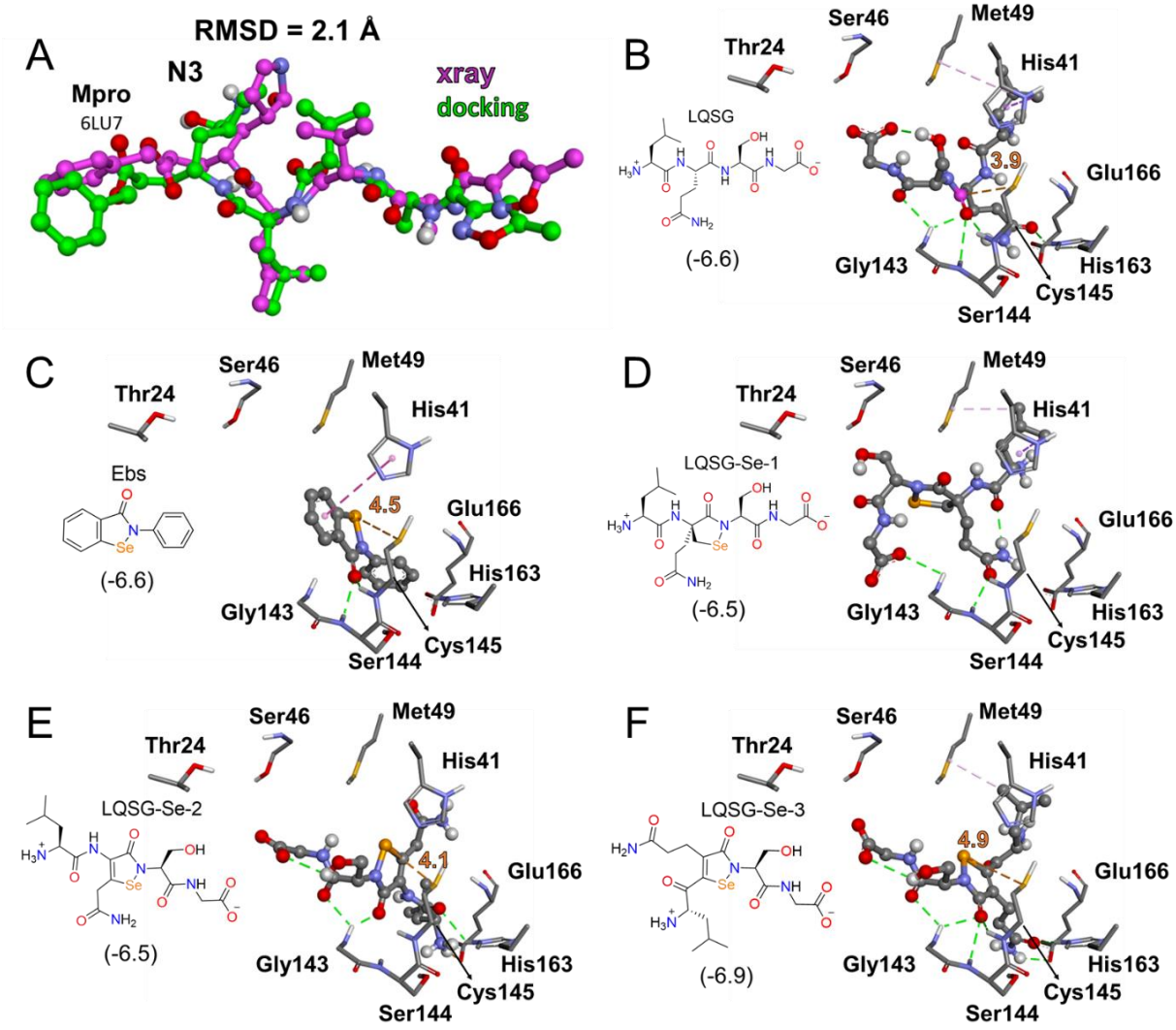

Fonte: autor.

O *docking* do Ebselen demonstrou que o composto interage com a His45 hidrofobicamente e realiza duas ligações de H com os grupos aminos dos resíduos Gly143 e Ser144 (C). A posição da porção isoselenazol e a distância (4,5 Å) entre os átomos de Se e S, sugerem que o ataque nucleofilico da Cys pode ocorrer, podendo levar a formação da ligação Se–S, e a consequente inibição enzimática.

Assim como o peptídeo LQSG, a molécula LQSG-Se-1 também demonstrou as interações hidrofóbicas entre a Leu e a His41 e Met49, no entanto, o átomo de Se do anel isoselenazol está afastado da Cys145 (D). Provavelmente devido o centro quiral presente neste composto

impossibilitar uma conformação adequada para interagir com a Cys145. Dessa maneira, planejou-se remover o centro quiral adicionado uma dupla ligação no anel isoselenazol (moléculas LQSG-Se-2 e LQSG-Se-3).

Já no composto LQSG-Se-2 a porção isoselenazol apesentou uma conformação similar ao Ebselen, com o Se a 4,1 Å de distância do S da Cys145 (E). No entanto, a cadeia lateral da Gln e resíduo de Leu demonstraram uma conformação distinta à apresentada pelo peptídeo LQSG. Dessa maneira, as posições equivalentes aos resíduos Gln e Leu no LQSG-Se-2 foram invertidas na molécula LQSG-Se-3.

Por fim, as simulações de *docking* para a molécula LQSG-Se-3 demonstraram que tem um modo de ligação similar ao peptídeo LQSG, onde o resíduo de Leu faz interações hidrofóbicas com a Met49 e His41, a cadeia lateral da Gln realiza ligações de H com a His163 e Glu166, e a carbonila do anel isoselenazol forma ligações de H com os grupos amino dos resíduos Gly143 e Ser144 (F). É importante destacar que a conformação adotada pela molécula poderia facilitar o ataque da Cys145 ao átomo de Se, uma vez que a distância é de 4,9 Å.

Os dados termodinâmicos de ΔG preditos pelo Vina variaram de -6,6 a -6,9, onde o composto LQSG-Se-3 apresentou o menor valor, indicando ser um potencial inibidor da Mpro, pois, o complexo formado é termodinamicamente mais favorável que o Ebselen e as moléculas LQSG-Se-1 e LQSG-Se-2. Assim como outros compostos carbonílicos e α,β-insaturados, considerados inibidores covalentes da Mpro (ULLRICH; NITSCHE, 2020), o grupo isoselenazol pode ser considerado um grupo eletrofílico importante no desenvolvimento de inibidores de cisteino-proteases.

Como método de avaliação de uma possível toxicidade, simulações de *docking* foram realizadas entre os compostos LQSG-Se-2 e LQSG-Se-3 e a δ-AlaD (Figura 4.3.3.3). Os resultados demonstraram que o grupo carboxílico terminal da Gly do peptídeo realiza uma coordenação com o átomo de Zn (~2,2 Å) e o átomo de Se não interage com os resíduos e Cys da δ-AlaD, indicando que a oxidação dos tióis proteicos pode não ocorrer (NOGARA; ORIAN; ROCHA, 2020). Desta forma, espera-se que esses compostos sejam mais seletivos para a enzima Mpro e apresentem uma menor toxidade frente a δ-AlaD.

Figura 4.3.3.3. Simulações de docking com a δ-AlaD. Os valores de ΔG (kcal/mol) estão em parênteses.

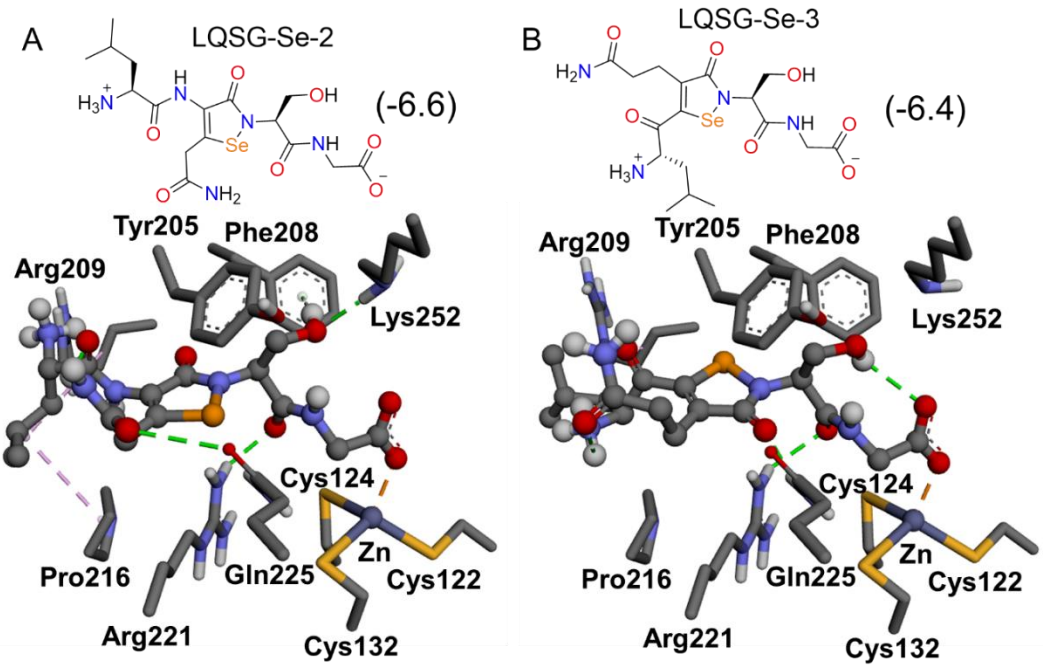

Fonte: autor.

4.3.4. Predição da toxicidade através do servidor pkCSM

Os testes de toxicidade são muito importantes para o desenvolvimento de fármacos, pois tem o objetivo de identificar os efeitos nocivos causados por essas substâncias, tanto em seres humanos e animais, como em plantas. Muitos fatores estão envolvidos na determinação da toxicidade de uma molécula, como por exemplo, a via de administração (oral, cutânea, inalação), dose (quantidade da substância), frequência da exposição (única/aguda ou múltiplas/crônica), duração da exposição (7 min, 12 h, 2 dias), variáveis biológicas (idade, sexo), propriedades físico-químicas do composto químico (solubilidade, estado físico, ponto de ebulição), além de suas propriedades ADME (absorção, distribuição, metabolismo e excreção) (KITCHEN et al., 2004; RAIES; BAJIC, 2016).

Além do uso de ensaios *in vivo* e *in vitro* para a determinação da toxicidade, os métodos *in silico* auxiliam nesse processo, minimizando a necessidade de testes em animais, reduzindo custos e o tempo dos ensaios. Uma grande vantagem dos métodos computacionais é poder testar uma molécula sem esta realmente existir, isto é, não foi sintetizada (RAIES; BAJIC, 2016). Além disso, certos parâmetros empíricos auxiliam na determinação/seleção de uma molécula como candidata a fármaco, como por exemplo as regras de cinco de Lipinski (massa molecular < 500 Da; nº doadores de ligações de H ≤ 5; nº receptores de ligações de H ≤ 10; coeficiente de partição octanol/água, logP ≤ 5) (LIPINSKI et al., 1997). Esse modelo foi baseado nas propriedades de vários medicamentos oralmente administrados.

Assim, a predição da toxicidade dos compostos aqui já apresentados com potenciais usos terapêuticos foi determinada através do servidor pkCSM (PIRES; BLUNDELL; ASCHER, 2015).

4.3.4.1. Materiais e métodos

A predição da toxicidade dos compostos foi determinada através do servidor pkCSM, disponível em: http://biosig.unimelb.edu.au/pkcsm/ (PIRES e colab., 2015).

4.3.4.2. Resultados e discussões

Os resultados (Quadro 4.3.4.1) demonstraram que todos os compostos mostraram um adequado valor de LogP, no entanto, a molécula LQSG-Se-2 apresentou um nº de doadores de H acima do aceitável, e o híbrido Ebs-Hist-Thaτ violou a regra da massa molecular (>500 g/mol).

Quadro 4.3.4.1. Propriedades físicas, químicas, e de toxicidade. Valores obtidos através do servidor pkCSM.

Moléculas	MM (g/mol)	LogP	Lig. Rot.	Ac. H	Do. H	Área (Å)	LD_{50} (mol/kg)	AMES	Hep.
Ebselen 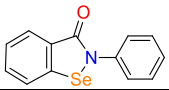	274,18	2,05	1	2	0	98,74	1,70	*sim*	não
Py-COOH-S 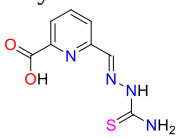	224,24	-0,05	4	4	3	90,82	2,21	não	não
Py-COOH-Se 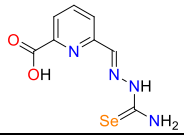	271,14	-1,08	4	4	3	93,56	2,03	não	não
Qui-OH-S 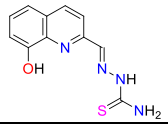	246,30	1,11	3	4	3	102,97	1,19	*sim*	não
Qui-OH-Se 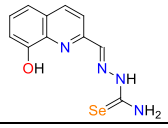	293,19	0,08	3	4	3	105,71	1,91	*sim*	não
Ebs-Hist-Thaτ 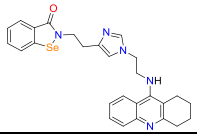	*516,51*	4,04	7	6	1	203,80	2,46	*sim*	*sim*
LQSG-Se-2 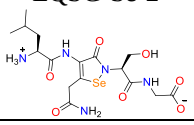	478,36	-3,02	11	8	*6*	171,76	1,46	não	*sim*
LQSG-Se-3 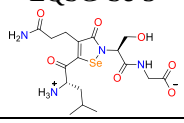	477,38	-2,38	12	8	5	172,57	1,03	não	*sim*

Fonte: autor. MM = massa molecular; LogP = coeficiente de partição, (P = [octanol]/[água]); Lig. Rot. = ligações racionáveis; Ac.H = nº de aceptores de ligações de H; Do. H = nº de doadores de ligações de H; Area = area superficial; LD_{50} = dose letal, considerando uma toxicidade aguda por via oral em ratos; Hep. = hepatotoxicidade. Dados em *itálico* indicam uma violação das regras de Lipinski e/ou indícios de toxicidade.

Os valores de dose letal (LD_{50}), aparentam estar subestimados, uma vez que precisaria de 1 a 2 mols de cada composto para matar metade de uma população de ratos. O valor experimental determinado para o Ebselen é de 0,4 mol/kg (NOGUEIRA; ROCHA, 2011), ou seja, cerca de 5

vezes menor que o predito. No entanto, estudos já demonstram que o Ebselen é um composto com baixa toxicidade, sendo já testado em humanos (MASAKI et al., 2016a, 2016b; JIN et al., 2020).

De acordo com o método AMES (que avalia o potencial mutagênico de moléculas usando bactérias), o Ebselen, Qui-OH-S, Qui-OH-Se, e Ebs-Hist-Thaτ poderiam apresentar certa genotoxicidade. Além disso, LQSG-Se-2, LQSG-Se-3 e Ebs-Hist-Thaτ demonstram uma potencial hepatoxicidade. Uma baixa citotoxidade e hepatotoxicidade são importantes fatores que devem ser considerados no planejamento de novas drogas (BANERJEE et al., 2018; LOPES et al., 2018), por exemplo, a tacrina, alvo da AChE, foi retirada do tratamento da DA justamente por ser hepatotóxica (SUGIMOTO et al., 2000).

Desta maneira, os compostos Py-COOH-S e Py-COOH-Se foram os únicos que não violaram nenhum dos parâmetros estudados, podendo assim serem considerados bons candidatos a fármacos, mais especificamente para a remoção do MeHg de tio(seleno)proteínas.

5. DISCUSSÃO

Considerando que a toxicidade do MeHg pode ser atenuada por compostos orgânicos de Se, o entendimento desse(s) mecanismo(s), a nível molecular, é importante para o desenvolvimento de um possível tratamento para os casos de intoxicação. Além disso, o próprio modo de como o MeHg se liga a seus alvos, causando a toxicidade, devem ser mais estudados para uma melhor compreensão do modo de ação deste, e para que possamos desenvolver métodos de remoção dessa toxina.

Nesse sentido, o estudo da interação de organosselênios com proteínas alvos é essencial para compreender sua farmacologia e toxicologia. É bem descrito na literatura que os organosselênios são miméticos da GPx (ORIAN; TOPPO, 2014; BARBOSA et al., 2017), mas também podem oxidar grupos tióis de proteínas (como no caso da δ-AlaD), além de serem substratos da TrxR (ZHAO; HOLMGREN, 2002; ROCHA et al., 2012; BARBOSA et al., 2017).

Para uma compreensão da toxicidade de organosselênios, estudos de *docking* molecular *in silico* com a enzima δ-AlaD foram realizados. Com base nos resultados apresentados (Capítulo 1), foi possível observar que a oxidação dos selenetos a selenóxidos, além de aumentar o caráter eletrofílico do átomo de Se, também faz com que estas espécies tenham uma maior afinidade pela δ-AlaD, provavelmente devido as ligações de hidrogênio e a coordenação Zn···O observados nos modelos simulados. O que justificaria o maior potencial de inibição selenóxidos quando comparados com seus respectivos selenetos. Além disso, a interação entre o átomo de Se e o grupo tiolato da Cys124 (Se···S) poderia gerar um aduto através da ligação Se–S, levando a desnaturação da enzima. De fato, estudos *in vitro* e *in vivo* da atividade de δ-AlaD indicam que esta enzima não é inibida significativamente pelo disseleneto de dicolesterila (DCDSe) (KADE et al., 2008; KADE; ROCHA, 2010), e as simulações de *docking* não mostraram a interação Se···S (Apêndice 9.5), como observado para os demais organosselênios estudados. No caso da AlaD de pepino, que não possui resíduos de Cys no sítio ativo, a Lys192 poderia reagir com o ácido fenilselenínico (PSA), o que justificaria a inibição desta enzima (NOGARA; ROCHA, 2018; NOGARA; ORIAN; ROCHA, 2020), indicando que pequenas moléculas eletrofílicas de Se seriam capazes de reagir covalentemente com grupos aminos nucleofílicos presentes em proteínas. Dessa maneira, as simulações de *docking* com δ-AlaD poderiam ser usadas como um método de predição da toxicidade de organosselênios.

A redução do DPDSe e Ebs pela TrxR tem um papel muito importante para a atividade antioxidante destes compostos. Além disso, a formação do grupo –SeH nessas moléculas podem estar associados a seus efeitos terapêuticos nos casos de toxicidade induzida por MeHg, uma vez os adutos R-Se–HgMe (R= Ebs, Ph) poderiam remover o MeHg de seus alvos celulares e serem excretados do organismo mais facilmente (BARBOSA et al., 2017; MEINERZ et al., 2017). Desta forma, o modo como essas moléculas interagem e são reduzidas pela TrxR devem ser melhor compreendidos. Os estudos de *docking* molecular aqui realizados com a TrxR demonstram que tanto disselenetos (Capitulo 1) como o Ebs (Apêndice 9.6) poderiam ser reduzidos por esta enzima, dado que estas moléculas acessam o sítio ativo de modo que um ataque nucleofilico da Sec498 sobre o átomo de Se nos ligantes possam ocorrer. Desta maneira, esses compostos podem serem considerados substratos da TrxR, uma vez que ensaios *in vitro* sugerem essa hipótese (ZHAO; HOLMGREN, 2002; SUDATI et al., 2018).

Com relação ao MeHg, a sua toxicidade pode estar relacionada com a inibição das selenoenzimas GPx e TrxR (BRANCO; CARVALHO, 2019; FARINA; ASCHNER, 2019). De acordo com o as simulações de encaixe, as espécies de MeHg (MeHgCl, MeHgOH, MeHgCys e MeHgGSH) poderiam acessar os sítios ativos dessas enzimas, onde o grupo –SeH da Sec poderia realizar um ataque nucleofilico ao Hg, formando o aduto Sec-Se–HgMe, e consequentemente inibindo-as, de acordo com a Reação de Rabenstein (Capitulo 2). Além disso, considerando a GPx inibida pelo MeHg, os cálculos de DFT sugerem que o resíduo Sec-Se–HgMe poderia ser oxidado, favorecendo assim reação de β-eliminação, levando a formação da Dha, e consequentemente removendo o átomo de Se da enzima. No caso da inibição covalente por MeHg (Sec-Se–HgMe), a ação de agentes sequestrantes de MeHg poderiam reativar a enzima inibida, no entanto, caso ocorra a β-eliminação essa inibição é irreversível, uma vez que o átomo de Se é removido da enzima (MA et al., 2003). Apesar da reação de β-eliminação poder ser considerada benéfica em compostos organocalcogênicos atuando como pro-drogas (ANDREADOU et al., 1996; ROOSEBOOM et al., 2002), ela também pode ser considerada tóxica, dado que ácidos selenínicos poderiam inibir a δ-AlaD (Capítulo 2) (NOGARA; ORIAN; ROCHA, 2020).

Neste sentido, o planejamento e desenvolvimento de compostos capazes de remover o MeHg do sítio ativo de selenoenzimas (ou outro alvo macromolecular), é essencial para auxiliar no tratamento de intoxicação. Estudos sugerem que a forma reduzida do Ebs e DPDSe poderiam formar os adutos Ebs-Se–HgMe e PhSe–HgMe que seriam menos tóxicos (BARBOSA et al., 2017;

MEINERZ et al., 2017). As simulações de *docking* demonstraram que tanto os grupos selenolato e selenol dos metabólitos do Ebs e DPDSe poderiam acessar o sítio ativo da GPx inibida por MeHg (GPx-Se–HgMe), apresentando a interação Se···Hg, indicando assim uma possível reação de troca, ou reação de Rabenstein, entre essas espécies (GPx-Se–HgMe + R–Se(H) → GPx-Se(H) + R–Se–HgMe, R = Ebs, Ph) (Capítulo 3). Além disso, aqui foi demonstrado que os compostos piridinil(quinolil)-tio(seleno)semicarbazidas também poderiam interagir com a GPx-Se–HgMe, indicando serem potenciais agentes sequestrantes de MeHg. Uma possível vantagem desses compostos é que o átomo de S e Se, nas formas de tionas e selenonas, são nucleófílos, sendo assim, a 'ativação' dessas moléculas pela TrxR não seria necessária.

Devido as inúmeras propriedades terapêuticas associadas aos organosselênios, sugerindo que essas moléculas possuem uma baixa seletividade frente a alvos macromoleculares celulares (BARBOSA et al., 2017; NOGARA; OLIVEIRA; ROCHA, 2020), o desenvolvimento de compostos mais seletivos é essencial. Considerando que o Ebs é um composto com baixa toxicidade, sua estrutura pode ser utilizada no planejamento de novos candidatos à fármacos. Nesse sentido, híbridos do Ebselen foram testados virtualmente frente a AChE, como possíveis agentes no tratamento da DA (LUO et al., 2013). Dentre os compostos testados, a molécula Ebs-Hist-Thaτ demonstrou a formação de um complexo muito estável com a AChE, indicando ser um possível inibidor da AChE (Capítulo 3). Além disso, levando em consideração a importância de organosselênios como agentes capazes de interagir com resíduos de Cys, em especifico o grupo 1,2-selenazol, moléculas derivadas do Ebs e peptídeos foram simuladas frente a enzima Mpro, um importante alvo terapêutico para o desenvolvimento de drogas para o tratamento da COVID-19 (SIES; PARNHAM, 2020). Assim, o composto LQSG-Se-3 mostrou resultados promissores, sendo um bom candidato a inibidor da Mpro, devido a interação Se···S com a Cys145 (Capítulo 3). Além disso, simulações da toxicidade desses compostos hipotéticos foram realizadas, através do *docking* com a δ-AlaD e do servidor pkCSM (Capítulo 3). Os dados sugerem que essas moléculas não são capazes de oxidar os resíduos de Cys da δ-AlaD, uma vez que não apresentaram a interação S···Se. No entanto, a predição da toxicidade sugere que somente os compostos Py-COOH-S e Py-COOH-Se poderiam ser atóxicos, assim, podendo serem considerados bons candidatos a fármacos em futuros estudos.

6. CONCLUSÃO

O uso de ferramentas *in silico* (*docking* molecular, modelagem por homologia, cálculos de DFT, e predição de toxicidade) foram essenciais para uma melhor compreensão da ação biológicas de compostos orgânicos de selênio e de mercúrio.

Desta forma, de acordo com os objetivos propostos neste estudo, verificou-se que:

(a) A inibição da δ-AlaD por organosselênios pode envolver a interação entre o átomo de Se e o grupo tiolato da Cys124. Ademais, as formas oxidadas dos compostos de Se são mais eletrofílicas que seus respectivos selenetos, e apresentam a coordenação Zn···O, o que poderia estar associado com o maior efeito inibitório dessas moléculas;

(b) O *docking* molecular entre organosselênios e enzima TrxR demonstrou que esses compostos são capazes de acessar o sítio ativo enzimático de modo que um ataque nucleofilico da Sec498 sobre o átomo de Se possa ocorrer, assim, reduzindo esses compostos para suas formas –Se^-/–SeH;

(c) As espécies de MeHg (MeHgCl, MeHgOH, MeHgCys e MeHgGSH) são capazes de interagir com o resíduos de Sec dos sítios ativos da GPx e TrxR, onde através da interação Se···Hg, a formação do aduto enzima-Se–HgMe poderia ocorrer, e consequentemente inibindo as enzimas;

(d) Os cálculos de DFT sugerem que o aduto entre a Sec e MeHg (Sec-Se–HgMe) após ser oxidado pela H_2O_2, pode sofrer uma reação de β-eliminação *syn*-intramolecular, que leva a formação da Dha e removendo o Se do sítio ativo, assim, podendo inibir irreversivelmente selenoenzimas, tais como a GPx.

(e) Novos compostos com potencial eficiência terapêutica foram planejados. Assim, piridinil-tio(seleno)semicarbazidas podem ser agentes sequestrantes de MeHg, o híbrido Ebs-Hist-Thaτ é um potencial inibidor da AChE humana, e o selenazoil-peptideos LQSG-Se-3 poderá ser um candidato a inibidor da Mpro viral.

Conjuntamente, os dados *in silico* apresentados podem auxiliar no entendimento da toxicologia do MeHg e organosselênios, além de guiar para o desenvolvimento de futuras moléculas quelantes de Hg e compostos com alta seletividade frente a seus alvos terapêuticos (tais como inibidores enzimáticos), colaborando desta forma para a ciência e saúde pública.

7. PERSPECTIVAS

Os dados aqui apresentados podem auxiliar no desenvolvimento de futuros trabalhos envolvendo organosselênios e MeHg. Novos organocalcogênios devem ser planejados visando uma alta seletividade a seus alvos proteicos e com menor toxicidade frente a inibição da δ-AlaD.

A atividade sequestrante de MeHg de piridinil-tio(seleno)semicarbazidas, e o potencial inibitório da AChE humana e Mpro viral pelos híbridos Ebs-Hist-Thaτ e LQSG-Se-3, respectivamente, podem ser avaliados em futuros testes *in vitro* e *in vivo*. Também, estudos práticos envolvendo a β-eliminação da Cys e Sec ligadas ao MeHg, bem como utilizando tio(seleno)proteínas, podem revelar informações importantes sobre o mecanismo de inibição desta neurotoxina e a formação de nanopartículas de HgSe.

8. BIBLIOGRAFIA

AKINCIOGLU, H.; GÜLÇIN, İ. Potent Acetylcholinesterase Inhibitors: Potential Drugs for Alzheimer's Disease. **Mini-Reviews in Medicinal Chemistry**, 2020.

ANDREADOU, I. et al. Synthesis of novel Se-substituted selenocysteine derivatives as potential kidney selective prodrugs of biologically active selenol compounds: Evaluation of kinetics of β-elimination reactions in rat renal cytosol. **Journal of Medicinal Chemistry**, v. 39, n. 10, p. 2040–2046, 1996.

ARAÚJO, M. De; FARIA, M. Mercuralismo metálico crônico ocupacional. **Revista de Saúde Pública**, v. 37, n. 1, p. 116–127, 2003.

ARNÉR, E. S. J.; HOLMGREN, A. Physiological functions of thioredoxin and thioredoxin reductase. **European Journal of Biochemistry**, v. 267, n. 20, p. 6102–6109, 2000.

ARNOLD, A. P.; TAN, K.; RABENSTEIN, D. L. Nucelar Magnetic Resonance Studies of the Solution Chemistry of Metal Complexes. 23. Complexation of Methylmercury by Selenohydryl-Containing Amino Acids and Related Molecules. **Inorganic Chemistry**, v. 25, n. 14, p. 2433–2437, 1986.

ARNOLD, K. et al. The SWISS-MODEL workspace: A web-based environment for protein structure homology modelling. **Bioinformatics**, v. 22, n. 2, p. 195–201, 2006.

BAJDA, M. et al. Structure-Based Search for New Inhibitors of Cholinesterases. **International Journal of Molecular Sciences**, v. 14, p. 5608–5632, 2013.

BANERJEE, M.; ROY, G. Cleavage of Hg-C Bonds of Organomercurials Induced by ImOHSe via Two Distinct Pathways. **Inorganic Chemistry**, v. 56, n. 21, p. 12739–12750, 2017.

BANERJEE, P. et al. ProTox-II: a webserver for the prediction of toxicity of chemicals. **Nucleic Acids Research**, v. 46, p. 257–263, 2018.

BARBOSA, N. V. et al. Organoselenium compounds as mimics of selenoproteins and thiol modifier agents. **Metallomics**, v. 9, n. 12, p. 1703–1734, 2017.

BAYSE, C. A.; ALLISON, B. D. Activation energies of selenoxide elimination from Se-substituted selenocysteine. **Journal of Molecular Modeling**, v. 13, p. 47–53, 2007.

BERNHOFT, R. A. Mercury toxicity and treatment: A review of the literature. **Journal of Environmental and Public Health**, v. 2012, p. 460508, 2012.

BRANCO, V.; CARVALHO, C. The thioredoxin system as a target for mercury compounds. **Biochimica et Biophysica Acta - General Subjects**, v. 1863, n. 12, p. 129255, 2019.

BRIGELIUS-FLOHÉ, R.; MAIORINO, M. Glutathione peroxidases. **Biochimica et Biophysica Acta - General Subjects**, v. 1830, n. 5, p. 3289–3303, 2013.

BROWN, K.; ARTHUR, J. Selenium, selenoproteins and human health: a review. **Public Health Nutrition**, v. 4, n. 2b, p. 593–599, 2001.

CAPPER, M. J. et al. The cysteine-reactive small molecule ebselen facilitates effective SOD1 maturation. **Nature Communications**, v. 9, n. 1693, p. 1–9, 2018.

CARVALHO, C. M. L. et al. Inhibition of the human thioredoxin system: A molecular mechanism

of mercury toxicity. **Journal of Biological Chemistry**, v. 283, n. 18, p. 11913–11923, 2008.

CARVALHO, I. et al. Introdução a modelagem molecular de fármacos no curso experimental de química farmacêutica. **Quimica Nova**, v. 26, n. 3, p. 428–438, 2003.

CHANDRA, S.; PARMAR, S.; KUMAR, Y. Synthesis, spectroscopic, and antimicrobial studies on bivalent zinc and mercury complexes of 2-formylpyridine thiosemicarbazone. **Bioinorganic Chemistry and Applications**, v. 2009, p. 851316, 2009.

CHANG, M. W. et al. Virtual screening for HIV protease inhibitors: A comparison of AutoDock 4 and Vina. **PLoS ONE**, v. 5, n. 8, p. 1–9, 2010.

CHEN, Y.-C. Beware of docking! **Trends in Pharmacological Sciences**, v. 36, n. 2, p. 78–95, 2015.

CHEN, Y. et al. Analytical methods, formation, and dissolution of cinnabar and its impact on environmental cycle of mercury. **Critical Reviews in Environmental Science and Technology**, v. 47, n. 24, p. 2415–2447, 2017.

CHEN, Y.; LIU, Q.; GUO, D. Emerging coronaviruses: Genome structure, replication, and pathogenesis. **Journal of Medical Virology**, v. 92, n. 4, p. 418–423, 2020.

CHIERRITO, T. P. C. et al. From dual binding site acetylcholinesterase inhibitors to allosteric modulators: A new avenue for disease-modifying drugs in Alzheimer's disease. **European Journal of Medicinal Chemistry**, v. 139, p. 773–791, 2017.

CLARKSON, T. W.; MAGOS, L. The toxicology of mercury and its chemical compounds. **Critical Reviews in Toxicology**, v. 36, n. 8, p. 609–662, 2006.

CUI, Q.; ELSTNER, M. Density functional tight binding: Values of semi-empirical methods in an ab initio era. **Physical Chemistry Chemical Physics**, v. 16, n. 28, p. 14368–14377, 2014.

DASSAULT SYSTÈMES BIOVIA. **Accelrys Discovery Studio Visualizer**San Diego, 2017. .

DE CLERCQ, E. Strategies in the design of antiviral drugs. **Nature Reviews Drug Discovery**, v. 1, p. 13–25, 2002.

DU, Q. S. et al. Polyprotein cleavage mechanism of SARS CoV M pro and chemical modification of the octapeptide. **Peptides**, v. 25, n. 11, p. 1857–1864, 2004.

DUARTE, H. A. Índices de reatividade química a partir da teoria do funcional de densidade: formalismo e perspectivas. **Química Nova**, v. 24, n. 4, p. 501–508, 2001.

DVIR, H. et al. Acetylcholinesterase : From 3D structure to function. **Chemico-Biological Interactions**, v. 187, p. 10–22, 2010.

EKINO, S. et al. Minamata disease revisited: An update on the acute and chronic manifestations of methyl mercury poisoning. **Journal of the Neurological Sciences**, v. 262, n. 1–2, p. 131–144, 2007.

FARINA, M. et al. Reaction of diphenyl diselenide with hydrogen peroxide and inhibition of delta-aminolevulinate dehydratase from rat liver and cucumber leaves. **Brazilian Journal of Medical and Biological Research**, v. 35, n. 6, p. 623–631, 2002.

FARINA, M.; ASCHNER, M. Methylmercury-Induced Neurotoxicity: Focus on Pro-oxidative Events and Related Consequences. **Advances in Neurobiology**, v. 18, p. 267–286, 2017.

FARINA, M.; ASCHNER, M. Glutathione antioxidant system and methylmercury-induced neurotoxicity : An intriguing interplay. **Biochimica et Biophysica Acta - General Subjects**, v. 1863, n. 12, p. 129285, 2019.

FARINA, M.; ASCHNER, M.; ROCHA, J. B. T. Oxidative stress in MeHg-induced neurotoxicity. **Toxicology and Applied Pharmacology**, v. 256, n. 3, p. 405–417, 2011.

FARINA, M.; ROCHA, J. B. T.; ASCHNER, M. Mechanisms of methylmercury-induced neurotoxicity: Evidence from experimental studies. **Life Sciences**, v. 89, n. 15–16, p. 555–563, 2011.

FERREIRA, L. G. et al. **Molecular docking and structure-based drug design strategies**. [s.l: s.n.]v. 20

FOLCH, J. et al. Current Research Therapeutic Strategies for Alzheimer's Disease Treatment. **Neural Plasticity**, v. 2016, p. 8501693, 2016.

FORLI, S. et al. Computational protein–ligand docking and virtual drug screening with the AutoDock suite. **Nature Protocols**, v. 11, n. 5, p. 905–919, 2016.

FRANCO, J. L. et al. Methylmercury neurotoxicity is associated with inhibition of the antioxidant enzyme glutathione peroxidase. **Free Radical Biology and Medicine**, v. 47, p. 449–457, 2009.

FRIEDMAN, R.; BOYE, K.; FLATMARK, K. Molecular modelling and simulations in cancer research. **Biochimica et Biophysica Acta - Reviews on Cancer**, v. 1836, n. 1, p. 1–14, 2013.

FRIESNER, R. A. Ab initio quantum chemistry: Methodology and applications. **Proceedings of the National Academy of Sciences of the United States of America**, v. 102, n. 19, p. 6648–6653, 2005.

FRISCH, M. J. et al. **Gaussian 09**Wallingford CTGaussian Inc., , 2009. .

GAJDOSECHOVA, Z. et al. In vivo formation of natural HgSe nanoparticles in the liver and brain of pilot whales. **Scientific Reports**, v. 6, n. September, p. 1–11, 2016.

GALIMBERTI, D.; SCARPINI, E. Old and new acetylcholinesterase inhibitors for Alzheimer's Disease. **Expert Opinion on Investigational Drugs**, v. 25, n. 10, p. 1181–1187, 2016.

GENHEDEN, S. et al. Computational Chemistry and Molecular Modelling Basics. In: MARTIN-SANTAMARIA, S. (Ed.). **Computational Tools for Chemical Biology**. London UK: Royal Society of Chemistry, 2017. p. 1–38.

GO, Y. M.; CHANDLER, J. D.; JONES, D. P. The cysteine proteome. **Free Radical Biology and Medicine**, v. 84, p. 227–245, 2015.

GOGOI, D. et al. 3D pharmacophore-based virtual screening, docking and density functional theory approach towards the discovery of novel human epidermal growth factor receptor-2 (HER2) inhibitors. **Journal of Theoretical Biology**, v. 411, p. 68–80, 2016.

GRANDJEAN, P. et al. Adverse effects of methylmercury: Environmental health research implications. **Environmental Health Perspectives**, v. 118, n. 8, p. 1137–1145, 2010.

GREGOIRE, D. S.; POULAIN, A. J. A physiological role for Hg II during phototrophic growth. **Nature Geoscience**, v. 9, n. 2, p. 121–125, 2016.

GUHA, R. On Exploring Structure-Activity Relationships. In: KORTAGERE, S. (Ed.). **Methods**

in Molecular Biology. Totowa, NJ: Humana Press, 2013. 993p. 81–94.

GUPTA, M.; SHARMA, R.; KUMAR, A. Docking techniques in pharmacology: How much promising? **Computational Biology and Chemistry**, v. 76, p. 210–217, 2018.

HAMPEL, H. et al. The cholinergic system in the pathophysiology and treatment of Alzheimer's disease. **Brain**, v. 141, n. 7, p. 1917–1933, 2018.

HEINEMANN, I. U.; JAHN, M.; JAHN, D. The biochemistry of heme biosynthesis. **Archives of Biochemistry and Biophysics**, v. 474, p. 238–251, 2008.

HEVERLY-COULSON, G. S.; BOYD, R. J. Theoretical Investigations on the Reaction of Monosubstituted Tertiary-Benzylamine Selenols with Hydrogen Peroxide. **The Journal of Physical Chemistry A**, v. 114, p. 10706–10711, 2010.

HINTELMANN, H. Organomercurials. Their Formation and Pathways in the Environment. In: SIGEL, A.; SIGEL, H.; SIGEL, R. K. O. (Ed.). **Metal Ions in Life Sciences**. [s.l.] Royal Society of Chemistry, 2010. p. 365–401.

HOLLINGSWORTH, S. A.; DROR, R. O. Molecular Dynamics Simulation for All. **Neuron**, v. 99, n. 6, p. 1129–1143, 2018.

HOWELL, J. A. S. DFT investigation of the interaction between gold (I) complexes and the active site of thioredoxin reductase. **Journal of Organometallic Chemistry**, v. 694, n. 6, p. 868–873, 2009.

HUGHES, J. P. et al. Principles of early drug discovery. **British Journal of Industrial Medicine**, v. 162, p. 1239–1249, 2011.

IWANAGA, Y. et al. Characterization of acetylcholinesterase-inhibition by itopride. **Japanese journal of pharmacology**, v. 66, n. 3, p. 317–22, 1994.

JAFFE, E. K. The porphobilinogen synthase family of metalloenzymes. **Acta Crystallographica Section D: Biological Crystallography**, v. 56, n. 2, p. 115–128, 2000.

JAFFE, E. K. The porphobilinogen synthase catalyzed reaction mechanism. **Bioorganic Chemistry**, v. 32, n. 5, p. 316–325, 2004.

JAGGER, B. R. et al. Multiscale simulation approaches to modeling drug–protein binding. **Current Opinion in Structural Biology**, v. 61, p. 213–221, 2020.

JANG, C. et al. Identification of novel acetylcholinesterase inhibitors designed by pharmacophore-based virtual screening, molecular docking and bioassay. **Scientific Reports**, v. 8, p. 14921, 2018.

JIN, Z. et al. Structure of Mpro from COVID-19 virus and discovery of its inhibitors. **Nature**, v. 582, p. 289–293, 2020.

JOHANSSON, L.; GAFVELIN, G.; ARNÉR, E. S. J. Selenocysteine in proteins - Properties and biotechnological use. **Biochimica et Biophysica Acta - General Subjects**, v. 1726, n. 1, p. 1–13, 2005.

JOHANSSON, M. P.; KAILA, V. R. I.; SUNDHOLM, D. AbInitio, Density Functional Theory, and Semi-Empirical Calculations. In: MONTICELLI, L.; SALONEN, E. (Ed.). **Biomolecular Simulations: Methods and Protocols**. New York: Springer, 2013. 924p. 3–27.

KADE, I. J. et al. Comparative Studies on Dicholesteroyl Diselenide and Diphenyl Diselenide as

Antioxidant Agents and their Effect on the Activities of Na+/K+ ATPase and δ-Aminolevulinic acid Dehydratase in the Rat Brain. **Neurochemical Research**, v. 33, n. 1, p. 167–178, 2008.

KADE, I. J.; ROCHA, J. B. T. Comparative study on the influence of subcutaneous administration of diphenyl and dicholesteroyl diselenides on sulphydryl proteins and antioxidant parameters in mice. **Journal of Applied Toxicology**, v. 30, n. 7, p. 688–693, 2010.

KAMP, M. W. Van Der; MULHOLLAND, A. J. Combined quantum mechanics/molecular mechanics (QM/MM) methods in computational enzymology. **Biochemistry**, v. 52, n. 16, p. 2708–2728, 2013.

KATSAMAKAS, S.; HADJIPAVLOU-LITINA, D. Computational Design of Multitarget Drugs Against Alzheimer's Disease. In: K., R. (Ed.). **Methods in Pharmacology and Toxicology**. New York, NY: Humana Press, 2018. p. 203–253.

KITCHEN, D. B. et al. Docking and scoring in virtual screening for drug discovery: methods and applications. **Nature Reviews Drug Discovery**, v. 3, n. November, p. 935–949, 2004.

KORBAS, M. et al. The chemical nature of mercury in human brain following poisoning or environmental exposure. **ACS Chemical Neuroscience**, v. 1, n. 12, p. 810–818, 2010.

KOSNETT, M. J. The Role of Chelation in the Treatment of Arsenic and Mercury Poisoning. **Journal of Medical Toxicology**, v. 9, n. 4, p. 347–354, 2013.

KRISTENSEN, A. K. B.; THOMSEN, J. F.; MIKKELSEN, S. A review of mercury exposure among artisanal small-scale gold miners in developing countries. **International Archives of Occupational and Environmental Health**, v. 87, n. 6, p. 579–590, 2014.

KRYUKOV, G. V. et al. Characterization of mammalian selenoproteomes. **Science**, v. 300, n. 5624, p. 1439–1443, 2003.

LEWARS, E. G. **Computational Chemistry: Introduction to the Theory and Applications of Molecular and Quantum Mechanics**. 3. ed. New York: Springer, 2016.

LI, G.; DE CLERCQ, E. Therapeutic options for the 2019 novel coronavirus (2019-nCoV). **Nature Reviews Drug Discovery**, v. 19, p. 149–150, 2020.

LIM, J. et al. Case of the index patient who caused tertiary transmission of coronavirus disease 2019 in Korea: The application of lopinavir/ritonavir for the treatment of COVID-19 pneumonia monitored by quantitative RT-PCR. **Journal of Korean Medical Science**, v. 35, n. 7, p. 1–6, 2020.

LIPINSKI, C. A. et al. Experimental and computational approaches to estimate solubility and permeability in drug discovery and development settings. **Advanced Drug Delivery Reviews**, v. 23, p. 3–25, 1997.

LOPACHIN, R. M.; GAVIN, T. Reactions of electrophiles with nucleophilic thiolate sites: Relevance to pathophysiological mechanisms and remediation. **Free Radical Research**, v. 50, n. 2, p. 195–205, 2016.

LOPES, J. P. B. et al. Design, synthesis , cholinesterase inhibition and molecular modelling study of novel tacrine hybrids with carbohydrate derivatives. **Bioorganic & Medicinal Chemistry**, v. 26, p. 5566–5577, 2018.

LÖWIG, C. Ueber Schwefelwasserstoff- und Selenwasserstoffäther. **Annalen Der Physik Und Chemie**, v. 113, n. 3, p. 550–553, 1836.

LU, J.; BERNDT, C.; HOLMGREN, A. Metabolism of selenium compounds catalyzed by the mammalian selenoprotein thioredoxin reductase. **Biochimica et Biophysica Acta - General Subjects**, v. 1790, n. 11, p. 1513–1519, 2009.

LUO, Z. et al. Synthesis and evaluation of multi-target-directed ligands against Alzheimer's disease based on the fusion of donepezil and ebselen. **Journal of Medicinal Chemistry**, v. 56, n. 22, p. 9089–9099, 2013.

MA, S. et al. Loss of selenium from selenoproteins: Conversion of selenocysteine to dehydroalanine in vitro. **Journal of the American Society for Mass Spectrometry**, v. 14, p. 593–600, 2003.

MADABENI, A. et al. Chalcogen-mercury bond formation and disruption in model Rabenstein's reactions: A computational analysis. **Journal of Computational Chemistry**, v. June, p. 1–10, 2020.

MALM, O. Gold Mining as a Source of Mercury Exposure in the Brazilian Amazon. **Environmental Research**, v. 77, p. 73–78, 1998.

MAO, F. et al. Novel tacrine-ebselen hybrids with improved cholinesterase inhibitory, hydrogen peroxide and peroxynitrite scavenging activity. **Bioorganic and Medicinal Chemistry Letters**, v. 23, n. 24, p. 6737–6742, 2013.

MARKOVIC, M.; BEN-SHABAT, S.; DAHAN, A. Computational simulations to guide enzyme-mediated prodrug activation. **International Journal of Molecular Sciences**, v. 21, n. 10, 2020.

MASAKI, C. et al. Effects of the potential lithium-mimetic, ebselen, on brain neurochemistry: A magnetic resonance spectroscopy study at 7 tesla. **Psychopharmacology**, v. 233, n. 6, p. 1097–1104, 2016a.

MASAKI, C. et al. Effects of the potential lithium-mimetic, ebselen, on impulsivity and emotional processing. **Psychopharmacology**, v. 233, n. 14, p. 2655–2661, 2016b.

MASON, R.; FITZGERALD, W.; MOREL, F. The biogeochemical cycling of elemental mercury: Anthropogenic influences. **Geochimica et Cosmochimica Acta**, v. 58, n. 15, p. 3191–3198, 1994.

MEHTA, M.; ADEM, A.; SABBAGH, M. New Acetylcholinesterase Inhibitors for Alzheimer's Disease. **International Journal of Alzheimer's Disease**, v. 2012, p. 728983, 2012.

MEINERZ, D. F. et al. Diphenyl diselenide protects against methylmercury-induced inhibition of thioredoxin reductase and glutathione peroxidase in human neuroblastoma cells: a comparison with ebselen. **Journal of Applied Toxicology**, v. 37, n. 9, p. 1073–1081, 2017.

MELNICK, J. G.; PARKIN, G. Cleaving mercury-alkyl bonds: A functional model for mercury detoxification by MerB. **Science**, v. 317, n. 5835, p. 225–227, 2007.

MELNICK, J. G.; YURKERWICH, K.; PARKIN, G. On the Chalcogenophilicity of Mercury: Evidence for a Strong Hg−Se Bond in [TmBut]HgSePh and Its Relevance to the Toxicity of Mercury. **Journal of the American Chemical Society**, v. 132, n. 2, p. 647–655, 2010.

MOLTER, A. et al. Synthesis, structures, 119Sn Mössbauer spectroscopic studies and biological activity of some tin(IV) complexes containing pyridyl functionalised selenosemicarbazonato ligands. **Journal of Organometallic Chemistry**, v. 701, p. 80–86, 2012.

MORRIS, G. M. et al. Automated Docking Using a Lamarckian Genetic Algorithm and an

Empirical Binding Free Energy Function. **Journal of Computational Chemistry**, v. 19, n. 14, p. 1639–1662, 1998.

MORSE, J. S. et al. Learning from the Past: Possible Urgent Prevention and Treatment Options for Severe Acute Respiratory Infections Caused by 2019-nCoV. **ChemBioChem**, v. 21, n. 5, p. 730–738, 2020.

MUGESH, G.; SINGH, H. B. Synthetic organoselenium compounds as antioxidants: Glutathione peroxidase activity. **Chemical Society Reviews**, v. 29, n. 5, p. 347–357, 2000.

MUNNIK, M. et al. Targeting the: Mycobacterium tuberculosis transpeptidase LdtMt2 with cysteine-reactive inhibitors including ebselen. **Chemical Communications**, v. 55, n. 69, p. 10214–10217, 2019.

MUSTACICH, D.; POWIS, G. Thioredoxin reductase. **Biochemical Journal**, v. 346, p. 1–8, 2000.

NIKOLIC, K. et al. Drug Design for CNS Diseases: Polypharmacological Profiling of Compounds Using Cheminformatic, 3D-QSAR and Virtual Screening Methodologies. **Frontiers in Neuroscience**, v. 10, p. 265, 2016.

NIRMALA, M. et al. Ruthenium(II) complexes of hybrid 8-hydroxyquinoline-thiosemicarbazone ligands: Synthesis, characterization and catalytic applications. **Applied Organometallic Chemistry**, v. 28, n. 1, p. 18–26, 2014.

NITSCHE, C. Proteases from dengue, West Nile and Zika viruses as drug targets. **Biophysical Reviews**, v. 11, n. 2, p. 157–165, 2019.

NOETZLI, M.; EAP, C. B. Pharmacodynamic , Pharmacokinetic and Pharmacogenetic Aspects of Drugs Used in the Treatment of Alzheimer's Disease. **Clinical Pharmacokinetics**, v. 52, p. 225–241, 2013.

NOGARA, P. A. et al. Methylmercury's chemistry: From the environment to the mammalian brain. **Biochimica et Biophysica Acta - General Subjects**, v. 1863, n. 12, p. 129284, 2019a.

NOGARA, P. A. et al. Mercury in Our Food. **Chemical Research in Toxicology**, v. 32, n. 8, p. 1459–1461, 2019b.

NOGARA, P. A.; OLIVEIRA, C. S.; ROCHA, J. B. T. Chemistry and pharmacology of synthetic organoselenium compounds. In: RANU, B. C.; BANERJEE, B. (Ed.). **Organoselenium Chemistry**. Berlin: De Gruyter, 2020. p. 305–346.

NOGARA, P. A.; ORIAN, L.; ROCHA, J. B. T. The Se…S/N interactions as a possible mechanism of δ-aminolevulinic acid dehydratase enzyme inhibition by organoselenium compounds: A computational study. **Computational Toxicology**, v. 15, p. 100127, 2020.

NOGARA, P. A.; ROCHA, J. B. T. In Silico Studies of Mammalian δ-ALAD Interactions with Selenides and Selenoxides. **Molecular Informatics**, v. 37, p. 1700091, 2018.

NOGUEIRA, C. W. et al. Organochalcogens effects on d-aminolevulinate dehydratase activity from human erythrocytic cells in vitro. **Toxicology**, v. 191, p. 169–178, 2003.

NOGUEIRA, C. W.; ROCHA, J. B. T. Toxicology and pharmacology of selenium: emphasis on synthetic organoselenium compounds. **Archives of Toxicology**, v. 85, p. 1313–1359, 2011.

NOGUEIRA, C. W.; ZENI, G.; ROCHA, J. B. T. Organoselenium and organotellurium

compounds: Toxicology and pharmacology. **Chemical Reviews**, v. 104, n. 12, p. 6255–6285, 2004.

OLIVEIRA, C. S. et al. Chemical Speciation of Selenium and Mercury as Determinant of Their Neurotoxicity. In: ASCHNER, M.; COSTA, L. G. (Ed.). **Neurotoxicity of Metals, Advances in Neurobiology**. New York: Springer International Publishing, 2017. 18p. 53–83.

OLIVEIRA, C. S. et al. Neurodevelopmental Effects of Mercury. In: ASCHNER, M.; COSTA, L. G. (Ed.). **Advances in Neurotoxicology**. London UK: Elsevier Inc, 2018. 2p. 27–86.

OLIVEIRA, C. S. et al. Biological thiols and their interaction with mercury. In: MCALPINE, C. C. (Ed.). **Thiols: Structure, Properties and Reactions**. New York, NY: Nova Science Publishers, 2019. p. 1–60.

ORIAN, L.; TOPPO, S. Organochalcogen peroxidase mimetics as potential drugs: A long story of a promise still unfulfilled. **Free Radical Biology and Medicine**, v. 66, p. 65–74, 2014.

PACYNA, E. G. et al. Global anthropogenic mercury emission inventory for 2000. **Atmospheric Environment**, v. 40, n. 22, p. 4048–4063, 2006.

PARKS, J. M. et al. Mechanism of Hg-C protonolysis in the organomercurial lyase MerB. **Journal of the American Chemical Society**, v. 131, n. 37, p. 13278–13285, 2009.

PATRICK, G. **An Introduction to Medicinal Chemistry**. 5. ed. Oxford: Oxford University Press, 2013.

PETTERSEN, E. F. et al. UCSF Chimera - A visualization system for exploratory research and analysis. **Journal of Computational Chemistry**, v. 25, n. 13, p. 1605–1612, 2004.

PIRES, D. E. V.; BLUNDELL, T. L.; ASCHER, D. B. pkCSM: Predicting small-molecule pharmacokinetic and toxicity properties using graph-based signatures. **Journal of Medicinal Chemistry**, v. 58, n. 9, p. 4066–4072, 2015.

PIRRONE, N. et al. Global mercury emissions to the atmosphere from anthropogenic and natural sources. **Atmospheric Chemistry and Physics**, v. 10, n. 13, p. 5951–5964, 2010.

RABENSTEIN, D. L. The Aqueous Solution Chemistry of Methylmercury and Its Complexes. **Accounts of Chemical Research**, v. 11, n. 3, p. 100–107, 1978.

RABENSTEIN, D. L.; EVANS, C. A. The mobility of methylmercury in biological systems. **Bioinorganic Chemistry**, v. 8, n. 2, p. 107–114, 1978.

RABENSTEIN, D. L.; ISAB, A. A.; REID, R. S. A proton nuclear magnetic resonance study of the binding of methylmercury in human erythrocytes. **Biochim. Biophys. Acta**, v. 696, n. 1, p. 53–64, 1982.

RABENSTEIN, D. L.; REID, R. S. Nuclear Magnetic Resonance Studies of the Solution Chemistry of Metal Complexes. 20. Ligand-Exchange Kinetics of Methylmercury(II)-Thiol Complexes. **Inorganic Chemistry**, v. 23, n. 9, p. 1246–1250, 1984.

RAIES, A. B.; BAJIC, V. B. In silico toxicology: computational methods for the prediction of chemical toxicity. **Wiley Interdisciplinary Reviews: Computational Molecular Science**, v. 6, n. April, p. 147–172, 2016.

REALE, M. et al. Butyrylcholinesterase and Acetylcholinesterase polymorphisms in Multiple

Sclerosis patients: implication in peripheral inflammation. **Scientific Reports**, v. 8, p. 1319, 2018.

RENZONI, A.; ZINO, F.; FRANCHI, E. Mercury Levels Along the Food Chain and Risk for Exposed Populations. **Environmental Research**, v. 77, p. 68–72, 1998.

RICE, K. M. et al. Environmental mercury and its toxic effects. **Journal of Preventive Medicine and Public Health**, v. 47, n. 2, p. 74–83, 2014.

ROCHA, J. B. T. et al. Aminolevulinate dehydratase (δ-ALA-D) as marker protein of intoxication with metals and other pro-oxidant situations. **Toxicology Research**, v. 1, n. 2, p. 85–102, 2012.

ROCHA, J. B. T.; PICCOLI, B. C.; OLIVEIRA, C. S. Biological and chemical interest in selenium: A brief historical account. **Arkivoc**, v. part ii, p. 457–491, 2017.

RODRIGUES, C. R. Processos modernos no desenvolvimento de farmacos: modelagem molecular. **Cadernos Temáticos de Química Nova na Escola**, v. 3, p. 43–49, 2001.

ROGOLINO, D. et al. Anti-proliferative effects of copper(II) complexes with hydroxyquinoline-thiosemicarbazone ligands. **European Journal of Medicinal Chemistry**, v. 128, p. 140–153, 2017.

ROOSEBOOM, M. et al. Comparative study on the bioactivation mechanisms and cytotoxicity of Te-phenyl-L-tellurocysteine, Se-Phenyl-L-selenocysteine, and S-Phenyl-L-cysteine. **Chemical Research in Toxicology**, v. 15, n. 12, p. 1610–1618, 2002.

ROSENBERRY, T. L. et al. Comparison of the binding of reversible inhibitors to human butyrylcholinesterase and acetylcholinesterase: a crystallographic, kinetic and calorimetric study. **Molecules**, v. 22, n. 12, p. 2098, 2017.

SANT'ANNA, C. M. R. Métodos de Modelagem Molecular para Estudo e Planejamento de Compostos Bioativos: Uma Introdução. **Revista Virtual de Química**, v. 1, n. 1, p. 49–57, 2009.

SANTI, C.; SANTORO, S.; BATTISTELLI, B. Organoselenium Compounds as Catalysts in Nature and Laboratory. **Current Organic Chemistry**, v. 14, n. 20, p. 2442–2462, 2010.

SARAIVA, R. A. et al. Molecular Docking Studies of Disubstituted Diaryl Diselenides as Mammalian δ -Aminolevulinic Acid Dehydratase Enzyme Inhibitors. **Journal ofToxicology and Environmental Health, Part A**, v. 75, p. 1012–1022, 2012.

SAUSEN DE FREITAS, A. et al. Reduction of Diphenyl Diselenide and Analogs by Mammalian Thioredoxin Reductase Is Independent of Their Gluthathione Peroxidase-Like Activity: A Possible Novel Pathway for Their Antioxidant Activity. **Molecules**, v. 15, n. 11, p. 7699–7714, 2010.

SAXENA, M.; DUBEY, R. Target Enzyme in Alzheimer's Disease: Acetylcholinesterase Inhibitors. **Current Topics in Medicinal Chemistry**, v. 19, n. 4, p. 264–275, 2019.

SCHMIDT, T.; BERGNER, A.; SCHWEDE, T. Modelling three-dimensional protein structures for applications in drug design. **Drug Discovery Today**, v. 19, n. 7, p. 890–897, 2014.

SHARMA, K. Cholinesterase inhibitors as Alzheimer's therapeutics (Review). **Molecular and Medicine Reports**, v. 20, p. 1479–1487, 2019.

SIES, H.; PARNHAM, M. J. Potential therapeutic use of ebselen for COVID-19 and other respiratory viral infections. **Free Radical Biology and Medicine**, v. 156, n. June, p. 107–112, 2020.

SILVA, F. D. et al. Molecular docking and in vitro evaluation of a new hybrid molecule (JM-20) on cholinesterase activity from different sources. **Biochimie**, v. 168, p. 297–306, 2020.

SINGH, M. et al. Acetylcholinesterase inhibitors as Alzheimer therapy: From nerve toxins to neuroprotection. **European Journal of Medicinal Chemistry**, v. 70, p. 165–188, 2013a.

SINGH, N. et al. A safe lithium mimetic for bipolar disorder. **Nature Communications**, v. 4, p. 1332–1337, 2013b.

STEINBRENNER, H.; SIES, H. Protection against reactive oxygen species by selenoproteins. **Biochimica et Biophysica Acta - General Subjects**, v. 1790, n. 11, p. 1478–1485, 2009.

STEWART, J. J. P. Optimization of parameters for semiempirical methods V: Modification of NDDO approximations and application to 70 elements. **Journal of Molecular Modeling**, v. 13, n. 12, p. 1173–1213, 2007.

STIGLIANI, J. L. et al. Cross-docking study on InhA inhibitors: A combination of Autodock Vina and PM6-DH2 simulations to retrieve bio-active conformations. **Organic and Biomolecular Chemistry**, v. 10, p. 6341–6349, 2012.

SUDATI, J. H. et al. Diselenoamino acid derivatives as GPx mimics and as substrates of TrxR:: In vitro and in silico studies. **Organic and Biomolecular Chemistry**, v. 16, n. 20, p. 3777–3787, 2018.

SUGIMOTO, H. et al. Donepezil Hydrochloride (E2020) and Other Acetylcholinesterase Inhibitors. **CurrentMedicinal Chemistry**, v. 7, p. 303–339, 2000.

TCHOUNWOU, P. B. et al. Environmental exposure to mercury and its toxicopathologic implications for public health. **Environmental Toxicology**, v. 18, n. 3, p. 149–175, 2003.

TE VELDE, G. et al. Chemistry with ADF. **Journal of Computational Chemistry**, v. 22, n. 9, p. 931–967, 2001.

TODOROVIĆ, T. R. et al. Synthesis and characterization of Zn(II) and Cd(II) complexes with 2,6-diacetylpyridine-bis(selenosemicarbazone). Crystal structure of a Ni(II) complex with a modified 2,6-diacetylpyridine-bis(selenosemicarbazone). **Inorganic Chemistry Communications**, v. 9, n. 8, p. 862–865, 2006.

TROTT, O.; OLSON, A. J. AutoDock Vina: Improving the Speed and Accuracy of Docking with a New Scoring Function, Efficient Optimization, and Multithreading. **Journal of computational chemistry**, v. 31, p. 455–461, 2010.

ULLRICH, S.; NITSCHE, C. The SARS-CoV-2 main protease as drug target. **Bioorganic and Medicinal Chemistry Letters**, v. 30, n. 17, p. 127377, 2020.

UNEP. **Global Mercury Assessment 2013: Sources, Emissions, Releases, and Environmental Transport**. Geneva: UNEP Chemicals Branch, 2013.

WAGNER, C. et al. In vivo and in vitro inhibition of mice thioredoxin reductase by methylmercury. **BioMetals**, v. 23, n. 6, p. 1171–1177, 2010.

WANG, L. et al. Ethaselen: A potent mammalian thioredoxin reductase 1 inhibitor and novel organoselenium anticancer agent. **Free Radical Biology and Medicine**, v. 52, n. 5, p. 898–908, 2012.

WU, C. et al. Analysis of therapeutic targets for SARS-CoV-2 and discovery of potential drugs by computational methods. **Acta Pharmaceutica Sinica B**, v. 10, n. 5, p. 766–788, 2020.

YAN, Y. et al. The First 75 Days of Novel Coronavirus (SARS-CoV-2) Outbreak: Recent Advances, Prevention, and Treatment. **International Journal of Environmental Research and Public Health**, v. 17, n. 7, p. 2323, 2020.

ZHANG, L. et al. Crystal structure of SARS-CoV-2 main protease provides a basis for design of improved α-ketoamide inhibitors. **Science**, v. 368, p. 409–412, 2020.

ZHAO, R.; HOLMGREN, A. A novel antioxidant mechanism of ebselen involving ebselen diselenide, a substrate of mammalian thioredoxin and thioredoxin reductase. **Journal of Biological Chemistry**, v. 277, n. 42, p. 39456–39462, 2002.

9. APÊNDICE

9.1. ARTIGO: MERCURY IN OUR FOOD

Chemical Research in Toxicology

ToxWatch

Cite This: *Chem. Res. Toxicol.* 2019, 32, 1459−1461

pubs.acs.org/crt

Mercury in Our Food

Pablo A. Nogara,[†] Marcelo Farina,[‡] Michael Aschner,[§] and Joao B. T. Rocha*[,†]

[†]Departamento de Bioquímica e Biologia Molecular, Centro de Ciências Naturais e Exatas, Universidade Federal de Santa Maria, Santa Maria, Rio Grande do Sul 97105-900, Brazil

[‡]Departamento de Bioquímica, Centro de Ciências Biológicas, Universidade Federal de Santa Catarina, Florianópolis, Santa Catarina 88040-900, Brazil

[§]Department of Molecular Pharmacology, Albert Einstein College of Medicine, Bronx, New York 10461, United States

ABSTRACT: The methylation of mercuric mercury (Hg^{2+}) in the aquatic sediments produces methylmercury (CH_3Hg^+), which is biomagnified along the food chain. The ingestion of piscivorous fish or aquatic mammals by pregnant women is of concern because it can cause long-lasting neurobehavioral deficits in their offspring.

Mercury (Hg) is one of the most toxic elements in the periodic table, particularly when in the cationic states (i.e., in the electrophilic Hg forms or E^+Hg forms, for example, Hg^{2+}, CH_3Hg^+, and $CH_3CH_2Hg^+$). Elemental Hg (Hg^0) is liquid at room temperature, and, as a consequence of this property, it has been exploited by humanity for centuries. Hg^0 is utilized in artisanal gold mining and mercury-vapor lamps. It can still be found in medical devices (sphygmomanometers and thermometers).[1,2] Exposure to ethylmercury ($CH_3CH_2Hg^+$) remains a concern in developing countries, where $CH_3CH_2Hg^+$ complexed with thiosalicylic acid forms the antimicrobial agent thimerosal (ethyl(2-mercaptobenzoato-(2-)-O,S) mercurate(1-) sodium). Thimerosal is used as a preservative in multiple-dose vaccine vials,[2] and newborns in developing countries are still commonly exposed to high levels of $CH_3CH_2Hg^+$ during the schedule of immunization just after birth and during the first years of life. The natural and anthropogenic release of Hg in the environment are of great neurotoxicological concerns because the developing mammalian brain is susceptible to low concentrations of CH_3Hg^+.[1−4] After the outbreaks of Minamata Bay in Japan, where humans were exposed to toxic levels of mercury released by Chisso Corporation, mercury became notorious for its neurotoxicity.[1−4] Fish and seafood from Minamata Bay, Japan, contained elevated levels of mercury (from 6 to 36 ppm of Hg),[2] and those who had fish as the primary source of protein developed neuropathological signs of intoxication (Minamata disease). The case of Minamata was instrumental in the history of environmental contamination by industrial waste products and to unravel the strong neuro-teratogenic effects of CH_3Hg^+ in mammals.[1−4] Indeed, the main lesson from the unfortunate outbreak in Minamata Bay was the tremendous susceptibility of the developing brain to CH_3Hg^+.[1−4]

The levels of mercury in fish from noncontaminated areas are lower than those found in Minamata Bay. For instance, piscivorous fish (shark, swordfish, cod, etc.) can have from 0.1 to 3 ppm of Hg in their muscles. Marine carnivorous mammals have even more, for instance, the liver of pilot whale (*Globicephalus meleanus*) can have nearly 10 ppm of Hg.[2] Consumption of fish from noncontaminated regions typically does not produce overt signs of neurotoxicity. However, several reports have indicated subtle and long-lasting neuropsychological effects resulting from relatively low-level CH_3Hg^+ exposures during periods of human brain development.[1−4] While debatable as to whether very low levels of mercury during critical periods of human brain development can cause long-lasting cognitive impairments, *in vitro* and *in vivo* experimental data strongly attest to the sensitivity of the developing brain to CH_3Hg^+.[1−4] Notably, the US EPA's Mercury Study Report to Congress[5] estimates that 8% of US women of childbearing age have blood mercury levels exceeding the reference-dose (RfD) of 0.1 μg Hg/kg body-weight/day. Furthermore, nearly 300 000 babies in the US may be at risk of having learning disabilities due to exposure to CH_3Hg^+ during the gestational period.[5]

The long-lasting disruption in synaptic transmission after CH_3Hg^+ intoxication has been demonstrated for excitatory and inhibitory neurotransmitters, for instance, glutamate and GABA.[2,4] The neurochemical disturbances caused by CH_3Hg^+ in neurotransmission are considered secondary molecular events that activate adverse outcome pathways (AOP) associated with CH_3Hg^+-induced neurotoxicity. However, our knowledge about the primary targets of CH_3Hg^+ is still limited. The identification of molecular initiating events (MIEs) involved in the toxicity of CH_3Hg^+ will require coordinate endeavors from neuroscientists, toxicologists, and analytical biochemists. Although different molecular targets of CH_3Hg^+ have been described, it is not clear whether they are the primary or secondary targets of CH_3Hg^+.[2,4]

Electrophilic mercury forms (CH_3Hg^+, $CH_3CH_2Hg^+$, and Hg^{2+}) have strong affinity for thiol and selenol groups (−S(e)H) and will form complexes with the sulfur or selenium atoms of −S(e)H groups (formation constants of CH_3Hg−S-R_1 and CH_3Hg−Se-R_2 complexes are in the range of 10^{15-20}). Physiologically, R_1- can be low molecular mass molecules (e.g., cysteine or glutathione) or thousands of high molecular mass thiol-containing proteins, whereas R_2- can be a few high molecular mass selenol-containing proteins (human genome encodes 25 types of selenoproteins). Despite the high formation constant, free $-S(e)^-$ (thiolate or selenolate) groups can attack the −S(e)−Hg− bound at the mercury atom, forming a new

Published: May 24, 2019

DOI: 10.1021/acs.chemrestox.9b00126
Chem. Res. Toxicol. 2019, 32, 1459−1461

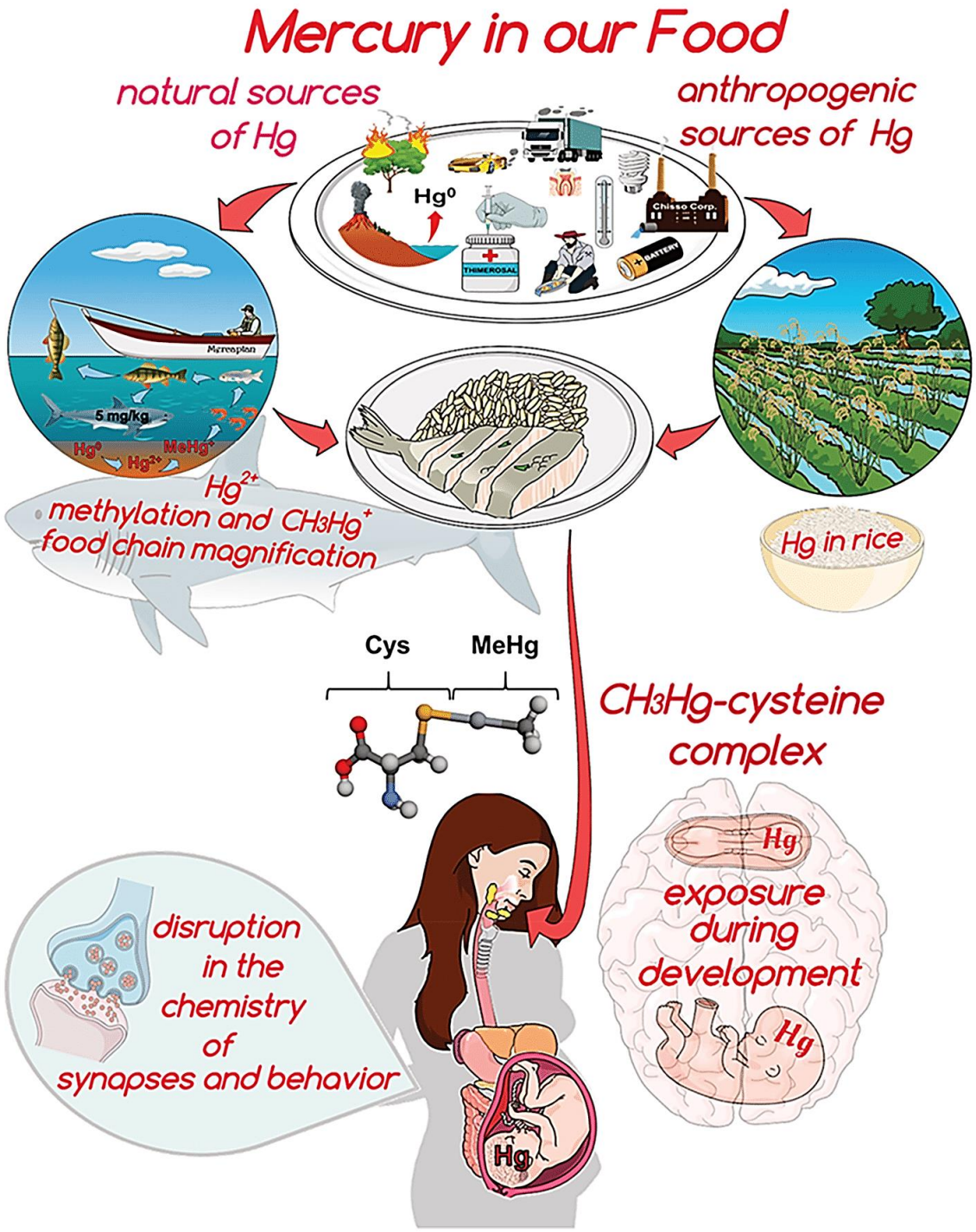

−S(e)−Hg− bond and releasing the formerly bound −S(e)H groups. Prof. Dallas Rabenstein first described this diffusion controlled type of exchange reaction in 1975.[2] Rabenstein's reactions can be represented as

$$R_1{-}S(e){-}HgCH_3 + R_2{-}S(e)H \leftarrow\rightarrow R_1{-}S(e)H + R_2{-}S(e){-}HgCH_3$$

Where CH_3Hg^+ can shift from on −S−Hg− bound to free $-S(e)H/-S(e)^-$ groups. The migration of CH_3Hg^+ from −Se−Hg− bonds to free $-SH/S^-$ is not thermodynamically favorable

DOI: 10.1021/acs.chemrestox.9b00126
Chem. Res. Toxicol. 2019, 32, 1459−1461

unless a molar excess of $-S^-$ over $-Se-Hg$ displace the Hg atom from the Se atom. Accordingly, the selenol have a stronger affinity for CH_3Hg^+ than thiol groups, implying that selenoproteins are the preferential targets of CH_3Hg^+. Given the stronger affinity of cationic mercurials for selenol over thiol, different groups of researchers have postulated that selenol-containing proteins (selenolproteins) are the preferential targets for E^+Hg forms of mercury. Since various selenoproteins (for instance, glutathione peroxidase and thioredoxin reductase) metabolize pro-oxidative species, their inhibition by CH_3Hg^+ can increase cellular sensitivity to redox imbalance.

The simultaneous targeting in the central nervous system (CNS) of a few antioxidant selenoproteins and thiol-containing proteins located in the external surface of the plasma membrane (receptors, channels, neurotransmitter carriers, ionic pumps, etc.) can work synergistically to disrupt the synaptic functioning and whole-cell metabolism. Glutamatergic neurotransmission is particularly important in mediating the neurotoxicity of CH_3Hg^+ because it is the main excitatory neurotransmitter in the mammalian CNS. Sustained increase in the extracellular levels of glutamate produces characteristic neuronal toxic effects, which collectively are termed excitotoxicity. Glutamatergic excitotoxicity is characterized by an overstimulation of ionotropic glutamatergic receptors (notably, *N*-methyl-D-aspartate (NMDA) receptors), which causes intracellular Ca^{2+} overload and triggers a cascade of events, which will culminate in cell dysfunction and death.[2,4]

The knowledge available so far allows us to conclude that CH_3Hg^+ is an electrophilic toxicant with strong affinity for thiol and selenol groups. In accordance, thiol-containing proteins involved in the transport, metabolism, or signaling of neurotransmitters as well as antioxidant selenoenzymes (for instance, glutathione peroxidases, and thioredoxin reductases) have been indicated as critical targets of CH_3Hg^+. Their targeting by CH_3Hg^+ deregulates normal brain cell physiology, particularly in the developing synapses. The disruption of the chemical processes involved in brain synaptic assembly and communication can cause permanent behavioral and cognitive impairments in humans. Although the CH_3Hg^+ affinity for selenols is significantly higher than that for thiols, there are not sufficient data to support that selenoproteins represent the preferential target for CH_3Hg^+. Looking to the future, it seems that *in vitro* studies focusing on the elucidation of the primary targets will be profitable to the understanding of CH_3Hg^+ neurotoxicity, as well as for the discovery of potential biomarkers for subtle intoxications, and more efficacious antidotes. Moreover, studies on the adverse outcome pathways (AOPs) associated with CH_3Hg^+ neurotoxicity could represent the basis for the development of *in silico* physiological based kinetics (PBK) models[6] to better predict the toxicity of CH_3Hg^+ in metazoan. Combined with system biology approaches,[7] the *in vitro* and *in silico* approaches will facilitate the precise identification of the AOPs mediating CH_3Hg^+ toxicity, thus imparting novel strategies to minimize its neurotoxic effects.

AUTHOR INFORMATION

Corresponding Author

*E-mail: jbtrocha@gmail.com.

ORCID

Joao B. T. Rocha: 0000-0003-3829-0595

Notes

Views expressed in this editorial are those of the authors and not necessarily the views of the ACS.

The authors declare no competing financial interest.

ACKNOWLEDGMENTS

The work described herein was supported by Conselho Nacional de Pesquisa e Desenvolvimento (CNPq), FAPERGS, FAPERGS/CAPES DocFix, CAPES-PROEX (Nos. 23038.005848/2018-31, 0737/2018, 88882.182123/2018-01), FINEP, CAPES-PRINT. M.A. was partially supported by grants from the National Institute of Environmental Health Sciences (NIEHS R01ES07331, NIEHS R01ES10563, and NIEHS R01ES020852).

REFERENCES

(1) Landrigan, P. J., Fuller, R., Acosta, N. J. R., Adeyi, O., Arnold, R., Basu, N. N., Baldé, A. B., Bertollini, R., Bose-O'Reilly, S., Boufford, J. I., et al. (2018) The Lancet Commission on pollution and health. *Lancet 391* (10119), 462−512.

(2) Nogara, P. A., Oliveira, C. S., Schmitz, G. L., Piquini, P. C., Farina, M., Aschner, M., and Rocha, J. B. T. (2019) Methylmercury's chemistry: From the environment to the mammalian brain. *Biochim. Biophys. Acta, Gen. Subj.*, DOI: 10.1016/j.bbagen.2019.01.006.

(3) Karagas, M. R., Choi, A. L., Oken, E., Horvat, M., Schoeny, R., Kamai, E., Cowell, W., Grandjean, P., and Korrick, S. (2012) Evidence on the Human Health Effects of Low-Level Methylmercury Exposure. *Environ. Health Perspect. 120*, 799−806.

(4) Atchison, W. D. (2005) Is chemical neurotransmission altered specifically during methylmercury-induced cerebellar dysfunction? *Trends Pharmacol. Sci. 26* (11), 549−557.

(5) US EPA. (1997) *Mercury Study Report to Congress, Volume V: Health Effects of Mercury and Mercury Compounds, EPA-452/R-97−0071997*, Office of Air Quality Planning & Standards and Office of Research and Development, US EPA.

(6) Punt, A. (2018) Toxicokinetics in Risk Evaluations. *Chem. Res. Toxicol. 31* (5), 285−286.

(7) Sturla, S. J., Boobis, A. R., FitzGerald, R. E., Hoeng, J., Kavlock, R. J., Schirmer, K., Whelan, M., Wilks, M. F., and Peitsch, M. C. (2014) Systems Toxicology: From Basic Research to Risk Assessment. *Chem. Res. Toxicol. 27* (3), 314−329.

DOI: 10.1021/acs.chemrestox.9b00126
Chem. Res. Toxicol. 2019, 32, 1459−1461

9.2. PROTONAÇÃO DAS CYS DA δ-ALAD HUMANA

O estado de protonação das Cys da δ-AlaD humana foi determinado utilizando dois modelos simplificados do sítio ativo: um composto apenas pelas 3 Cys, Zn e uma molécula de água (para completar a coordenação ao Zn tetraédrico), e um outro sistema, similar ao anterior, mas contendo os resíduos a 5,5 Å de distância do Zn (Figura 8.2.1), sendo variado o estado de protonação de cada Cys. Os modelos foram obtidos através do cristal PDB 5HMS, sendo os grupos metilamina e acetil adicionados aos resíduos de aminoácidos que apresentavam os grupos carboxi e amino-terminal, respectivamente. Os modelos foram otimizados através do programa MOPAC (STEWART, 2012) com o método PM6 (STEWART, 2007), considerando a constante dielétrica da água (74,0), com as ligações peptídicas fixas, e analisadas no programa Accelrys Discovery Studio 3.5 (DASSAULT SYSTÈMES, 2016).

Os resultados sugerem que as três Cys estão desprotonadas, pois o RMSD obtido (0,36 Å) para este sistema considerando os resíduos à 5,5 Å, foi o menor, quando comparado com as Cys protonadas (Tabela 8.2.1). Os resultados para os modelos de 3Å não apresentaram ser promissores, indicando que os resíduos ao redor das Cys e Zn, são importantes para que se mantenha a estrutura adequada.

Figura 9.2.1. Modelos otimizados do estado de protonação das Cys. Resíduos a 3 Å do Zn (A) e 5,5 Å (B). A estrutura do original do cristal está representada em amarelo. Para a visualização das cores, acessar a versão online.

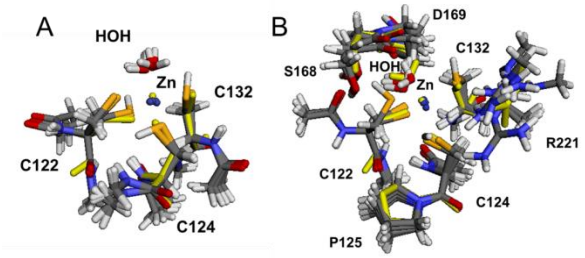

Tabela 9.2.1. Valores e RMSD (em Å) do estudo da protonação das Cys (C) da δ-AlaD. Valores em parênteses foram calculados considerando somente os átomos de S e Zn.

Cys protonada	Nenhuma	C122	C124	C132	Todas
Sistema 3 Å	0,75 (0,55)	1,09 (0,54)	0,88 (0,63)	0,69 (0,61)	1,3 (0,95)
Sistema 5,5 Å	0,36 (0,34)	0,42 (0,55)	0,40 (0,39)	0,42 (0,53)	0,66 (0,62)

9.3.

Supporting information

The Se···S/N interactions as a possible mechanism of δ-aminolevulinic acid dehydratase enzyme inhibition by organoselenium compounds: a computational study

P. A. Nogara[a], L. Orian[b], and J. B. T. Rocha[a*]

[a] Departamento de Bioquímica e Biologia Molecular, Universidade Federal de Santa Maria (UFSM), Santa Maria, 97105-900, RS, Brazil; *Corresponding author: jbtrocha@yahoo.com.br

[b] Dipartimento di Scienze Chimiche, Università degli Studi di Padova, Via Marzolo 1 35131 Padova, Italy.

S1. Protein sequence comparison and homology modeling

Homology modeling is the most accurate method to build protein structure models [1–3]. It is based on the fact that proteins with similar sequences adopt similar structures, and that 3D structure of proteins from the same family is more conserved than their amino acid sequences [4–6]. Based on the data from Table S2 and S3, the best protein model was selected. The Dmδ-AlaD-1L6S model from Swiss-Model showed a satisfactory protein structure. The validation parameters are in the range of native protein structure, with 91% of the residues in the most favorable regions, G-factor of -0.11, the ProSA Z-score of -9.38, 91% of the residues with an averaged 3D-1D score >0.2 (Verify 3D), and a good high-resolution structure with 95% of confidence (ERRAT) (Figure S3 and Table S2). The Dmδ-AlaD-1L6S model was used for the molecular docking simulations. For the Csδ-AlaD, the best protein model built was from Swiss-Model, using the PDB ID 3OBK as the template, because it presented all the validation parameters in the range of native protein structure (Figure S3 and Table S3). This structure was used in the molecular docking studies. The Csδ-AlaD structure modeled from Swiss-Model showed a satisfactory model, with 93.5% of the residues in the most favorable regions, G-factor of -0.13, the ProSA Z-score in the range of native proteins (-8.75), 81% of the residues with an averaged 3D-1D score >0.2 (Verify 3D), and a good high-resolution structure with 97% of confidence (ERRAT).

In addition, as a comparison method, we used the MODELLER software [7] to do the multi-template homology modelling for Dmδ-AlaD enzyme (templates PDB ID: H7N, 1L6S, and 5LZL). According to validation parameters, despite the 94% of the residues are in the most favorable regions, the G-factor of -0.10, the ProSA Z-score in the range of native proteins (-8.87), and 86% of the residues has an averaged

3D-1D score >0.2 (Verify 3D), the protein model generated showed a low-resolution structure with 88% of confidence, according to ERRAT.

S2. Docking protocol determination

The molecular docking protocols were validated by the RMSD (root-mean-square deviation) values from the PBG molecules, which give the relationship between the experimental and the theoretical data in a receptor-ligand complex. RMSD values lower than 2.0 Å indicate good quality of data reproduction [8–10].

Many docking protocols/configurations were studied (such as blind docking with the protein rigid, local docking on the active site with the protein rigid, docking on the active site with the side chain of Lys195, Phe204, Arg205, Arg217, Lys248 residues flexible (Dmδ-AlaD numbers as example), combination of different flexible residues, and different grid box sizes (from 15 to 40 Å3)), but the PBG binding pose obtained were different from the crystallographic data, with the RMDS > 2.0 Å. The best docking protocol was obtained using the ligands and the side chain of Arg209 and Lys252 residues from Hsδ-AlaD (Arg205 and Lys248 from Dmδ-AlaD-1L6S, and Arg301 and Lys344 from Csδ-AlaD-3OBK) flexible. As shown in Figure 3, PBG binding pose from the molecular docking presented practically the same conformation and interactions than the crystallographic data from PDB ID 1E51 and 3OBK.

The RMSD value, in relation to PBG cocrystallized in Hsδ-AlaD (PDB 1E51), for HsPBG, DmPBG and CsPBG were: 0.82 Å, 1.32 Å, and 1.23 Å, respectively (Figure S4). As the RMSD values were lower than 2.0 Å, we considered the docking protocol successful. The ΔG obtained were -7.4, -6.4, and -7.3 kcal/mol, respectively. It is important to mention that for the Hsδ-AlaD the docking using only the Lys252 side chain flexible also presented a good RMSD (0.57 Å; ΔG= -7.8 kcal/mol). However, to keep both enzymes with the same respective residues flexible, we choose to use the Hsδ-AlaD with Arg209 and Lys252 side chain flexible. To calculate the RMSD, the complexes enzyme-inhibitor (δ-AlaD-PBG) obtained from the docking were overlapped in the DSV program, taking into account the Hsδ-AlaD as reference structure (because this structure has the PGB cocrystallized). Only the heavy atoms from PBG best-docked conformation (lowest binding free energy) were considered for the RMSD determination.

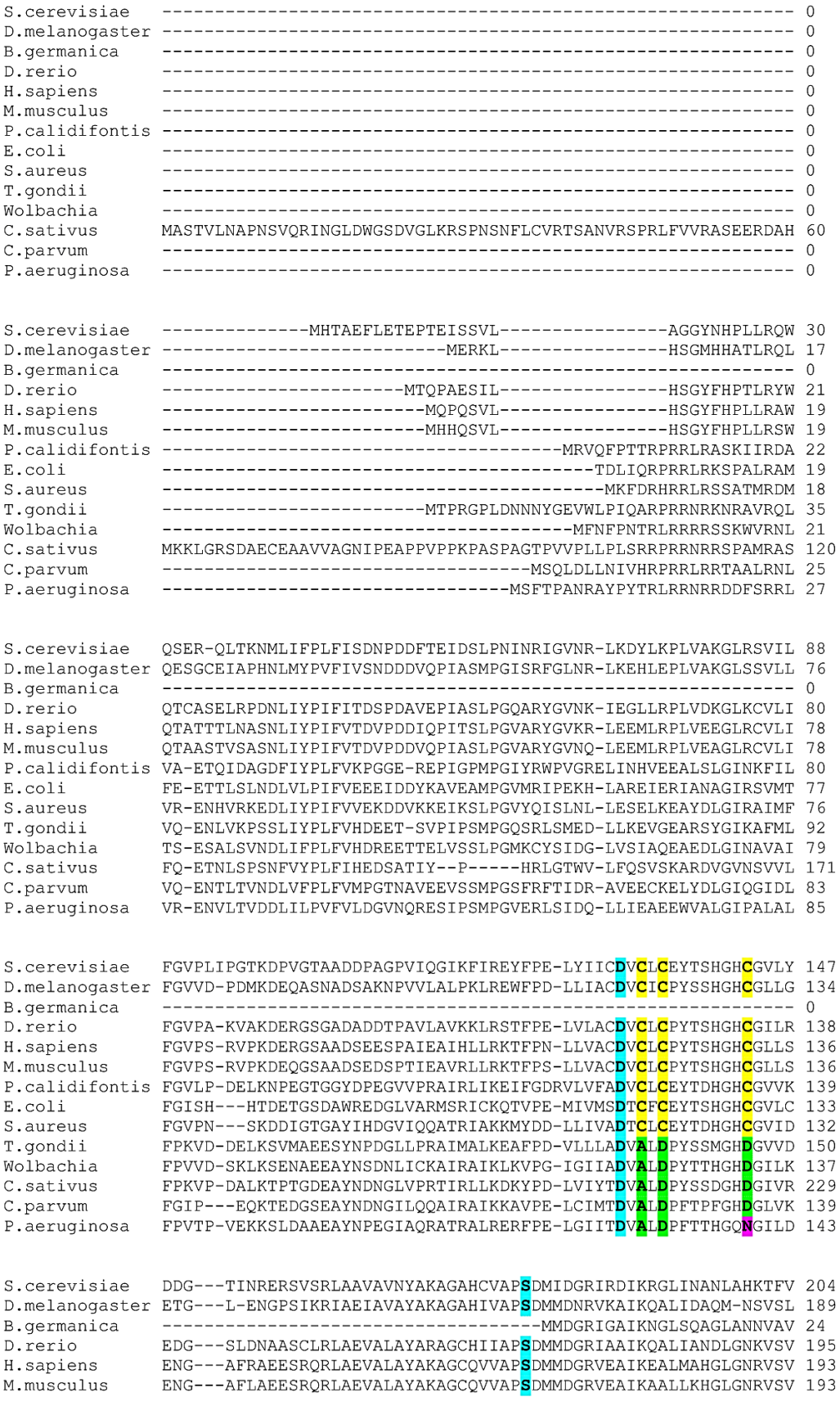
S.cerevisiae ---------- 0
D.melanogaster ---------- 0
B.germanica ---------- 0
D.rerio ---------- 0
H.sapiens ---------- 0
M.musculus ---------- 0
P.calidifontis ---------- 0
E.coli ---------- 0
S.aureus ---------- 0
T.gondii ---------- 0
Wolbachia ---------- 0
C.sativus MASTVLNAPNSVQRINGLDWGSDVGLKRSPNSNFLCVRTSANVRSPRLFVVRASEERDAH 60
C.parvum ---------- 0
P.aeruginosa ---------- 0
S.cerevisiae ----------MHTAEFLETEPTEISSVL----------AGGYNHPLLRQW 30
D.melanogaster ----------MERKL----------HSGMHHATLRQL 17
B.germanica ---------- 0
D.rerio ----------MTQPAESIL----------HSGYFHPTLRYW 21
H.sapiens ----------MQPQSVL----------HSGYFHPLLRAW 19
M.musculus ----------MHHQSVL----------HSGYFHPLLRSW 19
P.calidifontis ----------MRVQFPTTRPRRLRASKIIRDA 22
E.coli ----------TDLIQRPRRLRKSPALRAM 19
S.aureus ----------MKFDRHRRLRSSATMRDM 18
T.gondii ----------MTPRGPLDNNNYGEVWLPIQARPRRNRKNRAVRQL 35
Wolbachia ----------MFNFPNTRLRRRRSSKWVRNL 21
C.sativus MKKLGRSDAECEAAVVAGNIPEAPPVPPKPASPAGTPVVPLLPLSRRPRRNRRSPAMRAS 120
C.parvum ----------MSQLDLLNIVHRPRRLRRTAALRNL 25
P.aeruginosa ----------MSFTPANRAYPYTRLRRNRRDDFSRRL 27
S.cerevisiae QSER-QLTKNMLIFPLFISDNPDDFTEIDSLPNINRIGVNR-LKDYLKPLVAKGLRSVIL 88
D.melanogaster QESGCEIAPHNLMYPVFIVSNDDDVQPIASMPGISRFGLNR-LKEHLEPLVAKGLSSVLL 76
B.germanica ---------- 0
D.rerio QTCASELRPDNLIYPIFITDSPDAVEPIASLPGQARYGVNK-IEGLLRPLVDKGLKCVLI 80
H.sapiens QTATTTLNASNLIYPIFVTDVPDDIQPITSLPGVARYGVKR-LEEMLRPLVEEGLRCVLI 78
M.musculus QTAASTVSASNLIYPIFVTDVPDDVQPIASLPGVARYGVNQ-LEEMLRPLVEAGLRCVLI 78
P.calidifontis VA-ETQIDAGDFIYPLFVKPGGE-REPIGPMPGIYRWPVGRELINHVEEALSLGINKFIL 80
E.coli FE-ETTLSLNDLVLPIFVEEEIDDYKAVEAMPGVMRIPEKH-LAREIERIANAGIRSVMT 77
S.aureus VR-ENHVRKEDLIYPIFVVEKDDVKKEIKSLPGVYQISLNL-LESELKEAYDLGIRAIMF 76
T.gondii VQ-ENLVKPSSLIYPLFVHDEET-SVPIPSMPGQSRLSMED-LLKEVGEARSYGIKAFML 92
Wolbachia TS-ESALSVNDLIFPLFVHDREETTELVSSLPGMKCYSIDG-LVSIAQEAEDLGINAVAI 79
C.sativus FQ-ETNLSPSNFVYPLFIHEDSATIY--P-----HRLGTWV-LFQSVSKARDVGVNSVVL 171
C.parvum VQ-ENTLTVNDLVFPLFVMPGTNAVEEVSSMPGSFRFTIDR-AVEECKELYDLGIQGIDL 83
P.aeruginosa VR-ENVLTVDDLILPVFVLDGVNQRESIPSMPGVERLSIDQ-LLIEAEEWVALGIPALAL 85
S.cerevisiae FGVPLIPGTKDPVGTAADDPAGPVIQGIKFIREYFPE-LYIICDVCLCEYTSHGHCGVLY 147
D.melanogaster FGVVD-PDMKDEQASNADSAKNPVVLALPKLREWFPD-LLIACDVCICPYSSHGHCGLLG 134
B.germanica ---------- 0
D.rerio FGVPA-KVAKDERGSGADADDTPAVLAVKKLRSTFPE-LVLACDVCLCPYTSHGHCGILR 138
H.sapiens FGVPS-RVPKDERGSAADSEESPAIEAIHLLRKTFPN-LLVACDVCLCPYTSHGHCGLLS 136
M.musculus FGVPS-RVPKDEQGSAADSEDSPTIEAVRLLRKTFPS-LLVACDVCLCPYTSHGHCGLLS 136
P.calidifontis FGVLP-DELKNPEGTGGYDPEGVVPRAIRLIKEIFGDRVLVFADVCLCEYTDHGHCGVVK 139
E.coli FGISH---HTDETGSDAWREDGLVARMSRICKQTVPE-MIVMSDTCFCEYTSHGHCGVLC 133
S.aureus FGVPN---SKDDIGTGAYIHDGVIQQATRIAKKMYDD-LLIVADTCLCEYTDHGHCGVID 132
T.gondii FPKVD-DELKSVMAEESYNPDGLLPRAIMALKEAFPD-VLLLADVALDPYSSMGHDGVVD 150
Wolbachia FPVVD-SKLKSENAEEAYNSDNLICKAIRAIKLKVPG-IGIIADVALDPYTTHGHDGILK 137
C.sativus FPKVP-DALKTPTGDEAYNDNGLVPRTIRLLKDKYPD-LVIYTDVALDPYSSDGHDGIVR 229
C.parvum FGIP---EQKTEDGSEAYNDNGILQQAIRAIKKAVPE-LCIMTDVALDPFTPFGHDGLVK 139
P.aeruginosa FPVTP-VEKKSLDAAEAYNPEGIAQRATRALRERFPE-LGIITDVALDPFTTHGQNGILD 143
S.cerevisiae DDG---TINRERSVSRLAAVAVNYAKAGAHCVAPSDMIDGRIRDIKRGLINANLAHKTFV 204
D.melanogaster ETG---L-ENGPSIKRIAEIAVAYAKAGAHIVAPSDMMDNRVKAIKQALIDAQM-NSVSL 189
B.germanica ----------MMDGRIGAIKNGLSQAGLANNVAV 24
D.rerio EDG---SLDNAASCLRLAEVALAYARAGCHIIAPSDMMDGRIAAIKQALIANDLGNKVSV 195
H.sapiens ENG---AFRAEESRQRLAEVALAYAKAGCQVVAPSDMMDGRVEAIKEALMAHGLGNRVSV 193
M.musculus ENG---AFLAEESRQRLAEVALAYAKAGCQVVAPSDMMDGRVEAIKAALLKHGLGNRVSV 193

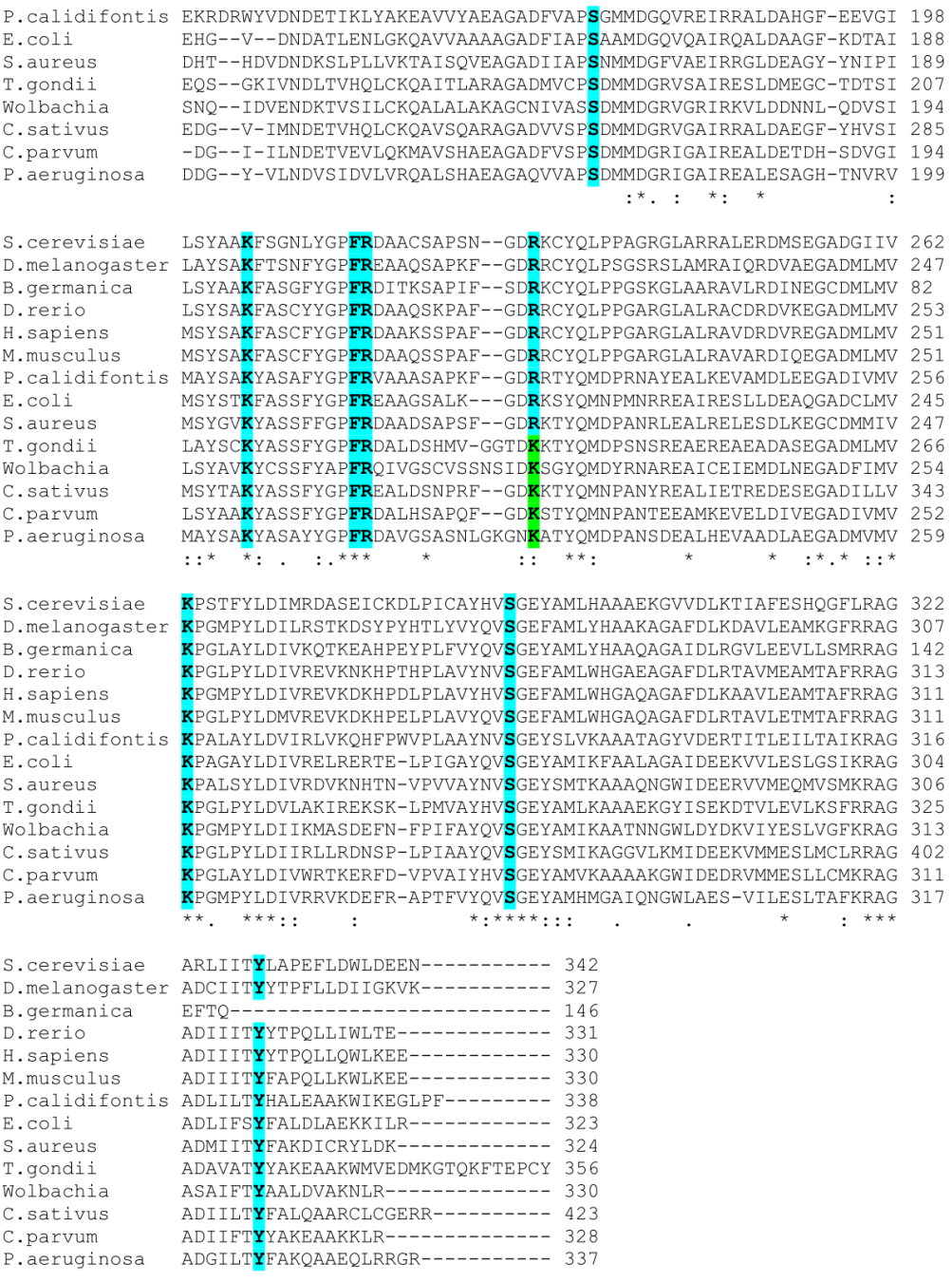

Figure S1. Multiple alignments of the δ-AlaD amino acids sequence of different species through Clustal Omega (1.2.4) (https://www.ebi.ac.uk/Tools/msa/clustalo). For more details, see the Materials and Methods article section. The residues from the active site are highlighted: Cys (yellow); residues that remain conserved (cyan), residues not conserved when compared to the human enzyme (green and pink). Legend of the symbols: asterisk (*) indicates positions which have a single fully conserved residue (conserved sequence); colon (:) indicates conservation between residues with groups of strongly similar properties (conservative mutations); period (.) denotes conservation between groups of weakly similar properties (semi-conservative mutations) and the lack of symbols indicates the non-conservative mutations ( ).

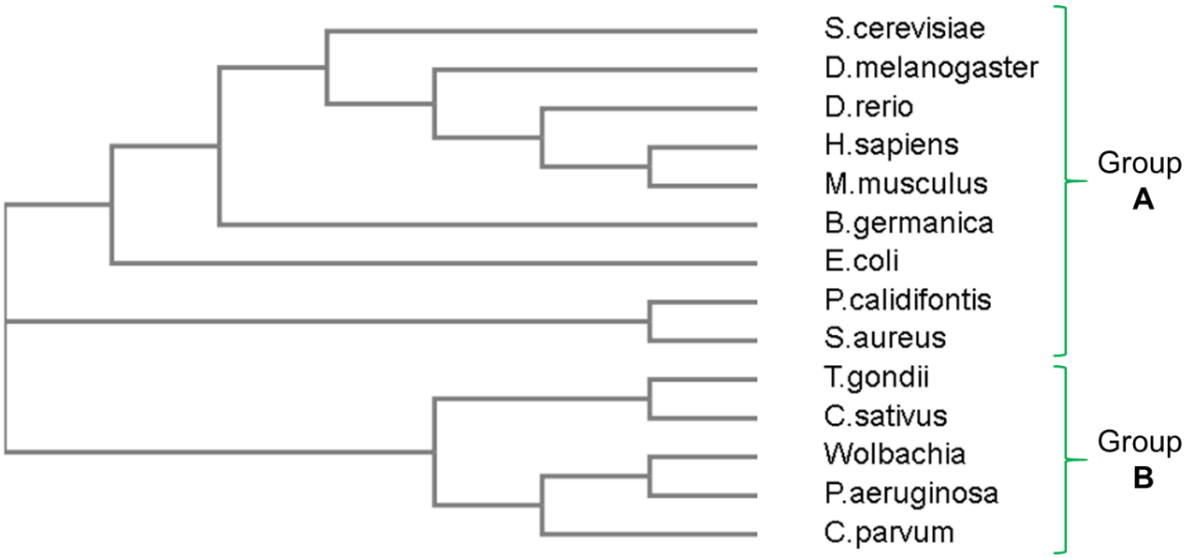

Figure S2. Phylogenetic tree of δ-AlaD enzymes from different organisms through Clustal Omega (1.2.4). Group A are the species that present Cys (C) residues in the active site, while the Group B are the species that have Asp (D) residues. Despite the *Blattella germanica* δ-AlaD lacks the residues corresponding to the cysteine's region, it belongs to Group A.

Table S1. The similarity between the δ-AlaD sequences expressed as percent sequence identity and percentage of positive substitutions*. Data from Geneious program (https://www.geneious.com).

Organism	*Drosophila melanogaster*		*Cucumis sativus*	
	identity	positive	identity	Positive
Blattella germanica	25.9	34.1	15.5	21.4
Chlorobaculum parvum [b]	33.7	57.6	39.2	50.8
Cucumis sativus	26.2	42.0	-	-
Danio rerio	59.6	74.0	28.2	41.1
Drosophila melanogaster	-	-	26.2	42.0
Escherichia coli [a]	36.0	55.5	34.3	47.3
Homo sapiens	58.7	74.1	28.9	42.3
Mus musculus	58.1	73.2	28.9	42.7
Pseudomonas aeruginosa [b]	35.7	55.2	33.7	47.3
Pyrobaculum calidifontis [a]	36.8	57.9	35.5	48.1
Saccharomyces cerevisiae [a]	45.9	63.7	27.0	40.2
Staphylococcus aureus	34.1	56.8	31.7	46.3
Toxoplasma gondii [b]	34.4	51.4	40.0	53.0
Wolbachia	32.2	54.0	33.6	45.6

*Specific amino acid substitution that preserves the physico-chemical properties of the original residue. The protein sequences here used are described in the Materials and Methods article section. [a] The δ-AlaD 3D structures from these organisms were used to build the *Dm*δ-AlaD models. [b] The δ-AlaD 3D structures from these organisms were used to build the *Cs*δ-AlaD models. For better visualization, the species from Group A have grey background.

Table S2. Validation of the 3D models of *Dm*δ-AlaD from protein homology modeling programs.

Program	Template	Verify 3D (%)	ProSA	PROCHECK					ERRAT
				Most favored region (%)	Additional allowed region (%)	Generously allowed region (%)	Disallowed region (%)	G-factor overall average	
	1H7N	88.92	-8.87	90.4	8.9	0.7	0.0	-0.12	79.479
Swiss Model	**1L6S**	**91.54**	**-9.38**	**90.6**	**9.4**	**0.0**	**0.0**	**-0.11**	**95.424**
	5LZL	91.16	-8.66	88.2	10.2	1.6	0.0	-0.19	94.681
	1H7N	84.92	-8.79	89.4	8.5	1.8	0.4	-0.19	72.843
Phyre2	1L6S	89.10	-8.53	87.1	12.2	0.7	0.0	-0.02	55.627
	5LZL	87.31	-8.84	81.4	15.7	2.9	0.0	-0.40	68.789
	1H7N	80.62	-8.96	78.0	19.9	2.1	0.0	0.25	93.375
Geno3D	1L6S	90.03	-8.75	76.0	20.8	2.5	0.7	0.21	91.262
	5LZL	92.92	-8.52	73.8	20.9	3.2	2.1	0.19	95.569

An ideal native protein model should have: Verify 3D: >80% residues with an averaged 3D-1D score > 0.2; PROCHECK: >90% of the residues in the most favored regions and an overall; G-factor > -0.5; ERRAT: >95%. The templates PDB ID 1H7N, 1L6S, and 5LZL correspond to the *Saccharomyces cerevisiae*, *Escherichia coli* and *Pyrobaculum calidifontis* organisms, respectively.

Table S3. Validation of the 3D models of *Cs*δ-AlaD from protein homology modeling programs.

Program	Template	Verify 3D (%)	ProSA	PROCHECK					ERRAT
				Most favored region (%)	Additional allowed region (%)	Generously allowed region (%)	Disallowed region (%)	G-factor overall average	
	1GZG	84.39	-7.89	92.0	8.0	0.0	0.0	-0.16	91.438
Swiss Model	2C1H	88.22	-8.13	92.7	6.2	0.7	0.4	-0.14	93.399
	3OBK	**81.17**	**-8.75**	**93.7**	**6.3**	**0.0**	**0.0**	**-0.13**	**97.315**
	1GZG	73.02	-8.13	91.6	7.7	0.7	0.0	0.11	83.025
Phyre2	2C1H	74.52	-8.03	88.2	10.3	1.5	0.0	0.08	61.852
	3OBK	73.90	-7.07	91.5	8.1	0.4	0.0	0.09	81.107
	1GZG	77.89	-6.99	79.6	18.1	1.5	0.8	0.23	91.156
Geno3D	2C1H	86.05	-6.95	79.5	19.4	0.4	0.8	0.23	96.918
	3OBK	78.90	-7.35	77.7	19.3	1.1	1.9	0.24	99.660

An ideal native protein model should have: Verify 3D: >80% residues with an averaged 3D-1D score > 0.2; PROCHECK: >90% of the residues in the most favored regions and an overall; G-factor > -0.5; ERRAT: >95%. The templates PDB ID 1GZG, 2C1H, and 3OBK correspond to the *Pseudomonas aeruginosa*, *Chlorobaculum parvum* and *Toxoplasma gondii* organisms, respectively.

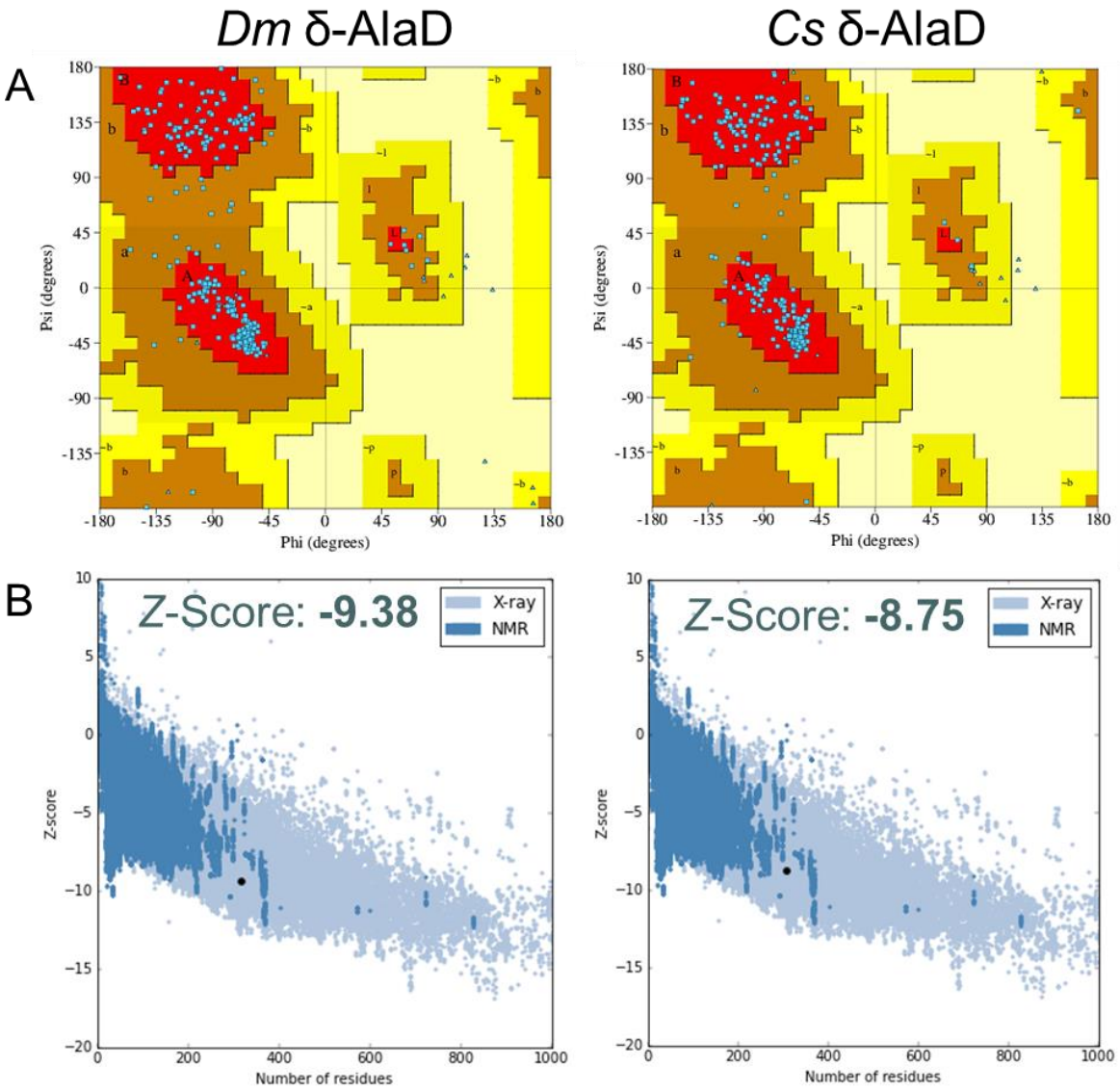

Figure S3. Ramachandran plot (A) and ProSa Z-score (B) for *Dm*δ-AlaD and *Cs*δ-AlaD models obtained from Swiss-model with the templates PDB ID 1L6S and 3OBK, respectively. The Ramachandran plots are divided into four regions based on the conformation of the amino acid residues (phi (φ) and psi (ψ) angles). The most favored regions (red) are labeled with A (α-helix), B (β-sheet), and L (left-handed α-helix). The additional allowed regions (brown) are labeled with a (α-helix), b (β-sheet), l (left-handed α-helix), and p (epsilon α-helix). The generously allowed regions (yellow) are labeled with ~a (α-helix), ~b (β-sheet), ~l (left-handed α-helix), and ~p (epsilon α-helix). Disallowed regions are colored in light yellow. Glycine residues are indicated as triangles (▲) because they lack a side chain. The ProSa plot shows the Z-scores of protein structures obtained by X-ray (light blue) and NMR (blue) sources that are used to check whether the Z-score of the protein model (•) is within the range of scores typically found for native proteins of similar size.

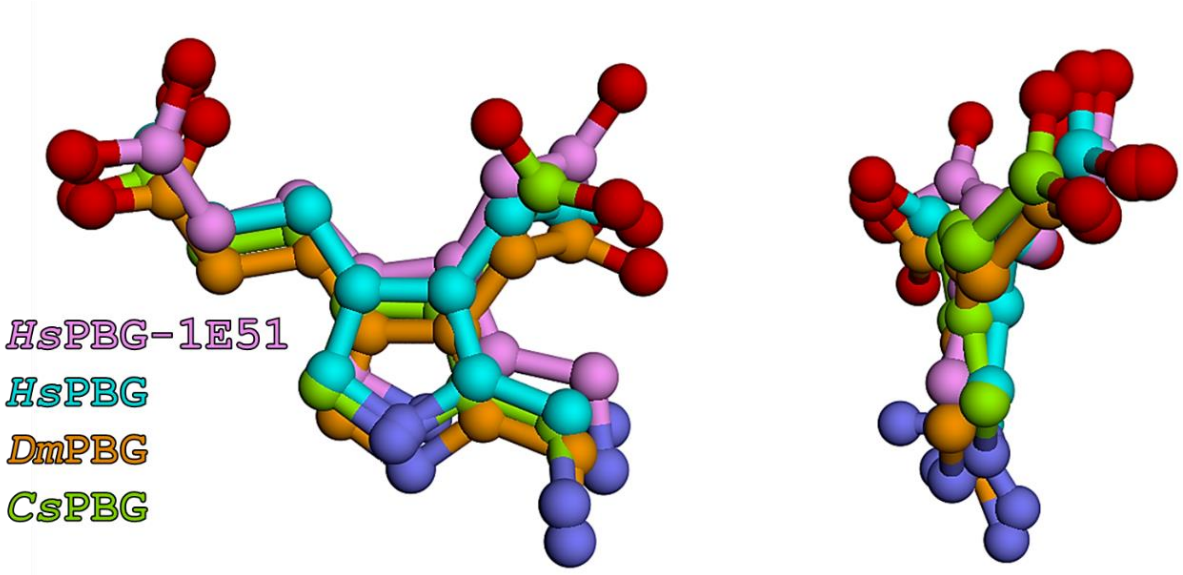

Figure S4. The overlapping and RMSD (root-mean-square deviation) calculations between the PBG molecules (front and side view). The PBG from *Homo sapiens* (crystal: *Hs*PBG-1E51; redocking: *Hs*PBG), *Drosophila melanogaster* (*Dm*PBG), and *Cucumis sativus* (*Cs*PBG) are represented with the carbon atoms in pink, blue, orange and green colors, respectively. Only the heavy atoms are shown. The RMSD value, in relation to *Hs*PBG-1E51, for *Hs*PBG, *Dm*PBG and *Cs*PBG were: 0.82 Å, 1.32 Å and 1.23 Å, respectively. As the RMSD values were lower than 2 Å, we considered the docking protocol successful [8–10].

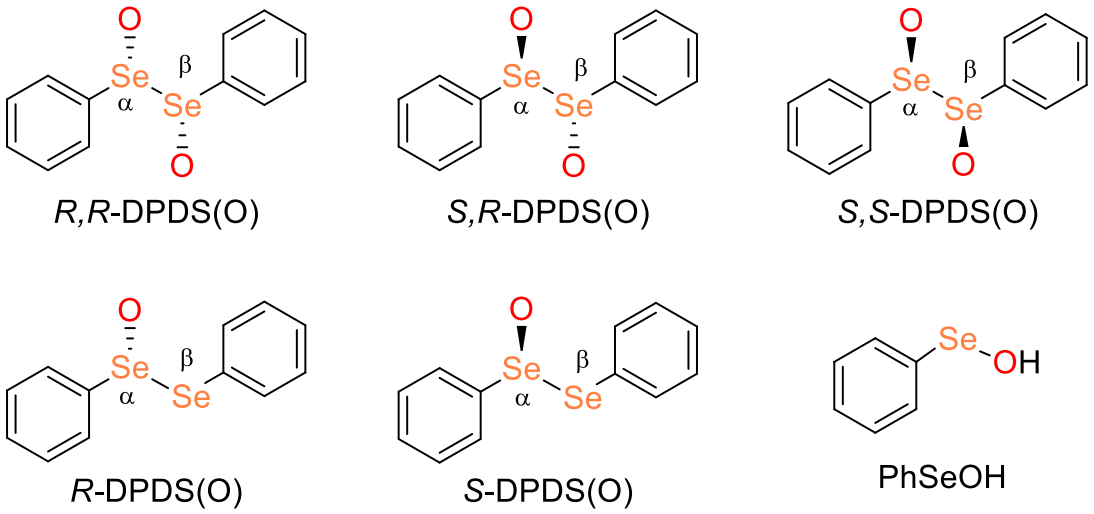

Figure S5. Chemical structures of putative oxidized organoselenium forms. "α" and "β" indicate the selenium atom (see **Table S4**).

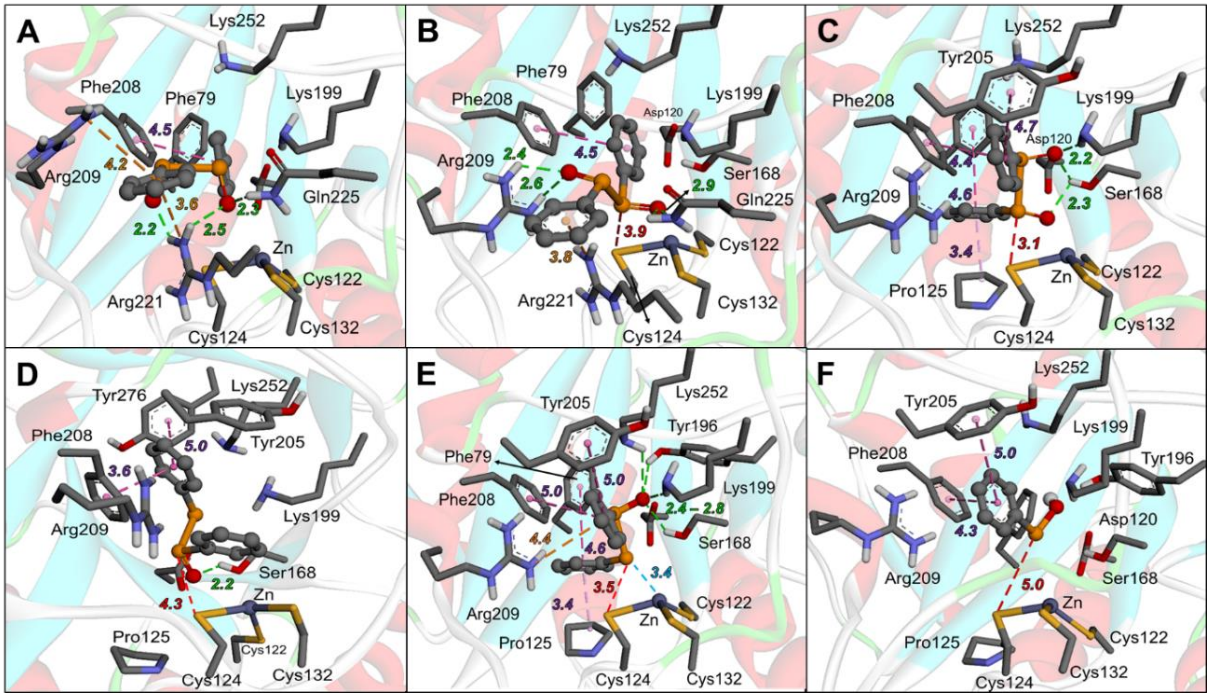

Figure S6. Molecular docking of oxidized organoselenium compounds with *Hs*δ-AlaD. A) *R*,*R*-DPDS(O); B) *S*,*R*-DPDS(O); C) *S*,*S*-DPDS(O); D) *R*-DPDS(O); E) *S*-DPDS(O); F) PhSeOH. H-bonds, cation-π, anion-π, and electrostatic and hydrophobic (π-π, alkyl-π) interactions, besides the zinc coordination, are represented by green, orange, purple, and blue dotted lines, respectively; the distances are in Å.

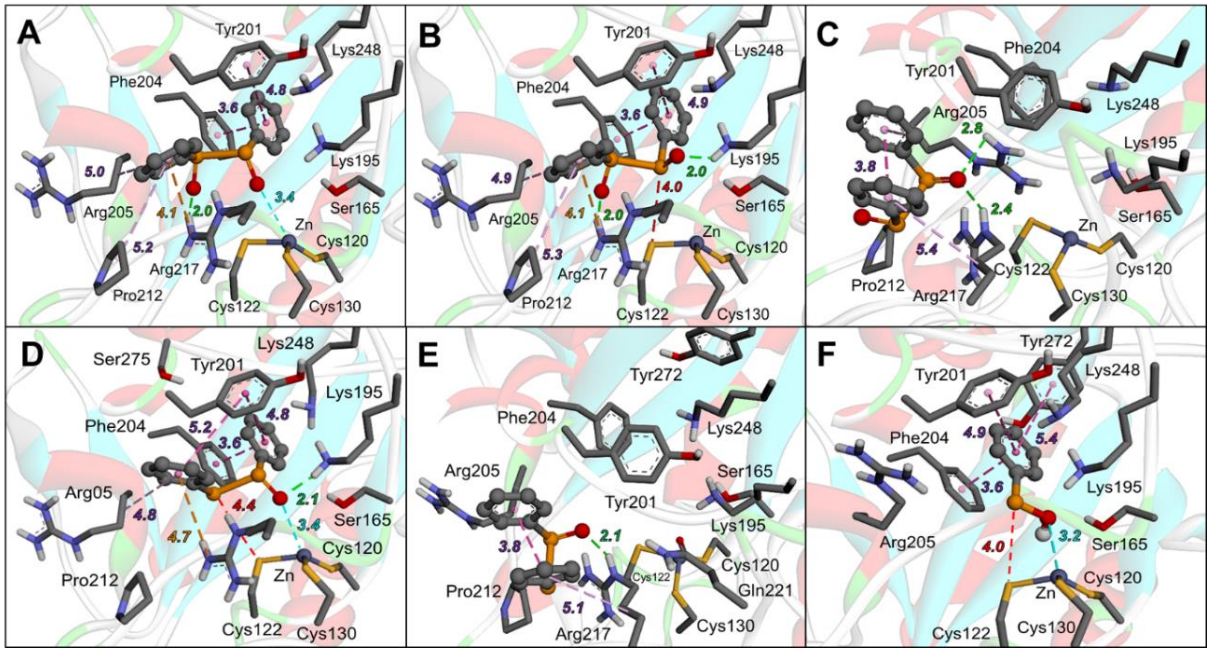

Figure S7. Molecular docking of oxidized organoselenium compounds with *Dm*δ-AlaD. A) *R*,*R*-DPDS(O); B) *S*,*R*-DPDS(O); C) *S*,*S*-DPDS(O); D) *R*-DPDS(O); E) *S*-DPDS(O); F) PhSeOH. H-bonds, cation-π, anion-π, and electrostatic and hydrophobic (π-π, alkyl-π) interactions, besides the zinc coordination, are represented by green, orange, purple, and blue dot lines, respectively; the distances are in Å.

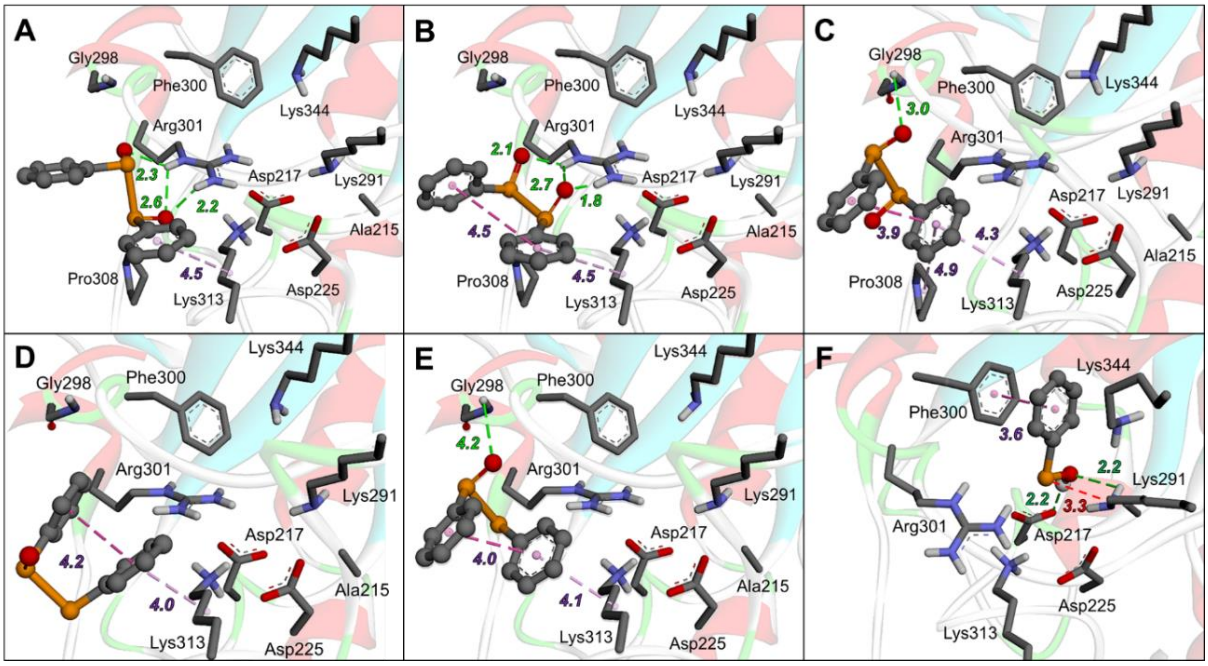

Figure S8. Molecular docking of oxidized organoselenium compounds with *Cs*δ-AlaD. A) *R*,*R*-DPDS(O); B) *S*,*R*-DPDS(O); C) *S*,*S*-DPDS(O); D) *R*-DPDS(O); E) *S*-DPDS(O); F) PhSeOH. H-bonds, cation-π, anion-π, and electrostatic and hydrophobic (π-π, alkyl-π) interactions, are represented by green, orange, and purple dot lines, respectively; the distances are in Å.

Table S4. Hirshfeld charges on selenium atoms computed at mPW1PW91/def2PVTZ level of theory.

Molecule	**Se$^{\alpha}$**	**Se$^{\beta}$**
PhSeOH	0.132	-
PSA (PhSeOO^{-})	0.257	-
PSA (PhSeOOH)	0.451	-
DPDS	0.005	0.005
R,*R*-DPDS(O)	0.326	0.326
S,*R*-DPDS(O)	0.349	0.349
S,*S*-DPDS(O)	0.326	0.326
R-DPDS(O)	0.358	-0.021
S-DPDS(O)	0.363	-0.014

"α" and "β" indicate the selenium atom. See **Figure S5**.

Table S5. XYZ coordinates and energy in gas (GP) and water (WP) phases, of the structures at mPW1PW91/def2PVTZ level of theory.

PhSeOOH
(GP= -2784.43594809 Ha; WP= -2784.44929995 Ha)

Se	1.419989	0.093801	-0.321723
C	-0.498207	0.049538	-0.118414
C	-1.082010	-1.168579	0.176091
C	-2.461815	-1.235982	0.298298
C	-3.231904	-0.096403	0.115984
C	-2.631141	1.117584	-0.188730
C	-1.253080	1.195525	-0.312685
O	1.608177	1.010236	1.223592
O	1.871061	-1.430842	-0.020684
H	-0.448197	-2.037056	0.310661
H	-2.936319	-2.179708	0.534958
H	-4.309014	-0.153663	0.209204
H	-3.236638	2.003627	-0.329862
H	-0.776915	2.140576	-0.544632
H	2.542502	1.231722	1.311733

EtNH2
(GP= -135.193779414 Ha; WP= -135.197982784 Ha)

C	0.049051	0.557402	0.053708
N	1.200507	-0.317625	-0.116858
C	-1.238568	-0.236859	-0.027453
H	0.064600	1.124819	0.996364
H	0.070474	1.294849	-0.752785
H	1.237412	-0.999158	0.630416
H	2.062583	0.209109	-0.077218
H	-1.294016	-0.975022	0.776643
H	-1.299569	-0.770496	-0.976505
H	-2.107930	0.416013	0.063562

PhSeONHEt
(GP= -2843.19105512 Ha; WP= -2843.20234058 Ha)

C	2.999627	0.520146	0.199556
N	1.543367	0.661108	0.190862
C	3.647556	1.798207	0.692770
H	3.328855	-0.327625	0.810977
H	3.316375	0.317015	-0.827060
H	1.185780	0.801327	1.131512
H	3.356178	2.013370	1.722961
H	3.354904	2.646236	0.073349
H	4.734406	1.707167	0.669190
H	-4.622877	1.251309	0.538998
C	-3.624694	0.883131	0.338323
H	-3.117881	2.526883	-0.946484
C	-2.780261	1.600805	-0.498770
C	-3.196053	-0.302470	0.915958
H	-3.857186	-0.859159	1.567984
C	-1.502401	1.133101	-0.762434
C	-1.918571	-0.779569	0.657843
H	-0.834817	1.691119	-1.407085
C	-1.086678	-0.050609	-0.171868
O	0.745575	-2.050821	0.513430
H	-1.545934	-1.699166	1.093980
Se	0.667732	-0.797238	-0.532355

H2O
(GP= -76.4401085779 Ha; WP= -76.4475550809 Ha)

O	0.000000	0.116510	0.000000
H	0.761254	-0.466042	0.000000
H	-0.761254	-0.466041	0.000000

PhSeOOH.EtNH2
(GP= -2919.63798158 Ha; WP= -2919.64907581 Ha)

C	3.912658	0.281473	0.028870
N	2.762198	0.801342	0.757570
C	4.544798	1.363633	-0.821960
H	4.677299	-0.155867	0.686510
H	3.559809	-0.528098	-0.614940
H	3.055048	1.530012	1.396660
H	2.328739	0.075722	1.315640
H	4.920298	2.180913	-0.201050
H	3.816588	1.780073	-1.519140
H	5.386898	0.969953	-1.392790
H	-3.375692	3.417640	0.135600
C	-2.774422	2.519831	0.065690
H	-0.913422	3.581661	0.189710
C	-1.389312	2.613791	0.095040
C	-3.393062	1.283930	-0.058530
H	-4.473282	1.217150	-0.085770
C	-0.610522	1.470271	0.001230
C	-2.626821	0.131771	-0.154240
H	0.473988	1.526472	0.030780
C	-1.247792	0.242721	-0.113360
O	0.440749	-1.410168	1.398580
O	-1.339731	-2.524609	-0.341930
H	-3.074631	-0.849229	-0.259600
Se	-0.197161	-1.376139	-0.284780
H	-0.314851	-1.533389	1.988270

PhSeONHEt.H2O
(GP= -2919.64746509 Ha; WP= -2919.65877091 Ha)

C	2.924110	0.677141	-0.095435
N	1.479647	0.674815	0.151151
C	3.585529	1.763759	0.728012
H	3.380327	-0.291626	0.135316
H	3.084259	0.867313	-1.160114
H	1.280773	0.380914	1.110523
H	0.415445	-1.662982	2.868055
H	3.443590	1.582191	1.794549
H	3.166988	2.741718	0.488846
H	4.658752	1.786366	0.533320
H	-4.709955	1.091681	0.848498
C	-3.716390	0.813079	0.520998
H	-3.093712	2.841033	0.194204
C	-2.809858	1.797250	0.150892
C	-3.353928	-0.524582	0.473247
H	-4.062529	-1.290185	0.762749
C	-1.536718	1.447408	-0.271107
C	-2.081734	-0.885854	0.053472
H	-0.817777	2.208182	-0.546116
C	-1.186637	0.106397	-0.305579
O	1.104420	-1.368188	2.271723
O	0.653040	-1.996711	-0.366015
H	-1.767196	-1.921576	0.014399
Se	0.550773	-0.455612	-0.949756
H	0.931295	-1.814322	1.416773

References

[1] V.K. Vyas, R.D. Ukawala, M. Ghate, C. Chintha, Homology Modeling a Fast Tool for Drug Discovery : Current Perspectives, Indian J. Pharm. Sci. 74 (2012) 1–17.

[2] T. Schmidt, A. Bergner, T. Schwede, Modelling three-dimensional protein structures for applications in drug design, Drug Discov. Today. 19 (2014) 890–897. https://doi.org/10.1016/j.drudis.2013.10.027.

[3] Z. Xiang, Advances in Homology Protein Structure Modeling, Curr. Protein Pept. Sci. 7 (2006) 217–227. https://doi.org/10.2174/138920306777452312.

[4] A. Fiser, Template-Based Protein Structure Modeling, in: Comput. Biol. Methods Mol. Biol., 2010: pp. 73–94. https://doi.org/10.1007/978-1-60761-842-3.

[5] K. Joo, I.S. Joung, S.Y. Lee, J.Y. Kim, Q. Cheng, B. Manavalan, J.Y. Joung, S. Heo, J. Lee, M. Nam, I.H. Lee, S.J. Lee, J. Lee, Template based protein structure modeling by global optimization in CASP11, Proteins. 84 (2016) 221–232. https://doi.org/10.1002/prot.24917.

[6] M.R. Pitman, R.I. Menz, Methods for protein homology modelling, Elsevier B.V, 2006. https://doi.org/10.1016/S1874-5334(06)80005-5.

[7] B. Webb, A. Sali, Comparative Protein Structure Modeling Using Modeller, Curr. Protoc. Bioinforma. 54 (2016) 5.6.1-5.6.37. https://doi.org/10.1002/cpbi.3.

[8] J.L. Stigliani, V. Bernardes-Génisson, J. Bernadou, G. Pratviel, Cross-docking study on InhA inhibitors: A combination of Autodock Vina and PM6-DH2 simulations to retrieve bio-active conformations, Org. Biomol. Chem. 10 (2012) 6341–6349. https://doi.org/10.1039/c2ob25602a.

[9] C.P. Vianna, W.F. De Azevedo, Identification of new potential Mycobacterium tuberculosis shikimate kinase inhibitors through molecular docking simulations, J. Mol. Model. 18 (2012) 755–764. https://doi.org/10.1007/s00894-011-1113-5.

[10] T.L. Gonzalez, J.M. Rae, J.A. Colacino, R.J. Richardson, Homology models of mouse and rat estrogen receptor-α ligand-binding domain created by in silico mutagenesis of a human template: Molecular docking with 17β-estradiol, diethylstilbestrol, and paraben analogs, Comput. Toxicol. 10 (2019) 1–16. https://doi.org/10.1016/j.comtox.2018.11.003.

9.4.

SUPPORTING INFORMATION

β-elimination reaction from methyl(mercury)chalcogen oxides: a theoretical study

P. A. Nogara[a,b], A. Madabeni[b], M. Bortoli[b], J. B. T. Rocha[a*], and L. Orian[b*]

[a] Departamento de Bioquímica e Biologia Molecular, Universidade Federal de Santa Maria (UFSM), Santa Maria 97105-900, RS, Brazil
[b] Dipartimento di Scienze Chimiche, Università degli Studi di Padova, Via Marzolo 1, 35131 Padova, Italy
[*] Corresponding authors. E-mail address: laura.orian@unipd.it (L. Orian), jbtrocha@yahoo.com.br (J.B.T. Rocha).

TABLE OF CONTENTS

Table S1. Optimized structures. GGA ZORA-BLYP(BJ)/TZ2P.

Molecule Energy (Ha)	Coordinates			Molecule	Coordinates		
H_2O -0.5067482	O	-0.812277	-3.797985	0.000000	**CH_2=CH_2** -1.13370981	C	-4.565764	-0.665644	-0.701049
	H	-0.555031	-2.860026	0.000000		H	-5.586332	-0.294731	-0.775633
	H	-1.784755	-3.783047	0.000000		H	-4.330135	-1.269386	0.173400
						C	-3.651559	-0.394313	-1.632532
						H	-3.887200	0.209401	-2.506998
						H	-2.631078	-0.765498	-1.558116
H_2O_2 -0.64253188	O	-0.950665	-3.866755	-0.829678					
	H	-1.218280	-2.948615	-0.622989					
	H	-1.584416	-4.334246	-2.577082					
	O	-0.836332	-3.759752	-2.317018					
R = HgMe					***R = Me***				
EtSHgMe -2.12313494	C	0.675791	1.940526	-0.716873	**EtSMe** -2.13843582	C	-0.689423	1.739835	-0.876133
	H	0.871215	2.741593	0.000609		H	-0.474961	1.618842	0.190914
	H	1.130181	2.180397	-1.681589		H	-0.331857	2.719851	-1.204171
	H	1.078117	0.996392	-0.339908		H	-0.177118	0.960810	-1.450497
	Hg	-1.436217	1.734717	-0.973139		S	-2.495304	1.699525	-1.187824
	S	-3.805221	1.550499	-1.275969		C	-2.862157	-0.001560	-0.574881
	H	-6.211854	0.150031	-0.258390		H	-2.259334	-0.713507	-1.151507
	C	-5.618828	-0.517967	-0.892934		H	-2.556308	-0.062982	0.476511
	H	-5.951094	-0.388096	-1.928940		C	-4.355912	-0.304757	-0.726264
	H	-5.825269	-1.553335	-0.591585		H	-4.962115	0.403568	-0.150334
	C	-4.123274	-0.218457	-0.756032		H	-4.665629	-0.245415	-1.775753
	H	-3.537481	-0.887597	-1.392986		H	-4.574469	-1.315826	-0.362421
	H	-3.798498	-0.348677	0.280415					
EtSeHgMe -2.09873783	C	0.734809	1.936052	-0.711523	**EtSeMe** -2.10637937	C	-0.582990	1.787385	-0.874937
	H	0.961192	2.788749	-0.066429		H	-0.412898	1.648076	0.194982
	H	1.210566	2.062873	-1.687164		H	-0.191380	2.757180	-1.189991
	H	1.079474	1.010328	-0.243176		H	-0.107526	0.990110	-1.450523
	Hg	-1.391490	1.817765	-0.982949		Se	-2.537597	1.814350	-1.248104
	Se	-3.883048	1.702356	-1.307532		C	-2.916746	-0.034845	-0.574128
	H	-6.251411	0.056366	-0.237894		H	-2.300111	-0.722489	-1.160455
	C	-5.646352	-0.576398	-0.896935		H	-2.594509	-0.067303	0.470862
	H	-6.003749	-0.438897	-1.923695		C	-4.405033	-0.352994	-0.714871
	H	-5.817496	-1.624214	-0.614195		H	-5.017893	0.347474	-0.136000
	C	-4.161706	-0.236793	-0.778662		H	-4.725371	-0.302409	-1.761856
	H	-3.555623	-0.851735	-1.446967		H	-4.612533	-1.366151	-0.347341
	H	-3.804324	-0.354020	0.246388					
EtTeHgMe -2.07383571	C	0.840618	1.951501	-0.712393	**EtTeMe** -2.07747688	C	-0.442981	1.852787	-0.875597
	H	1.138026	2.944883	-0.366781		H	-0.309306	1.694306	0.195498
	H	1.321283	1.722050	-1.666507		H	-0.000590	2.805952	-1.172188
	H	1.103621	1.198997	0.035436		H	-0.002223	1.038663	-1.452748
	Hg	-1.301059	1.931911	-0.985712		Te	-2.586532	1.971278	-1.321401
	Te	-3.976955	1.901384	-1.323561		C	-2.993450	-0.068116	-0.574872
	H	-6.310512	-0.076482	-0.218330		H	-2.363831	-0.738291	-1.165540
	C	-5.693016	-0.657146	-0.912973		H	-2.658183	-0.082202	0.465266
	H	-6.084924	-0.502559	-1.924644		C	-4.476009	-0.420817	-0.700542
	H	-5.814723	-1.720638	-0.663473		H	-5.102343	0.266448	-0.120103
	C	-4.220723	-0.259584	-0.817596		H	-4.809938	-0.384768	-1.743963
	H	-3.601645	-0.815339	-1.523634		H	-4.659200	-1.436857	-0.326171
	H	-3.828203	-0.387896	0.192404					
Monoxides									
EtSOHgMe-*S* -2.32109436	C	0.704815	1.919675	-0.671396	**EtSOMe-*S*** -2.35168595	C	-0.712046	1.730731	-0.841711
	H	0.835937	2.730993	0.048817		H	-0.600829	1.566732	0.234444
	H	1.196088	2.160071	-1.617423		H	-0.329285	2.716536	-1.116862
	H	1.087008	0.979373	-0.266815		H	-0.204296	0.951670	-1.419611
	Hg	-1.423317	1.687883	-1.047680		S	-2.512075	1.729245	-1.261260
	S	-3.931539	1.596087	-1.409586		C	-2.844805	0.009470	-0.623810
	O	-4.571655	2.485589	-0.347142		H	-2.250528	-0.672220	-1.245011
	H	-6.182558	0.132055	-0.183080		H	-2.472756	-0.015570	0.407243
	C	-5.625240	-0.544930	-0.838525		C	-4.342612	-0.288025	-0.697181
	H	-6.049262	-0.476213	-1.847203		H	-4.906326	0.454456	-0.123149
	H	-5.765639	-1.570244	-0.475265		H	-4.702085	-0.270575	-1.732773
	C	-4.139104	-0.179613	-0.838390		H	-4.553159	-1.279447	-0.280337
	H	-3.555104	-0.786643	-1.543135		O	-3.189574	2.688202	-0.310326
	H	-3.704516	-0.268467	0.162361					

EtSeOHgMe-*S*	C	0.757386	1.938404	-0.632406	**EtSeOMe-*S***	C	-0.596809	1.783312	-0.821895
	H	0.873866	2.781673	0.052517		H	-0.589801	1.651762	0.261976
	H	1.305925	2.113583	-1.560854		H	-0.179246	2.752245	-1.101137
-2.28089674	H	1.081912	1.008061	-0.160460	-2.30190277	H	-0.080892	0.967803	-1.336792
	Hg	-1.357806	1.755222	-1.116550		Se	-2.531535	1.803287	-1.388341
	Se	-3.973645	1.694352	-1.532906		C	-2.884378	-0.072456	-0.682429
	O	-4.594925	2.573184	-0.223727		H	-2.326320	-0.754309	-1.334295
	H	-6.132258	0.128732	-0.109114		H	-2.450290	-0.074291	0.321663
	C	-5.654622	-0.575478	-0.798957		C	-4.387036	-0.331685	-0.672105
	H	-6.168455	-0.514327	-1.765754		H	-4.902675	0.444641	-0.096347
	H	-5.794316	-1.590002	-0.403639		H	-4.801497	-0.342265	-1.687419
	C	-4.169243	-0.256499	-0.936814		H	-4.604829	-1.302546	-0.210188
	H	-3.659892	-0.855572	-1.700509		O	-3.285066	2.795706	-0.263036
	H	-3.638013	-0.335717	0.014713					
EtTeOHgMe-*S*	C	0.827804	1.950439	-0.592187	**EtTeOMe-*S***	C	-0.483272	1.847891	-0.775269
	H	1.078160	2.977972	-0.317502		H	-0.588162	1.789770	0.310538
	H	1.405470	1.630455	-1.462654		H	0.015064	2.773723	-1.068550
-2.26201189	H	0.991348	1.274702	0.250666	-2.28043890	H	0.041409	0.976688	-1.177152
	Hg	-1.291282	1.887993	-1.112928		Te	-2.540814	1.892535	-1.559672
	Te	-4.067455	1.887612	-1.576348		C	-2.926378	-0.157482	-0.791868
	O	-4.695872	2.634534	0.013304		H	-2.462228	-0.856746	-1.495986
	H	-6.057009	0.019552	0.018061		H	-2.388765	-0.186504	0.160731
	C	-5.668890	-0.634859	-0.770552		C	-4.429291	-0.371780	-0.619862
	H	-6.308273	-0.521699	-1.654398		H	-4.862820	0.424669	-0.004678
	H	-5.755190	-1.673157	-0.423398		H	-4.950055	-0.379771	-1.585177
	C	-4.213201	-0.293332	-1.083309		H	-4.627766	-1.331440	-0.125859
	H	-3.809200	-0.836927	-1.944237		O	-3.417297	2.899653	-0.277542
	H	-3.560495	-0.437669	-0.218978					
MeHgSOH	C	0.326594	1.735869	-0.295746	**MeSOH**	C	-0.638106	1.854699	-0.856012
	H	0.947718	2.632379	-0.364545		H	-0.412314	1.667785	0.198500
	H	0.748437	0.933748	-0.906166		H	-0.330818	2.863434	-1.147098
-1.16803542	H	0.244955	1.414257	0.745811	-1.18843648	H	-0.105884	1.121186	-1.475188
	Hg	-1.635486	2.201512	-1.016536		S	-2.406423	1.595757	-1.221856
	S	-3.867482	2.740586	-1.781346		O	-3.114206	2.864228	-0.320598
	O	-4.785739	2.293088	-0.377413		H	-3.340619	2.493900	0.553395
	H	-5.114056	1.393702	-0.560822					
MeHgSeOH	C	0.325391	1.682802	-0.325352	**MeSeOH**	C	-0.567051	1.837867	-0.866442
	H	0.814463	2.584562	0.050442		H	-0.370884	1.639810	0.188822
	H	0.911770	1.238783	-1.133447		H	-0.304085	2.861656	-1.138248
-1.14977429	H	0.187463	0.960260	0.482962	-1.16162084	H	-0.013904	1.128482	-1.492185
	Hg	-1.608845	2.216359	-1.093553		Se	-2.483476	1.532094	-1.281731
	Se	-3.926374	2.842744	-1.921423		O	-3.200635	2.925449	-0.274279
	O	-4.854326	2.358709	-0.351301		H	-3.408334	2.535629	0.595205
	H	-5.173672	1.455089	-0.529873					
MeHgTeOH	C	0.372303	1.662791	-0.360051	**MeTeOH**	C	-0.483334	1.815105	-0.878305
	H	1.097196	2.460212	-0.541174		H	-0.288924	1.583946	0.169376
	H	0.644365	0.763941	-0.918174		H	-0.262524	2.858382	-1.108144
-1.13775763	H	0.307449	1.444567	0.708783	-1.14575441	H	0.099000	1.154469	-1.528515
	Hg	-1.567220	2.337541	-1.030629		Te	-2.587342	1.449730	-1.342589
	Te	-4.050293	3.155561	-1.783123		O	-3.312040	2.982427	-0.230664
	O	-5.010392	2.220036	-0.234802		H	-3.513206	2.616929	0.649984
	H	-5.287128	1.353048	-0.583045					
Dioxides									
$EtSO_2HgMe$	C	0.766922	2.026728	-0.739259	**$EtSO_2Me$**	C	-0.676769	1.771089	-0.890593
	H	0.935113	2.841143	-0.030900		H	-0.484611	1.677335	0.180630
	H	1.166762	2.281210	-1.723463		H	-0.381837	2.761372	-1.246891
-2.56364367	H	1.209625	1.098217	-0.371350	-2.59637307	H	-0.170916	0.991654	-1.464871
	Hg	-1.355116	1.734376	-0.932403		S	-2.464708	1.659508	-1.184587
	S	-3.828975	1.523480	-1.192841		C	-2.881901	-0.012580	-0.565840
	O	-4.486883	2.360999	-0.163523		H	-2.268495	-0.711853	-1.143907
	H	-6.306300	0.151044	-0.240009		H	-2.573538	-0.033238	0.484837
	C	-5.744241	-0.488663	-0.926735		C	-4.380271	-0.280000	-0.734821
	H	-6.081709	-0.288363	-1.947881		H	-4.970186	0.448467	-0.170761
	H	-5.963558	-1.535168	-0.686271		H	-4.667947	-0.223646	-1.788808
	C	-4.240942	-0.235663	-0.794267		H	-4.616856	-1.282544	-0.362636
	H	-3.649330	-0.835091	-1.495410		O	-3.124761	2.644729	-0.321929
	H	-3.875394	-0.391952	0.226916		O	-2.685024	1.679691	-2.634228
	O	-4.172495	1.730877	-2.618644					
$EtSeO_2HgMe$	C	0.935505	2.108476	-0.739213	**$EtSeO_2Me$**	C	-0.514587	1.835683	-0.880939
	H	1.082256	2.920811	-0.024835		H	-0.353967	1.714851	0.191602
	H	1.312531	2.376894	-1.727897		H	-0.227024	2.830414	-1.223809
-2.47424503	H	1.387060	1.181086	-0.381821	-2.49013440	H	-0.042245	1.050481	-1.473413
	Hg	-1.190745	1.780283	-0.921021		Se	-2.478334	1.723430	-1.203363
	Se	-3.804495	1.532296	-1.182536		C	-2.947547	-0.122542	-0.546334

	O	-4.547750	2.466381	-0.023385		H	-2.324675	-0.787828	-1.151444
	H	-6.373552	0.129922	-0.239017		H	-2.619688	-0.126332	0.497357
	C	-5.845773	-0.533532	-0.931184		C	-4.443391	-0.354921	-0.720421
	H	-6.156256	-0.293266	-1.952763		H	-5.021714	0.374410	-0.144850
	H	-6.141698	-1.567659	-0.713295		H	-4.730735	-0.279985	-1.773745
	C	-4.338195	-0.388177	-0.775973		H	-4.700679	-1.359277	-0.363002
	H	-3.758682	-0.979325	-1.491777		O	-3.215789	2.822820	-0.217984
	H	-3.978734	-0.550223	0.244877		O	-2.727446	1.768782	-2.834064
	O	-4.207994	1.789208	-2.776202					
$EtTeO_2HgMe$	C	1.114366	2.173103	-0.721139	**$EtTeO_2Me$**	C	-0.336318	1.905699	-0.881863
	H	1.262301	2.880235	0.097172		H	-0.164658	1.762363	0.186387
	H	1.479194	2.577176	-1.667279		H	-0.031529	2.901376	-1.207835
-2.44958376	H	1.571458	1.207014	-0.499146	-2.46132815	H	0.123457	1.125077	-1.490434
	Hg	-1.020124	1.860448	-0.930340		Te	-2.494167	1.809811	-1.216471
	Te	-3.811626	1.590197	-1.234873		C	-3.025938	-0.217945	-0.527998
	O	-4.666169	2.638527	0.017474		H	-2.402826	-0.880429	-1.136223
	H	-6.454045	0.076633	-0.215039		H	-2.700874	-0.241081	0.516448
	C	-5.943819	-0.605750	-0.902522		C	-4.525205	-0.446021	-0.710406
	H	-6.264090	-0.372960	-1.923224		H	-5.109112	0.273245	-0.127101
	H	-6.262721	-1.629918	-0.668715		H	-4.814156	-0.357068	-1.762593
	C	-4.428026	-0.492060	-0.763734		H	-4.787650	-1.454935	-0.368794
	H	-3.871309	-1.108698	-1.475998		O	-3.291751	3.019248	-0.093241
	H	-4.064094	-0.660997	0.254441		O	-2.787093	1.890644	-3.024283
	O	-4.267817	1.840223	-3.003117					
$MeHgSO_2H$	C	0.034215	1.446358	-0.357325	**$MeSO_2H$**	C	-0.598475	1.829167	-0.903586
	H	0.773707	2.248978	-0.409838		H	-0.319193	1.647246	0.137297
	H	0.281369	0.644301	-1.056753		H	-0.441804	2.874186	-1.184879
-1.39155610	H	-0.049771	1.062302	0.661970	-1.42685660	H	-0.062905	1.157449	-1.579346
	Hg	-1.894991	2.272411	-0.932914		S	-2.384276	1.465353	-1.119658
	S	-4.161577	3.199991	-1.683016		O	-2.796000	2.755842	-0.060352
	O	-5.125420	2.499791	-0.441568		H	-3.751016	2.660883	0.125599
	H	-5.090502	1.525417	-0.533894		O	-2.722145	1.839643	-2.517997
	O	-4.458141	2.521352	-2.989593					
$MeHgSeO_2H$	C	-0.036043	1.363375	-0.318360	**$MeSeO_2H$**	C	-0.512547	1.809801	-0.898263
	H	0.749435	2.122406	-0.314027		H	-0.243334	1.651591	0.148287
	H	0.188155	0.573611	-1.038876		H	-0.422830	2.857091	-1.191846
-1.35273864	H	-0.184522	0.950112	0.681769	-1.37691144	H	0.047626	1.153741	-1.568026
	Hg	-1.890838	2.320473	-0.931966		Se	-2.443584	1.353917	-1.133823
	Se	-4.217029	3.335147	-1.749097		O	-2.863881	2.738459	0.078940
	O	-5.229092	2.585853	-0.333197		H	-3.840314	2.772414	0.119918
	H	-5.294321	1.631034	-0.540421		O	-2.796951	1.892755	-2.658109
	O	-4.528438	2.408191	-3.103739					
$MeHgTeO_2H$	C	0.000815	1.325109	-0.290125	**$MeTeO_2H$**	C	-0.425836	1.793401	-0.895034
	H	0.835517	2.008739	-0.461721		H	-0.180127	1.727744	0.167402
	H	0.096211	0.431671	-0.911493		H	-0.361747	2.819618	-1.262924
-1.34392393	H	-0.072470	1.058638	0.766771	-1.36489813	H	0.192346	1.118221	-1.491434
	Hg	-1.839796	2.345977	-0.860327		Te	-2.514987	1.233548	-1.166881
	Te	-4.298309	3.476564	-1.682891		O	-2.964336	2.663255	0.201031
	O	-5.377323	2.480579	-0.270342		H	-3.915997	2.872444	0.129956
	H	-5.481808	1.566580	-0.605204		O	-2.905132	2.001539	-2.785038
	O	-4.567386	2.470877	-3.208904					

Table S2. TS structures. GGA ZORA-BLYP(BJ)/TZ2P. Imaginary vibrational frequencies (imag freq) in cm^{-1}.

R= HgMe		***R= Me***	
Molecule Energy (Ha) imag freq	**Coordinates**	**Molecule Energy (Ha) imag freq**	**Coordinates**
Oxidation			
EtSHgMe + H_2O_2 -2.7522672 $O^{14}...H^{15}...O^{16}$ (-501.56)	C -9.690102 1.495198 -0.439780 H -9.661991 2.039697 -1.385521 H -10.230035 2.061318 0.321688 H -10.135166 0.506900 -0.570756 Hg -7.680916 1.250458 0.204101 S -5.314197 1.074116 0.834493 H -3.020549 0.201627 -0.821437 C -3.295156 -0.581367 -0.108411 H -2.736416 -0.424514 0.820704 H -3.001131 -1.552290 -0.526381 C -4.804117 -0.565635 0.141629 H -5.108850 -1.326311 0.868068 H -5.358768 -0.715316 -0.787982 O -5.348016 1.951786 -1.071878 H -5.021728 2.888038 -1.033511 O -5.240247 3.281927 -2.657655 H -4.544990 2.772016 -3.115157	**EtSMe + H_2O_2** -2.76822025 $O^{13}...H^{14}...O^{15}$ (-474.10)	C -1.114918 2.154175 -0.463180 H -1.275477 2.374631 0.595158 H -0.756020 3.049883 -0.975316 H -0.405758 1.332503 -0.601712 S -2.718053 1.728306 -1.209524 C -3.168111 0.259220 -0.207572 H -2.409227 -0.508219 -0.397457 H -3.112076 0.580092 0.837630 C -4.574067 -0.219179 -0.573670 H -5.306060 0.572389 -0.388389 H -4.634350 -0.520540 -1.625320 H -4.836224 -1.085469 0.044015 O -3.796397 2.972064 -0.034394 H -4.251999 3.642504 -0.597715 O -4.941893 4.467471 0.760425 H -5.617379 3.854437 1.107712
EtSeHgMe + H_2O_2 -2.73106059 $O^{14}...H^{15}...O^{16}$ (-414.81)	C -10.004473 1.275440 -0.176261 H -10.190357 2.047918 -0.925066 H -10.568894 1.474957 0.737194 H -10.251259 0.287732 -0.571945 Hg -7.921783 1.299343 0.302801 Se -5.421177 1.375497 0.800335 H -3.126595 0.282196 -0.865099 C -3.409096 -0.488026 -0.141786 H -2.839650 -0.335344 0.781757 H -3.133826 -1.467932 -0.553432 C -4.912416 -0.447715 0.111687 H -5.240806 -1.167497 0.865540 H -5.481286 -0.580761 -0.810074 O -5.090472 2.097603 -1.200609 H -4.639291 2.974817 -1.156831 O -4.373570 3.090817 -2.866155 H -3.693054 2.407953 -3.020716	**EtSeMe + H_2O_2** -2.73866362 $O^{13}...H^{14}...O^{15}$ (-414.15)	C -0.722614 2.088321 -0.630374 H -0.771446 2.173268 0.457087 H -0.302720 2.996495 -1.065981 H -0.140936 1.213406 -0.928782 Se -2.568980 1.915568 -1.335775 C -3.072853 0.276247 -0.302064 H -2.486670 -0.548358 -0.719075 H -2.753381 0.474541 0.724701 C -4.579281 0.050264 -0.399315 H -5.121649 0.918107 -0.012492 H -4.892776 -0.134424 -1.433301 H -4.855260 -0.827971 0.197151 O -3.720498 3.231099 -0.046920 H -3.223081 3.281133 0.801314 O -4.556194 4.192728 1.511417 H -4.594096 5.037968 1.025041
EtTeHgMe + H_2O_2 -2.71584254 $O^{14}...H^{15}...O^{16}$ (-288.60)	C -9.721431 1.543998 -0.574068 H -9.548524 1.972354 -1.562983 H -10.335939 2.203863 0.041371 H -10.168962 0.550790 -0.644676 Hg -7.798333 1.354784 0.358183 Te -5.218868 1.224475 1.285828 H -3.072603 0.255722 -0.906173 C -3.230555 -0.593760 -0.234983 H -2.532303 -0.512189 0.605680 H -2.988283 -1.513890 -0.784346 C -4.681414 -0.645867 0.236549 H -4.877675 -1.457558 0.940718 H -5.381522 -0.700145 -0.598549 O -5.309216 2.058518 -0.871317 H -5.132683 3.023513 -0.870891 O -5.471494 3.045768 -2.684871 H -4.722567 2.547273 -3.063261	**EtTeMe + H_2O_2** -2.72223125 $O^{13}...H^{14}...O^{15}$ (-197.47)	C -0.201328 1.762570 -0.837070 H -0.168231 1.872721 0.248199 H 0.425301 2.511557 -1.324010 H 0.087754 0.757167 -1.149092 Te -2.268385 2.119725 -1.435836 C -3.012985 0.365831 -0.343571 H -2.720834 -0.502890 -0.938978 H -2.439605 0.393998 0.586439 C -4.516670 0.443277 -0.090395 H -4.760592 1.325073 0.507133 H -5.089162 0.475793 -1.024729 H -4.836453 -0.448136 0.464868 O -3.037465 3.149345 0.429246 H -2.861348 4.106848 0.336525 O -3.766951 4.092172 2.052380 H -4.689594 3.939569 1.770494
EtSOHgMe + H_2O_2 -2.95830998 $O^{15}...H^{16}...O^{17}$ (-364.10)	C 0.684055 1.894445 -0.880264 H 1.099199 1.022673 -0.371215 H 1.034678 2.821516 -0.422725 H 0.904791 1.870599 -1.949113 Hg -1.453053 1.824424 -0.673656 S -3.971107 1.804198 -0.595585 O -4.635736 2.547476 0.536389 H -6.401452 0.326900 0.231752 C -5.837192 -0.261574 -0.498128 H -6.184003 -0.011901 -1.504588 H -6.035860 -1.323632 -0.312882 C -4.335939 0.000658 -0.364416	**EtSOMe + H_2O_2** -2.98027709 $O^{14}...H^{15}...O^{16}$ (-495.08)	C -0.477710 1.813613 -0.703631 H -0.163806 1.542465 0.307981 H -0.193648 2.844555 -0.927423 H -0.089786 1.132131 -1.462193 S -2.304492 1.756724 -0.759894 O -2.832731 2.581882 0.373003 H -4.641398 0.320517 0.324352 C -4.121762 -0.303113 -0.409562 H -4.545486 -0.116992 -1.400601 H -4.291716 -1.353897 -0.151084 C -2.619017 -0.019957 -0.401140 H -2.080638 -0.576548 -1.172422

	H	-3.748136	-0.515746	-1.128262		H	-2.166600	-0.192132	0.581775
	H	-3.960450	-0.241990	0.634771		O	-2.532809	1.489102	-2.684279
	O	-4.153528	1.568707	-2.553851		H	-2.298998	2.293259	-3.207051
	H	-3.954203	2.414186	-3.010011		O	-2.143498	1.287687	-4.660725
	O	-3.648436	1.370315	-4.516546		H	-3.059103	1.035877	-4.888851
	H	-4.532920	1.057433	-4.786376					
EtSeOHgMe + H_2O_2 -2.91288113 $O^{15}...H^{16}...O^{17}$ (-374.10)	C	1.108651	1.944370	-0.170667	**EtSeOMe + H_2O_2** -2.92475726 $O^{14}...H^{15}...O^{16}$ (-595.37)	C	-0.276674	1.822746	-0.614556
	H	1.194815	2.000774	0.915626		H	-0.064394	1.546816	0.420007
	H	1.485287	2.847792	-0.653378		H	0.057464	2.837775	-0.832621
	H	1.583628	1.046104	-0.568229		H	0.109782	1.102861	-1.337525
	Hg	-1.014045	1.811200	-0.638367		Se	-2.270115	1.839982	-0.803361
	Se	-3.667399	1.778843	-1.133384		O	-2.849671	2.823823	0.419724
	O	-4.382219	2.671450	0.089891		H	-4.760488	0.304288	0.118313
	H	-6.002844	0.318955	0.163220		C	-4.131800	-0.373561	-0.468286
	C	-5.573777	-0.357918	-0.582647		H	-4.409643	-0.295137	-1.523422
	H	-6.061226	-0.181543	-1.544944		H	-4.334393	-1.398406	-0.134324
	H	-5.779572	-1.389336	-0.269704		C	-2.653251	-0.062091	-0.271021
	C	-4.067188	-0.156060	-0.691717		H	-1.994345	-0.658456	-0.907722
	H	-3.604855	-0.717256	-1.509143		H	-2.331966	-0.103526	0.773765
	H	-3.540808	-0.339817	0.248719		O	-2.576943	1.464622	-2.805689
	O	-4.552883	1.531599	-2.963583		H	-2.307280	2.172475	-3.459022
	H	-4.560132	2.361936	-3.496808		O	-2.402567	1.305176	-4.844964
	O	-5.393321	1.559962	-4.849522		H	-3.366915	1.205786	-4.971040
	H	-6.301403	1.437634	-4.510068					
EtTeOHgMe + H_2O_2 -2.89970213 $O^{15}...H^{16}...O^{17}$ (-277.71)	C	1.441088	1.945947	0.601165	**EtTeOMe + H_2O_2** -2.90912153 $O^{14}...H^{15}...O^{16}$ (-513.00)	C	-0.236724	1.910752	-0.663267
	H	1.942503	0.978356	0.549472		H	-0.010945	1.598932	0.358206
	H	1.171714	2.212549	1.624228		H	0.124731	2.922146	-0.854698
	H	2.020321	2.732136	0.114187		H	0.131439	1.206407	-1.411423
	Hg	-0.437534	1.758095	-0.518935		Te	-2.410976	1.950924	-0.840685
	Te	-3.010558	1.705982	-1.843711		O	-2.993584	2.857942	0.673340
	O	-3.858737	3.042206	-0.890020		H	-4.663337	0.183974	0.612670
	H	-5.672816	0.761488	-0.390690		C	-4.257204	-0.438529	-0.191560
	C	-5.283705	-0.139664	-0.876533		H	-4.830654	-0.247382	-1.104816
	H	-5.682698	-0.190047	-1.893143		H	-4.406441	-1.489511	0.084849
	H	-5.644973	-1.012605	-0.317726		C	-2.768449	-0.168389	-0.402102
	C	-3.755949	-0.138024	-0.887456		H	-2.343396	-0.692986	-1.262181
	H	-3.323159	-0.957169	-1.470380		H	-2.169322	-0.356996	0.493870
	H	-3.321532	-0.126076	0.116279		O	-2.553086	1.588321	-2.971287
	O	-4.149732	1.141099	-3.569530		H	-2.268164	2.307422	-3.596668
	H	-4.101461	1.786195	-4.310222		O	-2.004559	1.341389	-4.950026
	O	-5.492942	0.874877	-5.122872		H	-2.902530	1.060756	-5.215968
	H	-6.252971	1.151766	-4.573420					
Elimination									
EtSOHgMe -2.28630531 $O^{7}...H^{8}...C^{9}$ (-1035.94)	C	0.079958	0.393469	2.122194	**EtSOMe** -2.31078648 $O^{6}...H^{7}...C^{8}$ (-1227.8)	C	-0.843238	0.742395	1.029604
	H	-0.137596	0.828735	3.100838		H	-0.469827	1.536161	1.681850
	H	1.038314	0.761554	1.747506		H	-0.093480	0.497380	0.268250
	H	0.089064	-0.697531	2.184089		H	-1.089621	-0.147361	1.615361
	Hg	-1.469233	0.996850	0.751529		S	-2.339551	1.332248	0.140338
	S	-3.306875	1.704816	-0.724150		O	-3.437165	1.477890	1.278059
	O	-4.512893	1.972857	0.296844		H	-3.999686	0.347740	1.235421
	H	-5.106379	0.817283	0.293790		C	-4.241223	-0.924997	0.765868
	C	-5.333950	-0.446450	-0.063265		H	-5.296078	-0.836079	0.502938
	H	-6.345242	-0.352702	-0.463426		H	-4.040846	-1.521607	1.656668
	H	-5.271380	-0.971939	0.891657		C	-3.302623	-0.957150	-0.278155
	C	-4.287919	-0.646449	-0.984586		H	-3.595598	-0.745942	-1.301944
	H	-4.443479	-0.514930	-2.050308		H	-2.345993	-1.459199	-0.164450
	H	-3.388609	-1.187983	-0.710449					
EtSeOHgMe -2.25995906 $O^{7}...H^{8}...C^{9}$ (-817.02)	C	0.071345	0.383883	2.161551	**EtSeOMe** -2.27607404 $O^{6}...H^{7}...C^{8}$ (-985.16)	C	-0.753085	0.770001	1.045607
	H	-0.025350	1.000251	3.058584		H	-0.382231	1.585769	1.667875
	H	1.059982	0.511307	1.714085		H	-0.001599	0.465772	0.310360
	H	-0.109339	-0.667572	2.397707		H	-1.066021	-0.078099	1.656869
	Hg	-1.415225	1.030376	0.733370		Se	-2.356154	1.414146	0.038385
	Se	-3.319205	1.797687	-0.829201		O	-3.539082	1.521543	1.308905
	O	-4.581180	2.004226	0.371370		H	-4.059805	0.316645	1.235913
	H	-5.123219	0.760976	0.336808		C	-4.244165	-0.914390	0.782561
	C	-5.288430	-0.457355	-0.044989		H	-5.303961	-0.889336	0.522439
	H	-6.324630	-0.435480	-0.390062		H	-4.014122	-1.516626	1.663303
	H	-5.141614	-1.026901	0.875747		C	-3.320228	-0.957877	-0.288868
	C	-4.292203	-0.607390	-1.046925		H	-3.646339	-0.801892	-1.312924
	H	-4.536977	-0.492826	-2.098300		H	-2.359104	-1.453536	-0.183973
	H	-3.370173	-1.143603	-0.847483					
EtTeOHgMe	C	0.169379	0.369043	2.202729	**EtTeOMe**	C	-0.645490	0.793260	1.075625
	H	-0.346909	0.325964	3.164853		H	-0.203109	1.611070	1.645699
	H	0.976649	1.104744	2.233564		H	0.074162	0.375719	0.366047

-2.24455324 $O^8...H^9...C^{10}$ (-782.80)	H 0.557045 -0.615604 1.930600 Hg -1.263266 0.988163 0.695281 Te -3.224263 1.782657 -1.070416 O -4.586852 2.097516 0.243964 H -5.157668 0.842284 0.276674 C -5.358591 -0.379968 -0.012876 H -6.398666 -0.362326 -0.347901 H -5.217858 -0.883451 0.947025 C -4.386550 -0.676894 -1.019194 H -4.662249 -0.683584 -2.069494 H -3.496417 -1.250966 -0.782549	-2.25754370 $O^6...H^7...C^8$ (-963.54)	H -1.030609 0.018074 1.740838 Te -2.379264 1.544859 -0.040153 O -3.664895 1.527806 1.367904 H -4.131238 0.289057 1.241081 C -4.268246 -0.926575 0.772171 H -5.330067 -0.947178 0.518340 H -4.009635 -1.530097 1.644713 C -3.354308 -0.963252 -0.319794 H -3.707175 -0.860239 -1.341730 H -2.389033 -1.453184 -0.221915
$EtSO_2HgMe$ -2.50705980 $O^8...H^9...C^{10}$ (-1327.55)	C 0.589569 0.700504 2.343095 H 0.213218 0.642460 3.366447 H 1.122770 1.638306 2.174103 H 1.222149 -0.157692 2.107560 Hg -1.108624 0.666238 1.014649 S -3.086152 0.722548 -0.533533 O -2.858087 1.749236 -1.598504 O -4.040678 1.204764 0.644694 H -5.131652 0.620138 0.262141 C -5.928972 -0.210597 -0.464330 H -6.628761 0.508034 -0.892850 H -6.336583 -0.838154 0.330120 C -4.958924 -0.767646 -1.312385 H -4.798932 -0.389993 -2.318374 H -4.488041 -1.719571 -1.082879	**$EtSO_2Me$** -2.52954537 $O^7...H^8...C^9$ (-1235.8)	C -0.558647 0.907048 1.028387 H -0.454251 1.910873 1.447966 H 0.176212 0.735100 0.238746 H -0.501830 0.142366 1.805998 S -2.219014 0.817828 0.248841 O -2.281374 1.892120 -0.776247 O -3.108117 1.042998 1.515298 H -3.983751 0.091423 1.293806 C -4.562070 -0.992953 0.736254 H -5.518318 -0.577199 0.416452 H -4.606178 -1.662536 1.596668 C -3.602064 -1.256580 -0.250196 H -3.722801 -0.909431 -1.272387 H -2.804342 -1.976217 -0.088719
$EtSeO_2HgMe$ -2.44805615 $O^8...H^9...C^{10}$ (-703.33) constraints $Hg^5...O^8$ = 3.26 Å	C 0.827575 0.763629 2.330919 H 0.496669 0.990855 3.345724 H 1.442788 1.566732 1.921482 H 1.341966 -0.197638 2.283474 Hg -0.941871 0.622643 1.097841 Se -3.071052 0.634411 -0.486062 O -2.735877 1.820528 -1.614959 O -4.136771 1.190567 0.785311 H -5.316460 0.532299 0.255706 C -5.987079 -0.199362 -0.501215 H -6.691135 0.509286 -0.944006 H -6.448822 -0.905369 0.193917 C -5.016695 -0.745862 -1.392112 H -4.854983 -0.322025 -2.379883 H -4.599842 -1.736433 -1.229910	**$EtSeO_2Me$** -2.45734157 $O^7...H^8...C^9$ (-645.78)	C -0.406083 0.966014 1.071328 H -0.342900 1.990874 1.438209 H 0.328143 0.763675 0.290181 H -0.380511 0.233555 1.879102 Se -2.213183 0.836138 0.203326 O -2.242334 2.043819 -0.935783 O -3.188576 1.134335 1.593893 H -4.117301 0.008965 1.318364 C -4.579872 -1.000243 0.771432 H -5.564093 -0.661736 0.438667 H -4.610407 -1.722958 1.590925 C -3.644150 -1.280910 -0.264007 H -3.813570 -0.956392 -1.287232 H -2.849678 -2.009758 -0.127686
$EtTeO_2HgMe$ -2.42986769 $O^8...H^9...C^{10}$ (-478.90) constraints $Hg^5...O^8$ = 3.5 Å	C 1.582177 0.336337 1.130026 H 1.896339 -0.679122 1.376653 H 1.507176 0.961885 2.020984 H 2.230567 0.786063 0.376260 Hg -0.405007 0.215902 0.269930 Te -2.938992 0.265584 -0.979823 O -2.620329 1.371696 -2.426974 O -3.749359 1.231129 0.455989 H -5.141826 0.656531 0.208472 C -6.002494 -0.023612 -0.314700 H -6.687508 0.727900 -0.717496 H -6.424714 -0.587270 0.522275 C -5.341919 -0.826605 -1.311757 H -5.365964 -0.543289 -2.361676 H -5.098112 -1.867934 -1.118182	**$EtTeO_2Me$** -2.43644697 $O^7...H^8...C^9$ (-430.51)	C -0.249595 1.003047 1.124105 H -0.172040 2.041470 1.449004 H 0.516835 0.747864 0.390794 H -0.276025 0.308784 1.965077 Te -2.199376 0.883895 0.114715 O -2.176969 2.297042 -1.063203 O -3.296407 1.181149 1.623342 H -4.218159 -0.048369 1.325815 C -4.632188 -1.044766 0.787921 H -5.639837 -0.758413 0.473586 H -4.622694 -1.783607 1.594731 C -3.731791 -1.333262 -0.294325 H -3.969123 -1.053483 -1.317510 H -2.938707 -2.068693 -0.187312

9.5. INTERAÇÕES DO DCDSe COM A δ-ALAD DE MAMÍFERO

Figura 9.5.1. *Docking* do DCDSe com a δ-AlaD.

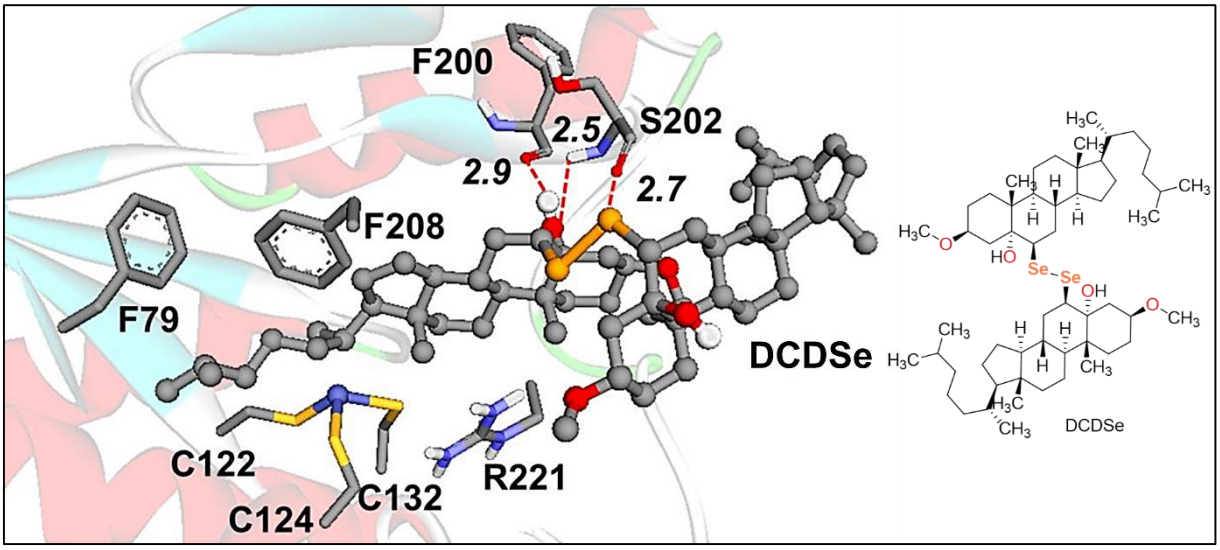

Fonte: autor. ΔG = -5,5 kcal/mol. Metodologia de acordo com NOGARA *et al*. 2020.

9.6. *DOCKING* DA TrxR COM EBSELEN.

Figura 9.6.1. *Docking* entre o Ebselen (A) e o disseleneto de Ebselen (B) com a enzima TrxR (1H6V).

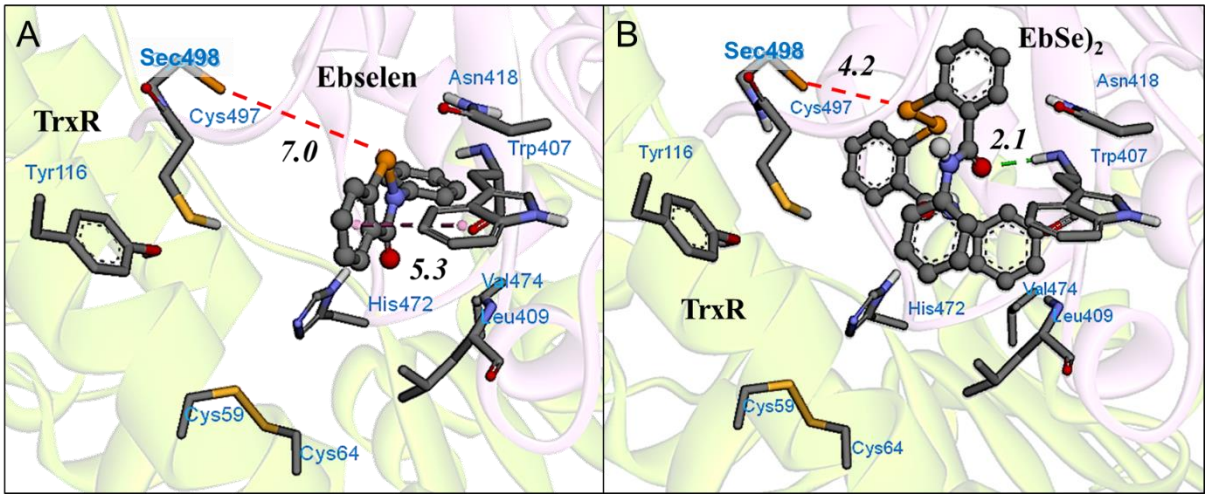

Fonte: autor. Metodologia de acordo com SUDATI *et al*. 2018. ΔG = -7,1 e -10,6 kcal/mol, respectivamente.

9.7. SOFTWARES UTILIZADOS

A tabela 9.7.1 descreve de maneira geral os programas e suas respectivas funções neste estudo.

Tabela 9.7.1. Programas e suas funções.

Softwares	**Função**
ADF	Cálculos de DFT
AutoDockTools	Conversão para o formato de arquivo *.pdbqt*
Avogadro	Desenho dos ligantes 3D
Chimera	Edição da estrutura da proteína
Clustal Omega	Alinhamento da sequência de aminoácidos das proteínas
Discovery Studio Visualizer	Visualização de estruturas 3D
ERRAT	Avaliação da estrutura proteica
Gaussian	Cálculos de DFT
Geneious	Análise de sequências de aminoácidos
Geno3D	Homologia de proteínas
MOPAC	Otimização geométrica semiemprírica de moléculas
Notepad++	Editor de texto
PROCHECK	Gráfico de Ramachandran e avaliação da estrutura proteica
Phyre2	Homologia de proteínas
pkCSM	Predição da toxicidade
ProSA	Avaliação da estrutura proteica
Swiss-Model	Homologia de proteínas
Verify3D	Avaliação da estrutura proteica
Vina 1.1.1	Simulações de *docking* molecular